

THE UNIVERSITY OF HULL

**BIOIMPRINTING TECHNOLOGIES FOR REMOVAL OF
MYELOBLASTS FROM PERIPHERAL BLOOD**

A thesis submitted for the Degree of Doctor of Philosophy
to the University of Hull

Jevan Medlock

MChem (University of Hull)

September 2018

Acknowledgements

Firstly, I would like to thank my academic supervisors Professor Vesselin Paunov and Dr Leigh Madden for their support and guidance. I'm sincerely grateful for the opportunity you have given me. Also massive thanks to Dr David Allsup and all those at the Queen's Centre for Oncology and Haematology at Castle Hill Hospital; it was inspiring to see the work you do.

Thank you to all those at The University of Hull who have made my time so enjoyable; particularly to Bobby, Ben, Andy and Anupam. To my Arabic tutors Saba, Mohammed, Osama, Khaled and Ahmed - شكرا جزيلا . Also, to the support staff who are often overlooked; cheers to Rich, Nigel, Chris and Dean and to Tony Sinclair for his help in collecting SEM images.

To my family, particularly my parents, Clive and Lehan, who have always done the upmost to help, care and nurture me throughout my life for which I will always be grateful. A massive thank you to Brogan for being there for me, for the things we do and places we go. I am the luckiest person in the world.

On to pastures new, thanks to Dr Jackson Kirkman-Brown MBE and all those at the Centre for Human Reproductive Science for their kind welcome to the group.

Lastly, thanks to the staff of BBC's Test Match Special whose coverage has provided an excellent soundtrack over my experiments and writing up.

Abstract

Acute Myeloid Leukaemia (AML) is a malignancy occurring in the bone marrow and blood whereby immature and defective blast cells are overproduced. As a genetic condition, no cure is available. The condition is traditionally managed by treatment reliant on non-specific cytotoxic chemotherapy and bone marrow transplantation. Treatment is associated with causing discomfort and mortality and is ultimately ineffective; relapse is common and survival rates are poor.

Bioimprinting is a technology whereby the size, shape and morphology of biological templates are recreated in polymer matrices. Studies aim to mimic and exploit specific binding reliant on complementary size and shape interactions as seen in a number of biological processes. The field has developed from the templating of rudimentary macromolecules to whole cells with extracellular features accurate on a nanometre scale.

This study aimed to fabricate AML specific bioimprints able to discriminate neoplastic cells from patient aspirate. Myeloblasts provide an ideal target due to their inherent size difference and morphological irregularity. Bioimprints incorporated into a high throughput device could provide a vehicle for selectivity of myeloblasts, yielding an alternate treatment pathway in reducing the leukaemic burden in AML sufferers.

Herein, methods were devised and evaluated to reliably fabricate high quality bioimprints, representative of the templated cell. Key in the protocol design is the control over the proportion of the cell surface exposed to the curing polymer matrix which dictates the size of the cavities produced and in-turn the ability of uptake of target cells to the bioimprint substrates. This method should be compatible with roll-to-roll nanoimprint lithography which has been highlighted as a viable method to upscale the imprints in order to deplete very high myeloblast cell populations in AML sufferers. Bioimprints of various cell types and polymer particles of similar size were made and further used to produce positive imprints and subsequent negative replica imprints. Ultimately, a methodology was devised and bioimprints of an AML *in vitro* cultured cell line were fabricated and reproduced into an area of hundreds of square metres.

The success of bioimprinting technology was evaluated with high resolution microscopy and surface profiling; characterising bioimprinted cavities in comparison with the template cell

type. Surface modifications were trialled in order to incur an attraction between substrates and incubated cell populations. A coating of weak cationic surface charge was introduced on the bioimprint surface, to attract the negative charges of extracellular groups. This interaction is amplified by an increased surface area contact, allowing binding of cells fitting flush into cavities. Cells unable to fit into cavities did not receive this attraction and remained unbound. With the intended use in mind, a method using materials approved for clinical use was found.

Once produced and functionalised, the retention of incubated cell populations was examined under flow conditions. In doing, a bespoke microfluidic device was designed in order to control the hydrodynamics experienced by the bioimprint allowing for a comparison of retention per surface modification parameters. Retention of target cells to bioimprints made using the same cell type was measured as a function of incubated cell suspension concentration; analysis confirmed cells were retained and localised to the bioimprinted cavities. This was compared to cells incubated on bioimprints produced from microparticles of the same size distribution. Significantly poorer retention was observed, indicating the importance of cell shape and cellular surface properties in bioimprint capture.

The preference of the bioimprints to the target cell type was assessed by exposure to binary cell mixtures of myeloblasts and PBMCs. Cell populations were characterised on account of size and shape and separately fluorescently labelled for identification and automated enumeration. Bioimprint selectivity towards the targeted cells (myeloblasts) was compared by the proportions of each cell type retained to the bioimprints. In each instance the bioimprint showed a preference for capture of the target cell type over the healthy control. It is anticipated that by reapplying or recirculating patient aspirate, myeloblasts can be completely depleted from samples due to the higher affinity. This effect was confirmed by comparison of the bioimprint path length on selectivity; using larger areas of bioimprint at fixed cell concentration to represent a recirculated population.

Table of Contents

1. Introduction	1
1.1. Leukaemia	1
1.1.1. Acute myeloid leukaemia	3
1.1.2. Treatment	6
1.1.3. Prognosis.....	8
1.1.4. Weaknesses of current therapy	9
1.2. Bioimprinting	10
1.2.1. Molecular recognition	10
1.2.2. Molecularly imprinted polymers - macromolecules	11
1.2.3. Whole cell Bioimprints	12
1.2.4. Applications of bioimprinting.....	16
1.2.5. Current methods of cell sorting and targeting.....	27
1.2.6. Bioimprint replication and area augmentation.....	35
1.2.7. Summary of bioimprinting.....	38
1.3. Bioimprint rationale	39
1.3.1. Attractive dispersion forces	39
1.3.2. Electrostatic interaction due to overlapping of electric double layers	40
1.3.3. Interaction energy between a spherical cell and flat substrate.....	44
1.3.4. Interaction energy between a spherical cell and bioimprint	46
1.4. Aim of this project.....	49
1.4.1. Presentation of this thesis.....	50
1.5. References	52

2. Experimental 59

2.1. Materials.....	59
2.1.1. Water.....	59
2.1.2. Solvents.....	59
2.1.3. Cell lines and processing	59
2.1.4. Particles.....	60
2.1.5. Imprinting materials.....	61
2.1.6. Charged materials	62
2.1.7. Dyes	62
2.1.8. Miscellaneous	63
2.2. Methods.....	64
2.2.1. Cell line handling.....	64
2.2.2. Bioimprint production.....	67
2.2.3. Bioimprint surface modification	72
2.2.4. Bioimprint cell retention study	74
2.3. References	78

3. Fabrication of Bioimprints 79

3.1. Cell fixation.....	81
3.2. Template deposition	84
3.2.1. Cell sedimentation	84
3.2.2. Adhesive tape capture	91
3.2.3. Cytospin centrifuge method.....	93
3.2.4. Glucose protective coating spreading	95
3.3. Bioimprint casting	99

3.3.1.	Sedimentation imprints	100
3.3.2.	Cytospin bioimprints.....	103
3.3.3.	Glucose imprints bioimprints.....	110
3.4.	Positive imprints.....	117
3.4.1.	Cytospin-mediated positive imprints	118
3.4.2.	Glucose positive imprints	121
3.5.	Imprint augmentation	125
3.5.1.	Cytospin augmentation	126
3.5.2.	Glucose protective layer	130
3.6.	Conclusions	134
3.7.	References	136
4.	Bioimprint Characterisation and Modification	137
4.1.	Bioimprint characterisation	137
4.1.1.	Cavity diameter.....	137
4.1.2.	Nanoscale analysis	147
4.2.	Surface modification	150
4.2.1.	Oxygen plasma & APTES	150
4.2.2.	Hydrophobic recovery of PDMS	155
4.2.3.	Limitations of PDMS as a material for negative bioimprints	157
4.2.4.	Matrix entanglement	160
4.3.	Conclusions	161
4.4.	References	163

5. Cell retention on Bioimprints 164

5.1. PDMS bioimprints	164
5.1.1. Jurkat Bioimprint	164
5.1.2. Jurkat Cells.....	165
5.1.3. Jurkat cells retention onto PDMS imprints.....	167
5.2. Flow cell experiments	174
5.2.1. Substrate.....	175
5.2.2. Retention of cells from single cell suspension.....	180
5.2.3. HL60 retention to particle imprints.....	183
5.3. Conclusions	186
5.4. References.....	188

6. Bioimprint Selectivity 189

6.1. Cell populations.....	189
6.2. Cell staining.....	193
6.3. Examination of the bioimprint selectivity towards myeloblasts	196
6.3.1. Channel path length comparison.....	205
6.4. Conclusions	210
6.5. References	212

7. Summary of Conclusions and Future Work 214

7.1. Conclusions.....	214
7.1.1. Bioimprint production.....	214
7.1.2. Bioimprint characterisation and modification	215

7.1.3.	Retention of single cells to bioimprints	216
7.1.4.	Selectivity from binary mixtures	217
7.2.	Future work.....	218
7.2.1.	Optimise surface modification.....	218
7.2.2.	Examination of effluent	218
7.2.3.	Unfixed cells	218
7.2.4.	Flow conditions.....	219

List of Abbreviations

Acronym	Description
AFM	Atomic force microscopy
ALL	Acute lymphoblastic (or interchangeably, lymphocytic) leukaemia
AML	Acute myeloid leukaemia
bPEI	Branched poly(ethylenimine)
BSA	Bovine serum albumin
CD	Cluster of differentiation
CLL	Chronic lymphocytic leukaemia
CLSM	Confocal laser scanning microscopy
CTC	Circulating tumour cell
DLVO	Derjaguin-Landau-Verwey-Overbeek
DNA	Deoxyribonucleic acid
EDL	Electric double layer
EpCAM	Epithelial cell adhesion molecule
FAB	French-American-British [classification]
GvHD	Graft versus host disease
GvL	Graft versus leukaemia [effect]
HL60	Human Leukaemia 60 [cell line]
HLA	Human leukocyte antigen
HSC	Haematopoietic stem cell
HSCT	Haematopoietic stem cell transplant
HTSMU	High throughput micro-sampling unit
mAb	Monoclonal Antibody
MCF-7	Michigan cancer foundation 7 [cell line]
MIP	Molecularly imprinted polymer
MRD	Minimal residual disease
NIR	Near infrared
NPs	Nano-particles
PBMC	Peripheral blood mononuclear cell
PBS	Phosphate buffer saline
PCR	Polymerase chain reaction
PDAC	Poly(diallyldimethylammonium chloride)
PDMS	Polydimethyl siloxane
PET	Polyethylene terephthalate
pMA	Polymethacrylate
PMMA	Polymethyl methacrylate
pST	Polystyrene
PU	Polyurethane
QCM	Quartz crystal microbalance

R2R	Roll-to-roll
RNA	Ribonucleic acid
SELEX	Systematic evolution of ligands by exponential enrichment
SEM	Scanning electron microscopy
SPIONS	Superparamagnetic iron oxide nanoparticles
TEM	Transmission electron microscope
UV	Ultraviolet
VEGF	Vascular endothelial growth factor
VW	Van der Waals

1. Introduction

This thesis will introduce leukaemia, a hitherto uncured disease, and bioimprinting as a relatively underdeveloped field of biomaterials chemistry, which may be able to develop an alternative therapy for patients with leukaemia.

1.1. Leukaemia

Leukaemia is cancer of the blood.^{1,2} More accurately, it is a collective term for a family of heterogeneous, haematological disorders which manifest as an overproduction and accumulation of ineffective blast cells in the bone marrow, and subsequently, blood.³ In the UK, 9,800 cases were diagnosed in 2015 with incidence increasing 9% over the last decade. This rise is predicted to continue by a further 5% by 2035.⁴

The overproduction occurs as a result of an arrested development in *haematopoiesis*; the process whereby the body regenerates blood. In healthy subjects, haematopoietic stem cells (HSCs), a type of pluripotent stem cell, differentiate via the myeloid or lymphoid lineages through various stages of progenitors to yield blood cells. Figure 1.1, below, shows the myeloid pathways that HSCs can progress through; lymphoblastic leukaemias affect production of the lymphoid lineage. This process is constantly recurring and ensures new cells are produced and in correct proportions.¹

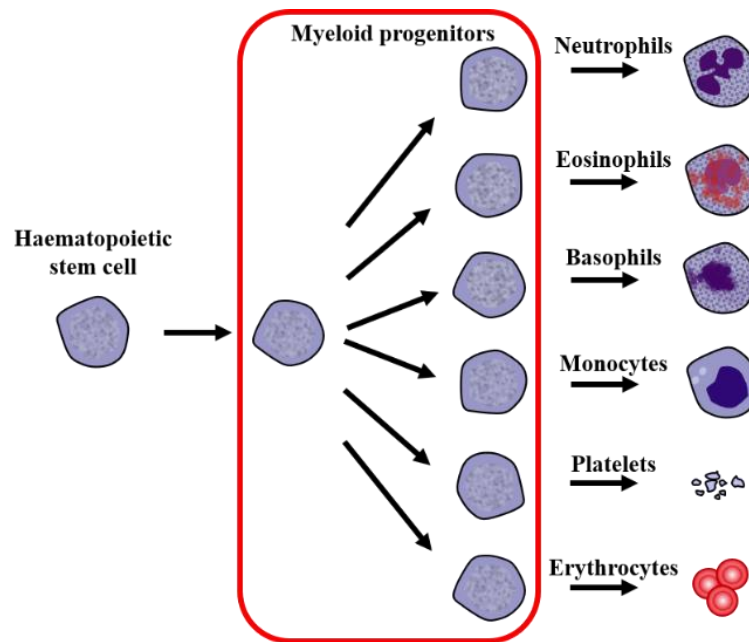


Figure 1.1 Tree diagram showing the differentiation cascade of pluripotent stem cells during haematopoiesis. This can occur via various precursors of the myeloid (shown) or lymphoid lineage. Leukaemia halts the development of progenitors early, yielding immature and ineffective cells. Produced via information from Harmening.¹

For leukaemia sufferers, aberrations on chromosomes 5 and 7 prevent the maturation of haematopoietic intermediaries, resulting in the uncontrolled production of ineffective cells that are unable to provide the functionality of their mature counterparts.⁵ This block of differentiation results in a deficiency of healthy cells being developed and a production of blasts the body is unable to regulate.⁵

As the condition progresses, blasts comprise an increasing proportion of the bone marrow until they reach a sufficient number to ‘crowd out’ into the blood.^{1,5} Subsequently, the blast count in peripheral blood increases over time with a significance two-fold.¹⁰ Firstly, the patient is deficient of the cells of the type blasts failed to differentiate into; leading to symptoms of anaemia (erythrocytes), thrombocytopenia (platelets) or reduced immune system capacity (various cell types).⁶ It is in this stage that patients are likely to seek medical attention, presenting with a group of symptoms indicative that the body is under stress namely: unexplained weight-loss, fatigue, persistent infection or bone and joint pain. Secondly, a complication termed hyperleukocytosis can occur whereby the blast count is so high the bloods

viscosity is increased. In turn, hyperleukocytosis can cause occlusion of blood vessels and attributed ischaemic damage.⁷⁻⁹

Leukaemia can be divided into sub-types dependant on the HSCs progress through either the myeloid (shown in Figure 1.1) or lymphoid lineage and via various subsequent intermediates to yield fully matured blood cells. Though it may appear counterintuitive, the arrested production of erythrocytes (a myeloid cell) is still leukaemia as the progenitors appeared white in early rudimentary aspirate examinations.¹⁰ The condition can be further divided by the speed of onset with chronic leukaemias being the slowest such that the condition can be managed over a period of years, acute cases develop more aggressively over a period weeks-to-months.⁹ This gives the four most common sub types: acute or chronic myeloid or lymphoblastic leukaemia. This thesis focuses on the most prevalent and difficult to treat subtype; Acute Myeloid Leukaemia (AML).

1.1.1. Acute myeloid leukaemia

AML accounted for around a third (3126) of newly diagnosed cases of leukaemia in the UK in 2015.⁴ A diagnosis is confirmed when morphological analysis of blood and/or bone marrow smears yield greater than 20% of blasts in peripheral blood or 30% nucleated cells in bone marrow (minimum of 200 and 500 cells assessed respectively). With AML these can be further subcategorised depending on the type of myeloid cell line, each convoluting identification and management of patients. The traditional description being the French-American-British (FAB) classification as proposed in 1974; see Table 1.1.

Table 1.1 French, American and British sub-type classification of acute myeloid leukaemia determined by morphological analysis. Table reproduced from information from National Health Service website.¹²

Subtype	Morphological description
M0	Undifferentiated acute myeloblastic leukaemia
M1	Acute myeloblastic leukemia with minimal maturation
M2	Acute myeloblastic leukemia with maturation
M3	Acute promyelocytic leukaemia
M4	Acute myelomonocytic leukaemia (M4EOS with eosinophilia)
M5	Acute monocytic leukaemia
M6	Acute erythroid leukaemia
M7	Acute megakaryocytic leukaemia

FAB classifications have been largely superseded by WHO guidelines which detail the epigenetic information of each condition. However, in this instance, FAB classifications are useful to highlight the heterogeneity of the condition from a morphological standpoint.¹³ Leukaemic blast cells show a different morphology to their healthy counterparts but also there is a disparity between each subtype.^{1,3,11} Myeloid blasts are significantly larger in size and, dependent on subtype and degree of maturation, highly irregular in shape with a maximum diameter around 15-20 μm . The nucleus is also distinctive on account of its shape and large size; taking up almost entirely the cell interior. In approximately 60% of patients, granulations known as Auer rods can be seen on the cell membrane.^{1,3} Auer rods are a surface characteristic often though not uniformly seen in subtypes, and are helpful in distinguishing and diagnosing myeloid over lymphoblastic leukaemia. Figure 1.2, below, shows the variation between FAB subtypes.

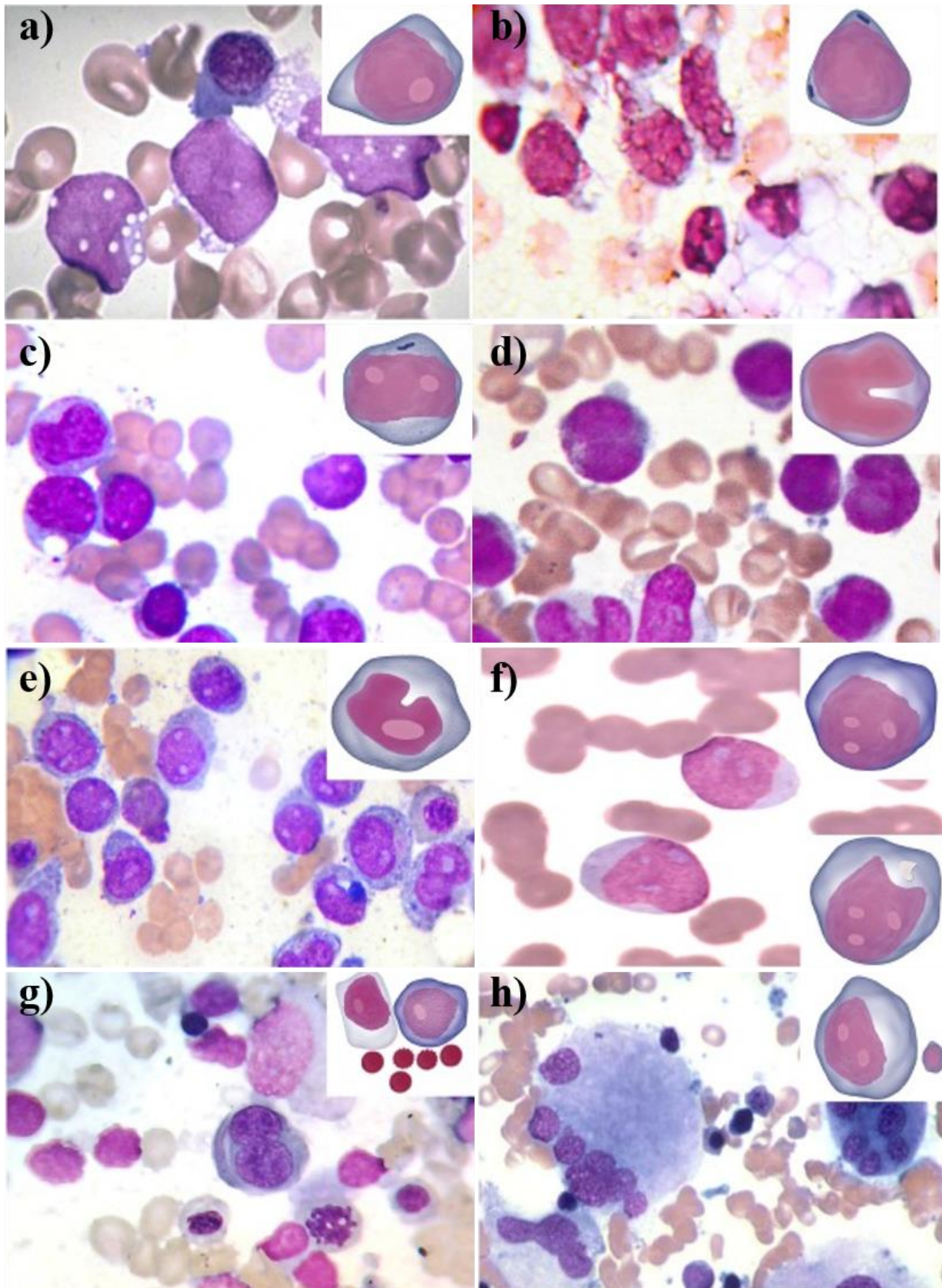


Figure 1.2 Morphological differences of FAB types a) M0, b) M1, c) M2, d) M3, e) M4, f) M5, g) M6 and h) M7. Image reproduced from Ladines-Castro *et al.*³

Blast lineage can be confirmed by diagnostic immunophenotyping via flow cytometry; particularly useful for AML with minimal differentiation which present without morphologic or cytochemical evidence of differentiation.^{14,15} Cytogenetic testing is done by comparing the karyotype of cells from bone marrow aspirate to that of blood specimens. Chromosomal aberrations indicative of a poor prognosis are found in around 55% of AML cases; 10-14% of cases have multiple unrelated cytogenetic abnormalities.^{14,16-18}

1.1.2. Treatment

Treatment for AML is given in two stages: *induction* and *consolidation*.¹⁹⁻²² The induction phase aims to remove the circulating blast cells from the patient's system in order to reduce the circulating leukaemic load.²³ Unlike other cancers that manifest primarily as a tumour, the malignancy cannot be surgically extracted due to the fluid nature and complexity in blood. The traditional mainstay of induction therapy is by via intravenous chemotherapy. These cytotoxic agents ablate blasts by interrupting DNA synthesis of dividing cells.^{24,25} Due to the inability to specifically target malignant cells, significant and discomforting side effects are common namely: stomach cramps, vomiting and hair loss. Traditionally, chemotherapy is given in a '7 + 3' regimen of 7 days cytarabine followed by 3 days of anthracycline.^{22,26} After chemotherapy, patients become immunocompromised so are given antibiotics and kept in relative isolation. If the condition is persistent and the blast count remains high, further cycles are administered often in a '5 + 2 day' format. Induction therapy typically removes 10¹² leukaemic cells to a cytologically undetectable level.^{1,15,27}

In the interest of completeness in specifically targeting cancer cells it is important to consider leukapheresis; an application of apheresis for *in vitro* separation of blood sample to reduce the white count.^{8,28,29} This involves an intermittent flow and centrifugation procedure discriminating the blood components by density. Unfortunately, blasts cannot be adequately separated from the peripheral blood and are discarded together with healthy white blood cells which obliterates the patient's immune system. Ultimately, no clinical link has been found to an improved AML survival rate after leukapheresis.^{8,28} In general, the method is reserved for patients unable to undertake chemotherapy immediately or as a bridge treatment in very severe cases of hyperleukocytosis (white cell count >100 10⁹ L⁻¹) to allow other treatment to take hold.⁸ Leukapheresis is not given routinely and only available in 8 centres in the UK; for

example, the Queen's Centre for Oncology & Haematology at Castle Hill Hospital (Hull, UK) in which this research was allied with does not offer leukapheresis.

Consolidation therapy aims to prolong the effects of induction treatment and prevent or slow down the return of the malignancy.^{30,31} Three modalities are available dependant on the condition of the patient and the subtype cytogenetics of the condition. Firstly, further rounds of high dose chemotherapy given administered on days 1, 3 and 5 in 6-day cycles, typically over 3-4 rounds. Due to cerebellar toxicity this is generally unavailable to geriatric (>60 years) patients.²⁰ Alternatively, an allogeneic bone marrow transplant (allo-BMT), one given from a close genetic match can be administered and is considered the preferred treatment for patients with unfavourable cytogenetics.^{19,26}

Allo-BMT present with challenges of finding a suitable donor, typically a close family member. The degree of matching is balanced against the risk of rejection by the patient's immune system in a condition known as graft-versus-host disease (GVHD) which is fatal 10-25% of cases.^{6,32,33} A similar immune response termed the graft-versus-leukaemia (GVL) effect can also be beneficial.^{34,35} Herein, the T-lymphocytes within the administered graft eliminate malignant cells in the patient's system in an alloimmune response due to their expression of non-self antibodies. This immune response is comparable to that of the body against foreign pathogens. Clinicians aim to yield the beneficial effects of GVL whilst reducing the GVHD; possible by suppression of the patient's immune system prior to allo-BMT.³⁵ Trials suggest that allo-BMT perform the best with regards to reducing relapse rate for consolidation therapy modalities.⁶

For those patients too weak or without a human leukocyte antigen (HLA) donor match, an autologous bone marrow transplant (auto-BMT) can be administered. In this case, stem cells are harvested prior to myeloablative conditioning and reinfused to the patient in order to replenish the low white blood cell count. Auto-BMTs have shown to improve disease-free survival though have no effect in overall length of survival.^{2,19} It may be pertinent with respect to the nature of this research to consider the purging process in which bone marrow aspirate is filtered prior to reinfusion.¹

Remission after induction and consolidation therapy is achieved in the majority (50-85%) of cases.³⁶ A patient enters remission when blasts in patient aspirate are cytologically undetectable, defined as <5% of a smear. Traditionally this was termed the minimal residual disease (MRD) stage as the blast count is lower than the sensitivity of morphological examination.³⁷ More recently, these can be characterised by combinations of reverse

transcription polymerase chain reaction (PCR) testing.³⁷ To date no approach or further classification of MRD has been used successfully as part of clinical practice. At this stage, the best prognostic indicator for a patient is the duration of the remission.^{19,38} Unfortunately, relapse rates are dismal.⁵ Patients are re-evaluated for their suitability for further rounds of chemotherapy and bone marrow transplants. Long-term survival depends on further curative treatment; relapsed AML cases unfit for bone marrow transplants are almost always fatal over a period of weeks to months.^{36,39}

1.1.3. Prognosis

Due to the high relapse rate, the prognosis for AML sufferers is poor.^{21,40} Ossenoeppele and Lowenberg reported though 50-60% cases achieved remission, due to the likelihood of relapse this translates to a 2-year survival rate of 15-20%.³⁸ According to Cancer Research UK, approximately only 15% of patients are expected to survive 5 years from diagnosis.⁴ For geriatric cases, this is reduced to 10% with a median survival time of a period of several months; salient given more than half of patients are >66 years old and over a third are >75.^{5,6,28,31,38,41} During treatment, patients are risk stratified according to their condition and the genetic abnormality. The former considers adverse factors, namely age and comorbidity, which are indicative of the likelihood of treatment related mortality.²³ Genetic landscape and chromosomal abnormalities predict the resistance to treatment. Karyotyping is the strongest prognostic factor for response to induction therapy and survival.^{16,18,20,29}

Intensive treatment protocols have shown to yield the best first-remission rates and ultimately long-term survival.^{19,23,31} A trade-off exists between the strength of the patient and the intensity of treatment.²⁸ Unfortunately, as the majority of sufferers are elderly, preferred intensive induction and consolidation therapy is unavailable in most cases. Patients in less favourable prognostic groups require further rounds of low dose treatment, clinically shown to be inadequate.^{24,38,39} Furthermore, repeated rounds of chemotherapy may cause malignancy in another site. The antithesis of this is secondary leukaemia caused in patients having treatment for cancer elsewhere in the body which would constitute an example of severe comorbidity.⁴ Modest improvements in survival rates are attributed to improved antibiotic and sterile care of immunocompromised patients. Relapse and therefore death rates remain poor. In 2016, 2601 patients died in the UK as a result of AML.⁴

1.1.4. Weaknesses of current therapy

AML therapy is maligned by the inability to preferentially target myeloblasts and cytotoxic treatments have a collateral effect on healthy tissues. By applying a broad-spectrum agent, healthy cells are also affected causing at best discomfort and at worst organ dysplasia and death. As alluded to previously, the condition is characteristically heterogeneous and complex and as such, myeloid neoplasms prove difficult targets using conventional techniques. Myeloblasts show a range of maturation, size, morphology and extra-cellular features; the presence of Auer rods and expression of surface antigens known as clusters of definition (CD) are not uniform.

Further complicating cell targeting, myeloblasts do not present with a distinctive CD antigen to target. Instead, research in the area has used combinations of monoclonal antibodies (mAbs) to target commonly overexpressed antigens. In 2000 the FDA approved the use of gemtuzumab ozogamicin, an anti-CD33 immuno-conjugate intended for the use in geriatric patients after relapse. By 2010 this had been withdrawn from the market due to an unacceptable increase in 30-day mortality.^{36,39} Combinations of chemotherapeutic agents have been trialled and shown to yield improved remission rates though this does not obviate the side effects or risk of patient mortality.

In summary, acute myeloid leukaemia is a diverse condition with considerable complications between patients. Though a treatment pathway has been in place for a number of decades, only modest improvements in overall survival rate have been observed. Chemotherapy is discomforting, dangerous and ineffective for the majority of patients. Though most patients enter a first remission, the majority of patients will relapse and die within 2 years of diagnosis. Though morphologically different, myeloblasts have proved a difficult target via conventional methods due to their heterogeneity and overall volume. Though research into targeted AML therapy shows promise, no clinical treatment is currently in place.

1.2. Bioimprinting

Bioimprinting is a relatively new field in materials chemistry aimed at capturing specific size and shape information of targeted moieties (whole cell or biomolecules) into polymer matrices. This section will introduce the field, its applications and show the potential for using artificial entities for selective cell targeting.

1.2.1. Molecular recognition

Highly specific binding reliant on shape is ubiquitous in nature and is vital for life.⁴²⁻⁴⁴ Cell signalling, cell growth and the body's immune system are all mediated by the selective affinities of macromolecules to target receptors.⁴⁴ Sterically and electrostatically complementary surfaces of antibodies, enzymes, DNA and hormones bind specifically to receptors to provoke a desired biological response.⁴⁵ The action was first described by the 'lock-and-key' rationale over half a century ago.⁴⁵ Figure 1.3, below, depicts complementary shape fit of biological moieties and receptors. Studies have attempted to exploit this effect by replicating bioactive agents particularly antigen/antibody combinations for use in catalysis, diagnostics and biochemical reactions.⁴⁶

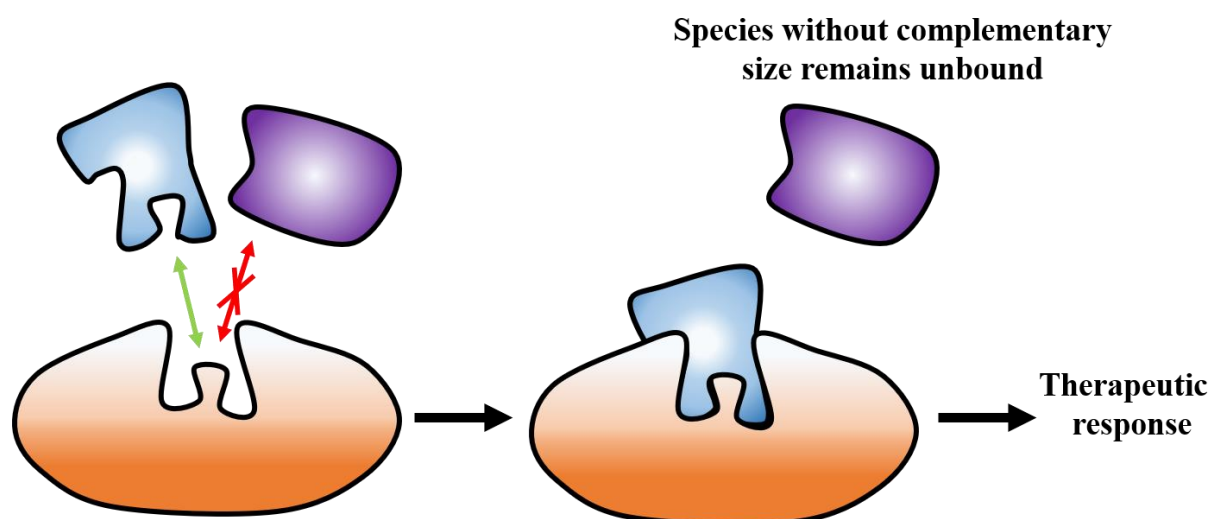


Figure 1.3 Schematic showing the action between biological agents and receptors. Species need a shape complementary to that of the receptor in order to bind sufficiently, thus producing a chemical response.^{45,46}

Polymer-based imprinted systems are relatively cheap and are both mechanically and chemically robust, allowing prolonged storage life and reuse. All manner of materials can be used as the template due to their bespoke nature, showing great potential for the area.^{42,45,47,48}.

1.2.2. Molecularly imprinted polymers - macromolecules

The field of molecularly imprinted polymers (MIPs) has shown promise in circumventing such problems.^{42-44,49-52} MIPs are biocompatible cross-linked polymer matrices cured in the presence of a template material to yield cavities of bespoke size, shape and functional group orientation. Fabricated artificial receptors are complementary to a desired functionality or epitope, able to mimic the highly specific interactions seen in nature.^{43,47,49,50,53} The field has great versatility, able to exchange the polymer matrix to encompass a range of applications and in various configurations such as bulk, thin films, fibres or monoliths. Figure 1.4 shows the rationale of bulk phase molecularly imprinted polymers.

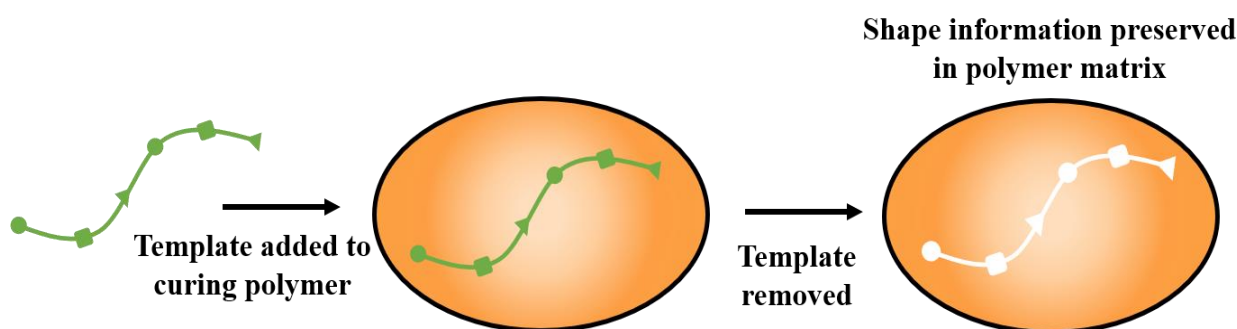


Figure 1.4 Schematic showing a bulk molecularly imprinted polymer (MIP) being produced. Produced from information from Schirhagl.⁴⁶

Molecular imprinting studies have been reported since the 1970s where initial studies struggled to replicate larger, more chemically and spatially complex templates.^{50,54} Success in the area was originally inhibited by intricacies in structure such as high molecular weight, branching and variation in regions of charge or hydrophobicity.^{43,55} Pioneering MIP studies used bulk imprinting techniques in which the template was dispersed in a porous polymer matrix. After curing, the template could be chemically removed to yield internal sites in the material with cavities of complementary shape to the template moiety. However, relying on movement through a porous material vastly limited the size of the target epitope or macro molecule being used.⁴⁶

To overcome this problem, further studies made MIPs by dispersing template materials in the bulk of non-porous pre-polymers, curing the matrix and grinding the resultant system into beads. The template could then be chemically removed and the beads sieved to achieve the desired bead diameter. A wider range of moieties and macromolecules have been successfully imprinted using this technique such as: drugs, amino acids, carbohydrates, nucleotide bases, pesticides, glycosides, hormones and co-enzymes.^{42,49,54,56} However, little control of the degree or uniformity of grinding can be achieved and the quality and reproducibility of imprinted cavities varies significantly.^{42,43,55}

A key application of bulk imprinted polymers is in separation science. Imprinted polymers are incorporated onto the stationary phases used in conjunction with chromatography or sorbents for solid phase extraction. Molecular imprints have been shown to vastly improve the selectivity of devices, increasing affinity of the target molecule to the stationary phase.^{57,58} The cavities allow selective binding to the template material while species not of the same size and shape are eluted off. Though grinding has been highlighted as a weakness when exposing the imprinted sites, devices have shown selectivity on a nanometre scale able to distinguish enantiomers in racemic mixtures.⁵⁹ Due to the arrangements of groups in space, even species with identical chemical formulas can be targeted. Ansell (2005) highlighted molecular imprinting as a viable method for enantiomeric separation of drug candidates to overcome stringent legislation from regulating bodies. Regulators only approve one enantiomer as a lead candidate as the second enantiomer may cause catastrophic effects as seen most notably with thalidomide.⁶⁰

Though early studies had limited success when capturing the morphology of larger molecules, a landmark publication by Dickert *et al.* (2001) showed the first case of whole cell imprinting.⁶¹ A distinction between the two will be made hereon describing macromolecule imprints as MIPs and those of whole cells as bioimprints.

1.2.3. Whole cell Bioimprints

The landmark publication by Dickert *et al.* showed the first case of a surface imprinting technique.⁶¹ The first bioimprinting publication described a surface micro-contact imprinting technique that was able to express the morphology of yeast cells in sol-gel surfaces.⁶¹ Unlike bulk methods, the group immobilised yeast to glass substrates in order to form a cell ‘stamp’

which could then be pressed into a curing sol-gel material (Figure 1.5a). Once polymerised, the imprint was removed, washed and analysed with atomic force microscopy (AFM)(Figure 1.5b and Figure 1.5c). The imprint was shown to yield a densely packed, regular honeycomb lattice of cell cavities in a complementary shape to the template yeast.

As template cells were not fully immersed in the matrix, problems associated with uneven grinding and sample elution are negated. The sol-gel material was reported as an ideal imprinting matrix due to the ease of formulation and resistance to scratching.⁶¹ Furthermore by imprinting quartz crystal microbalance (QCM) electrodes, the study was able to accurately test the retention of cells back on to the imprinted surface.^{61,62} When incubated with several strains of yeast, imprinted sol-substrates showed a high affinity to the target cell type with on-line monitoring. This effect was attributed to the large contact surface area between cells and the bioimprint cavity.⁶² See Figure 1.5 below, showing AFM analysis of b) yeast cells retained to a bioimprinted substrate and c) bioimprinted cavities showing complementary shape of template yeast cells.

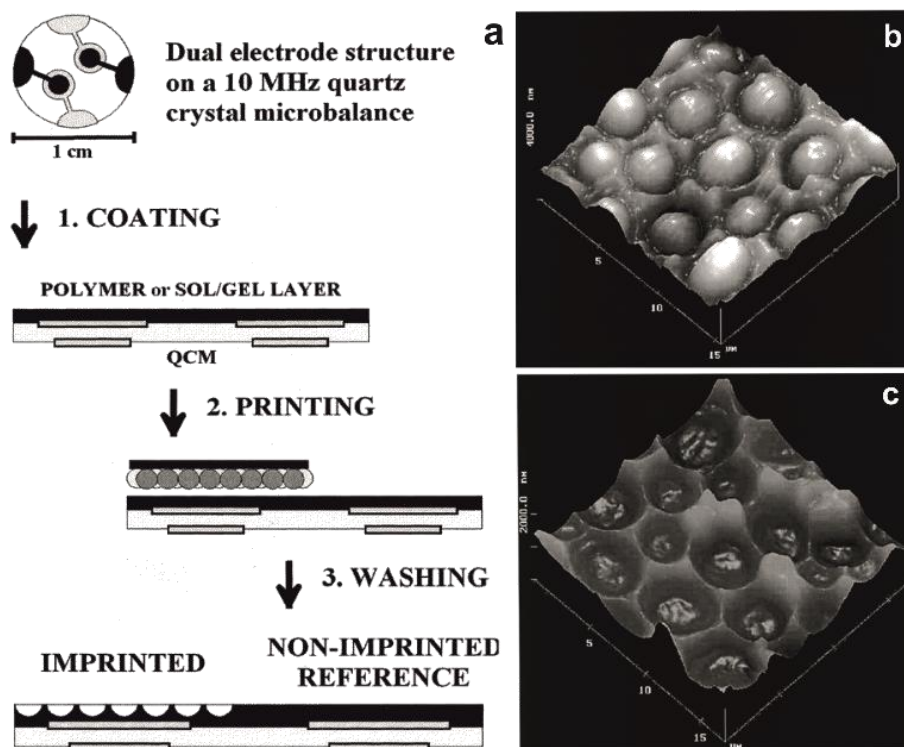


Figure 1.5 a) Schematic of the protocol reported by Dickert *et al.*, to fabricate imprints onto the surface of quartz crystal microbalance electrodes. b) AFM images of sol-gel layers from titanium (IV) ethylate whilst curing in contact with *S. Cerevisiae* and c) AFM images of cured bioimprint with densely packed layer of biomimetic receptors. Reproduced from Dickert *et al.*.⁶²

The group followed up their pioneering study by expanding the range of template materials captured into bioimprints such as enzymes and viruses.^{63,64} The latter proposed a method to screen complex matrices, in this case tobacco plant sap, circumventing time-consuming sample preparation for virus detection. Substrates could be analysed using real-time QCM analysis. Imprinted substrates selectively captured micro-organisms from aqueous suspensions with high adsorption affinities showing the scope for inclusion in biosensors.⁶⁵ Following these studies, a wealth of whole cell imprints have been recorded using spores,⁶⁶ yeast,⁶⁷⁻⁷⁰ bacteria⁷¹⁻⁷³ and most relevantly a multitude of mammalian cells.^{51,58,74,75}

Jenik *et al.*⁶⁶ reported a surface imprinting technique using two different pollen grains into polydimethylsiloxane (PDMS). When coupled with a QCM sensor, bioimprints were able to show in real-time, the selective uptake of pollen to the biosensor device. Though nanoscale printing of macromolecules and even whole cells had been achieved, this study showed bioimprinting to be effective at targeting comparatively large analytes. Pollen grains vary in size between 10-50 μm .⁷⁰ See Figure 1.6a showing AFM analysis of pollen-imprinted polyurethane.

Lin *et al.* reported surface imprinting and recognition of algae cells into poly(ethylene-co-vinyl alcohol) films; shown in Figure 1.6b.⁷⁶ The group were able to examine algal cell metabolism and hydrogen production by incorporating bioimprints on biofuel cells. Fuel cells showed increased output, likely due to the increased expression due to the artificial microenvironment created.⁷⁶ Cohen *et al.* reported the successful imprinting of various strains of bacteria into sol-gel films.⁷³ Bacteria with differing cell morphologies and extra cellular features were incubated on imprinted substrates and the retention analysed by a combination of AFM, scanning electron microscopy (SEM) and confocal laser scanning microscopy (CLSM). The study noted a 90% affinity to the target organism type due to their distinct 'macromolecular fingerprint'. Figure 1.6c shows SEM images of bacterial bioimprints and Figure 1.6d shows bacteria retained to imprinted surface after incubation.

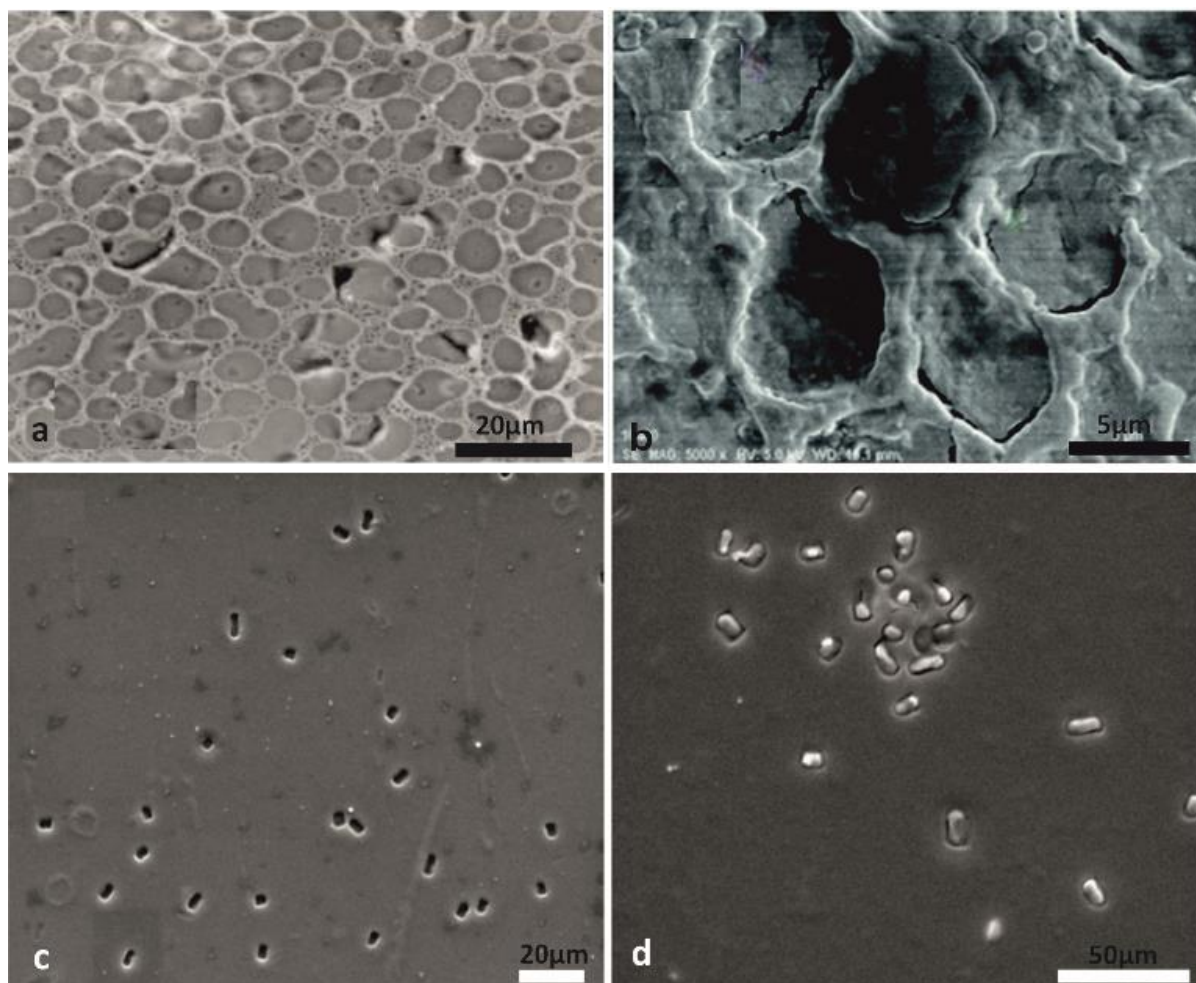


Figure 1.6 a) Contact mode AFM image of pollen imprinted polyurethane,⁶⁶ b) SEM image of algal cell imprint captured on poly(ethylene-co-vinyl alcohol) film⁷⁶ and c) images of *Cryptosporidium Parvum* oocysts and d) adsorption of new oocysts in suspension after incubation with the imprint.⁷³

Bao *et al.* reported a new approach where a bacterial imprints on polymer of outer surface charge heterogeneity was synthesized for highly specific bacterial recognition.⁷⁷ The charge distribution on the outer surface of the bacterial cells was captured by the bioimprint during polymerization by the self-assembly of the two different monomers around the template (Figure 1.7a-c). Subsequent covalent binding of this template monomer arrangement into the bioimprinting matrix created chemical imprints for bacterial recognition. These authors demonstrated that by using this novel approach, target bacteria can be preferentially captured due to stronger electrostatic interactions (Figure 1.7d). The study emphasized the versatility of this fabrication strategy since a variety of charged monomers could be exploited as building blocks in surface-initiated atomic transfer radical polymerization. This approach can also be

extended to recognize bio-macromolecules or other biologic entities associated with distinctive charge distribution.⁷⁷

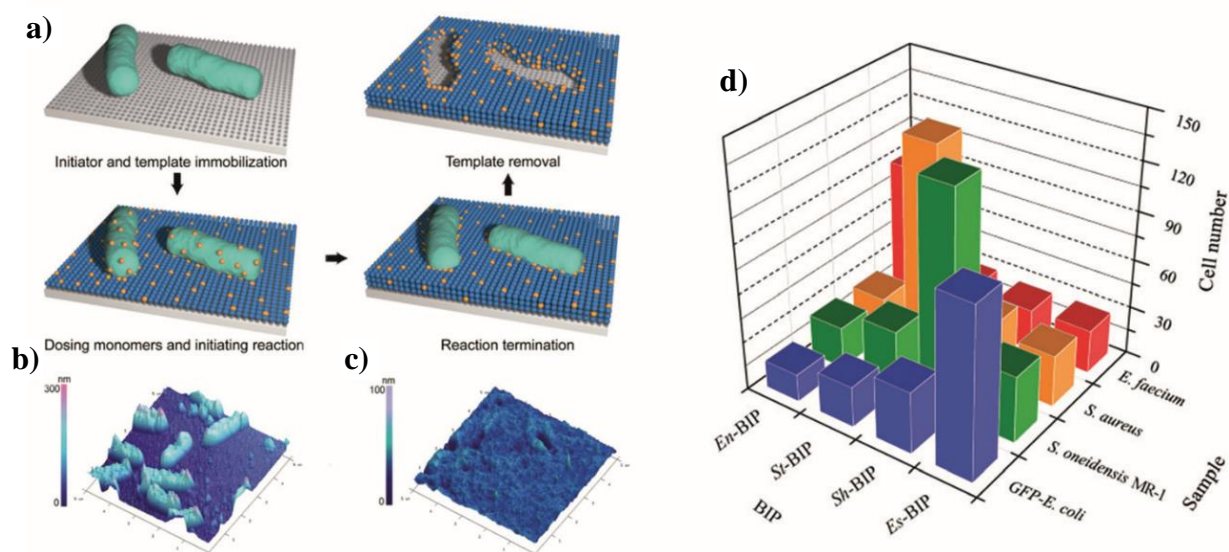


Figure 1.7 a) Schematic diagram of the bioimprint fabrication process with surface charge heterogeneity. AFM images of the polymeric bioimprint before b) and after c) removal of the *E. coli* template. d) Numbers of different bacterial cells captured on the bacteria-imprinted polymer imprinted with different cell templates.⁷⁷

1.2.4. Applications of bioimprinting

Thus far, this thesis has introduced bioimprinting of particulates, rudimentary microorganisms and even less robust mammalian cells captured in to an array of polymer matrices. The following section will focus on the intended real-world applications possible for bioimprinted surfaces. The first of which is incorporated into biosensor devices providing an alternative vehicle for cell discrimination on account of very closely matched size characteristics.

1.2.4.1. Bioimprinted biosensors

Biosensors are bioanalytical instruments containing a specific recognition entity coupled with a physiochemical transducer.^{78,79} There is large scope for such devices in quality control or health and safety applications such as water quality monitoring. In a healthcare setting, biosensors aim to provide rapid diagnoses with small sample size. Lowering the limits of

detection for such devices is of importance as early discovery and treatment of disease can improve patient prognosis.^{78,80}

Dickert *et al.* were able to create a biosensor device for ABO blood grouping.^{70,75} By using erythrocytes of the blood groups (A, B, AB and O) they produced bioimprinted layers in polyvinyl pyrrolidone. Erythrocytes of different blood group possess the same geometrical size and shape and differ only by varied surface antigens. AFM analysis of the bioimprints with retained erythrocytes and positive imprints were made by addition of polymer to the bioimprint (Figure 1.8). As all cells are erythrocytes, the selectivity reported is reliant only on hydrogen bonding between interaction sugar residue antigens and the bioimprinted surface.⁷⁵ The report characterised the selectivity of substrates imprinted with erythrocytes of blood groups A, B, AB and O by incubating cells of each type. Though imprints had mixed results, there was a clear preference to the blood group used to template the bioimprints. Selectivity experiments were initially carried out in buffer solution though the group also progressed to use whole blood. Though a loss of sensitivity was noted, the group have shown the viability of bioimprinted substrates in use with whole blood samples with very little sample preparation.

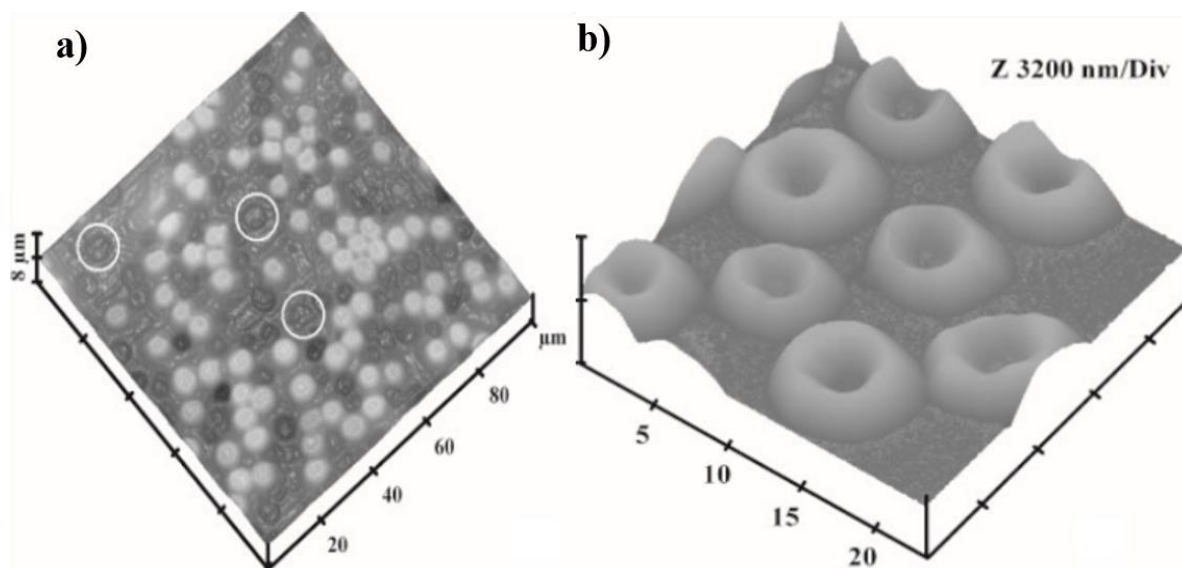


Figure 1.8 AFM analysis of a) erythrocyte imprinted polyvinyl pyrrolidone with cavities highlighted. Cells are also seen retained from the imprinting process b) positive imprints of erythrocytes made from subsequent imprinting procedures.^{70,75}

A subsequent study was further able to discriminate between subtypes of erythrocytes of blood group A, known as A₁ and A₂.⁷⁰ The work described the retention of erythrocytes to be dependent on type, abundance and orientation of cell membrane antigens. Bioimprints were able to discriminate analytes on a nanometre scale identical in overall size and curvature. Retention of mismatched erythrocytes was found to be negligible; similar to cells retained to non-imprinted substrates. The ability of bioimprints to discriminate between cells identical on a micrometre scale, due to differences in nanometre scale signifies possible use in biosensor devices.⁷⁰

Eersels *et al.* combined cell surface imprinting with heat transfer resistant measurement in order to detect human cancer cells and macrophages.⁵¹ The entrapment of the cells in the cavities of the surface imprinted polymer (SIP) layer resulted in the significant increase in thermal resistance at the solid-liquid interface. This property was used in order to detect the immobilisation of immortalised breast cancer cells, ZR-75-1, on the printed polyurethane substrate. ZR-75-1 cells were spread and allowed to sediment on a PDMS substrate forming a dense monolayer coverage. The cells morphology was captured in polyurethane resin layer by pressing the cell-rich PDMS stamp against a curing polyurethane surface (Figure 1.9). AFM was used to analyse the topography of the imprint surface. The imprint was mounted to a copper base and heated to a constant 37 °C (T₁) and the temperature of the cancer cell effluent (T₂) monitored. Taking into account the power used to heat the imprint surface a thermal transfer resistance was calculated as cell adhered to the imprint. The study reported specific binding of cells to the imprinted cavities noticeably increase the thermal resistance at the solid-liquid interface.⁵¹

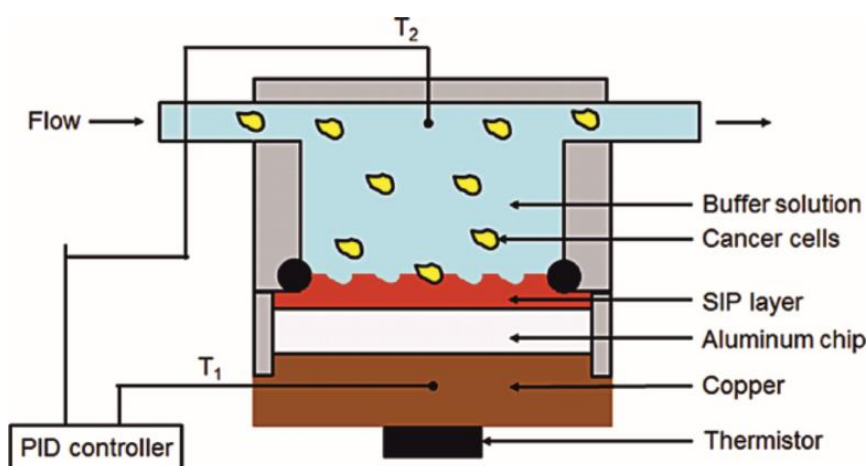


Figure 1.9 Schematic view of the device used to detect uptake of target macrophages to bioimprinted surfaces by thermal resistance measurement by the heat-transfer method.⁵¹

Eersels *et al.* reported MCF-7 breast cancer cell imprints which were characterised using the optical microscope, shown to have an average cell diameter of 20 μm (Figure 1.10a).⁸¹ This agreed with the AFM analysis image of the polyurethane imprints (Figure 1.10b). The results showed the selective nature of the imprints with 15-20% imprint response compared to 1.4 - 5.2% of cross contamination from non-imprinted cells. The gradual rinsing of the imprint resulted in significant decrease in cross-contamination from non-imprinted cells as evident from Figure 1.10d-e; indicating an increased adhesion to the target cells. The application of excess forces by rinsing was adequate to eliminate any non-specifically attached cells.

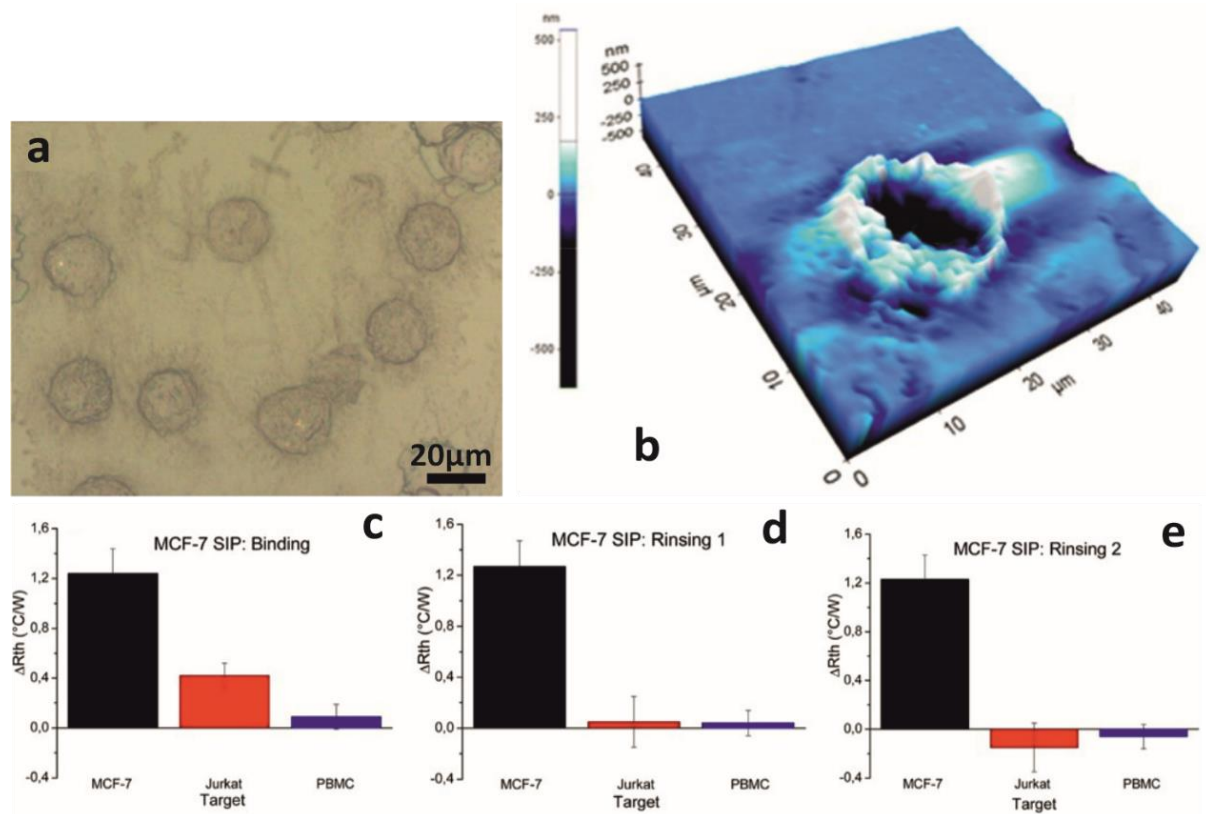


Figure 1.10 a) Optical microscope image of the surface imprinted polymer (SIP) for MCF-7 breast cancer cells, b) AFM representation of a single MCF-7 imprint on polyurethane, graphical representation of change in thermal resistance ΔR_{th} of MCF-7 SIP upon exposure to MCF-7 cells with attachment c) and d & e) consecutive rinsing steps.⁸¹

In a clinical setting, biosensors provide a diagnosis by detection of cells or other species from patient samples. The next group of studies uses bioimprinting to interrogate cells further by nanoscale analysis of cell membranes.

1.2.4.2. Cell surface analysis via bioimprints

Protocols to analyse cell topologies with both SEM and transmission electron microscopy (TEM) are commonplace, however, do not achieve a sufficient resolution for nanometre scale analysis.^{73,82,83} Difficulties using AFM for such analysis are also well documented; with a high pressure applied to cell membranes via the scanning cantilever, irreparable damage can be caused to the cells of the living tissue. Moreover, deformation or movement of living cell membranes mean direct analysis yielding results not truly representative of the cell structure.⁸⁴ AFM has been used to analyse both negative and positive bioimprints as an alternative to direct cell imaging.⁸⁵

Muys *et al.* immobilised living rat pituitary cells and captured the morphology into a polymer matrix.⁸⁶ After curing, the topology of the bioimprints were analysed by tapping mode AFM which showed cell shapes with no evidence of dehydration. Membrane pits and depressions were seen on the surface of the imprinted cells, consistent with those used for cellular exocytosis.⁸⁶ Similar results were achieved by the group using human endometrial cancer cells as templates.⁸⁶ Bioimprints can potentially circumvent problems in analysing fragile biological samples using positive imprints as proxy cells. Analysis of extracellular membrane features on nanometre scale can yield information on cell signalling and proliferation.^{83,86}

Samsuri *et al.* expanded the templating of endometrial cancer cells (Figure 1.11 a-b). They were able to correlate numbers of cellular membrane pores to on bioimprints with the quantity of vascular endothelial growth factor (VEGF) excreted from cells.⁸³⁻⁸⁴ Both authors achieved nanometre scale resolution of extracellular structures on endometrial cells, able to be analysed by AFM.^{83,84,86} They used a biocompatible UV curable matrix in order to achieve rapid curing in ambient conditions to successfully imprint live human muscle cells.^{87,88} Upon AFM analysis, microstructures and cell membrane features were imaged with nanoscale resolution. Figure 1.11c-d below shows AFM images of imprinted muscle fibres. Processes such as neurotransmission, enzyme secretion or hormone release can be attributed to nanoscale transformations on the cell membrane. The ability to characterise variations in structure and morphology of cell membranes may be indicative of malignancies and other disease. Moreover, membrane abnormalities on a molecular level may provide a valuable tool in providing a diagnosis and prognosis of a multitude of conditions and diseases.^{82,84,86}

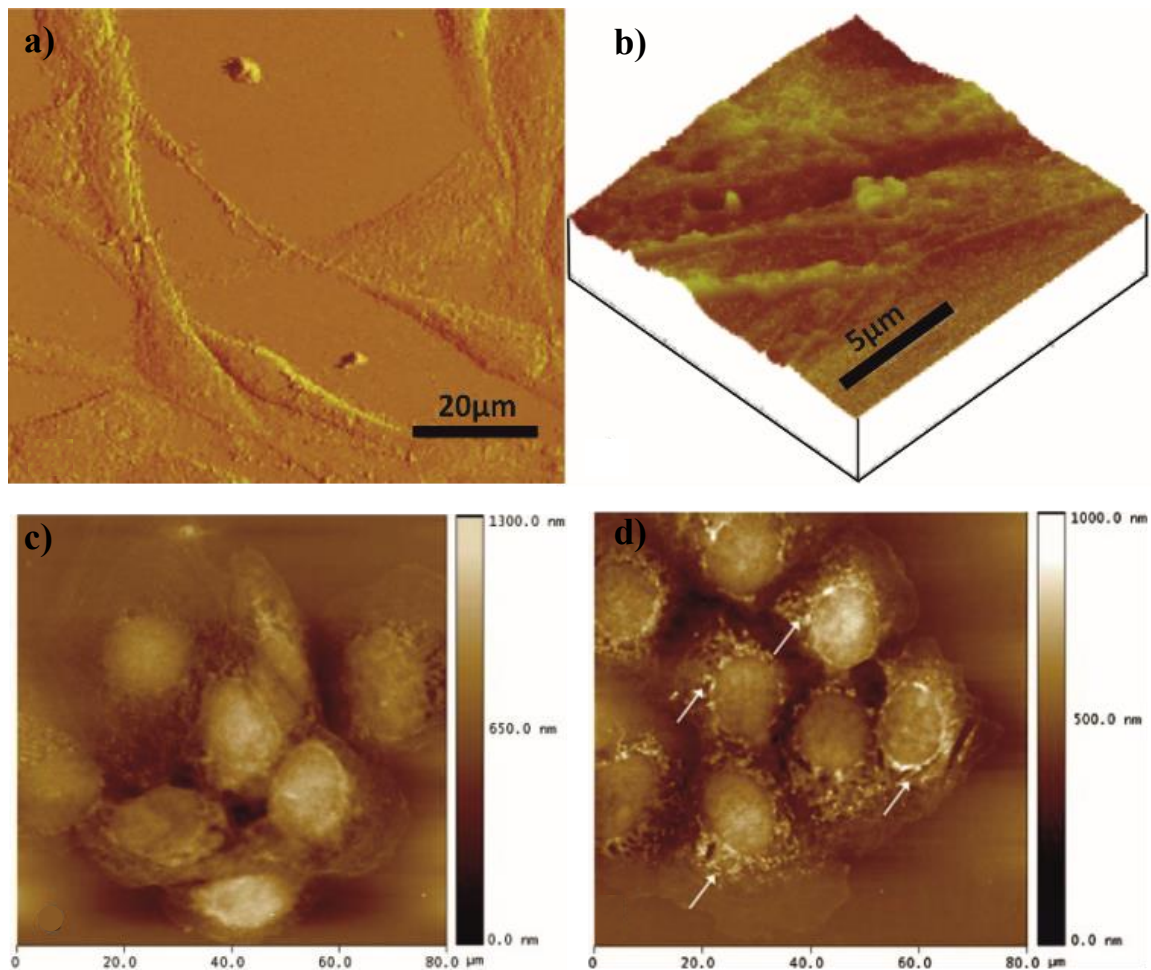


Figure 1.11 AFM images of a) imprint showing muscle cell characteristics and b) angular view of imprint showing muscle cell membrane roughness.⁸⁷ AFM images of Ishikawa endometrial cancer cell bioimprint; c) in native conditions and d) cancer cell replica made from cells exposed to CoCl_2 to induce their membrane pores to open.^{58,84}

Such studies show bioimprinting as an indirect method of assessing possible cell signalling by monitoring nanoscale changes to membrane topography before and after stimulation. Interaction between the cell membrane and surrounding physical environment affect cell proliferation. The following section details studies aiming to use bioimprinted surfaces to optimise the environment cells are grown *in vitro*.

1.2.4.3. Bioimprinted cell culture platforms

Extracellular environments have been shown to affect the growth of dividing cells.⁸⁹⁻⁹¹ Reports have detailed the use of bioimprinted substrates to mimic *in vivo* growth conditions in order to

study the proliferation of cell lines. The progression of cancers can be monitored in environments representative of the body.⁵⁸ In particular, the effect of topographical mechanical signals have on the progress and action of any adherent cell lines can be classified.^{74,88}

McNaughton *et al.* imprinted immortalised human cell lines: human cervical cancer (HeLa), human kidney (HEK-293) and human lung (MRC-9) into various polyacrylamide hydrogels.⁹¹ The various cell types were incubated aseptically on each individual bioimprint surface. Dense cell growth was noted confined to the imprinted areas of the substrate.⁹¹ Though results were mixed the study showed the culture surfaces cell cavities which act as cues to promote cell adhesion and growth.⁹¹ Jeon *et al.* imprinted fixed osteoblast-like cells (MG63) on a PDMS matrix.⁸⁹ MG63 cells were cultured on the surface of imprints and cell viability, alkaline phosphate activity and mineralisation were monitored. Results showed that imprinted substrates increased cell activities when compared with smooth culture substrates.⁸⁹

Vigneswaran *et al.* proposed bioimprinted substrates to be scaffolds for the development of tissue engineering technology.^{90,92} Both studies imprinted Ishikawa endometrial cancer cells into a UV fast-cure polymer. The results agreed with other studies showing the topology of bioimprints to be representative of template cells on a micro and nanoscale. The authors indicated that bioimprinting can be used as a novel tool to improve understanding of the proliferation of cancer cells, vaccine preparation and other drug studies.⁹⁰ The study proceeded to characterise the ideal properties of scaffold used in implants, and demonstrate the promise of such bioimprinting approach on cell growth.⁹²

Tan *et al.* also report the imprinting of Ishikawa endometrial cancer cells, using polymethacrylate (pMA) and polystyrene (pST).⁵⁸ The study compared a culture of cells on each bioimprint type and to flat (non-imprinted) substrates. Characteristics such as morphology, cell-responses and antigen expression were monitored by AFM analysis of positive bioimprint structures. Results showed increased proliferation of endometrial cancer cells on pMA, producing cells with a larger average diameter than cultured on flat substrates or pST. On both imprinted materials, cells showed an increased expression of β -1-integrin, focal adhesion kinase and cytokeratin-18. The study shows the microenvironment in which cell are cultured modulates cell signalling and ultimately their proliferation.⁵⁸ By monitoring cancers development in such *in vitro* environments allows an improved understanding of how the condition progresses in patients.

Bioimprints have also been used to examine the effect of chemotherapeutic agents on cancer proliferation. In another study, Tan *et al.* produced imprints of endometrial cancer cells into polystyrene.⁵⁸ They showed that by culturing Ishikawa cells on imprinted substrates, the effect of chemotherapeutic agents could be evaluated on caspase-3-expression, proliferating nuclear antigen (PCNA) expression, VEGF secretion and overall cell numbers. The study examined how the physical environment modified the sensitivity of cells to treatment.⁵⁸ It was found that positively and negatively imprinted platforms were preferred by different chemotherapeutic agents when administered in single doses.⁵⁸ This study used the shape recognition interactions between cells and bioimprints to monitor the effects of chemotherapeutic agents. The next section will focus on studies intending to use the same relationship to expose harmful effects to a single cell type.

1.2.4.4. Bioimprinting in direct therapy

As mentioned previously (section 1.1.2), the success of chemotherapy is maligned by an inability to focus cytotoxic effects directly on neoplastic cells. Despite trials of new drug species, combination therapy and altered dose, iatrogenic harm and mortality remain a concern.^{93,94} Bioimprinting presents as a vector in which to introduce selectivity to chemotherapeutic treatment. If cytotoxic materials can be focussed directly on cancerous cells, higher doses can be used to ablate cancerous tissue and causing fewer side effects.⁹⁵⁻⁹⁷ Unlike studies detailed thus far, the majority of imprinted drug delivery vehicles have been made with particles functionalised with recognition entities.

Colloid antibodies for cell shape recognition and targeting were reported by Paunov *et al.*, see Figure 1.12a.⁹⁸⁻¹⁰⁰ A silica coating was applied to the target cells, cured and fragmented yielding partial shells with an interior void of the complementary shape to templated cells. When incubated in cell suspensions, colloid antibodies showed excellent selectivity binding the target microbial cells in a suspension containing other cells of different shape and size.⁷⁸ The authors expanded the study to selectively kill target cells by embedding gold nanoparticles to the inner side of colloid antibodies.⁷⁹⁻⁹⁸ In this study, template cell membranes were functionalised with gold nanoparticles which was engulfed in the silica material when imprinted. After fracturing the silica shells with ultrasound and bleaching the cell templates they produced ‘photothermal colloid antibodies’, in which the silica hemi-shells matching the

shape of the target cells had gold nanoparticles on their inner surface; see Figure 1.12b). Such photothermal colloid antibodies were then used to selectively bind to the target cells in a cell mixture and the whole sample irradiated with a green laser at a wavelength where the gold nanoparticles absorb the laser irradiation more strongly than the surrounding material. Due to the localized heating around the illuminated gold nanoparticles on the colloid antibody inner surface, the authors demonstrated that they can specifically kill only the shape-matching target cells. The study shows the ability of causing cell-death directly to template cell types.^{98–100}

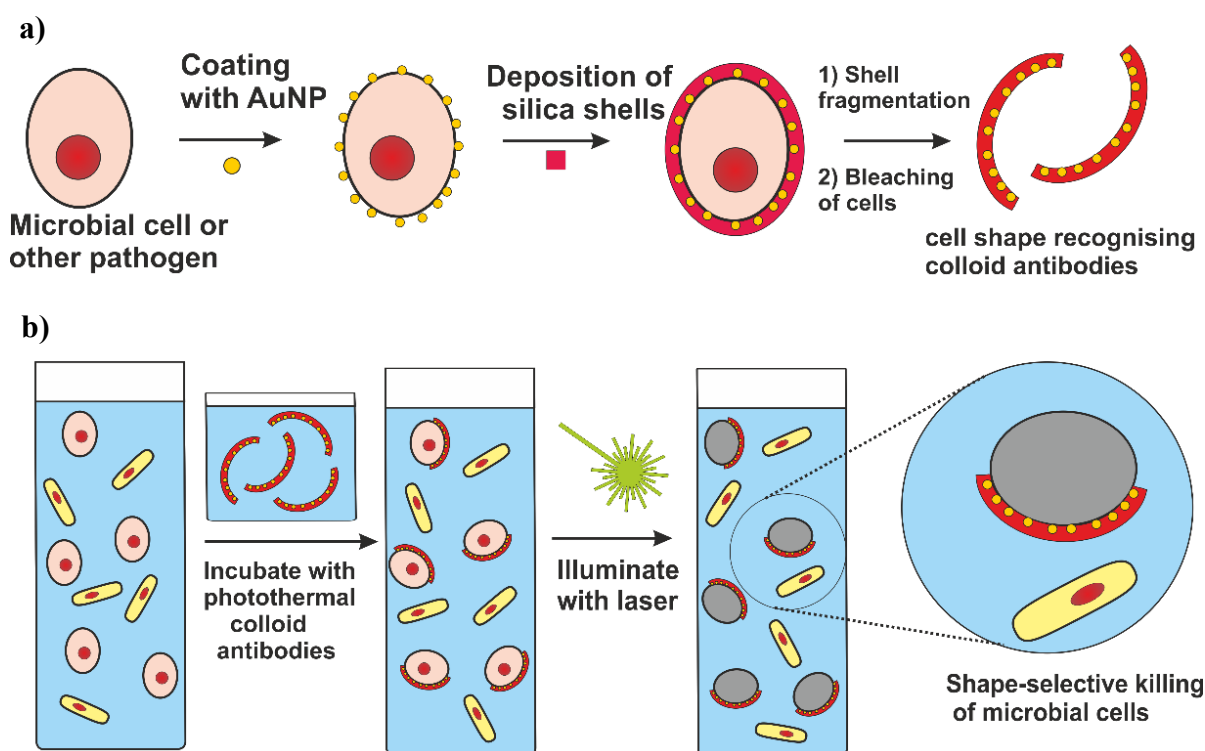


Figure 1.12 a) Schematic of the production and action of colloid antibodies reported by Paunov *et al.* where b) explains the action of the photothermal killing of cells to use in conjunction with colloid antibodies.^{99,100}

Liu *et al.* also produced functionalised nanoparticles (NPs) to exhibit a selective action on cancer cells. The study targeted malignant tissues on account of over exposure of polysaccharides on the cell membrane sialic acid; a universal feature of cancer cells. Nanoparticles whose surface was imprinted with monosaccharides showed an affinity to the specific monosaccharides expressed on the cancerous cells surface. In this study the NPs were doped with a fluorescent tag to improve selective imaging of malignant cells. However, the authors speculate that with minor adjustment, the technique suitable in probes for targeted photothermal therapy for cancer.¹⁰¹

Doyle *et al.* also attempted specific targeting via hydrogel microparticles.¹⁰² They aimed to build on previous findings to optimise particle design for cancer therapy. For instance, the flexibility of particles dictates the overall circulation around the body and, therefore, the bioavailability. Micro-particle shape has also been investigated with rod-like particles showing increased uptake by cancer compared to more spherical species. Various shapes of hydrogel microparticles functionalised with an anti-epithelial cell adhesion molecule (EpCAM) were fabricated. By systematically changing the particle shape the study was able to characterise the effect of surface area, hydrodynamic effects and steric effect uptake of particles to cells. Breast cancer cells (SKBR3s) which express EpCAM were used to confirm the uptake of the octopus-like shaped hydrogel microparticles. SKMEL28s cells were also monitored and shown not to adhere to the microparticles. Specifically, the study showed that octopus-like shaped microparticles offered the best shape for cell capture due to the heightened surface area contact.¹⁰²

Wang *et al.* investigated the topographic interactions between three MCF-7 cancer cell lines with differentiated morphologies and their imprinted replica surfaces.¹⁰³ They demonstrated two levels of topographic interactions between cancer cells and their replica surfaces. The nanostructures on template surfaces led to structural matching between nanoscale components on the cell surface and these nanoscale structures on the imprinted substrates. They report that in addition to the nanostructure, the microscale topography also enhances the topographic interaction between the cancer cells and their replica surfaces by the trapping effect; see Figure 1.13. The authors conclude that bioimprints that replicated multiscale structures exhibit improved affinities with cancer cells by synergistic effect of cooperative topographic interactions and molecular recognition which shows much higher capture efficiency compared to flat substrates. The suggested explanation is that the cell recognition is enhanced by the protrusions from the cell surface and their imprint. This approach is likely to advance the smart design of multiscale bioimprints with highly specific cell recognition and provides an alternative to investigate interfacial properties of the cancer cells.¹⁰³

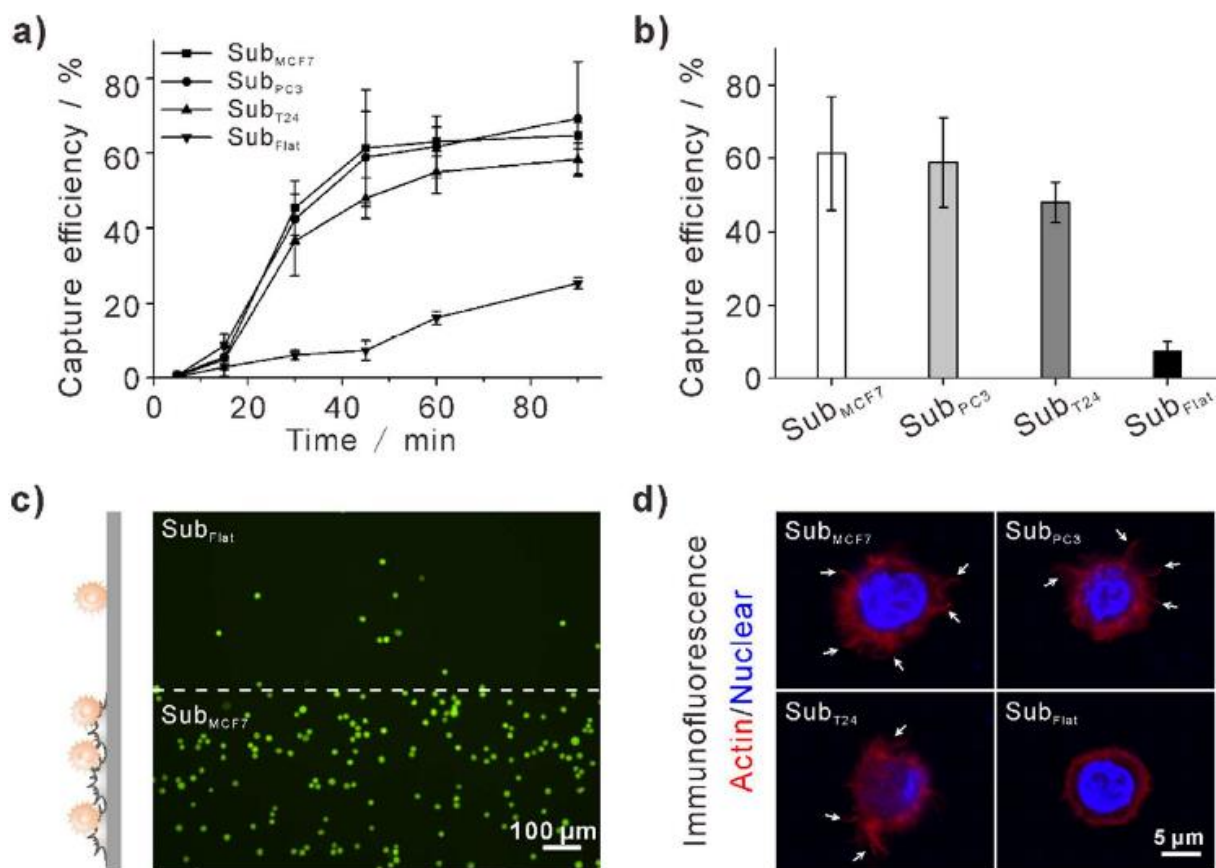


Figure 1.13 Evaluation of MCF-7 cells capture performances on the as-prepared cell replica surfaces after anti-EpCAM modification. a) With the increase of incubation time, the capture efficiencies of MCF-7 cells increase significantly and reach a maximum value around 45 min. b) In comparison with other surfaces, SubMCF-7 and SubPC3 show higher capture efficiencies of MCF-7 cells at incubation time of 45 min. The capture efficiencies of MCF-7 on cell replicated surfaces are much higher than that on the anti-EpCAM modified flat glass. c) A fluorescent image of captured MCF-7 cells on SubMCF-7 and SubFlat in a close experiment setup. d) Immunofluorescence images (actin, red; nuclear, blue) of captured MCF-7 cells on different surfaces. MCF-7 cells own more protrusions on SubMCF-7 and SubPC3, while exhibit less protrusions on the other two surfaces. Arrows indicate the protrusions of MCF-7 cells.¹⁰³

Thus far this chapter has introduced leukaemia as a condition maligned by an inability to target specific cell types and identified bioimprinting as a possible vehicle for selectivity. The following section aims to compare both conventional cell targeting and other research focuses.

1.2.5. Current methods of cell sorting and targeting

Cell targeting exploit a combination of chemical and physical differences between the cell types. Physical sorting methods typically require a large difference in properties such as cell size, shape or density as can be seen when using microfiltration and density centrifugation.^{104,105} However, these tend not to be selective to isolate specific cell types and are used more as a sample preparation. For instance, Ficoll-Paque extraction of PBMCs (peripheral blood mononuclear cells) from whole blood can separate erythrocytes, plasma and leukocytes but does not discriminate between lymphocytes and monocytes.^{105,106} When used in sample preparation, larger sample sizes are needed or subsequent cell culturing which convolutes analysis making it more time and cost intensive.

1.2.5.1. Label free isolation

Various microfluidic devices have been reported for isolation of rare cells on account of hydrodynamic properties in a field known as label-free isolation.¹⁰⁷ For instance, Chung *et al.* created microfluidic devices incorporated with powerful magnetic filters and size based cell sorters.¹⁰⁸ The microfluidic design of the device ensured efficient and accurate capture of cancerous cells from complex whole blood mixtures.¹⁰⁸ Chen *et al.* also used a microfluidic device however exploited differences in size by hydrodynamic forces. Deterministic lateral displacement arrays allowed rapid isolation of cancer cells from diluted whole blood samples.¹⁰⁹ Circulating liver cancer cells were trapped by size gradated microfluidic channels termed a ‘mechanical sieve’ by Moon *et al.*¹¹⁰ The study characterised the cancers progress by enumerating circulating tumour cells (CTCs) per millilitre of whole blood. The method showed excellent precision, with a single cancerous cell per millilitre of blood detected and a 98.9% recovery of cancer cells. Isolation used small sample volumes (typically ~ 4 ml) which in a clinical setting would place less stress on weak patients and allow for aspirate to be harvested at more regular intervals. Such classification can be a key prognostic marker in cancer treatment.¹¹⁰

Flow cytometry is a mainstay of cell targeting from heterogeneous populations on account of light scattering properties.^{111,112} Cells or particles are flowed through a laser beam and the relative light-scattering of each can be observed. Differentiation of cell types can be carried out based on difference in size and complexity allowing real time distributions to be observed.

Cells can be isolated due to their fluorescence behaviour by addition of fluorochromes to the membrane, cytoplasm, nucleus or conjugated to antibodies.¹¹³ Cell sorting allows sub-populations with desired characteristics to be separated by charging and differentiating electrostatically. Dependant on flow rates and sample cell concentration, thousands of cells can be sorted per second.^{112,113}

Chemical identification and separation techniques use unique cell membrane features. Cell separation using the microfluidic device based technology was found to be superior compared to the macroscale technologies due to higher cell-substrate interaction^{105,114} and flow techniques¹¹⁴ with off-chip purification in order to obtain target cancer cells with enhanced purity.¹¹⁵ Though this thesis aims to target leukaemia in which the primary tumour is circulating, it important to consider studies in which only residual cancerous cells are circulating. Currently the only chemical identification modality for CTC capture approved by the U.S. FDA (Food and Drug Administration) is CellSearch.¹⁰⁴

1.2.5.2. CellSearch

CellSearch is primarily used to detect (CTCs) in early cancer diagnosis, working by immunomagnetic cell selection. The majority of CTCs have over expressed (EpCAM) on their surface that are targeted by anti-EpCAM antibodies immobilised on the surface of magnetic nanoparticles.¹⁵ The CTC connected magnetic nanoparticles were then extracted from the blood sample using an external magnet. The aspirated cells were then put through immunofluorescent staining and observed under a fluorescence microscope. A number of studies have aimed to capture CTCs using CellSort in conjunction with flow cytometry.^{113,116,117}

Lang *et al.* used EpCAM binding to target ten breast cancer cell lines from phosphate buffer saline (PBS) solution and spiked into PBMC mixtures to mimic CTCs in blood.¹¹⁶ The study yielded variable results with the highest being MCF-7 with 99.3% recovered from PBS though as low as 0.002% for Hs578T. Zhang *et al.* reported the *in vivo* targeting of CTCs to circumvent limitations associated with standard *in vitro* blood tests.¹¹⁵ Herein, nylon substrates were functionalised with anti-EpCAM antibody via 3-aminopropyltriethoxysilane and carboxymethacrylate coupling. Uptake of CTCs onto the biomimetic device was examined and the results showed an affinity to tumour cells expressing EpCAM. The biocompatibility of nylon as a substrate was also reviewed and shown to be suitable for *in vivo* assays. The authors

suggest this method will overcome problems associated in sample size attributed to blood harvesting or negate the need for further culturing. Both could vastly improve the diagnosis of cancer. Moreover, by optimisation of the experimental apparatus and methodology limits of detection of the analysis can be lowered.¹¹⁵

This inability to target all cancers significantly reduces the scope of the technique in a clinical setting. Furthermore, when delivered from a more complex PBMC solution, the retention rates were significantly poorer requiring additional sample preparation time. Lastly, the study also reported a rapid decline in retention as a function of time after blood harvesting making it difficult to incorporate into a clinical setting.¹¹⁶ The main disadvantage of this process is the non-detection of non-EpCAM expressing CTCs which have been found.¹⁰⁴ CellSearch has shown to be expensive, time consuming and of variable efficiency on account. Nevertheless, this technique provides the better enrichment results compared to other selection methods comprised of several extraction steps. Hence, the need for alternative efficient separation processes which are simpler and cost effective.¹⁰⁴

1.2.5.3. Antibody based cell capture

Antibody-antigen assays are commonplace, which when linked with FACS or extraction steps such as magnetic bead separation, provide analysis or purification of complex samples. The obvious short falling of such assays in targeting leukaemia, particularly AML, is the lack of a specific antibody interaction to target. Myeloblasts antibody expression is highly heterogeneous, both in type and quantity, dependant on the maturation stage of the arrested haematopoiesis. Commonly found target antigens are targeted in combinations.

Jackson *et al.* used a microfluidic device with combinations of other antibodies grafted into a polymer matrix.¹¹⁴ A microfluidic device was produced, comprised of three chambers each targeting a separate surface antigen commonly expressed on the surface of leukaemic cells: CD33, CD34 and CD117. Using antibody stains on other antigens, the group were able to identify each cell type retained to the imprinted substrate. When applied to samples from remission patients suffering from AML, the microfluidic method showed vastly superior sensitivity to standard bone marrow and blood aspirate analysis. Moreover, the method was able to detect relapse in a patient 57 days after stem cell transplant compared to the 85 days

seen in conventional diagnoses.¹¹⁴ In direct treatment this method shows little scope due to the inherent quantity of leukaemic cells; upwards of 10^{12} .¹

Size dependant extraction has been extensively used for the recognition and capture of CTCs in the recent past using various binding agents in the form of antibodies, aptamers and peptides. Antibodies as binding agents are widely reported compared to aptamers and peptides selection. Specifically, EpCAM has been targeted extensively for this purpose. *In vitro* grown ovarian cancer cells (SKOV3) were successfully separated from whole blood using centrifugation and electrochemical (eLOAD) integrated microfluidic device.¹¹⁸ The anti-EpCAM antibodies were immobilised on gold electrode substrate using L-cysteine as the binding agent and the SKOV3 cells expressing the EpCAM bound to the gold electrode efficiently. The process optimisation resulted in the minimum capture efficiency of 87% and around 214 captured cells per mm^2 of the gold electrode surface.¹¹⁸

Anti-EpCAM antibodies were also used to modify a soft polystyrene nanotube substrate (PS NT) in order to detect and capture breast cancer cells. A BSA-Biotin (Bovine serum albumin) conjugate was attached to the pillars using the hydrophobic interaction with further modification carried out using streptavidin, followed by biotinylated anti-EpCAM antibodies, breast cancer cells were able to attach efficiently to the anti-EpCAM antibodies on the pillars via the over-expressed EpCAM on its surfaces. Non-patterned surfaces showed a lower cell retention compared to those with protruding filopodia on the PS NT substrate (Figure 1.14).¹¹⁹

The release of the cells were controlled by decreasing the temperature to $20\text{ }^{\circ}\text{C}$ resulting in the transformation of the soft PS NT substrate to hydrophilic and henceforth the separation of the BSA-Biotin conjugate which finally is responsible for the release of the cancer cells.¹¹⁹ The cells retained their viability due to the soft nature of the substrate and treatments. This method resulted in the capture efficiency of 95% of viable cells and could provide new prospect of surface modification for high-quality cancer cell detection platform.¹¹⁹

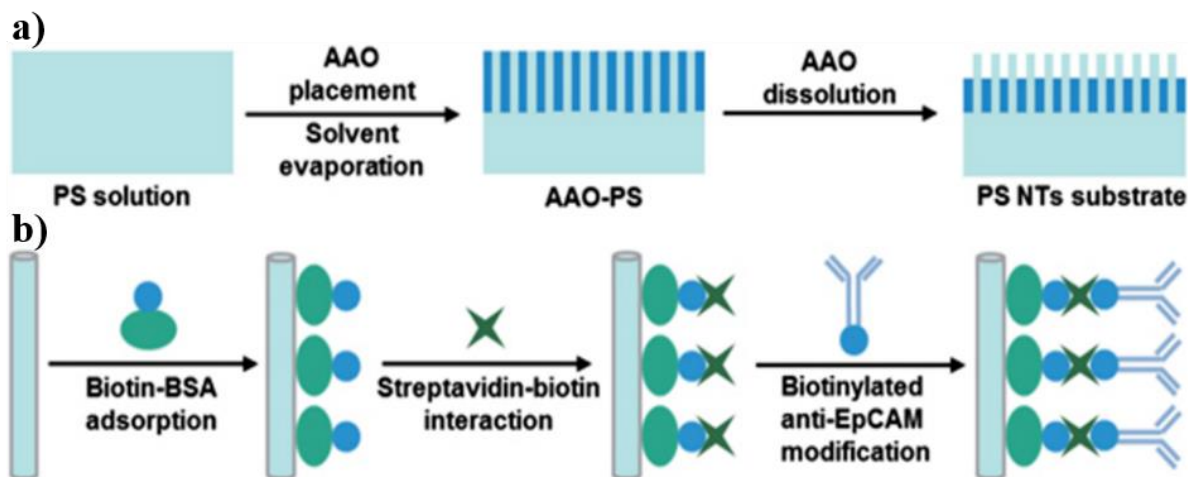


Figure 1.14 Schematics showing the production and modification of soft polystyrene (PS) nanotube (NT) substrate. a) Fabrication process of the PS NT substrate using the replication method with anodic aluminium oxide as the template and b) Functionalisation of the PS NT substrate surface with anti-epithelial cell adhesion molecule (EpCAM).¹¹⁹

Huang *et al.* also used the filopodias present on the surfaces of macrophages for the efficient separation of MCF-7 breast cancer cells from blood samples.¹²⁰ Smart particles were produced using the process of silicification and calcination of macrophages integrated with citrate-coated superparamagnetic iron oxide nanoparticles (SPION) as shown in Figure 1.15. These multifunctional smart particles which were silanised with biotinylated anti-EpCAM antibodies were capable of capture and release of the EpCAM positive breast cancer cells. EpCAM antibodies were attached to the MSP using the streptavidin-modified disulphide linker and hence the attached cells can be released by inducing a cleavage in the disulphide linker as shown in Figure 1.15f.¹²⁰ The results of this study showed 50% capture efficiency along with 90% efficiency in the release of the captured cells.¹²⁰

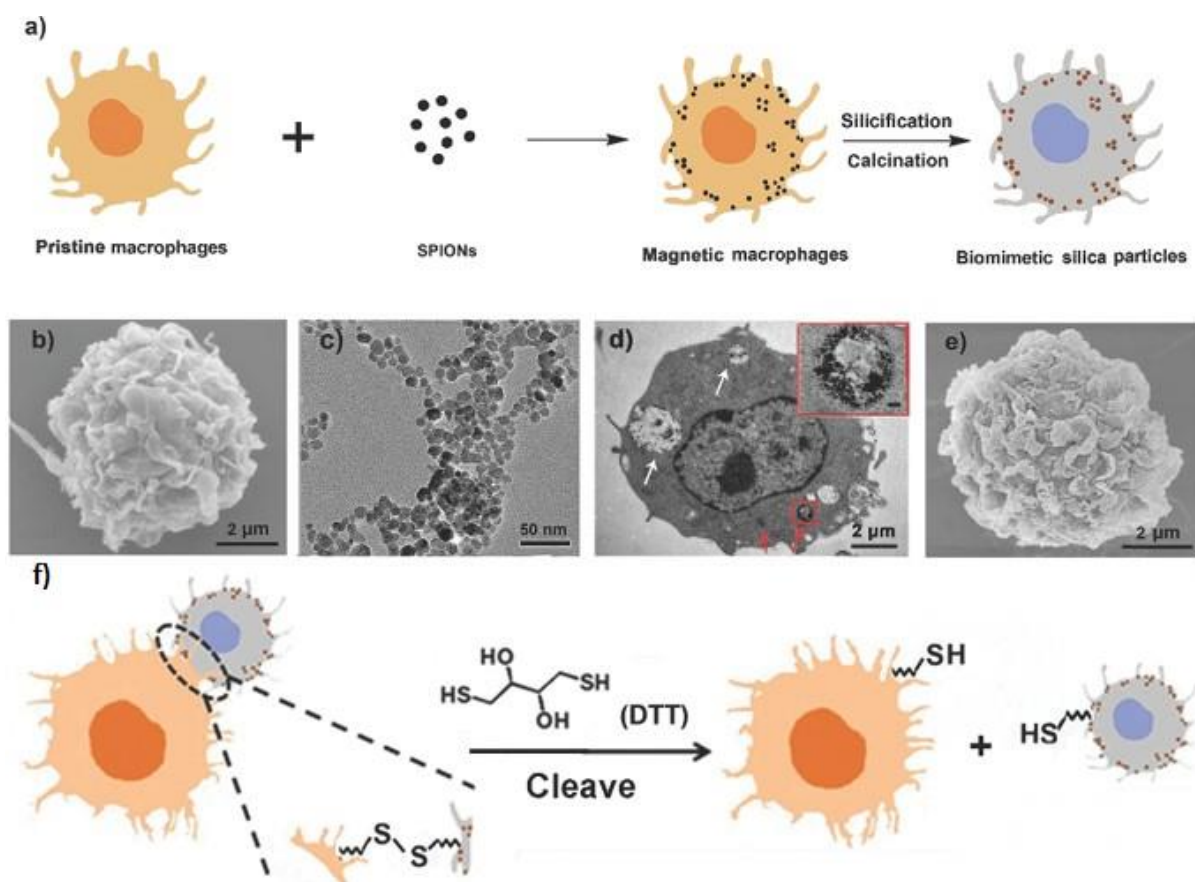


Figure 1.15 a) Schematic of the preparation of multifunctional smart particles using the live template strategy. b) SEM image of pristine macrophage. c-d) TEM images of SPIONs and magnetic macrophage, respectively. White and red arrows indicate the SPIONs in vesicles or cytoplasm, respectively. Insert picture shows a higher magnification view of internalized SPIONs. Scale bar is 100 nm. e) SEM image of the biomimetic silica particle and f) Schematic showing the mechanism of cleavable disulfide bonds-based cell release.¹²⁰

In another interesting approach, Lv *et al.* used photo-responsive immuno-magnetic nano-carriers for capture and release of CTCs.¹²¹ Similar antigen-antibody interactions were used for the separation of the rare cancer cells from blood but with the addition of a photo trigger in the form of 7-aminocoumarin. It acts as a connection between anti-EpCAM antibody and the magnetic beads. The 7-aminocoumarin moieties cleaved the C–O bond under both ultraviolet (UV) and near-infrared (NIR) light illumination, resulting in the release of the captured CTCs from the magnetic beads. The process was done while preserving the viability of the cells involved. This specific technology resulted in 90% efficiency and 85% purity of the MCF-7 breast cancer cells. Under the irradiation of UV and NIR light, 73% and 52% of

captured cells were released with a viability of 90% and 97%, respectively. This whole process was carried out on whole blood samples of cancer patients and hence opens new routes to cancer diagnosis and personalised therapy.¹²¹

The antibody-antigen interaction offers an attractive way for selective capture and release of specific cells, but at the same time the process is not cost effective and the availability is moderate. Antigen-antibody isolation techniques suffer from disadvantages inherent to their biological nature; antibodies are expensive and have a relatively limited storage time. Moreover, combinations of various clusters of definition may not be available to target particular cell types as immature cancer cells show heterogeneous expression of antibodies. Hence, in order to counter these limitations, the other subsection of natural receptors in the form of epitopes or aptamers (oligonucleotides) have been studied.

1.2.5.4. Aptamer based cell targeting

Aptamers made using the systematic evolution of ligands by exponential enrichment (SELEX) technology produce oligonucleotides with high target affinity.¹²² These aptamers were used extensively for cell recognition and ideally a replacement for antibodies in cancer diagnostics and therapies.^{122,123} An aptamers unique interaction with its target comes from the specific 3D folding of the RNA or DNA oligonucleotides which enables its recognition. To overcome disadvantages associated with antigen-antibody interactions, Zheng *et al.* developed a technique of screening specific cells from complex suspensions using the so-called 'barcode particles' coated with dendrimer amplified aptamer probes.¹²⁴

Such barcode particles were made using similarly sized silica nanoparticles packed in an emulsion droplet which was used as a template. The evaporation of the solvent resulted in the formation of closely packed spherical colloidal clusters. The surfaces of these particles were then coated with dendrimers and DNA aptamer probes as shown in Figure 1.16. The DNA aptamers help in the detection and binding to specific target molecules on the surface of the cancer cells among the pool of other cells. The use of aptamers has many advantages over the use of anti-EpCAM in CTC detection. DNA aptamers are synthesised for very specific cell types hence can differentiate between cells from different tumours signifying possible use of these techniques in cancer diagnostics. There are other advantages of non-toxicity, less immunogenicity, higher stability and less blood residence time. An overall capture efficiency

of 90% was obtained by Zheng *et al.* using the cell specific synthesised DNA aptamers.¹²⁴ The barcode particles were modified using three different synthesised aptamers segment ‘TD05’, ‘Sgc8’, and ‘Sgd5’ for affinity towards Ramos (human lymphoma), CCRF-CEM (human leukaemia) cells and the last as control respectively. The results showed a capture efficiency of 98% for Ramos and 97% for CCRF-CEM. Cell viability was maintained at 97% in the study. The use of exonuclease I resulted in the 86% release of the CTC from the barcode particles.¹²⁴

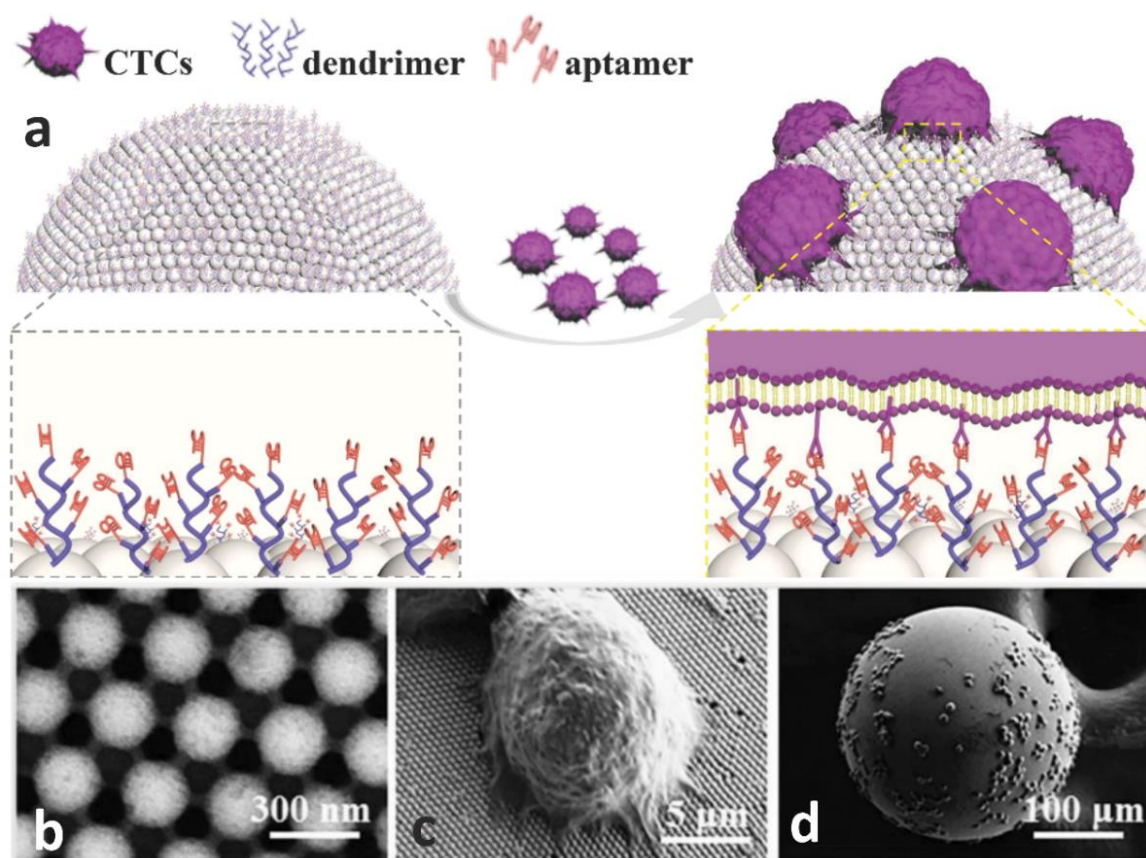


Figure 1.16 Schematics and Field-emission SEM images of the barcode particles used for the detection and capture of CTCs; a) Schematic showing the mechanism of the capture of CTCs using barcode particle surfaces modified with dendrimers and DNA aptamers. b) FESEM images of individual barcode particles coated with the aptamers, c) morphology and d) distribution of the captured CTC on the barcode particles.¹²⁴

In another study, specific antigen aptamers were synthesised and used for the detection of prostate tumour cells.¹²⁵ These prostate tumour cells express prostate specific membrane antigen on the cell surface which can be easily detected and captured using the specific antigen aptamers. The anti-PSMA aptamers were immobilised on the surface of a microchip made of polymethyl methacrylate (PMMA) and modified into a high throughput micro-sampling unit

(HTMSU). The HTMSU was used for screening the prostate tumour cells from highly heterogeneous clinical samples (peripheral blood matrix). The HTMSU contained 51 ultra-high aspect ratio parallel curvilinear channels with a channel dimensions similar to that of the prostate cancer cells. An extraction efficiency of 90% was obtained using this device for LNCaP cells.¹²⁵

Captured cells were also released using trypsin after separation. The HTMSU device also incorporated a contact conductivity sensor in order to determine the number of captured prostate cancer cells upon release and hence there is no requirement for staining individual cells for quantitative analysis. The authors were also able to separate prostate cancer cells from samples containing breast cancer cells which shows the specificity and sampling efficiency of the HTMSU device.¹²⁵ In another modification to the aptamer based cell cancer cell retrieval technology Zhao *et al.* used multiple monovalent aptamer units on a 3D DNA network with size of over tens of micrometres in the solution.⁵⁶ The science was inspired from marine organisms with long tentacles containing multiple adhesive domains in order to capture food.

This approach resulted in the amplification of the cell capture and retrieval of leukaemic cells compared to the use of antibodies and monovalent aptamers. The 3D DNA network was created using the rolling circle amplification (RCA) method with specific control over the DNA sequence, graft density and length. The RCA aptamer immobilised on the DNA network binds specifically to the protein tyrosine kinase-7 (PTK7) which is overexpressed on different human cancer cell surfaces. This multivalent aptamer technology (along with herringbone microfluidic device) for cancer cell detection and separation significantly outperformed other monovalent aptamer antibody integrated microfluidic cell capture technologies.⁵⁶

1.2.6. Bioimprint replication and area augmentation

The studies reviewed thus far have produced size and shape recognition entities accurate on a nanometre length scale. However, the total surface area of the imprint usually cover only a few square centimetres; which when incorporated into a myeloblast capture device will not provide sufficient surface area to significantly obviate malignancy from patient aspirate. For the areas required it is inconceivable to produce primary bioimprints of a suitable area for clinical use. For instance, by taking the diameter of a myeloblast as 15 μm , the area of bioimprint required to accommodate the number of blast cells per litre of patient blood at diagnosis is

around 0.2 – 0.5 m². For this calculation, a healthy white cell count of 4 – 11 × 10⁹ L⁻¹ was considered, with 20% of white count being myeloblasts at diagnosis with cells deposited in a square array. Typically, the studies discussed thus far have produced bioimprints in a range of square millimetres to centimetres. In the interests of upscaling the produced bioimprint into multiple square metres, a method for continuous reproduction is needed.

Nanoimprint lithography (NIL) was designed in order to circumvent low throughput restraints associated with the micro- and nano- fabrication of semiconductors and electronics on an industrial scale. Here, a mould is prefabricated displaying the reciprocal structure to the desired functionality which are then replicated by mechanical deformation of a secondary polymer. The nanometre scale resolution achieved with NIL is well within the range of the extracellular features seen on and significantly smaller than the micron range of whole cells. Three high through-put modalities are commercially available; plate-to-plate, plate-to-roll and roll-to-roll (R2R) NIL.

Plate-to-plate NIL involves a rigid, flat stamp used to emboss polymer matrix; which may be done in one step with the entire substrate used or as a multiple-step of sequential embossing of smaller areas. Multiple step imprinting negates the problems of very high processing pressure and air bubble entrapment which both compromise the imprint. Both have comparatively poor processing speed.

Roll-to-plate NIL involves a roller press mechanism ensuring a drum is rolled with constant force along a planar substrate; here the mold can be mounted to the drum or plate.¹²⁶ The area of contact between the master imprint and receiving polymer is equal to a narrow band along the circumference of the drum embossed into the drum. This offers the dual advantage of requiring significantly less imprinting force and reduced capacity for trapping air thus achieving an increased overall throughput.^{127,128}

The third conformation is roll-to-roll NIL (R2RNIL). Here, both the master imprint and receiving polymer are mounted to the circumference of imprinting drums. The continuous nature of the procedure results in the highest output, requiring no resetting as seen in roll-to-plate. R2RNIL is compatible with both thermal and UV curable polymer matrices.¹²⁹ Here, the polymer combinations can be substituted to suit the requirements of the intended use of the substrate. This project will focus on UV photoresists cured with high energy UV radiation; the setup can be seen in Figure 1.17, below.

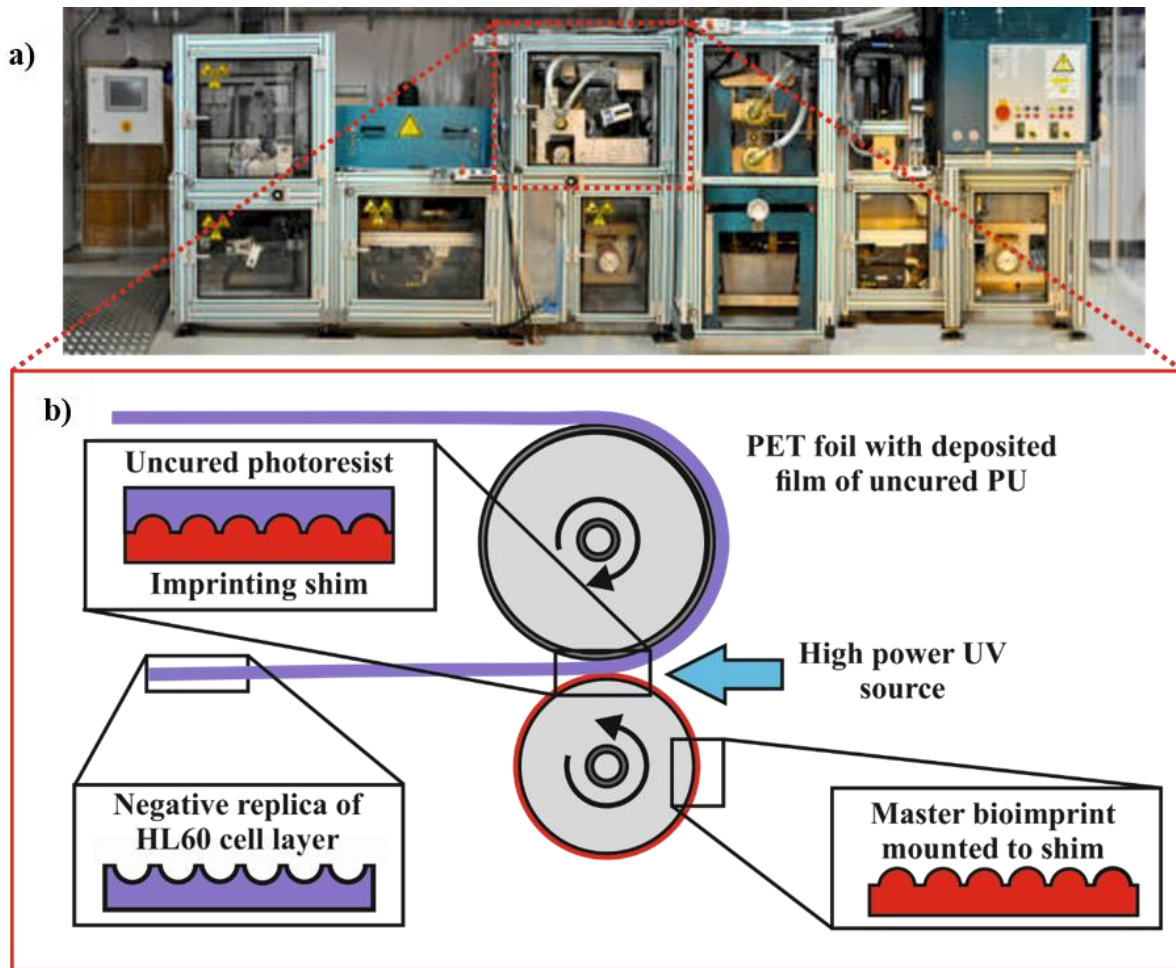


Figure 1.17 a) Roll-to-roll nanoimprinting lithography apparatus and b) schematic showing the action of the high throughput nanoimprinting lithography (NIL) process using a UV curable photoresist mounted on foils of polyethylene terephthalate (PET).¹²⁶

Metallic layers (or silicone-based polymer castings) are often used to lower surface adhesion from imprint drum to allow detachment of the resist material. Due to their flexibility, nickel layers are used, able to meet the mechanical demands of the imprinting process.¹³⁰ If significant adhesion were seen, the structure of the master imprint drum is compromised. Though the production of nickel coated master imprints further convolutes the production process, in this case producing the original bioimprint, Odom *et al.* highlighted the advantage of alternatives to silicone master imprints which incur feature loss due to the low elastic modulus due to deformation under high processing forces.¹³¹ Ultimately, by using materials with inherent low surface energy, the process does not compromise integrity of the master imprint showing a high fidelity over hundreds of cycles. Publications show the production of imprinted films on an area of hundreds of square metres.^{126,132}

1.2.7. Summary of bioimprinting

This section introduced the area of bioimprinting; the production of artificial recognition entities into polymer matrices to exploit size and shape dependant relationships. Studies have developed from the imprinting of macromolecules to whole cells into various polymer matrices. Such materials have the advantage of being cheap to produce, robust and create a bespoke target-substrate relationship.

Though publications describe various applications, particularly as cell culture supports, the majority of the studies envisage bioimprinted substrates as part of a biosensor, able to detect trace numbers of cells from complex media. Very few bioimprinting studies are focused on cancer detection, rather aiming to capture bacteria or other pathogens which have more distinctive size and aspect ratio discrepancies. There has been little evidence of bioimprints being incorporated into a flow device in order for clinical application. Moreover, bioimprints tend to cover an area in the square centimetre range with no attention paid to upscaling for real-world applications.

1.3. Bioimprint rationale

When considering the action of bioimprints in selective cell targeting, it is important to first discuss the interactions involved. Attractive and repulsive forces between colloids have significance in colloid chemistry such as surfactant adsorption, adhesion, and colloid stability.^{133–135} Adsorption of micron-scale cells is dependent on colloidal interactions, quantitatively described by the Derjaguin-Landau-Verwey-Overbeek (DLVO). The phenomenon is the net energy (U_T) of the long range attraction of dispersive forces (U_A) and short range electrostatic repulsion (U_R) described by DLVO theory.^{136–138}

$$U_{Total} = U_{Attractive} + U_{Repulsive} \quad (1.1)$$

To view the model as a whole, constituent DLVO forces will be discussed separately beginning with the Van der Waals (VW) attractive forces, below.

1.3.1. Attractive dispersion forces

Long range attraction, on a molecular and macroscopic scale, is the result of Van der Waals (VW) forces. VW forces between molecules are weak interactions, typically one or two orders of magnitude smaller than a chemical bond energy.¹³⁸ Though relatively weak when compared to chemical bonds, VW are ubiquitous and are significant on a 1-100 nanometre length scale.

There are three distinct types of the interaction, the first being the Keesom force; the interaction between opposing permanent dipole moments in adjacent molecules. Dipole-dipole interactions become more significant in small molecules with a larger dipole moment. When discussing interactions between electron deficient hydrogen atoms bonded to highly electronegative atoms such as oxygen or nitrogen, interactions become much stronger and are given the more specific term ‘hydrogen bonding’. The second type of VW force is the induction or Debye force; when a permanent dipole induces a dipole in a neighbouring polarizable molecule. The last type of VW force are the London dispersion forces. Dispersion forces are the most significant as they are ubiquitous; not reliant on the presence of electronegative constituents. Here, the interaction is on account of fluctuating charge distribution in a molecule causing an instantaneous dipole and generating a short-lived electric field. In turn this induces dipoles to neighbouring molecules causing a net coulombic interaction between two molecules.

All VW forces are non-directional and therefore dipoles in all orientations can correlate to yield a cumulative attraction. VW interactions between the two molecules are given by the equation:

$$U_{12}(r) = -\frac{c_{12}}{r^6} \quad (1.2)$$

Here U_{12} is the Van der Waals interaction between molecules 1 and 2, across a vacuum of distance r . Attractive Van der Waals energy (U_{VW}) between two flat surfaces interacting across media at a surface-to-surface separation, h , can be given by:

$$U_{VW}(h) = -\frac{A_H}{12\pi h^2} \quad (1.3)$$

A_H is the compound Hamaker constant, a function of molecules polarizabilities and dipole moments, density and polarizability:

$$A_H = A_{12} + A_{33} - A_{13} - A_{23} \quad (1.4)$$

Here 1, 2 and 3 denote the phases of the cell, planar substrate and aqueous media and A_{ij} are the simple Hamaker constants, corresponding to two surface interacting across vacuum, e.g. for A_{12} ($i=1, j=2$) one can write:

$$A_{12} = \pi^2 C_{12} \rho_1 \rho_2 \quad (1.3)$$

ρ_1 and ρ_2 are the densities of the materials 1 and 2 and C_{12} is the van der Waals constant of interaction of two molecules of type 1 and 2 in vacuum. A compound Hamaker constant can be calculated to account for separation of phases by aqueous media. VW forces can be attractive or repulsive dependent on the sign of the compound Hamaker constant.¹³⁶

1.3.2. Electrostatic interaction due to overlapping of electric double layers

Electrostatic forces arise from the appearance of a charged surfaces in aqueous media. When a surface of a material is placed in an aqueous solution, an electrical surface charge is produced by: ionization or dissociation of surface groups (-OH, -COOH etc.), adsorption of ions from solution to the surface or by charge transfer between two dissimilar surfaces at low separation. An electric double layer is formed as oppositely charged ions (counter-ions) from solution form a diffuse layer in the vicinity of the surface charge. Adjacent to this is a region of counter and

co-ions termed the electric double layer (EDL) characterised by the Debye parameter (κ). The Debye length, $(1/\kappa)$ is inversely proportional related to the square root of the electrolyte concentration in the aqueous media and characterises the effective thickness of the EDL.¹³⁶ The EDL structure and relative potential as a function of separation from the surface is shown in Figure 1.18a and the effect of overlapping electrical double layers from two like-charged surfaces at low separation shown in Figure 1.18b.¹³⁶

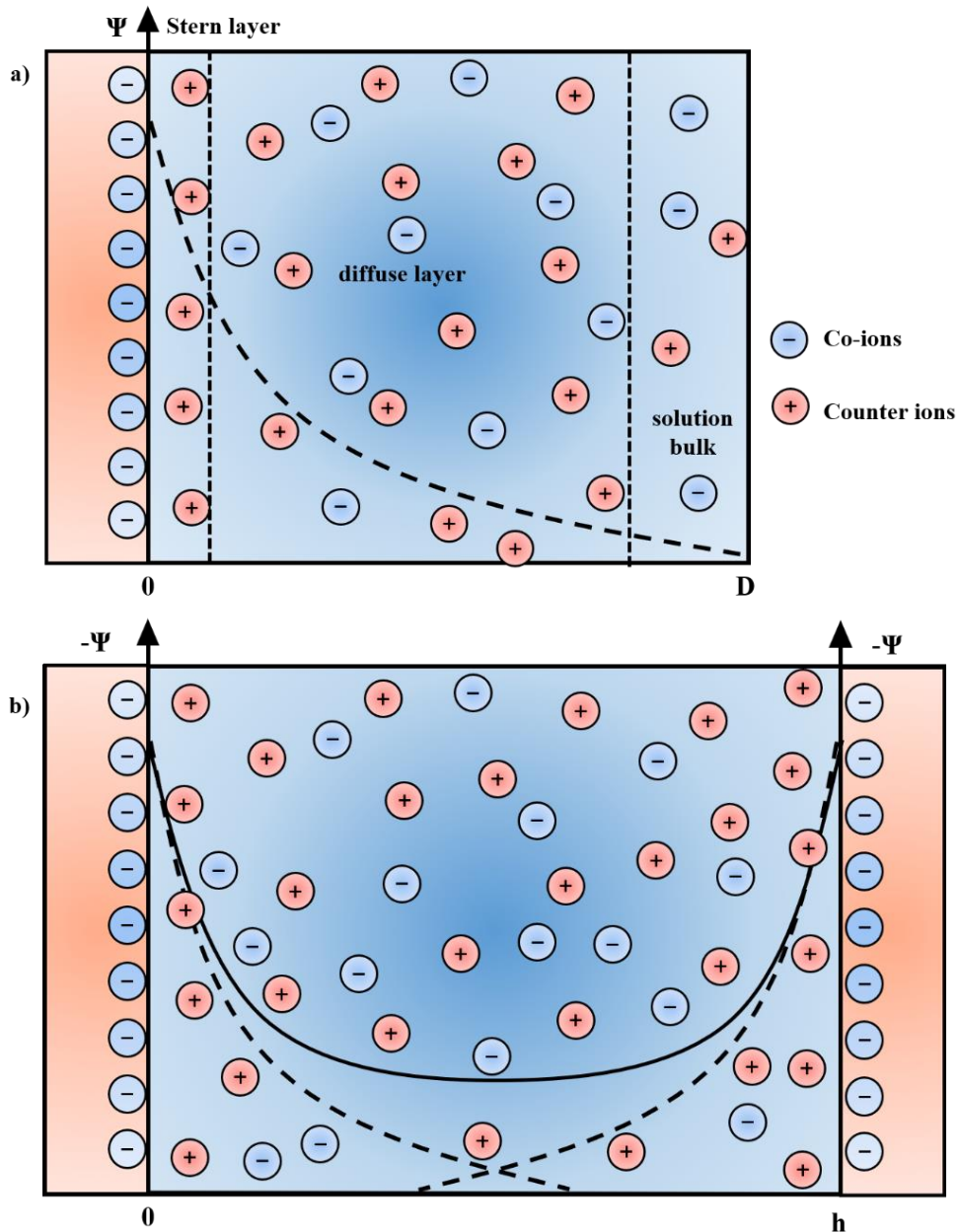


Figure 1.18 a) The electric double layer (EDL) formed as a result of a layer of oppositely charged ions (Stern layer) adsorbed to the immobilised surface charge and b) repulsion when approaching surfaces have overlapping double layers.

The total interaction energy (U_T) between the colloid particle and planar substrate is the sum of Van der Waals forces (U_{VW}) and electrostatic double layer (U_{EL}). Figure 1.19 shows the DLVO theory schematically as DLVO theory shown by overlaid plots of attractive dispersion forces (Van der Waals) and repulsive electrostatic interactions between like-charged surfaces. The net interaction can be shown as a function of separation distance.

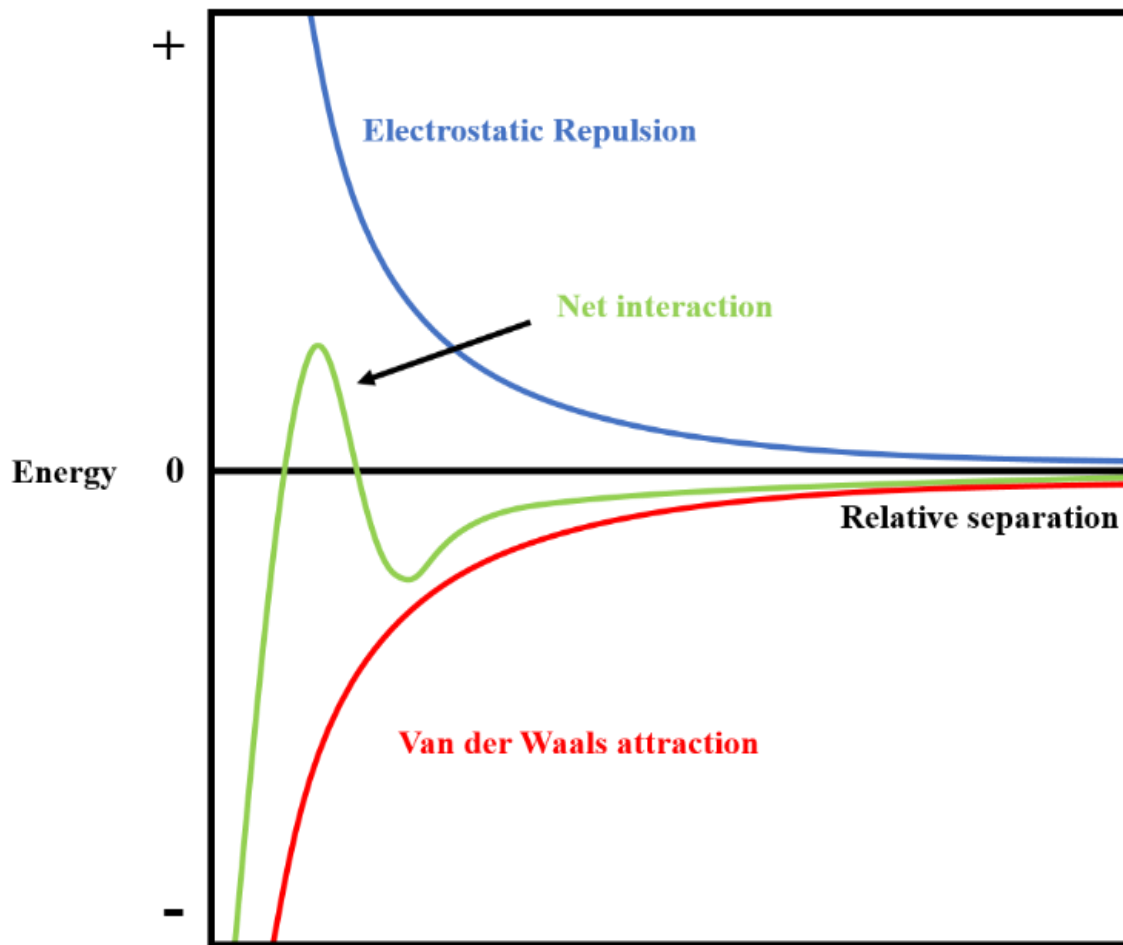


Figure 1.19 DLVO theory shown by overlaid plots of attractive dispersion forces (Van der Waals) and repulsive electrostatic interactions between like-charged surfaces. The net interaction can be shown as a function of separation distance.

The DLVO theory of stability of colloids in aqueous media predicts that at very close proximity, interactions between the cell and substrate are dominated by the attractive VW forces, yielding a net attraction termed the primary minimum. At low electrolyte concentration and intermediate separations, the electrostatic interaction between like-charged surfaces dominate over the VW attraction as shown by a net positive potential energy resulting in repulsion between the two surfaces. At larger separations the VW interactions become dominant once more, predicted to decay as an inverse power of particle separation compared to an exponential decrease observed for electrostatic interactions.

The method of action for selective cell capture reliant on size and shape matching can be shown by comparison of the DLVO interactions between cells and bioimprints and cells of a flat substrate. Borovička *et al.* characterised the energy of cell interactions of cells and colloidal antibodies (discussed in 1.2.4.4).^{99,100,139} The same approach is valid for the case of a

hemispherical bioimprint cavity and a cell of matching size and curvature. The terms for classical DLVO interactions will now be discussed for myeloblast cell interaction with a planar substrate and with a bioimprint cavity of complementary size and curvature; as described by Figure 1.20, below.

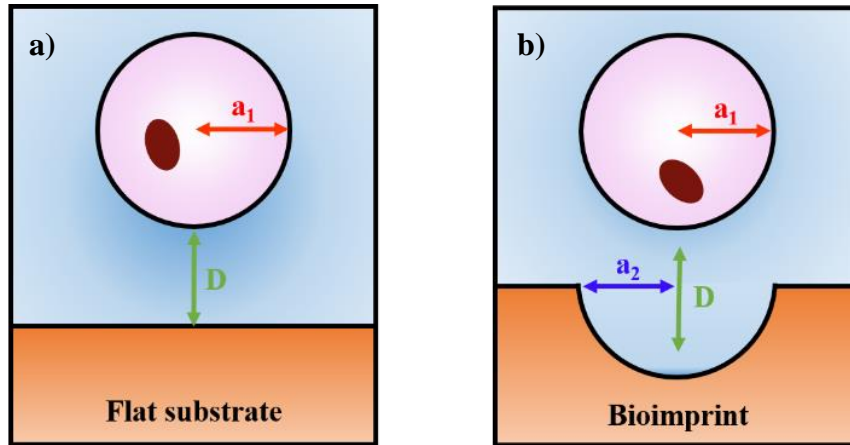


Figure 1.20 Schematic representation showing the interaction of a target cell with a) a planar surface and b) a bioimprinted hemisphere of matched radius and curvature.

1.3.3. Interaction energy between a spherical cell and flat substrate

Using the Derjaguin approximation, colloidal interactions between particles of different radii can be calculated per unit area of interaction as two planar geometries. This simplification is valid when the separation is significantly smaller than the radius of curvature of the particle in question. The Derjaguin approximation calculates the energy of interaction $U(D)$ between two different spherical particles separated by a surface-to-surface distance, D , by:

$$U_{VW}(D) = \frac{2\pi a_1 a_2}{a_1 + a_2} E(D) \quad (1.6)$$

Where a_1 and a_2 are the radii particles and $E(D)$ is the free energy of interaction between plane-parallel surfaces of the same materials across the same media. The approximation is valid when $a_1 \gg D$ and $a_2 \gg D$, as described in Figure 1.21.

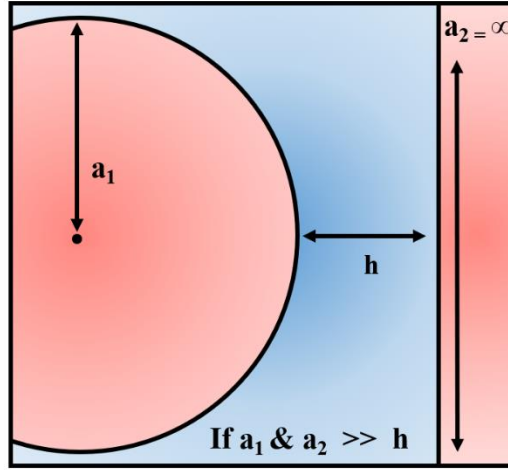


Figure 1.21 Schematic showing when the Derjaguin approximation is also applicable for the interaction between a spherical particle of radius a_1 and a planar substrate when $a_2 \rightarrow \infty$.

In this case the term for the Van der Waals interaction energy yields:

$$U_{VdW} = \frac{A_H a_1 a_2}{6(a_1 + a_2)D} \quad (1.7)$$

Which can be simplified when $a_1 = a$, $a_2 \rightarrow \infty$, then:

$$U_{VdW} = -\frac{A_H a}{6D} \quad (1.8)$$

The electrostatic component of cell-flat plane interaction can be calculated in a similar fashion. Here using the expression for the electrostatic free energy of interaction between two flat surfaces per unit area:

$$E_{EL}(h) = B e^{(-\kappa h)} \quad (1.9)$$

where

$$B = 32 \varepsilon_0 \varepsilon_r \kappa \gamma_1 \gamma_2 \left(\frac{kT}{ve} \right)^2 \quad (1.10)$$

When ε_0 is the permittivity of the vacuum and ε_r is the relatively dielectric permittivity, respectively, κ is the inverse Debye screening length. $\gamma_i = \tanh(\varphi_i/4)$ and $\varphi_i = ve\psi_i/kT$. ($i = 1, 2$ for the two interacting surfaces across aqueous media). In addition, k is the Boltzman constant, v is the valency of the electrolyte ions, e is the electronic charge, T is the absolute

temperature and ψ_i are the surface potentials for the cell and the planar substrate. By using the Derjaguin method, once more the term for the electrostatic energy of interaction between two particles of different radii, a_1 and a_2 , becomes:

$$U_{EL} = 2\pi B \left(\frac{a_1 a_2}{a_1 + a_2} \right) \frac{1}{\kappa} e^{(-\kappa D)} \quad (1.11)$$

This equation is simplified for a particles and a flat surface, when $a_1 = a$, $a_2 \rightarrow \infty$:

$$U_{EL} = \frac{2\pi a B}{\kappa} e^{(-\kappa D)} \quad (1.12)$$

The DLVO theory described the net interaction of the dispersion and electrostatic interactions and therefore yield the term:

$$U_{Total}(flat\ plane) = -\frac{A_H a}{6D} + \frac{2\pi a B}{\kappa} e^{(-\kappa D)} \quad (1.13)$$

1.3.4. Interaction energy between a spherical cell and bioimprint

Borovička *et al.* adapted the Derjaguin approximation to account the geometry of the imprinted colloid antibody recognition site.¹³⁹ Here the radius of the imprinted hemisphere (a_2) is greater than or equal to the radius of the target cell a_1 ; $a_1 \leq a_2$. By approximating both spherical surfaces to paraboloids of surfaces of the same size and integration of the Derjaguin approximation the following terms for the energy of VW and electrostatic interactions could be achieved.

$$U_{VW} = -\frac{a^2 A_H}{12D^2} \quad (1.14)$$

$$U_{EL} = \pi a^2 B e^{(-\kappa D)} \quad (1.15)$$

In accordance with the Derjaguin approximation, this integration can only be achieved within two radius lengths of the target cell. Combination of both terms to fit the DLVO theory yields:

$$U_{Total}(imprint) = -\frac{a^2 A_H}{12D^2} + \pi a^2 B e^{(-\kappa D)} \quad (1.16)$$

The ratio of the combined terms for the case of spherical cell interacting with a matching bioimprint cavity ($a_1=a_2=a$) compared to a cell interacting with a planar surface can be calculated by:

$$\frac{U_{VW} (imprint)}{U_{VW} (flat substrate)} = \frac{a}{2D} \gg 1 \quad (1.17)$$

$$\frac{U_{EL} (imprint)}{U_{EL} (flat substrate)} = \kappa a/2 \gg 1 \quad (1.18)$$

In the case of the Van der Waals interactions where the Derjaguin approximation stipulates that the surface-to-surface distance D is to be smaller than a , the ratio shows the numerator to be significantly smaller than the denominator of the term. This shows that the forces from the Van der Waals interaction between the cell and the bioimprint are much stronger than those of the same cell and a flat substrate. This amplification is of the same magnitude of difference between a and D ; thus, dependent on the minimal possible separation. Since for myeloblasts $a \approx 6.5 \mu\text{m}$ and the minimal distance between the surface of the cell and the imprint surface can be $D_{min} \sim 1 \text{ nm}$ it is obvious that the ratio in Eq.(1.17) is always much larger than 1, i.e. the bioimprint would attract the cell much stronger than an equivalent flat surface.

The electrostatic forces present in both cases can be compared in a similar fashion; by adding the average radius of the target cell as $a = 6.5 \mu\text{m}$, at a salt concentration of 0.1 M yields the inverse Debye screening length $\kappa = 1 \text{ nm}$. Substitution of these values shows the interaction of electrostatic forces for the case of a matched bioimprint to be ~ 3250 times greater than that of a cell with a flat substrate. Thus, electrostatic interactions from bioimprinted cavities of a matched size are of 3 magnitudes higher than the interaction with a flat substrate. According to the DLVO theory, the sign interaction being amplified is dependent on the separation of the cell and substrate; causing significantly larger attraction when in close proximity or larger separations. This amplification of the attractive interaction will facilitate the adsorption and retention of cells to bioimprints.

Note that the myeloblasts cells carry a negative surface charge due to dissociation of surface carboxylic groups, which corresponds to negative surface potential, $\psi_1 < 0$. If the bioimprint surface also carries a negative surface charge, the cells and the bioimprint would repel stronger than a cell and a flat surface of the same material. However, if the bioimprint surface is modified with a cationic polyelectrolyte, its surface potential can be reversed from negative to positive ($\psi_2 > 0$) which according to Eq. 1.15 would mean that the bioimprint would effectively attract the cell by electrostatic attraction. In this case, when $\psi_2 > 0$ and $\psi_1 < 0$, the

bioimprint would attract stronger the cell by electrostatic attraction than the equivalent flat surface. This is the situation engineered in work throughout this thesis which leads to cell shape recognition. In this case, both the van der Waals and the electrostatic energy of interaction would contribute to an attraction, which is very different from the classical case of the DLVO theory, as presented in Figure 1.18 which describes the interaction between like-charged surfaces.

1.4. Aim of this project

This thesis has introduced acute myeloid leukaemia (AML); a fast onset, fatal cancer. Relatively little progress has been made in therapy and prognoses remain dismal. Treatment is maligned by an inability to direct toxic effects of chemotherapeutic to neoplastic cells. Iatrogenic discomfort and mortality are commonplace. Adverse age or comorbidity preclude effective treatment protocols for most patients and in the vast majority of cases, the condition relapses. Bioimprinting has been identified as a field in which specific complementary shape interactions can be exploited. By capturing size and shape information from the templated cells, bespoke recognition entities can be made for the selective capture of cells from complex systems.

This study aims to introduce bioimprinting as a vehicle for selectivity towards leukaemia cells in patient aspirate. Due to their distinctive size difference from matured blood cells, myeloblasts provide an ideal target for using bioimprints for their separation from normal white blood cells. Moreover, the bespoke nature of the field helps to overcome the heterogeneity seen in myeloblasts samples. For instance, antibody assays are unsuitable due to the lack of an AML specific antigen to exploit. This is further convoluted as antigen expression is non-uniform in myeloblasts, depending on the subtype and maturation stage of the cells. Myeloblast morphology also varies between subtypes, as described by the FAB classification system. Bioimprinting is able to circumvent the heterogeneity as imprints of each subtype can be made.

The majority of bioimprinting studies detail their use in lowering the detectable limits in biosensors. This application is highly relevant for AML patients in remission particular in the minimal residual disease (MRD) phase where leukaemic cells are too few to detect. By lowering detection limits, AML relapse can be identified earlier which is prognostically vital; patients can undergo subsequent therapy to avoid full relapse. Another foreseen application of bioimprints in treating leukaemia is by their incorporation into a flow device for direct discrimination as seen with leukapheresis. It is important to note that leukapheresis already is an alternate method to remove malignancy though does not correlate clinically with an improvement in length of remission or survival. This may be as the method is not selective enough to discriminate between myeloblasts and healthy peripheral blood mononuclear cells (PBMCs). Instead, in typical leukapheresis, all PBMCs healthy and malignant are removed from AML patient's peripheral blood by centrifugation. However, it is anticipated that in doing leukapheresis with the help of bioimprints the patients' leukaemic burden may be reduced

leaving the healthy PBMC, containing vital parts of the immune system intact, which is expected to improve AML patient outcomes.

1.4.1. Presentation of this thesis

The aim of this work is to produce bioimprints from layers of blood cancer cells (myeloblasts) and apply them for cell shape recognition towards the myeloblasts in mixtures with PBMCs in order to explore the effectiveness of bioimprinting mediated removal of these malignant cells from the peripheral blood of patients with blood cancer.

The main idea of the use of the bioimprinting method to target AML is based on the following premise: the bioimprint holes match better the size of the myeloblast cells than the PBMCs. When the cell mixture of myeloblasts and PBMCs get in contact with the imprint, both types of cells are attracted to the surface of the functionalised imprint but the myeloblasts attraction to the surface is stronger as their contact area with the imprint surface is much larger than this of the PBMCs, as it matches the surface of the bioimprint holes much closer. When the mixture of these types of cells on the imprint is flushed with pump, the loosely attached PBMCs get blown off easier which provides a differentiation in their retention. This is how the cell recognition is expected to work for removal of the myeloblasts from the peripheral blood of patients with AML.

Chapter 2 details the materials used throughout this study and describes all experimental procedures for the production, replication, modification and examination of bioimprints of blood cancer cells. Here the instrumentation and parameters are also detailed.

Various methods of depositing both blood cancer cell and microparticle templates are explored to produce densely packed, uniform bioimprints in a variety of polymer matrices. Conversion of each bioimprint and replication into a very large area by using roll-to-roll nanolithography (by hundreds of square metres) are also discussed in Chapter 3.

In Chapter 4, bioimprint cavity size and surface topography were quantitatively assessed and compared with analysis of the template cell material. The performance was tested for various resins for bioimprinting of layers of myeloblasts cells. Various methods chemically modifying the bioimprint surfaces were assessed and characterised in order to introduce a weak attraction towards the cells.

The retention of the templated cell type by its bioimprint was assessed under static conditions in Chapter 5. For more accurate results, bioimprints were incorporated into bespoke flow chambers to control the hydrodynamic forces involved. The effect of the imprinted cell topography was assessed by comparison of retention to bioimprints produced from monodisperse microparticles with relatively little asperity.

Cell retention studies progressed to examining the selectivity of bioimprints to the template cell types from binary cell mixtures of a myeloblast cell line (HL60) and PBMCs from healthy volunteers in Chapter 6. Here, cell types expected in AML patient aspirate were used.

The thesis concludes in Chapter 7 with a summary of the project's findings, identifying areas deemed prudent for further study.

1.5. References

- 1 D. Harmening, *Clinical & fundamentals of Hemostasis*, F. A. Davies Company, Philadelphia, 1997.
- 2 J. Saultz and R. Garzon, *J. Clin. Med.*, 2016, **5**, 33.
- 3 W. Ladines-Castro, G. Barragán-Ibañez, M. A. Luna-Pérez, A. Santoyo-Sánchez, J. Collazo-Jaloma, E. Mendoza-García and C. O. Ramos-Peñafiel, *Rev. Médica del Hosp. Gen. México*, 2016, **79**, 107–113.
- 4 Cancer Research UK, <https://www.cancerresearchuk.org/health-professional/cancer-statistics/statistics-by-cancer-type/leukaemia-aml>, (accessed August 2018).
- 5 E. H. Estey and H. Dohner, *Lancet*, 2006, **368**, 1894–18907.
- 6 F. Ferrara and C. A. Schiffer, *Lancet*, 2013, **381**, 484–495.
- 7 S. Oberoi, T. Lehrnbecher, B. Phillips, J. Hitzler, M. C. Ethier, J. Beyene and L. Sung, *Leuk. Res.*, 2014, **38**, 460–468.
- 8 I. Berber, I. Kuku, M. A. Erkurt, E. Kaya, H. Gozukara Bag, I. Nizam, M. Koroglu, M. Ozgul and S. Bazna, *Transfus. Apher. Sci.*, 2015, **53**, 185–190.
- 9 K. Hölig and R. Moog, *Transfus. Med. Hemotherapy*, 2012, **39**, 241–245.
- 10 K. R. Kampen, *Leuk. Res.*, 2012, **36**, 6–13.
- 11 J. W. Vardiman, N. L. Harris and R. D. Brunning, *October*, 2002, **100**, 2292–2302.
- 12 NHS Blood and Transplant, <https://www.nhsbt.nhs.uk/what-we-do/diagnostic-and-therapeutic-services/therapeutic-apheresis/>, (accessed August 2018).
- 13 M. R. O'Donnell, M. S. Tallman, C. N. Abboud, J. K. Altman, F. R. Appelbaum, D. A. Arber, V. Bhatt, D. Bixby, W. Blum, S. E. Coutre, M. De Lima, A. T. Fathi, M. Fiorella, J. M. Foran, S. D. Gore, A. C. Hall, P. Kropf, J. Lancet, L. J. Maness, G. Marcucci, M. G. Martin, J. O. Moore, R. Olin, D. Peker, D. A. Pollyea, K. Pratz, F. Ravandi, P. J. Shami, R. M. Stone, S. A. Strickland, E. S. Wang, M. Wieduwilt, K. Gregory and N. Ogba, *J. Natl. Compr. Cancer Netw.*, 2017, **15**, 926–957.
- 14 H. Döhner, E. H. E. Estey, S. Amadori, F. R. F. R. Appelbaum, T. Büchner, A. K. a. K. Burnett, H. Dombret, P. Fenau, D. Grimwade, R. a. R. A. Larson, F. Lo-Coco, T. Naoe, D. Niederwieser, G. J. Ossenkoppele, M. A. Sanz, J. Sierra, M. S. Tallman, B. Löwenberg, C. D. Bloomfield and Others, *Blood*, 2010, **115**, 453–474.
- 15 J. E. Kolitz, *Br. J. Haematol.*, 2006, **134**, 555–572.
- 16 F. Stölzel, B. Mohr, M. Kramer, U. Oelschlägel, T. Bochtler, W. E. Berdel, M. Kaufmann, C. D. Baldus, K. Schäfer-Eckart, R. Stuhmann, H. Einsele, S. W. Krause, H. Serve, M. Hänel, R. Herbst, A. Neubauer, K. Sohlbach, J. Mayer, J. M. Middeke, U. Platzbecker, M. Schaich, A. Krämer, C. Röllig, J. Schetelig, M. Bornhäuser and G. Ehninger, *Blood Cancer J.*, 2016, **6**, 7–10.
- 17 O. Emma, S. Prideaux and T. Chevassut, 2014, **2014**, DOI:10.1155/2014/103175.
- 18 B. J. Wouters and R. Delwel, *Blood*, 2015, **127**, 42–53.

- 19 H. Dombret and C. Gardin, *Blood*, 2016, **127**, 53–62.
- 20 G. Tamamyian, T. Kadia, F. Ravandi, G. Borthakur, J. Cortes, E. Jabbour, N. Daver, M. Ohanian, H. Kantarjian and M. Konopleva, *Crit. Rev. Oncol. Hematol.*, 2017, **110**, 20–34.
- 21 J. M. Rowe, *Best Pract. Res. Clin. Haematol.*, 2016, **29**, 315–319.
- 22 N. J. Short and F. Ravandi, *Clin. Lymphoma, Myeloma Leuk.*, 2016, **16**, S25–S29.
- 23 A. K. Burnett, *Hematol. Am Soc Hematol Educ Progr.*, 2012, **2012**, 1–6.
- 24 N. A. Podoltsev, M. Stahl, A. M. Zeidan and S. D. Gore, *Blood Rev.*, 2017, **31**, 43–62.
- 25 C. C. Coombs, M. Tavakkoli and M. S. Tallman, *Blood Cancer J.*, 2015, **5**, 304–9.
- 26 D. Shafer and S. Grant, *Blood Rev.*, 2016, **30**, 275–283.
- 27 C. U. Michael J. Burke, Linda Burns, Michael A. Linden, Bruce Lindgren, Michael R. Verneris, Daniel Weisdorf, *Am. J. Hematol.*, 2014, **88**, 826–827.
- 28 S. Oberoi, T. Lehrnbecher, B. Phillips, J. Hitzler, M. C. Ethier, J. Beyene and L. Sung, *Leuk. Res.*, 2014, **38**, 460–468.
- 29 M. Schulz, G. Bug, H. Bialleck, H. Serve, E. Seifried and H. Bönig, *Vox Sang.*, 2013, **105**, 47–53.
- 30 F. R. Appelbaum, *Best Pract. Res. Clin. Haematol.*, 2016, **29**, 365–371.
- 31 W. R. Sperr, A. W. Hauswirth, F. Wimazal, P. Knöbl, K. Geissler and P. Valent, *Wien. Klin. Wochenschr.*, 2003, **115**, 505–514.
- 32 C. S. Viele, *Semin. Oncol. Nurs.*, 2003, **19**, 98–108.
- 33 N. Cieri, S. Mastaglio, G. Oliveira, M. Casucci, A. Bondanza and C. Bonini, *Immunol. Rev.*, 2014, **257**, 165–180.
- 34 A. M. Dickinson, J. Norden, S. Li, I. Hromadnikova, C. Schmid, H. Schmetzer and H. Jochem-Kolb, *Front. Immunol.*, 2017, **8**.
- 35 H. J. Kolb, *Hematology*, 2011, **112**, 4371–4383.
- 36 J. L. Shipley and J. N. Butera, *Exp. Hematol.*, 2009, **37**, 649–658.
- 37 G. J. Schuurhuis, M. Heuser, S. Freeman, M.-C. Béné, F. Buccisano, J. Cloos, D. Grimwade, T. Haferlach, R. K. Hills, C. S. Hourigan, J. L. Jorgensen, W. Kern, F. Lacombe, L. Maurillo, C. Preudhomme, B. A. van der Reijden, C. Thiede, A. Venditti, P. Vyas, B. L. Wood, R. B. Walter, K. Döhner, G. J. Roboz and G. J. Ossenkoppele, *Blood*, 2018, **131**, 1275–91
- 38 G. Ossenkoppele and B. Lowenberg, *Blood*, 2015, **125**, 767–774.
- 39 J. P. Sasine and G. J. Schiller, *Blood Rev.*, 2015, **29**, 1–9.
- 40 J. J. Cornelissen and D. Blaise, *Blood*, 2016, **51**, 1411–1412.
- 41 D. A. Pollyea, H. E. Kohrt and B. C. Medeiros, *Br. J. Haematol.*, 2011, **152**, 524–542.
- 42 Y. Ge and A. P. F. Turner, *Trends Biotechnol.*, 2008, **26**, 218–224.

- 43 S. Li, S. Cao, M. J. Whitcombe and S. A. Piletsky, *Prog. Polym. Sci.*, 2014, **39**, 145–163.
- 44 J. P. Renault, A. Bernard, D. Juncker, B. Michel, H. R. Bosshard and E. Delamarche, *Angew. Chemie. Int. Ed.*, 2002, **41**, 2320–2323.
- 45 A. Turner and S. Piletsky, *Electroanalysis*, 2002, **14**, 317–323.
- 46 R. Schirhagl, *Anal. Chem.*, 2014, **86**, 250–261.
- 47 C. Algieri, E. Drioli, L. Guzzo and L. Donato, *Sensors*, 2014, **14**, 13863–912.
- 48 L. Li, X. Ying, J. Liu, X. Li and W. Zhang, *J. Appl. Polym. Sci.*, 2015, **132**, 1–9.
- 49 H. Nishino, C. S. Huang and K. J. Shea, *Angew. Chemie - Int. Ed.*, 2006, **45**, 2393–2396.
- 50 G. Vasapollo, R. Del Sole, L. Mergola, M. R. Lazzoi, A. Scardino, S. Scorrano and G. Mele, *Int. J. Mol. Sci.*, 2011, **12**, 5908–5945.
- 51 K. Eersels, B. Van Grinsven, A. Ethirajan, S. Timmermans, K. L. Jiménez Monroy, J. F. J. Bogie, S. Punniyakoti, T. Vandenryt, J. J. A. Hendriks, T. J. Cleij, M. J. A. P. Daemen, V. Somers, W. De Ceuninck and P. Wagner, *ACS Appl. Mater. Interfaces*, 2013, **5**, 7258–67.
- 52 D. M. Hawkins, D. Stevenson and S. M. Reddy, *Anal. Chim. Acta*, 2005, **542**, 61–65.
- 53 D. E. Hansen, *Biomaterials*, 2007, **28**, 4178–91.
- 54 M. K. Kempe M, *J Chromatogr*, 1995, **691**, 317–23.
- 55 M. J. Whitcombe and E. N. Vulfson, *Adv. Mater.*, 2001, **13**, 467–78.
- 56 W. Zhao, C. H. Cui, S. Bose, D. Guo, C. Shen, W. P. Wong, K. Halvorsen, O. C. Farokhzad, G. S. L. Teo, J. A. Phillips, D. M. Dorfman, R. Karnik and J. M. Karp, *Proc. Natl. Acad. Sci.*, 2012, **109**, 19626–31.
- 57 A. Mujahid, N. Iqbal and A. Afzal, *Biotechnol. Adv.*, 2013, **31**, 1435–1447.
- 58 L. H. Tan, P. H. Sykes, M. M. Alkaisi and J. J. Evans, *Int. J. Nanomedicine*, 2015, **10**, 4883–4895.
- 59 A. Sukswan, L. Lomlim, F. L. Dickert and R. Suedee, *J. Appl. Polym. Sci.*, 2015, **132**, 1–14.
- 60 R. J. Ansell, *Adv. Drug Deliv. Rev.*, 2005, **57**, 1809–1835.
- 61 O. Hayden and F. L. Dickert, *Adv. Mater.*, 2001, **13**, 1480–1483.
- 62 F. L. Dickert and O. Hayden, *Anal. Chem.*, 2002, **74**, 1302–1306.
- 63 O. Hayden, R. Bindeus, C. Haderspöck, K. J. Mann, B. Wirl and F. L. Dickert, *Sensors Actuators, B Chem.*, 2003, **91**, 316–319.
- 64 F. L. Dickert, O. Hayden, R. Bindeus, K. J. Mann, D. Blaas and E. Waigmann, *Anal. Bioanal. Chem.*, 2004, **378**, 1929–1934.
- 65 F. L. Dickert, P. Lieberzeit and O. Hayden, *Anal. Bioanal. Chem.*, 2003, **377**, 540–549.
- 66 M. Jenik, A. Seifner, P. Lieberzeit and F. L. Dickert, *Anal. Bioanal. Chem.*, 2009, **394**, 523–528.

- 67 K. Seidler, P. A. Lieberzeit and F. L. Dickert, *Analyst*, 2009, **134**, 361–366.
- 68 K. Seidler, M. Polreichová, P. A. Lieberzeit and F. L. Dickert, *Sensors*, 2009, **9**, 8146–8157.
- 69 H. Lee, D. Hong, J. Y. Choi, J. Y. Kim, S. H. Lee, H. M. Kim, S. H. Yang and I. S. Choi, *Chem. An Asian J.*, 2015, **10**, 129–132.
- 70 M. Jenik, A. Seifner, S. Krassnig, K. Seidler, P. A. Lieberzeit, F. L. Dickert and C. Jungbauer, *Biosens. Bioelectron.*, 2009, **25**, 9–14.
- 71 A. Ahmed, J. V. Rushworth, N. A. Hirst and P. A. Millner, *Clin. Microbiol. Rev.*, 2014, **27**, 631–46.
- 72 P. Qi, Y. Wan and D. Zhang, *Biosens. Bioelectron.*, 2013, **39**, 282–88.
- 73 T. Cohen, J. Starosvetsky, U. Cheruti and R. Armon, *Int. J. Mol. Sci.*, 2010, **11**, 1236–52.
- 74 L. M. Murray, V. Nock, M. M. Alkaisi, J. J. M. Lee and T. B. F. Woodfield, *J. Vac. Sci. Technol. B, Nanotechnol. Microelectron. Mater. Process. Meas. Phenom.*, 2012, **30**, DOI:10.1088/1758-5090/7/2/025002
- 75 O. Hayden, K. J. Mann, S. Krassnig and F. L. Dickert, *Angew. Chemie - Int. Ed.*, 2006, **45**, 2626–2629.
- 76 M. Lee, J. L. Thomas, M. Lai and H. Lin, *RSC Adv.*, 2014, **4**, 61557–61563.
- 77 H. Bao, B. Yang, X. Zhang, L. Lei and Z. Li, *Chem. Commun.*, 2017, **53**, 2319–2322.
- 78 I. E. Tothill, *Semin. Cell Dev. Biol.*, 2009, **20**, 55–62.
- 79 V. Perumal and U. Hashim, *J. Appl. Biomed.*, 2014, **12**, 1–15.
- 80 V. Murlidhar, PhD thesis, University of Michigan, 2016.
- 81 K. Eersels, B. Van Grinsven, T. Vandenryt, K. L. Jiménez-Monroy, M. Peeters, V. Somers, C. Püttmann, C. Stein, S. Barth, G. M. J. Bos, W. T. V. Germeraad, H. Diliën, T. J. Cleij, R. Thoelen, W. De Ceuninck and P. Wagner, *Phys. Status Solidi Appl. Mater. Sci.*, 2015, **212**, 1320–1326.
- 82 X. Zhou, J. Shi, F. Zhang, J. Hu, X. Li, L. Wang, X. Ma and Y. Chen, *Lab Chip*, 2010, **10**, 1182–1188.
- 83 J. J. Muys, M. M. Alkaisi, D. O. S. Melville, J. Nagase, P. Sykes, G. M. Parguez and J. J. Evans, *J. Nanobiotechnology*, 2006, **4**, 1.
- 84 F. Samsuri, M. M. Alkaisi, J. J. Evans, K. Chitcholtan and J. S. Mitchell, *Microelectron. Eng.*, 2011, **88**, 1871–1874.
- 85 J. Muys, M. Alkaisi and J. Evans, 2006 *Int. Conf. Nanosci. Nanotechnol.*, 2006, 294–297.
- 86 J. J. Muys, M. M. Alkaisi and J. J. Evans, *J. Biomed. Nanotechnol.*, 2006, **2**, 11–15.
- 87 F. Samsuri, J. S. Mitchell, M. M. Alkaisi and J. J. Evans, *AIP Conf. Proc.*, 2009, **1151**, 71–74.

- 88 L. M. Murray, V. Nock, J. J. Evans and M. M. Alkaisi, *J. Biomed. Mater. Res. - Part A*, 2016, **104**, 1638–1645.
- 89 H. Jeon and G. Kim, *Langmuir*, 2012, **28**, 13423–30.
- 90 N. Vigneswaran, F. Samsuri and K. N. Kalyani, *2014 Int. Conf. Sci. Eng. Manag. Res.*, 2014, 1–4.
- 91 S. M. Deporter, I. Lui and B. R. McNaughton, *Soft Matter*, 2012, **8**, 10403–10408.
- 92 N. Vigneswaran, F. Samsuri and K. N. Kalyani, *Biomed. Pharmacol. J.*, 2015, **8**, 337–43.
- 93 J. B. King and M. W. Robins, *Cancer Biology*, Pearson, London, Third., 2006.
- 94 V. DeVita, T. S. Lawrence and S. A. Rosenberg, *Cancer: principles & practice of oncology*, Wolters Kluwer Health/Lippincott Williams & Wilkins, Philadelphia, Ninth., 2011.
- 95 O. Kotrotsiou, K. Kotti, E. Dini, O. Kammona and C. Kiparissides, *J. Phys. Conf. Ser.*, 2005, **10**, 281–284.
- 96 P. Luliński, *Acta Pol. Pharm.*, 2013, **70**, 601–9.
- 97 M. Esfandyari-Manesh, B. Darvishi, F. A. Ishkuh, E. Shahmoradi, A. Mohammadi, M. Javanbakht, R. Dinarvand and F. Atyabi, *Mater. Sci. Eng. C*, 2016, **62**, 626–633.
- 98 J. Borovička, S. D. Stoyanov, V. N. Paunov, *MRS Proc.*, 2013, **1498**, 127–132.
- 99 J. Borovička, W. J. Metheringham, L. A. Madden, C. D. Walton, S. D. Stoyanov and V. N. Paunov, *J. Am. Chem. Soc.*, 2013, **135**, 5282–5285.
- 100 J. Borovička, S. D. Stoyanov and V. N. Paunov, *Nanoscale*, 2013, **5**, 8560–8568.
- 101 S. Wang, D. Yin, W. Wang, X. Shen, J.-J. Zhu, H.-Y. Chen and Z. Liu, *Sci. Rep.*, 2016, **6**, 22757.
- 102 L. Chen, H. Z. An, R. Haghgoie, A. T. Shank, J. M. Martel, M. Toner and P. S. Doyle, *Small*, 2016, **12**, 2001–2008.
- 103 W. Wang, H. Cui, P. Zhang, J. Meng, F. Zhang and S. Wang, *ACS Appl. Mater. Interfaces*, 2017, acsami.7b01147.
- 104 A. L. Bole and P. Manesiotis, *Adv. Mater.*, 2016, 5349–5366.
- 105 H. W. Hou, M. E. Warkiani, B. L. Khoo, Z. R. Li, R. A. Soo, D. S. W. Tan, W. T. Lim, J. Han, A. A. S. Bhagat and C. T. Lim, *Sci. Rep.*, 2013, **3**, 1–8.
- 106 J. M. Walker and R. Rapley, *Molecular biometrics handbook: Second edition*, 2008.
- 107 D. R. Gossett, W. M. Weaver, A. J. Mach, S. C. Hur, H. T. K. Tse, W. Lee, H. Amini and D. Di Carlo, *Anal. Bioanal. Chem.*, 2010, **397**, 3249–3267.
- 108 J. Chung, D. Issadore, A. Ullal, K. Lee, R. Weissleder and H. Lee, *Biomicrofluidics*, 2013, **7**, DOI:10.1063/1.4821923.
- 109 Z. Liu, F. Huang, J. Du, W. Shu, H. Feng, X. Xu and Y. Chen, *Biomicrofluidics*, 2013, **7**, 0118011 - 10.

- 110 H. S. Moon, K. Kwon, K. A. Hyun, T. Seok Sim, J. Chan Park, J. G. Lee and H. Il Jung, *Biomicrofluidics*, 2013, **7**, 0141051 - 9.
- 111 P. Allen, D. Barnett, D. Davies, U. Johansson, M. W. Lowdell, M. G. Macey, D. McCarthy, J. T. Reilly and G. Warnes, *Flow cytometry: Principles and A*, New Jersey, 1st edn., 2007.
- 112 M. Assenmacher, U. M. Behrens-Jung, S. C. Brown, C. Chen, C. Esser, J. A. Fantes, D. W. Galbraith, C. Gottlinger, D. K. Green, L. A. Herzenberg, S. P. Hinnisdaels, S. Irlenbusch, S. Jung, M. Kubbies, K. Kato, S. Lucretti, R. Manz, D. Marie, B. Mechtold, K. L. Meyer, S. Miltenyi, W. Muller, R. F. Murphy, U. Nohrenberg, F. J. Otto, A. Radbruch, G. Rothe, A. Scheffold, J. Schmitz, S. Schumacher, G. Siebenkotten, A. Tarnok, H. Ulrich, G. Valet, J. Veuskens, H. J. Vollmer and W. Weichel, *Flow cytometry and cell sorting*, Springer, Berlin, 2nd edn., 2010, ch. 1, pp. 3-25.
- 113 T. Hristozova, R. Konschak, V. Budach and I. Tinhofer, *Cytometry A*, 2012, 489–495.
- 114 J. S. Peper and R. E. Dahl, *Analyst*, 2015, **22**, 134–139.
- 115 H. Wang, G. Yue, C. Dong, F. Wu, J. Wei, Y. Yang, Z. Zou, L. Wang, X. Qian, T. Zhang and B. Liu, *ACS Appl. Mater. Interfaces*, 2014, **6**, 4550–4559.
- 116 A. Ring, N. Mineyev, W. Zhu, E. Park, C. Lomas, V. Punj, M. Yu, D. Barrak, V. Forte, T. Porras, D. Tripathy and J. E. Lang, *Oncotarget*, 2015, **6**, 44623–34.
- 117 W. He, H. Wang, L. C. Hartmann, J. X. Cheng and P. S. Low, *Proc. Natl. Acad. Sci. U. S. A.*, 2007, **104**, 11760–11765.
- 118 C. E. Nwankire, A. Venkatanarayanan, T. Glennon, T. E. Keyes, R. J. Forster and J. Ducreé, *Biosens. Bioelectron.*, 2015, **68**, 382–389.
- 119 X. Liu, L. Chen, H. Liu, G. Yang, P. Zhang, D. Han, S. Wang and L. Jiang, *NPG Asia Mater.*, 2013, **5**, e63.
- 120 C. H. Dr, G. Yang, Q. Ha, J. M. Dr and S. W. Prof, *Adv. Mater.*, 2015, **27**, 310–313.
- 121 S.-W. Lv, J. Wang, M. Xie, N.-N. Lu, Z. Li, X.-W. Yan, S.-L. Cai, P.-A. Zhang, W.-G. Dong and W.-H. Huang, *Chem. Sci.*, 2015, **6**, 6432–6438.
- 122 J. Zhang, S. Li, F. Liu, L. Zhou, N. Shao and X. Zhao, *PLoS One*, 2015, **10**, 1–9.
- 123 M. Darmostuk, S. Rimpelova, H. Gbelcova and T. Ruml, *Biotechnol. Adv.*, 2014, **33**, 1141–1161.
- 124 F. Zheng, Y. Cheng, J. Wang, J. Lu, B. Zhang, Y. Zhao and Z. Gu, *Adv. Mater.*, 2014, **26**, 7333–7338.
- 125 U. Dharmasiri, S. Balamurugan, A. A. Adams, P. I. Okagbare and S. A. Soper, 2010, **30**, 3289–3300.
- 126 M. Leitgeb, D. Nees, S. Ruttloff, U. Palfinger, J. Götz, R. Liska, M. R. Beleggratis and B. Stadlober, *ACS Nano*, 2016, **10**, 4926–4941.
- 127 L. J. Guo, *Adv. Mater.*, 2007, **19**, 495–513.
- 128 S. H. Ahn and L. J. Guo, *ACS Nano*, 2009, **3**, 2304–2310.
- 129 N. Kooy, K. Mohamed, L. T. Pin and O. S. Guan, *Nanoscale Res. Lett.*, 2014, **9**, 1–13.

- 130 A. V. Shneidman, K. P. Becker, M. A. Lukas, N. Torgerson, C. Wang, O. Reshef, M. J. Burek, K. Paul, J. McLellan and M. Lončar, *ACS Photonics*, 2018, **5**, 1839–1845.
- 131 T. W. Odom, J. C. Love, D. B. Wolfe, K. E. Paul and G. M. Whitesides, *Langmuir*, 2002, **18**, 5314–5320.
- 132 P. Yi, H. Wu, C. Zhang, L. Peng and X. Lai, *J. Vac. Sci. Technol. B, Nanotechnol. Microelectron. Mater. Process. Meas. Phenom.*, 2015, **33**, 060801.
- 133 M. Hermansson, *Colloids Surfaces B Biointerfaces*, 1999, **14**, 105–119.
- 134 H. Hayashi, S. Tsuneda, A. Hirata and H. Sasaki, *Colloids Surfaces B Biointerfaces*, 2001, **22**, 149–157.
- 135 P. K. Sharma and K. Hanumantha Rao, *Colloids Surfaces B Biointerfaces*, 2003, **29**, 21–38.
- 136 D. Myers, *Surfaces, Interfaces and Colloids — Principles and Applications*, 2nd ed., Wiley-VCH, New York, 1999, vol. 51, ch 4 and 5, 2000, pp. 40-96.
- 137 J. A. L. Kemps and S. Bhattacharjee, *Langmuir*, 2005, **21**, 11710–11721.
- 138 D. Guo, G. Xie and J. Luo, *J. Phys. D. Appl. Phys.*, 2014, **47**, 013001 - 25.
- 139 J. Borovička, S. D. Stoyanov and V. N. Paunov, *Phys. Rev. E - Stat. Nonlinear, Soft Matter Phys.*, 2015, **92**, 22–24.

2. Experimental

In this chapter, the materials and experimental procedures used throughout this research project are described.

2.1. Materials

2.1.1. Water

Water was purified by passing through an Elgastat Prima Reverse Osmosis Unit followed by a Millipore MilliQ reagent water system consisting of one carbon filter and two ion-exchange filters.

2.1.2. Solvents

The solvents methanol ($\geq 99.8\%$), ethanol ($\geq 99.8\%$) and acetone ($\geq 99.8\%$) for cleaning glassware, microscope slides were all analytical grade and purchased from VWR Chemicals. Biological samples were cleaned using 70% ethanol in MilliQ water.

2.1.3. Cell lines and processing

2.1.3.1. Immortalised cell lines

Immortalised human cell lines HL60 (AML), Jurkat E6.1 (T-lymphocyte) and MOLT-4 (ALL) cell lines were purchased as frozen cultures from Public Health England.

2.1.3.2. Human donor blood

Whole blood samples (40 ml) were harvested in the Phlebotomy Department at the Queen's Centre for Haematology and Oncology, Castle Hill Hospital, Hull and East Yorkshire NHS Trust, United Kingdom. Samples were collected from patients diagnosed with Acute Myeloid Leukaemia (AML) prior to chemotherapy and from sufferers of Chronic Lymphoblastic Leukaemia (CLL) deemed in the remission phase of the condition. Patient identity and further data were available only to clinicians involved in

this project. Ethical approval for the study was granted by the Hull and East Riding Research Ethics Committee (REC reference number 08/H1304/35). In accordance with GCP, informed consent was taken from each participant prior to being enrolled into the research stream.

2.1.3.3. Microorganisms

Saccharomyces Cerevisiae (Baker's yeast) were purchased from Sigma-Aldrich.

2.1.3.4. Cell media

Immortalised cell lines were cultured in Roswell Park Memorial Institute Medium (RPMI) 1640 containing L-glutamine (Gibco), with added 10% foetal bovine serum (Gibco), 10 ml penicillin (Gibco) and 10 ml streptomycin (Gibco). Phosphate buffer saline (PBS, Gibco) solution was made in deionised water, yielding a pH of 7.4. Freezing media made of 10% dimethyl siloxane (DMSO, Sigma-Aldrich) in PBS solution. Cells were frozen in 10% v/v dimethylsiloxane (DMSO, Sigma-Aldrich) in PBS. Lymphoprep Ficoll-Paque density gradient was purchased and used as received from StemCell technologies. Yeast were cultured in media comprising peptone (2% w/v, Fisher), yeast extract (1% w/v, Sigma-Aldrich) and D-glucose (2% w/v, Sigma-Aldrich) in MilliQ water.

2.1.3.5. Cell fixation agents

Paraformaldehyde and glutaraldehyde were purchased from Sigma-Aldrich.

2.1.4. Particles

Monodisperse cross-linked PMMA microparticles of three discreet sizes, $10 \pm 1 \mu\text{m}$, $15 \pm 1 \mu\text{m}$ and $20 \pm 2 \mu\text{m}$, (CA10, CA15 and CA20) were used as purchased from Spheromers (Norway).

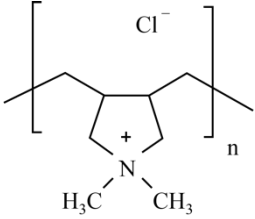
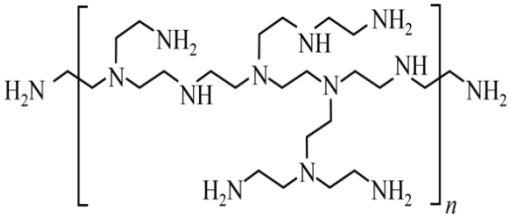
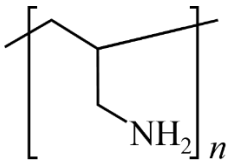
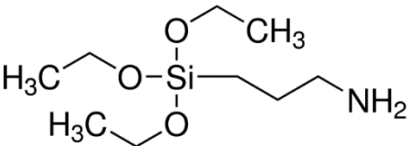
2.1.5. Imprinting materials

Xanthan gum was purchased from Sigma-Aldrich and used at 0.1 % (w/v) in water to increase the viscosity of cell suspensions being spread in glucose solutions. Hydroxypropylmethylcellulose (HPMC) was purchased from Sigma-Aldrich and used at 5 mM in PBS.

Sylgard 184 polydimethylsiloxane (PDMS) was purchased from Dow Corning and was used in a 10:1 mixture of elastomer to accelerator. To provide structural support to large PDMS bioimprints, a synthetic fabric sheet (Boyes UK, dimensions 65 cm × 30 cm × 0.1 cm) was added to the curing PDMS. UV curable polyurethane photoresist and rolls of polyethylene terephthalate (PET) sheet (1 mm thick) were gifts from the Joanneum Research Forschungsgesellschaft, Weitz, Austria. Norland Optical Adhesive 68 (NOA 68) was used as received from Norland Products Incorporated; cured by UV irradiation from 2 × 6 W lamps at a distance of 5 cm.

2.1.6. Charged materials

Table 2.1 Charged materials used throughout the project with their molecular weights, structures, and supplier.

Polyelectrolyte	Average MW (g mol ⁻¹)	Structure	Supplier
Poly (diallyldimethylammonium chloride) (PDAC)	200,000 - 350,000		Sigma-Aldrich
Polyethyleneimine (PEI)	~ 10,000		PolySciences Inc.
Poly (allylamine hydrochloride) (PAH)	~ 15,000		Sigma-Aldrich
(3-Aminopropyl) triethoxysilane (APTES)	221		Sigma-Aldrich

2.1.7. Dyes

Trypan blue was used as received from Lonza as 0.04% (w/v) in water for cell viability assays. As trypan blue is able to partition the membrane of dead cells, it was also used to identify fixed cells during optical microscopy.¹⁻³

Lipid conjugated fluorescent dyes 1,2-dioleoyl-sn-glycero-3-phosphoethanolamine-N-(lissamine rhodamine B sulphonyl) (ammonium salt) and 1,2-dioleoyl-sn-glycero-3-phosphoethanolamine N(carboxyfluorescein) were purchased from Avanti Lipids and used in 0.025% (w/v) in ethanol. Both are common fluorophores conjugated to a long chain lipid; these were used to avoid leaching of fluorescent dyes between cell types.

Stilbene 420 (Sigma Aldrich) was used in 0.01% (w/v) solution in MilliQ water. Carboxyfluorescein succinimidyl (CFSE) proliferation kits (Thermo Fisher) were diluted to a 0.1 (w/v) % solution and used to fluorescently tag living cells.⁴ Cell staining was carried out aseptic conditions in a biosafety cabinet class II with laminar flow (MSC-AdvantageTM, Thermo Scientific)

2.1.8. Miscellaneous

Potassium hydroxide (< 99.9%) was purchased from Fisher Scientific and used in 10% (w/v) in MilliQ water for cleaning glass substrates.

Cell culture areas were kept aseptic using Neodisher LaboClean A8 used at 0.5% (w/v) in MilliQ water and trigene. Both purchased from VWR, UK. For safe disposal, biological waste was added to Rely⁺On Virkon disinfectant, purchased from Du Pont and used at 1% (w/v) in MilliQ water.

2.2. Methods

2.2.1. Cell line handling

This section details the procedures used to handle and process cell lines and samples used throughout the project.

2.2.1.1. Immortalised cell line culture

All live cell culture and handling were carried out aseptically in a biosafety cabinet class II with laminar flow (MSC-Advantage™, Thermo Scientific). Prior to use the culture hood was irradiated with UV light (220 nm, 40 minutes) then wiped thoroughly with trigen disinfectant solution and 70% ethanol. Cell passaging equipment was purchased pre-sterilised or autoclaved (Classic, Prestige Medical) and wiped with 70% ethanol prior to introducing to the culture hood.

Immortalised cell lines were cultured by suspending in Roswell Park Memorial Institute (RPMI) 1640 media containing foetal bovine serum (FBS) (10% v/v), penicillin (2% v/v) and streptomycin (2% v/v). Media was warmed to ~ 37 °C before use and stored in the refrigerator (4 °C) between passages. Spent media was removed by centrifugation at 400 g for 4 minutes and suspensions of 5×10^5 cells in 25 ml of media were incubated in 75 cm² growth area (T75) tissue culture flasks (Sarstedt) at 37 °C and 5% CO₂ in a humidified atmosphere. Mechanical or enzymatic dissociation from growth vessels was not required as the cells grow in suspension culture. All tissue culture consumables were sterile prior to use; single use flasks and equipment were purchased pre-sterilised and glassware were autoclaved at 121 °C for 15 minutes.⁵

Aliquots of HL60, Jurkat and MOLT-3 cells were preserved by storing in the liquid phase of liquid nitrogen. Samples were frozen at a concentration of 1×10^7 cells ml⁻¹ in 1 ml of 10% dimethyl sulfoxide (DMSO) in FBS. Ampules were placed in a Mr Frosty Freezing Container (Thermo Scientific) containing propan-1-ol and frozen at -80 °C for minimum of 24 hours, then transferred to liquid nitrogen storage.

2.2.1.2. Whole blood fractionation

Whole blood samples were harvested from donors at the Queen's Centre for Oncology and Haematology at Castle Hill Hospital, Hull and East Yorkshire NHS Trust, United Kingdom. A dichotomy of sample types were received firstly, from apparently healthy and AML sufferers. The former from donors deemed in the remission phase of Chronic Lymphocytic Leukaemia (CLL), the latter from AML sufferers immediately prior to chemotherapy.

Peripheral Blood Mononuclear Cells (PBMCs) were extracted from whole blood by Ficoll-Paque density centrifugation. Blood samples (40 ml) were diluted with equal volumes with sterile Phosphate Buffer Saline (PBS) solution and added dropwise to the surface of Lymphoprep (15 ml, STEMCELL Technologies) density gradient media. Prior to use, PBS was sterilised by autoclaving at 121 °C for 15 minutes. Samples were centrifuged at 4 °C, 400 g for 30 minutes with no brake. The 'buffy coat' (phase between plasma and gradient media) was decanted and washed in PBS solution. Platelet contamination was removed by centrifugation at 120 g for 10 minutes and resuspension in PBS, done three times. Figure 2.1, below, shows a whole blood sample after density centrifugation. Distinct layers of plasma, buffy coat, density gradient media and erythrocytes can be seen.

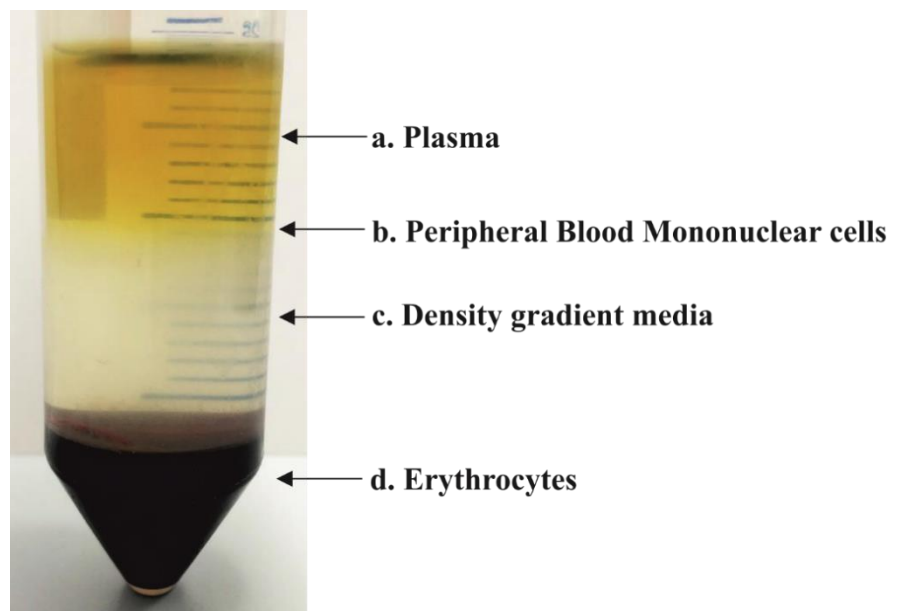


Figure 2.1 Whole blood sample after density centrifugation. Blood sample taken from an apparently healthy donor centrifuged at 400 g for 30 minutes with no brake. Distinct

layers are present in blood of a) plasma, b) 'buffy coat' containing PBMCs, c) density gradient media and d) erythrocytes.

2.2.1.3. Yeast

Yeast from *Saccharomyces cerevisiae* (Sigma) were cultured in media comprised of peptone (2% w/v), yeast extract (1% w/v) and D-glucose (2% w/v) in MilliQ water. Cultures were incubated at ~ 36 °C, agitated by stirring. Before addition of yeast, media solutions were autoclaved to reduce risk of contamination. All culture materials were used pre-sterilised or flame treated. The culture area was washed before and after passage with 70% ethanol solution.

2.2.1.4. Cell fixation

Chemical fixation was trialled using ethanol, methanol, an ethanol and methanol (1:1) mixture, paraformaldehyde (4% w/v) and glutaraldehyde (2.5% w/v) for a period of 1 hour. After flow cytometry comparison of cell size and shape with unfixed populations, all fixation was done by dropwise addition of cell suspension in PBS (10 ml) to a stirred 0.5% (v/v) glutaraldehyde (100 ml) solution. Glutaraldehyde was removed by centrifugation at 400 g for 4 minutes, the supernatant discarded and replaced with fresh PBS. Fixed cells were washed three times prior to use.

2.2.1.5. Cell analysis

While passaging, cell counts and viability assessments were carried out manually by diluting suspensions in a 0.04% (w/v) trypan blue solution imaged on an improved Neubauer haemocytometer (Hawksley). For further experiments, automatic counting was done with a Cellometer AutoX4 cell counter (Nexcelom). Viability was assessed automatically by addition of 1 mM fluorescein diacetate (FDA) and fluorescently active cells counted. Here, viability was given as a percentage of fluorescent (live) cells over the total number counted automatically counted by bright field microscopy.

Flow cytometry was carried out using a FACSCalibur device (BD Biosciences) in conjunction with CellQuest software (V.6).

2.2.2. Bioimprint production

This section details the protocols used to produce and replicate bioimprints.

2.2.2.1. Bioimprints produced replicating cells deposited using Cytospin centrifuge

Microscope slides (Menzel-Gläser, Thermo Scientific, dimensions 72 x 26 mm) were used as a substrate on which to deposit cell suspensions. Glass slides were washed by immersion in acetone, ethanol and MilliQ water and dried in air. Substrates were functionalised using oxygen plasma (32 W, 147 Pa) for 180 seconds and immersion in 20% w/v poly(diallyldimethylammonium chloride) (PDAC) for 1 hour. Excess PDAC was removed by immersion in ethanol and MilliQ and dried between and after immersions using compressed air.

Template cells or particles were deposited via cytopspin centrifuge (Shandon Cytospin III, Thermo Scientific). Cell or particle suspensions (1.5 ml in MilliQ water) were loaded into the cytofunnel, as seen in Figure 2.2 a) with filter card cut to leave a rectangular aperture (38 mm × 20 mm). Centrifugation was carried out at 450 g for 2 minutes with a cell concentration of 2×10^7 cells ml⁻¹. Sylgard 184 polydimethylsiloxane (PDMS) was mixed (10:1 ratio of elastomer to accelerator) was poured onto the deposited cell multilayers and allowed to cure at 30 °C for 48 hours. After curing, the glass substrate and PDMS were separated yielding a bioimprint (dimensions of 38 mm × 20 mm). Cell debris was washed from the bioimprint by application and removal of adhesive tape and subsequently rinsed with surfactant solution and by sonication in ethanol.

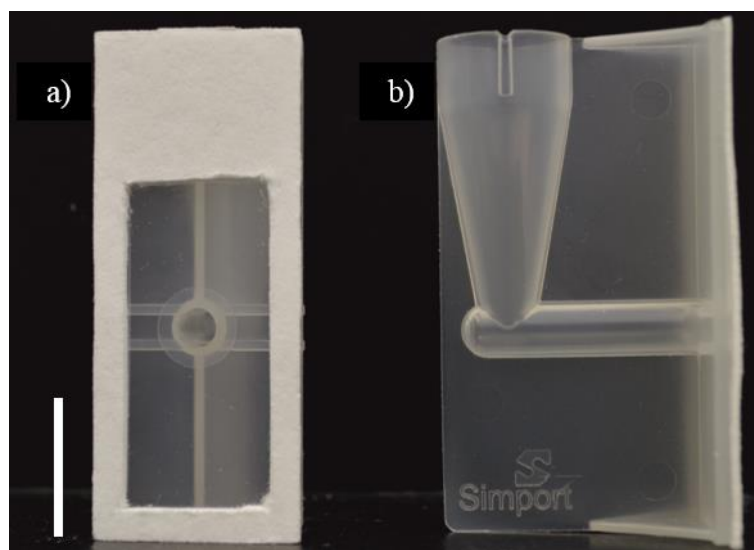


Figure 2.2 Cytospin cytofunnel showing a) the extended aperture cut to increase surface area (38 mm × 20 mm) of bioimprints b) Side-on view of the cytofunnel showing the inlet and outlet position. Scale bar represents 2 cm.

2.2.2.2. Positive imprints

Positive imprints were cast by curing UV photoresist in on the bioimprint surface. NOA 68, Norland Adhesive (20 μ l) was spread on a glass substrate and pressed against the bioimprint surface. The system was exposed to UV light ($\lambda = 365$ nm, 2×6 W lamps, distance of 5 cm) for 1 hour. The PDMS was peeled from the positive imprint and both the negative and positive cleaned with ethanol and MilliQ water.

A proprietary polyurethane (PU) resin-based photoresist, received from the Joanneum Institute, was also used to make positive imprints cured for 30 minutes under the same UV conditions.

2.2.2.3. Glucose protective layer imprints

Glass substrates (70 cm × 40 cm) were cleaned with acetone and 10% potassium hydroxide (Sigma Aldrich) for 1 hour, rinsed with MilliQ water and treated with 20% v/v poly(diallyldimethylammonium chloride) (PDAC) for 30 minutes. Substrates were cleaned with MilliQ water and dried with compressed air.

Fixed HL60 cells (6 g wet weight) and glucose (2.5 g) were spread in a 0.1% (w/v) xanthan gum solution. Spreading was done using a bespoke glass tool comprised of a square made of four glass strips, one of which was offset by 100 μm . Figure 2.3 shows the design and method of action of the spreading tool. Cell suspension was added to the squares interior and the device was moved along the substrate in one continuous motion in the direction opposite to the higher side, allowing a film (40 cm \times 70 cm) of uniform thickness to be deposited. The film of cells were allowed to dry at room temperature in a laminar flow cabinet to avoid contamination.

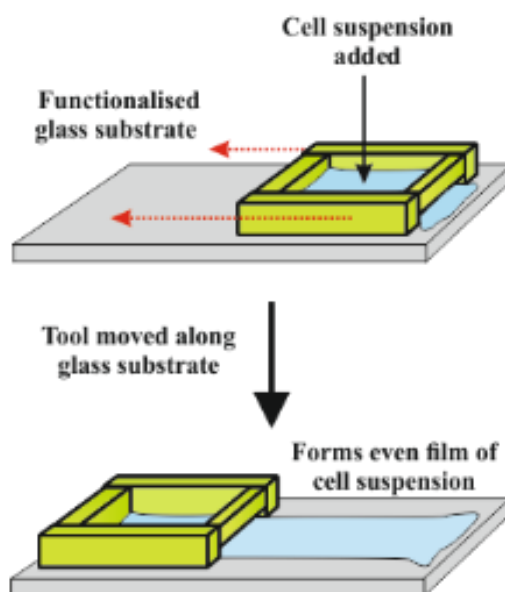


Figure 2.3. Schematic showing how a bespoke tool spreads cell or particulate suspension to yield a relatively even, large area film.

A frame (interior space 70 cm \times cm 40 cm \times 4 cm) was added around the deposited cells and PDMS (900 ml) poured evenly and allowed to dry at room temperature for 48 hours. Curable PDMS was mixed at a 10:1 ratio of Sylgard 184 elastomer to accelerator and degassed by centrifugation (1000 g, 10 minutes). To provide structural support, a synthetic fabric sheet (Boyes UK, dimensions 70 cm \times 40 cm \times 0.1 cm) was added to the curing PDMS. Cured bioimprints were removed from the glass surface and washed using warm water then ethanol and MilliQ dried using compressed air.

2.2.2.4. Glucose solution positive imprints

Cleaned bioimprints were treated with 0.1% (w/v) hydroxypropyl methylcellulose (HPMC) in (5 mM in PBS) and layered with UV curable polyurethane resin using a glass spreading tool (see 2.2.2.3).

The PET sheet of similar dimension to the PDMS imprint was also layered with polyurethane using the same glass tool with 60 μm clearance. The polyurethane coated PET foil was carefully placed over the PDMS imprint clipped from both sides and was pressed uniformly using a glass tool to rid any trapped air. It was cured using UV lamps for 30 minutes through two glass panes used as weight for uniform contact between the PDMS and the polyurethane. A schematic of the overall process is shown below in Figure 2.4.

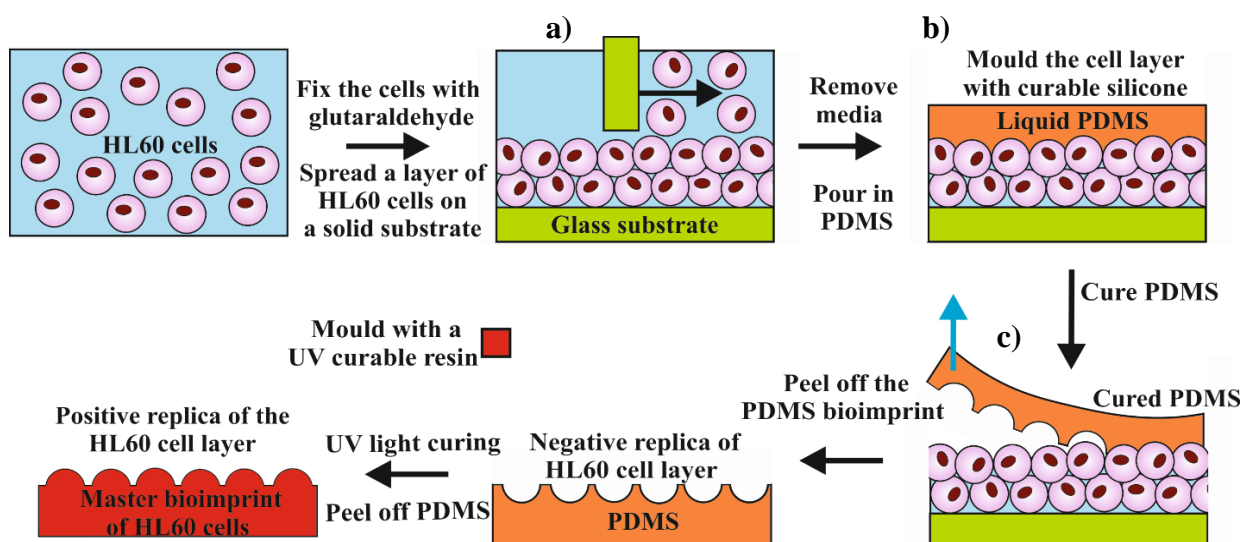


Figure 2.4 Schematic representation of negative and positive bioimprint production. a) Fixed HL60 cells are spread in glucose solutions on glass substrates b) Liquid PDMS is added to the cell layers and allowed to cure; c) PDMS can be separated from the glass and further used to produce positive imprint.

2.2.2.4.1. Replication of bioimprints by Roll-to-Roll printing

Roll-to-Roll nanoimprint lithography (R2RNIL) was done in collaboration with Joanneum Research Forschungsgesellschaft mbH, Austria.⁶ Herein, the bioimprint to be copied was applied to the circumference of an imprinting cylinder. This shim was rolled and pressed against a polyethylene terephthalate (PET) with a film (thickness $\sim 100 \mu\text{m}$)

of UV photoresist, cured by a 2.2 W cm^{-2} mercury vapour lamp. R2RNIL was done at 1 m s^{-1} for a used defined length.

When copying imprints produced by the cyto-centrifugation method, bioimprints ($2 \text{ cm} \times 2 \text{ cm}$) were used sequentially to produce positive imprints in NOA 68. Each copy was made adjacent to the last yielding a grid of positive imprints of $10 \text{ cm} \times 10 \text{ cm}$. In turn, the $10 \text{ cm} \times 10 \text{ cm}$ grid was copied by plate-to-plate lithography and sequentially added to the circumference of an imprinting drum (dimensions $30 \text{ cm} \times 10 \text{ cm}$). Between positive-negative replications, NOA 68 positive imprints were coated with evaporated gold (thickness of $\sim 50 \text{ nm}$). Replicas of $0.1 \times 50 \text{ m}$ were produced from bioimprints made via the cytospin centrifuge method.

Bioimprints made via the spreading of cells from glucose suspensions were able to be produced in a significantly larger size such that a single imprint (dimensions $40 \text{ cm} \times 70 \text{ cm}$) was mounted the imprinting shim. Replica bioimprints of dimensions $0.4 \text{ m} \times 100 \text{ m}$ were made.

2.2.2.5. Assessment of the bioimprint topology

Qualitative assessment of the surface topology and coverage was carried out using bright field and scanning electron microscopy (SEM). The former done with an Olympus BX51 microscope coupled with a DP70 camera and ImageProPlus and the latter a Hitachi TM-1000 benchtop or a Zeiss Evo 60. Prior to being analysed, all samples were coated with $\sim 100 \text{ nm}$ of gold by evaporation. SEM analysis was carried out both from perpendicular to the bioimprint surface and also with the sample tilted by 70° to yield images with a deeper perspective of the imprinted cavities.

The length mean diameter [1,0] of bioimprint cavities were measured in ImageJ using high resolution SEM images. Each measurement was taken horizontally at the widest part of the imprinted cavity to reduce the influence of the non-symmetrical shape. The process was repeated using fixed cell or particle suspension to enable a comparison of the template material and bioimprints produced.

Tapping mode atomic force microscopy scanning was carried out using a Dimension Edge (Bruker) with TESPA-V2 probes (Bruker). A scan rate of 0.1 Hz was used with 1024 or 512 lines for a $50 \mu\text{m}$ scan range.

2.2.3. Bioimprint surface modification

PDMS bioimprints were functionalised by exposure to oxygen plasma (Harrick Plasma PDC-32G) at 147 Pa, using an RF power of 16 W. To characterise the wetting properties of functionalised substrates, the contact angle of a sessile water drop was measured on unimprinted PDMS and polyurethane substrates. PDMS surfaces were made from a 10:1 mixture of Sylgard 184, degassed at 4000 g and poured into petri dish (10 cm × 10 cm × 1 cm) to cure for 48 hours at room temperature. Samples were cut into 2 × 2 cm tiles washed by sonication in absolute ethanol for 5 minutes, and then dried in air.

Contact angles were measured via a Krüss Drop Shape Analysis System DSA10 MK2 goniometer. The angle between the flat surface and the tangent of the water drop was measured with the angle left and right side of each drop averaged. The Laplace-Young method was used to calculate the contact angle. Each measurement was repeated three times using fresh MilliQ water droplets. See Figure 2.5, below, where contact angle of water on functionalised PDMS substrates was measured. Between measurements, the water drop was removed and the surface dried in air. Subsequently, PDMS bioimprints were exposed to 20% (w/v) aqueous (3-aminopropyl)triethoxysilane (APTES) for 30 minutes. Substrates were washed by sonication in ethanol for 5 minutes and dried in air.



Figure 2.5 Contact angle measurement of a sessile drop of MilliQ water on PDMS substrates.

The hydrophobic recovery of PDMS after oxygen plasma functionalisation was examined by contact angle measurements at 30-minute intervals after treatment. Substrates were stored in MilliQ water between measurements and dried in air.

Bioimprints replicated via roll-to-roll printing were functionalised to incur an attraction between target cells and bioimprints. Polyelectrolyte polyethyleneimine, (PEI, 0.1 – 0.9% w/v) a cationic polyelectrolyte with low toxicity, was spread in mixtures with uncured UV photoresist (0.9 – 0.1% w/v) from ethanol solutions. Spreading was done with a glass tool as seen when spreading cell suspension (see section 2.2.2.3) whereby square of four glass strips was made. In this instance, the tool did not have one side offset in order to form a thinner uniform film (height $\sim 10\ \mu\text{m}$).

Polyelectrolyte and UV photoresist solution in ethanol (5 ml) was added to the centre of a square frame (without a gap) and the tool moved across the imprinted substrate. As the PU and bPEI comprised 1 % of a film spread $\sim 10\ \mu\text{m}$ thick, the added layer was predicted to be $< 0.1\ \mu\text{m}$ thick. After evaporation of the ethanol, the photoresist was cured for 20 minutes with UV light (365 nm, $2 \times 6\ \text{W}$, at a distance of 30 cm). Figure 2.6 shows the immobilisation of the cationic polyelectrolyte bPEI on the bioimprint surface by steric entanglement in a PU matrix.

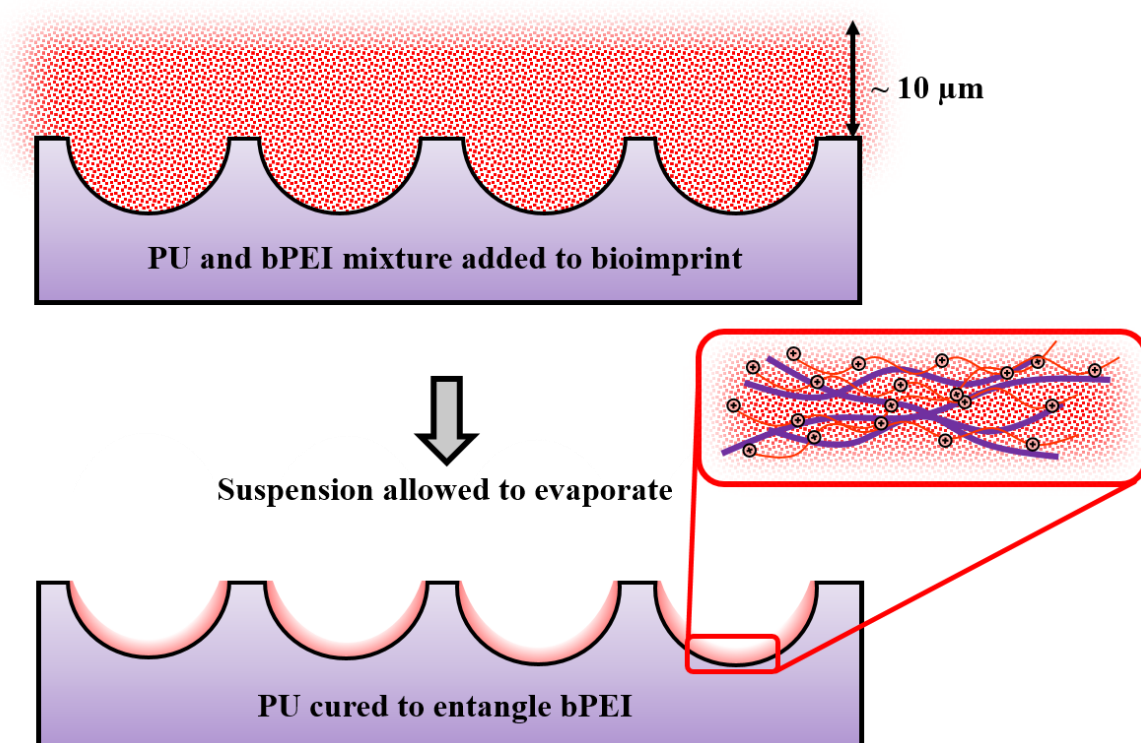


Figure 2.6 Schematic showing how thin films of cationic polyelectrolyte can be deposited and retained to bioimprints by spreading and entrapment in trace amounts of polymer matrix.

The proportion of bPEI to PU was investigated with the overall concentration of additive in ethanol remaining 1% (w/v). See Table 2.2, below, details the concentrations of bPEI and PU in ethanol solutions used to functionalise polyurethane bioimprints.

Table 2.2 Bioimprint functionalisation solutions. Concentrations of polyelectrolyte (bPEI) and non-cured resin (PU) in ethanol solutions used to functionalise bioimprints. Overall additive concentration was kept at 1% w/v.

[bPEI] /wt.%	PU / wt.%
0.9	0.1
0.75	0.25
0.5	0.5
0.25	0.75
0.1	0.9
0	1

2.2.4. Bioimprint cell retention study

This section will detail experiments to investigate the bioimprints ability to retain cell populations when exposed to single and binary cell suspensions.

2.2.4.1. Fluorescence staining and microscopy

Cell populations were fluorescently labelled to allow numeration and identification of cells retained to bioimprints. HL60 cells were stained by dropwise addition of 100 μ l of 0.025% (w/v) 1,2-dioleoyl-sn-glycero-3-phosphoethanolamine N(carboxyfluorescein) in ethanol. PBMCs were stained in via a similar method with 1,2-dioleoyl-sn-glycero-3-phosphoethanolamine-N(lissamine rhodamine B sulphonyl) (ammonium salt). Excess dye was removed by washing and replacing media with PBS. An Olympus BX51 microscope coupled with a mercury excitation source, DP70 camera and ImageProPlus was used to capture images of cell populations.

2.2.4.2. Cell retention examination

Cell suspensions (20 μ l) were incubated on the bioimprint surface, retained in place by adding a clean glass cover slip. After a period of 1 hour, the coverslip was removed and the unbound cells removed from the imprint by immersion in MilliQ water. A fresh coverslip was then placed to prevent drying. Bright field and fluorescence microscopy of various sites ($n = 20$) was captured.

Initially, cell populations were counted manually from bright field images with cells indicated by trypan blue staining. This progressed on to automatic numeration in ImageJ; the threshold was adjusted and binary images made prior to counting. Cells were counted using a macro created in ImageJ which thresholded and made each image binary. Conjoined cells were separated by the watershed function. Cells could be counted using binary images showing fluorescent features seen as black on a white background. A lower boundary of cell size was used to prevent fluorescent cell fragments and debris being counted as a whole cell, this was found from analysis of fluorescently tagged cell populations. Results were compared as the average number of cells per metre squared, hereafter termed the cell area density.

2.2.4.3. Flow cell experiments

Bioimprints were incorporated into flow-through chips made from a glass slide and a moulded PDMS channel. PDMS strips ($3 \times 6 \times 1$ cm) were made yielding an exposed channel ($0.5 \times 4 \times 0.1$ cm) which was punctured to allow inlet and outlet tubing to be fed (internal diameter 1 mm). The PDMS substrate and a clean glass microscope slide were treated in oxygen plasma (32 W, 147 Pa) for 2 minutes. A sample of functionalised bioimprint (0.5×4 cm) was trapped between the activated glass and PMDS substrates, with the bioimprint in the embossed channel. The system was clamped to ensure a seal and cured at 40 °C for 30 minutes. See Figure 2.7, below, for a schematic of the flow chip design and an image of a prepared HL60 bioimprint chip.

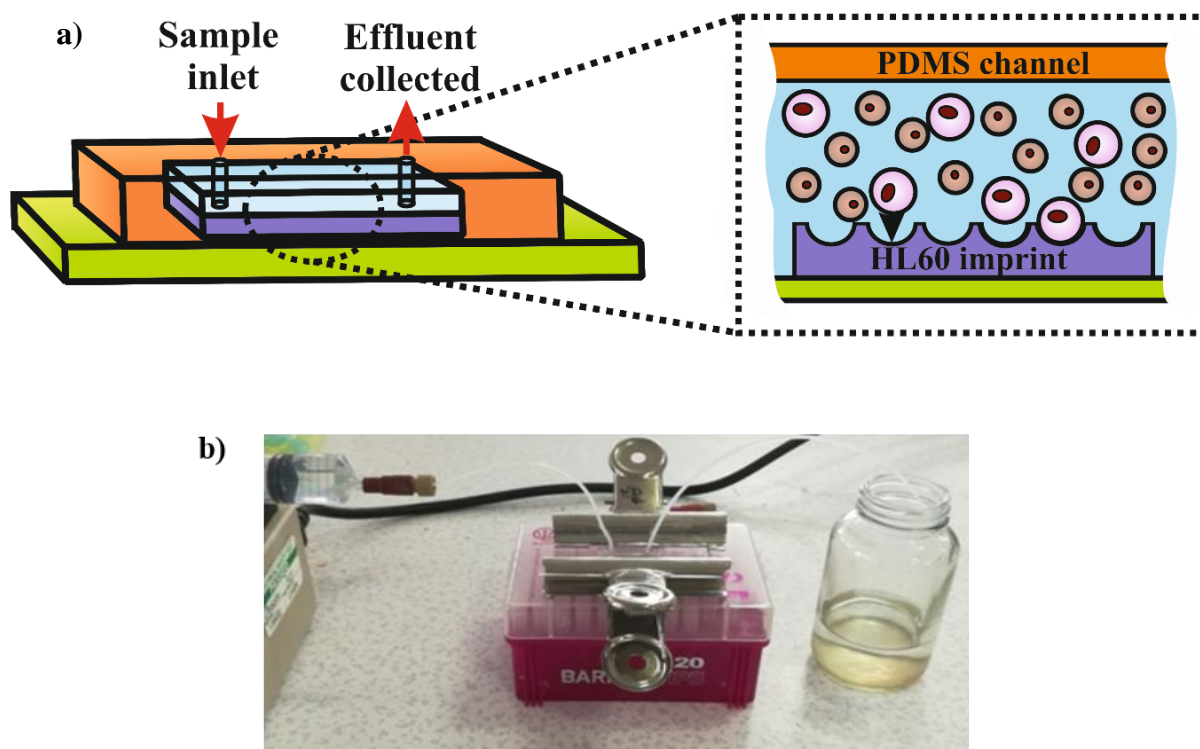


Figure 2.7 Flow-through chips used to examine retention of cells to bioimprints. a) Schematic representation of the method of action of the flow through chip. b) Photograph of prepared flow-through chips containing HL60 bioimprints.

Retention of fixed HL60 cells was investigated as a function of the seeded cell suspension concentration for a range of substrate functionalisation parameters. Suspensions of fluorescently tagged, fixed, HL60 cells in MilliQ water (100 μ l) were made at a range of concentrations. Cell samples were injected into flow-through chips containing HL60 imprints and left for 1 hour. Inlet and outlet tubing (internal diameter 1 mm) was fitted to opposite ends of the bioimprint. Unbound cells were washed from the bioimprint by elution of MilliQ water (10 ml, 100 ml h^{-1}). Retention of HL60 cells was assessed by bright field and fluorescence microscopy at various sites across the bioimprint ($n = 20$).

Cells were enumerated via the automatic method in ImageJ, described previously. This was done using images collected using fluorescein isothiocyanate (FITC) and tetramethylrhodamine isothiocyanate (TRITC) filter sets in order to separately assess each cell type collected at each site. Selectivity experiments characterised the numbers of each cell type retained to bioimprints.

2.2.4.4. Selectivity studies

The bioimprints preference towards HL60 cells from binary mixtures with PBMC was investigated. Suspensions of a fixed overall concentration (20×10^6 cell ml⁻¹) were made with different ratios between the cell types: 10:90, 25:75, 50:50 and 75:25 for HL60:PBMC. Cell samples were injected into flow-through chips containing HL60 imprints and left for 1 hour. Inlet and outlet tubing (internal diameter 1 mm) was fitted to opposite ends of the flow through chip. Unbound cells were washed from the bioimprint by elution of MilliQ water (10 ml, 100 ml h⁻¹). Quantification and identification of retained cells was done by fluorescence microscopy using FITC and TRITC filters for HL60 and PBMCs respectively. The study was repeated for various bPEI functionalisation concentrations.

The effect of column length on selectivity was investigated. Flow through chips containing bioimprints of: 2, 4, and 8 cm exposed to binary cell suspensions.

2.3. References

- 1 W. Strober, Trypan Blue Exclusion Test of Cell Viability. *Current Protocols in Immunology*, John Wiley and Sons, Inc., New York, 2001, pp. 221 - 229.
- 2 S. Atlman, L. Randers and G. Rao, *Biotechnol. Prog.*, 1993, **9**, 671–674.
- 3 A. Tholudur, L. Giron, K. Alam, T. Thomas, E. Garr, G. Weatherly, K. Kulowiec, M. Quick and S. Shepard, *Bioprocess Int.*, 2006, 28-34.
- 4 M. W. Wessendorf and T. C. Brelje, *Histochemistry*, 1992, **98**, 81–85.
- 5 S. Collins, *Blood*, 1987, **70**, 1233-1244.
- 6 M. Leitgeb, D. Nees, S. Ruttloff, U. Palfinger, J. Götz, R. Liska, M. R. Belegatis and B. Stadlober, *ACS Nano*, 2016, **10**, 4926–4941.

3. Fabrication of Bioimprints

This section details the capture of size and shape information from template cells and microparticles into a polymer matrix in order to fabricate bioimprints. The bioimprinting procedure used throughout this project followed a similar rationale to the whole cell bioimprinting reported by Dickert (2002).¹ The technique involved depositing and immobilising a layer of the template material to a substrate to form a cell ‘stamp’. The stamp was then embossed into a pre-polymer matrix capturing the topography of the attached biomaterial. The quality of the retained cell layer was critical as it forms the print positive of the bioimprint. Cells needed to be densely packed on the surface to produce a bioimprint with a good spatial efficiency; having more binding sites per area. It was also important that the layer of cells did not dry out sufficiently to cause cracks in the film, yielding areas un-patterned or with cell aggregates of multiple layers. Numerous methods were trialled to reproducibly produce dense and uniform coverage of the substrate.

When designing a protocol to produce an even, densely packed area of cells it was important to consider the nature of the cavities being produced. The size and shape of the cell cavities produced is key to the success of a highly selective cell capture device. Even by using the same template cells, a variation in size can arise dependent on the proportion of the cell exposed to the curing polymer. By varying the proportion of the cell that pressed against the curing print surface, the size of the resultant cell cavity could vary significantly even for monodisperse cell samples. Firstly, if too little of the cell is exposed, the cell cavity produced would be too shallow and will offer unsatisfactory surface contact to an identical cell when the imprint is exposed to cell suspensions. Conversely, too great a coverage will yield cell cavities with a protruding lip around the circumference, prohibiting uptake of cells into the cavity (Figure 3.1).

An effective area of the cell printed into the polymer layer is proposed as between one half and one third. This would yield a cavity able to allow entry by cells from suspension and have a large surface area to amplify any weak interaction incurred between imprint and cells.

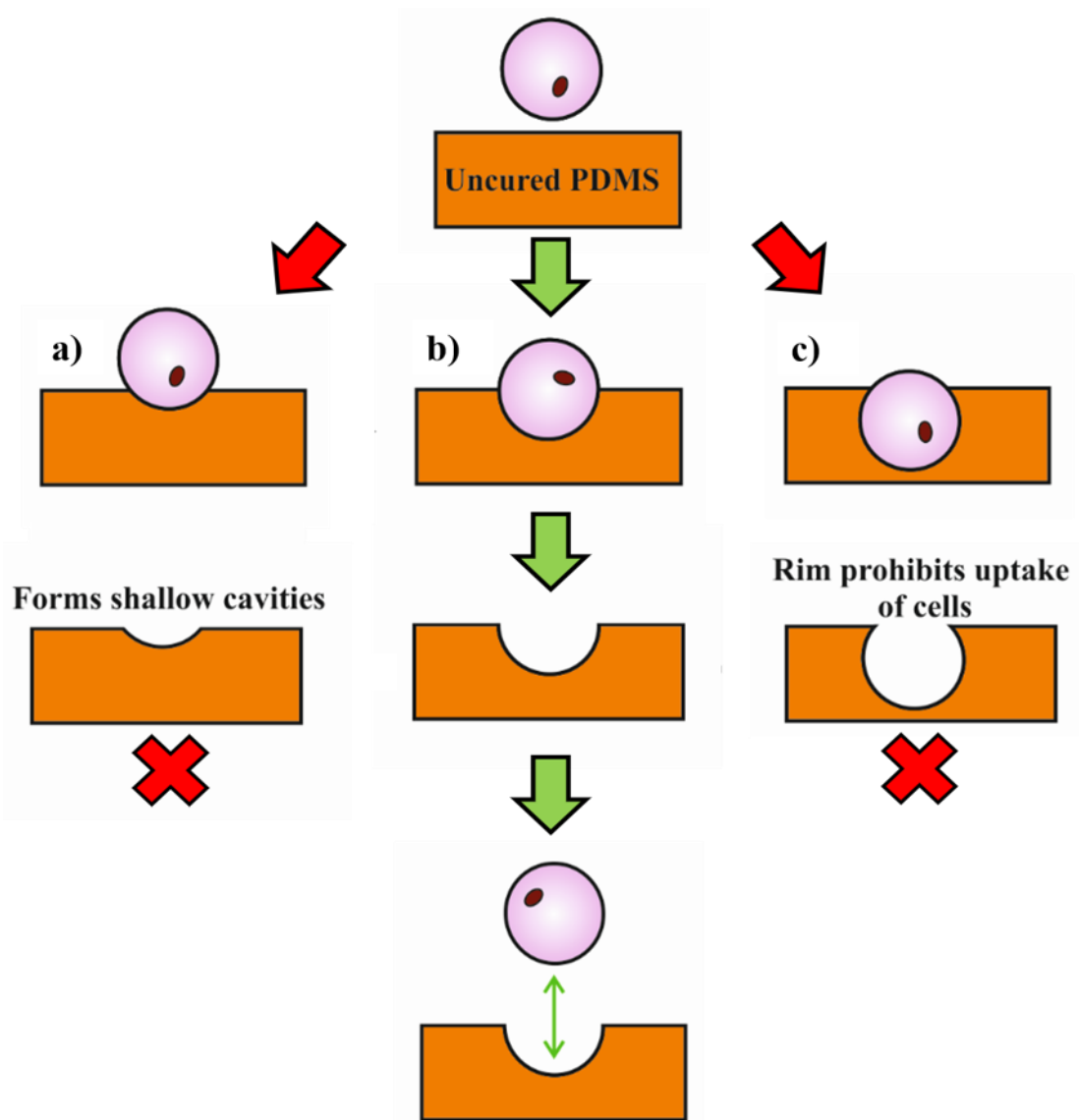


Figure 3.1 Schematic showing how identical cells can form cavities of a range of sizes dependant on how much of the original cell surface is exposed to the curing polymer. a) shows a shallow cell cavity from too little coverage, b) proposed ideal area of cells exposed: between a third and a half which maximises the contact area while still being accessible and c) a cell cavity with too much coverage forming a rim around the circumference.

This section aims to elucidate a method to spread cell suspension in order to produce bioimprints. Prior to rigorous handling, cell templates need to be chemically fixed to preserve their shape and size information, which may otherwise potentially change upon exposure to the resins or during the formation of the cell layer.

3.1. Cell fixation

The fabrication of a myeloblast removal device will involve the imprinting of an immortalised cell line model as a surrogate for AML myeloblasts. HL60 cell line was taken from an acute promyelocytic leukaemia sufferer, denoted as M3 under the FAB classification. However, as proof of principle examinations of preparing bioimprints require a relatively large volume of cells, a wider array of more readily available templates was used. Jurkat cells are lymphocytes from leukaemia sufferers and show similar properties to HL60. Further yet more readily available and robust templates were also used; yeast from *Saccharomyces Cerevisiae* and monodisperse cross-linked PMMA Spheromer® microparticles of three discreet sizes, $10 \pm 1 \mu\text{m}$, $15 \pm 1 \mu\text{m}$ and $20 \pm 2 \mu\text{m}$, (CA10, CA15 and CA20) purchased from www.micro-beads.com.

As biological matter, cells are susceptible to changes in their environment such as molarity, pH and physical deformation. As size and shape is paramount to the success of the project, all cell types cells were fixed as a precaution against robust treatment. A variety of fixation protocols are commonplace in literature though not all focus on the exterior properties; other studies aim preserve other aspects of the cell such as DNA. In this study, various crosslinking agents were trialled to ensure the fixed cell was representative of the unfixed cell. Though a variety of fixatives are available, the ones trialled function by crosslinking extracellular membrane groups, advantageous in this instance by providing structural rigidity.

An examination of the effect of fixing cells was carried out using Jurkat cells. Flow cytometry was used to measure the forward and side scatter of Jurkat cells before and after fixation with paraformaldehyde, glutaraldehyde, methanol, ethanol and a methanol and ethanol mixture. The forward and side scatter of unfixed cells was compared with the range of fixative agents (see in Figure 3.2, below).

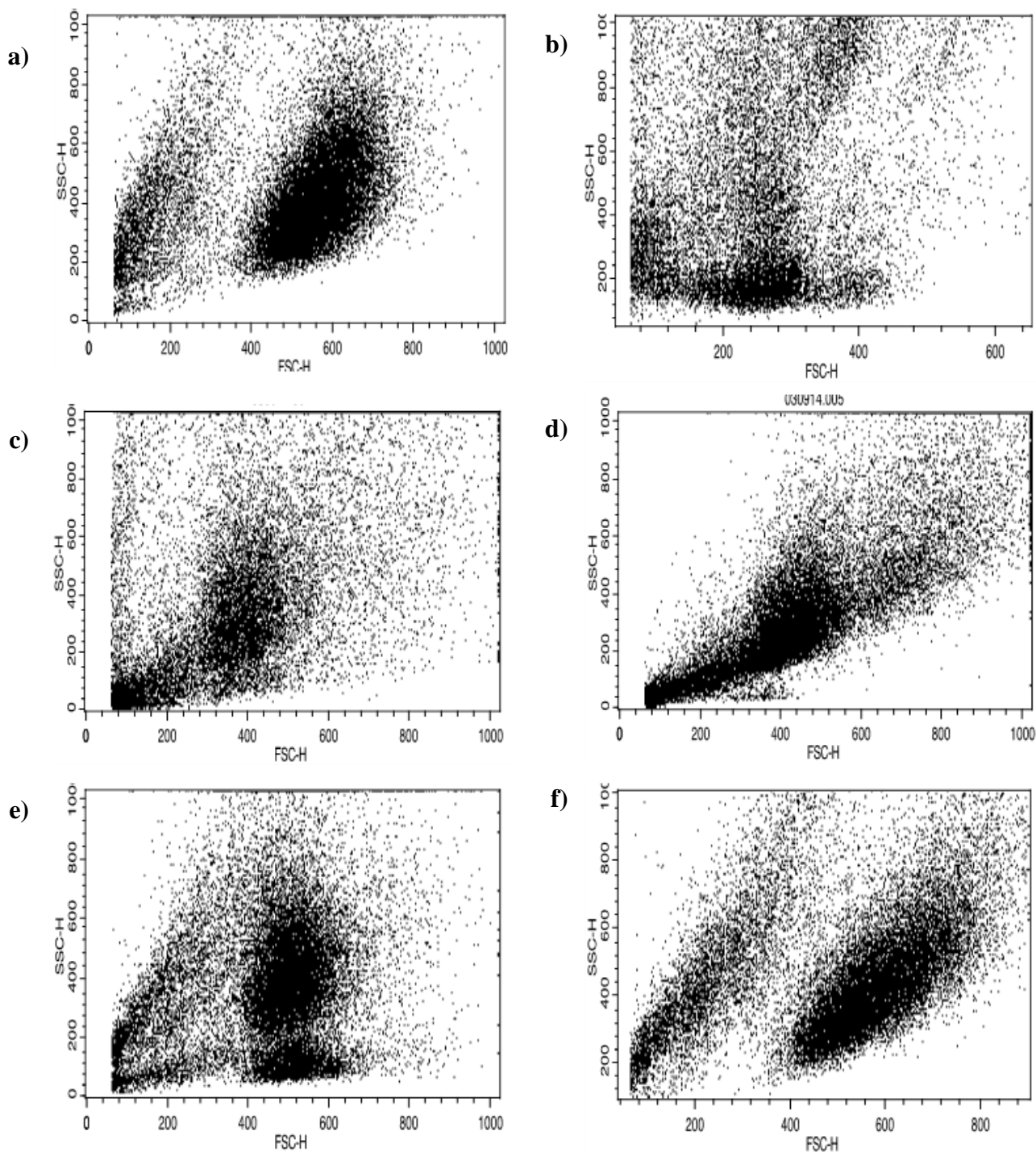


Figure 3.2 Forward and side scatter of Jurkat cells a) prior to and post fixing with b) methanol, c) ethanol, d) an ethanol and methanol (1:1) mixture, e) paraformaldehyde (4% w/v) and f) glutaraldehyde (2.5% w/v). Forward scatter (x-axis) denotes cell size and side scatter (y-axis) describes membrane complexity.

As can be seen from Figure 3.2 the agent that best resembled the unfixed cells was glutaraldehyde. The methanol fixed population that showed a poor distribution with fixed cells larger and smaller than the unfixed and would be unsuitable for further use in the study. For the purposes of this study, the fixed cells are more robust against physical

deformation and damage from changes in osmotic pressure. Initially, cell aggregation was observed from crosslinking of extracellular groups from neighbouring cells; the aggregates were difficult to separate with sonication and risked deformation of the cell shape. To avoid aggregation, the cell suspension was added dropwise to a stirred 0.5% w/v glutaraldehyde solution. Bright field microscopy of template Jurkat compared the size and shape of the template Jurkat cells before and after crosslinking fixation by glutaraldehyde solution (see Figure 3.3a-b). Glutaraldehyde fixation was confirmed using a HL60 cell line; an immortalised AML cell line which will be used hereafter due to the likeness with myeloblasts (Figure 3.3c-d).

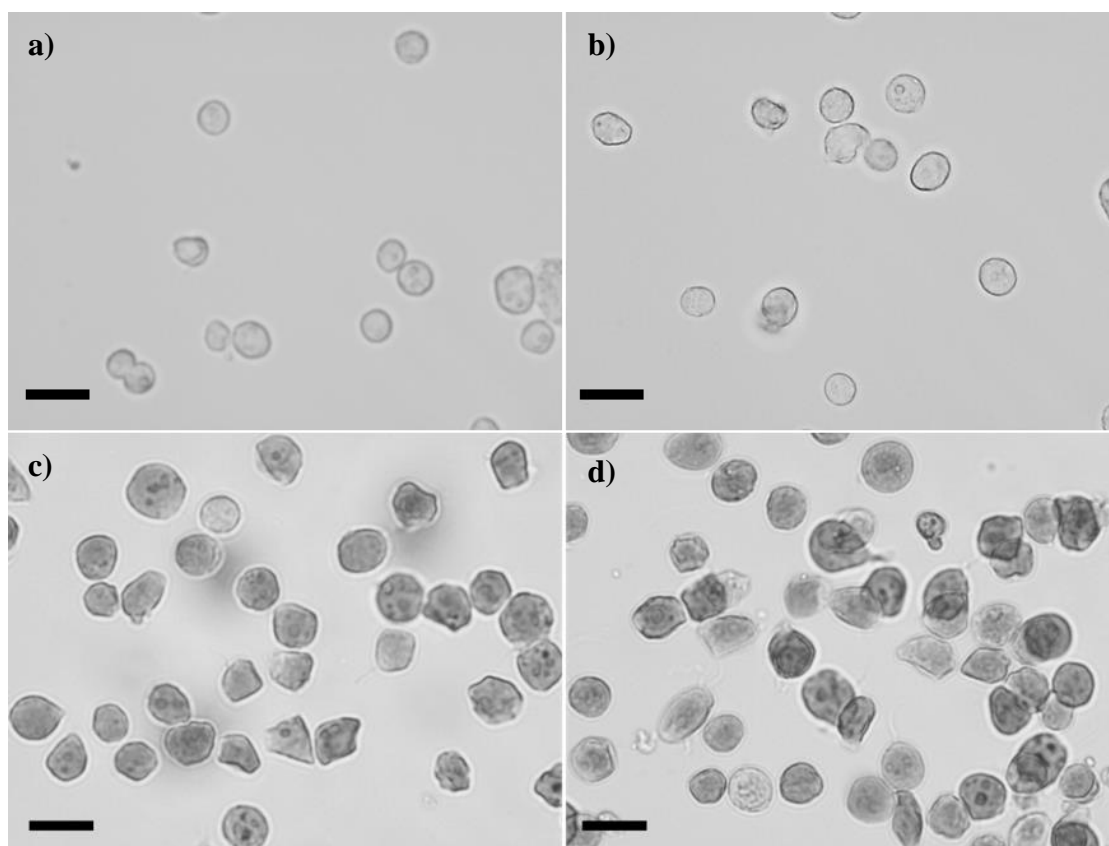


Figure 3.3 Bright field microscopy of unfixed Jurkat and HL60 cells a) and c) respectively, and after fixing by dropwise addition to glutaraldehyde (100 ml, 0.5% (w/v) in PBS) b) and d) for Jurkats and HL60. Scale bar represents 20 μm .

Microscopic and flow cytometry analysis confirmed the cell fixation process did not compromise the integrity of the cell shape or morphology. Template cells were fixed to

be more resistant to harsh treatment during the bioimprint preparation. When suspended in MilliQ water cells did not lyse due to osmotic shock as expected of unfixed cells.^{2,3}

In order to produce a bioimprint, a method was needed to reproducibly and reliably spread the template material evenly across a solid flat substrate. Various methods to deposit cells have been trialled and will be discussed in the following section.

3.2. Template deposition

3.2.1. Cell sedimentation

Firstly, fixed cells were allowed to sediment from suspension onto polyelectrolyte functionalised glass substrates. Cells were used in volumes in excess of the target area in order to improve the chances of achieving at least one single layer on the functionalised substrate. With this approach, a multilayer is likely to be observed for the areas on the substrate though this is insignificant provided that the top layer is captured into the curing polymer layer. Glass substrates were pre-treated with potassium hydroxide and the cationic polyelectrolyte PDAC, used to facilitate cell adhesion material on account of the cells negative surface charge. This net negative charge is the result of dissociation of carboxylic groups in extracellular proteins and carbohydrates.^{2,4-6}

Initially, the cell layers produced were poor as cells were weakly immobilised on the substrate making the cell multilayer brittle and subject to breaking and cracks. At lower concentrations, the cell layer prepared showed poor, sparse coverage (Figure 3.4). As cells were not strongly bound on the glass substrate, a large proportion of the cells in suspension did not adhere, making the method inefficient and difficult to reproducibly make larger imprints. There was also little control over the uniformity of substrates with regions having no attached cells. It is important to note the cell films were not allowed to dry. The procedure was repeated multiple times using yeast and Jurkat templates though showed poor reproducibility. Moreover, various sections of the same bioimprint were of a range of quality.

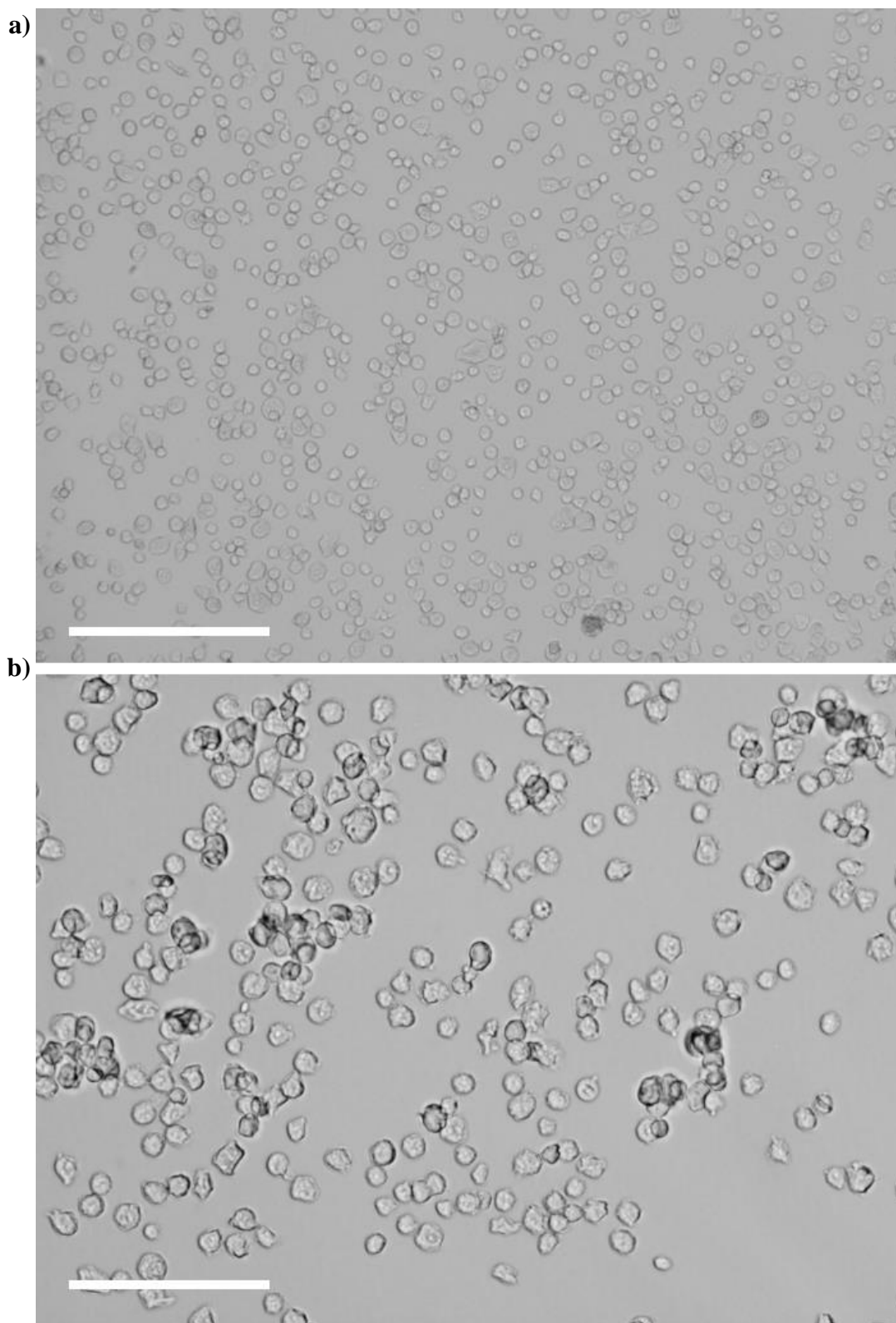


Figure 3.4 Bright field microscopy of PDAC treated substrates after incubation with Jurkat cells suspensions (15×10^6 cells ml^{-1}) for 1 hour. Scale bars represent a) 100 μm and b) 20 μm , respectively.

Experiments were repeated using yeast cell templates which were more readily available and easier to make very concentrated cell suspension. Increasing the cell concentration

was shown to improve the cell layer though the method was both irreproducible and an inefficient use of cells. Most cells remained unbound and were washed away (Figure 3.5).

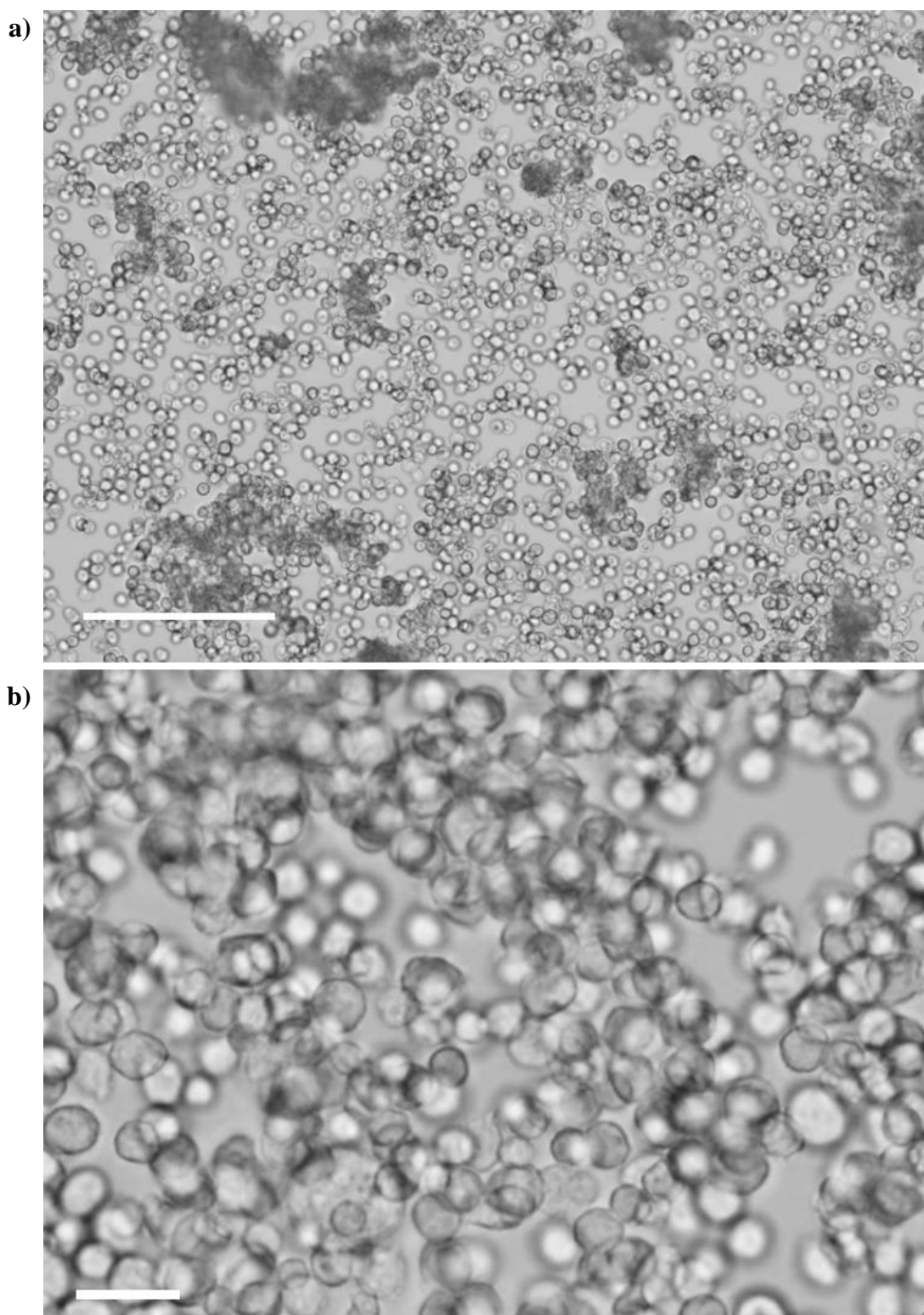


Figure 3.5 Bright field microscopy of PDAC treated substrates after incubation with yeast cells suspensions (20×10^6 cells ml^{-1}) for 1 hour. As can be seen, densely packed areas can be seen though this is not uniform across the substrate. Scale bars represent a) 100 μm and b) 20 μm , respectively.

Further attempts were made using a fixed yeast cell template which allowed a significantly larger volume and concentration of cell suspension to be incubated with the substrate in an attempt to overcome poorly packed areas. This was done for exploratory purpose as both yeast and blood cancer cells are negatively charged at neutral pH, so it was expected that they would deposit similarly when incubated with the glass substrates pre-treated with cationic polyelectrolyte.^{1,2,6,7}

The key disadvantage of the system was the inability to control the stability of the residual liquid layer once it has been immobilised to the substrate. Two problems with this approach were identified. Firstly, if the cell layer dried out, lateral capillary forces cause the layer to rupture and aggregate.^{8,9} Once imprinted, the PDMS print surface shows periodic clumps of cell cavities with a poor overall coverage of the polymer surface (Figure 3.6). The cavities created also formed channels in which the cell cavities are linked together, limiting the performance of both in cell retention. Figure 3.6, below, shows a schematic of the effect of drying in the immobilised cell layer and bright field microscopy before and after drying. Due to the lack of control and overall inefficiency, the method of allowing the cells to sediment from suspension over an oppositely charged substrate was discontinued as an approach to produce cell layers for fabrication of bioimprints.

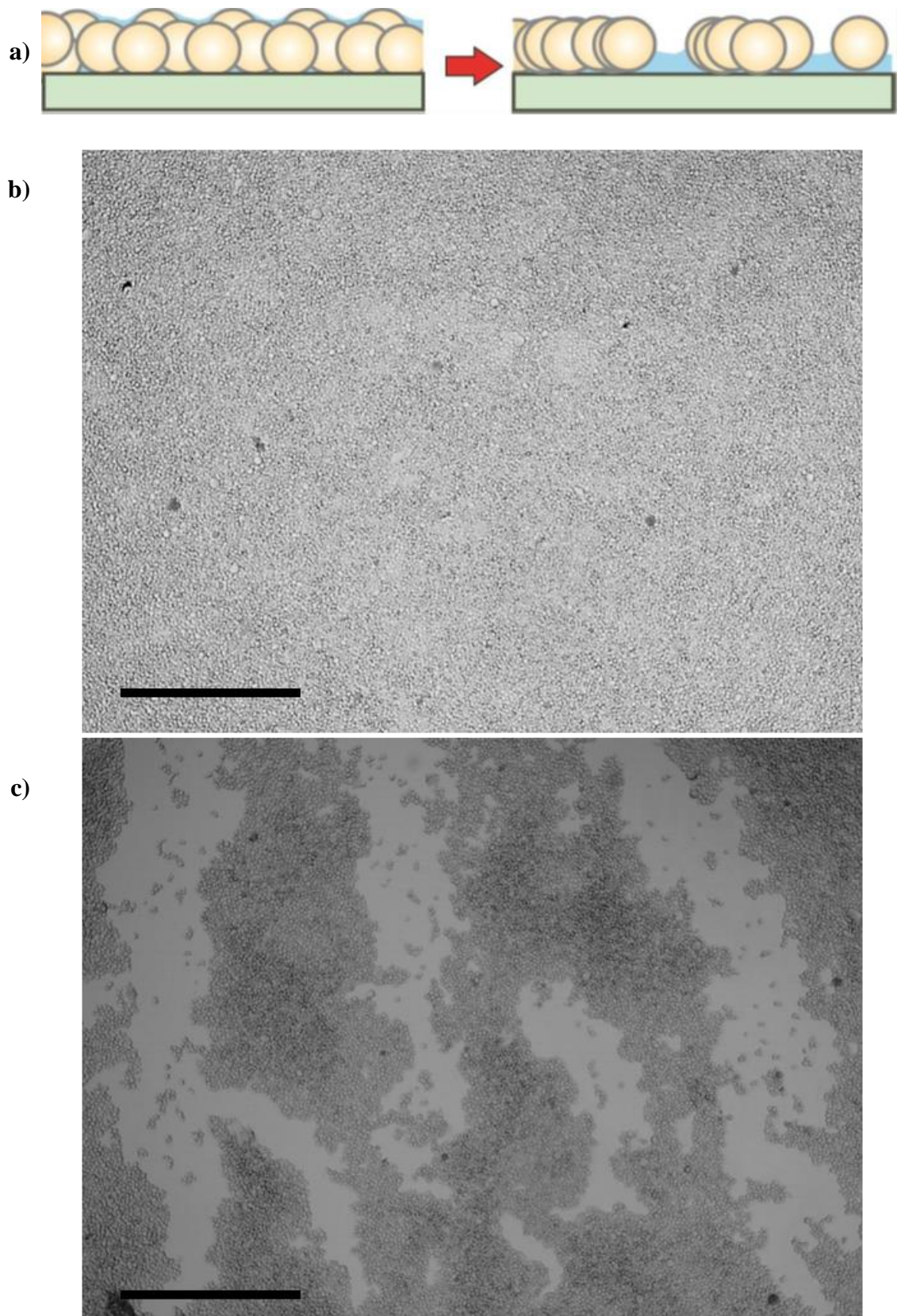


Figure 3.6 The effect of the cell layer drying shown as a) schematic and bright field microscopy of b) before and c) after drying. As can be seen, drying causes aggregation and cracking of the uniform layer. Scale bars for b) and c) represent 500 μm .

Secondly, by having too much liquid in the biofilm layer, not enough of the cell surface was exposed to the curing polymer matrix. The water meniscus surrounding the cells in the monolayer shields a large fraction of the cells surface as the cells are hydrophilic and does not allow the PDMS to capture accurately the cells size and shape information.^{2,5,6} In this case, the bioimprint produced yielded shallow cell cavities not representative of the full cell morphology unlikely to achieve a high enough contact area with cells for capture in future retention experiments. Figure 3.7 below, shows scanning electron microscopy of bioimprints produced from cell layers that have a) over dried and b) have too much water present, resulting in an overprotection of the cell material .

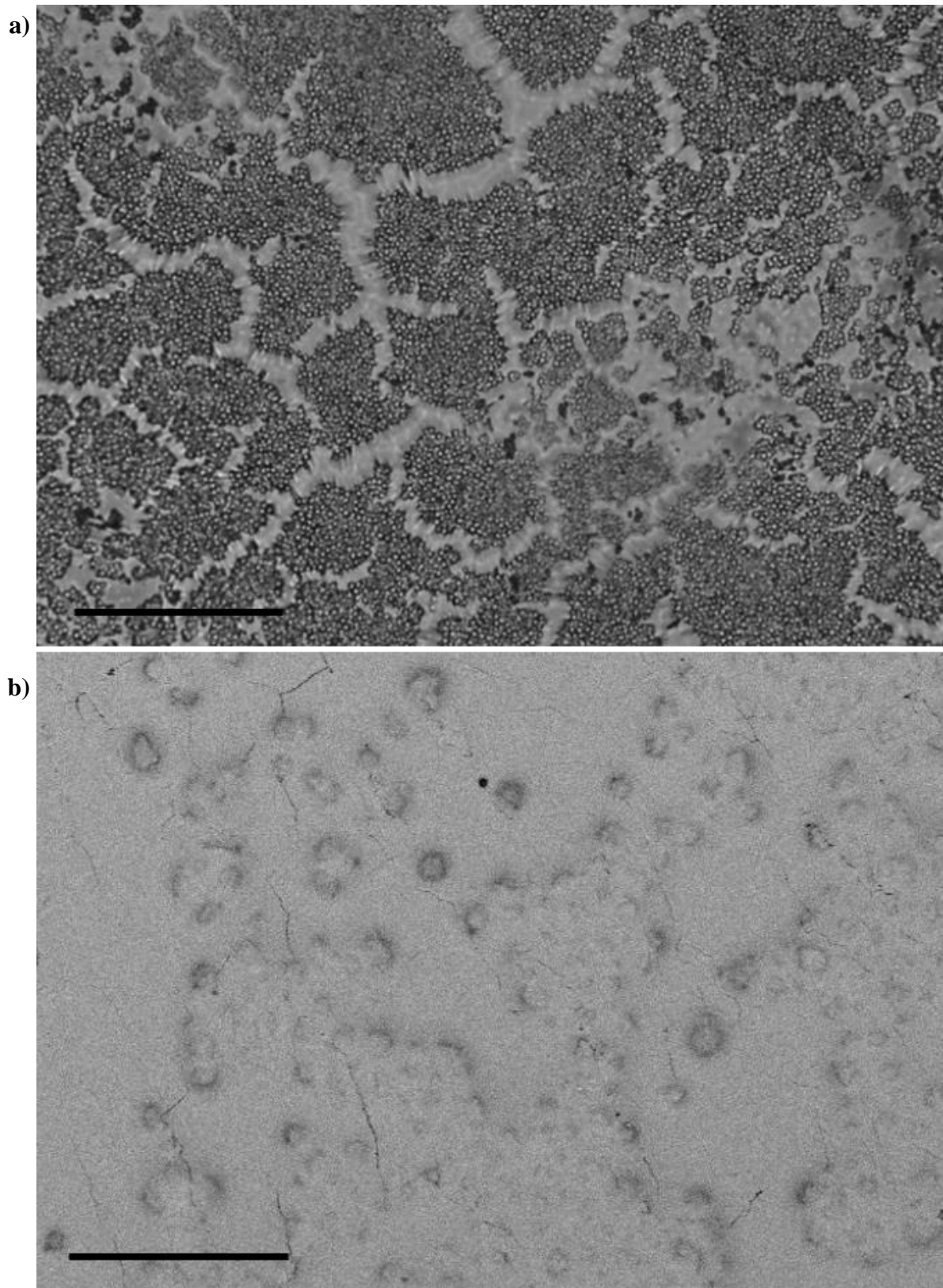


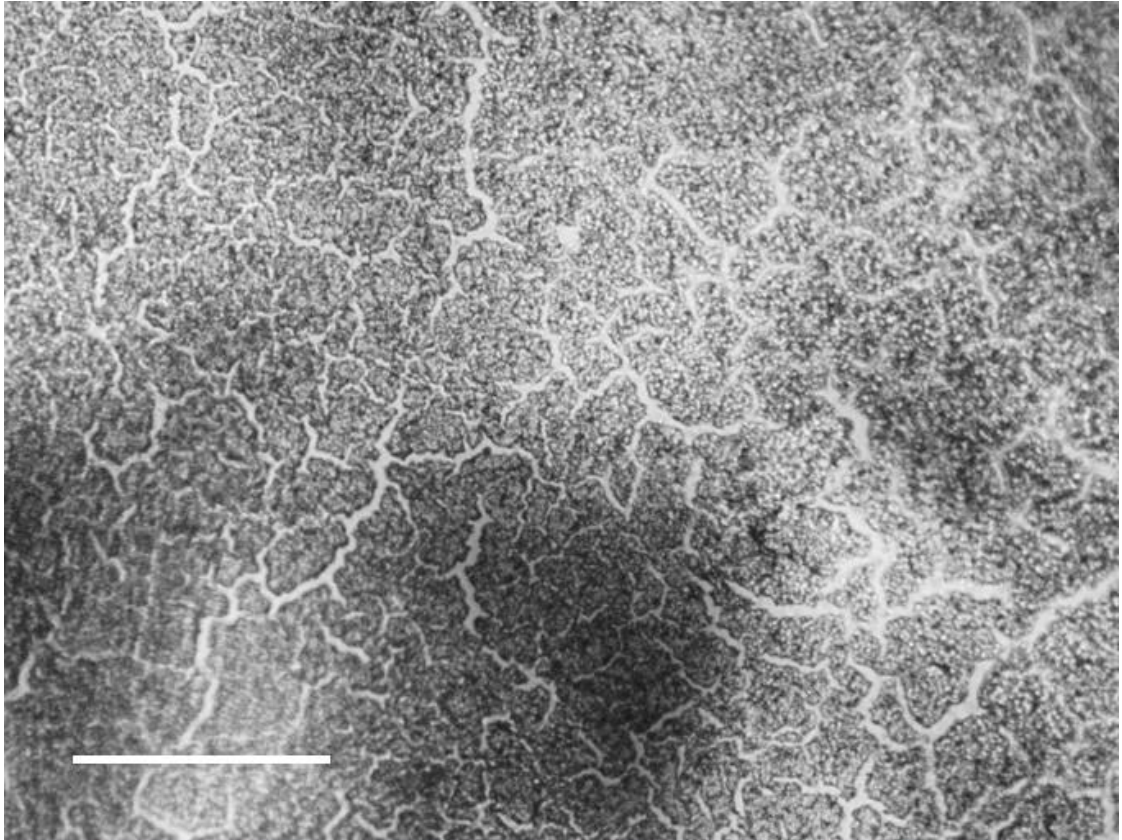
Figure 3.7 a) Brightfield microscopy of the cured PDMS bioimprints produced from cell layers too little water where the cell layer has ruptured and cells aggregated as seen in Figure 3.5c; here vast areas are left unimprinted; scale bar represents 500 μm b) SEM of bioimprint from a cell layer where water has shielded the cell shape. Scale bar represents 100 μm .

The samples produced were not consistent despite using an identical imprinting methodology. To overcome this problem, approaches were considered to increase the interaction between the glass substrate and cells. Herein, a substrate adorned with adhesive tape was used to actively trap the template material to the cell layers.

3.2.2. Adhesive tape capture

To overcome the problems associated with the drying of the biofilm, a method to produce cell layers on adhesive tape was trialled. The rationale was that by increasing the interaction between cells and the substrates would both improve the number of cells retained and circumvent the problems associated with over drying of the substrates. It was predicted that the cell layers would be relatively even due to the even layer of adhesive on commercially available tape. Cells were stained with lissamine-rhodamine (fluorescently tagged lipid) prior to deposition to allow analysis of the opaque cell layers via fluorescence microscopy.^{10,11} Yeast cells were used for the study due to the ease of culture. Analysis shows that cells are retained by the adhesive material though this was not uniform across the stamp surface; leaving large areas without cells (see Figure 3.8).

a)



b)

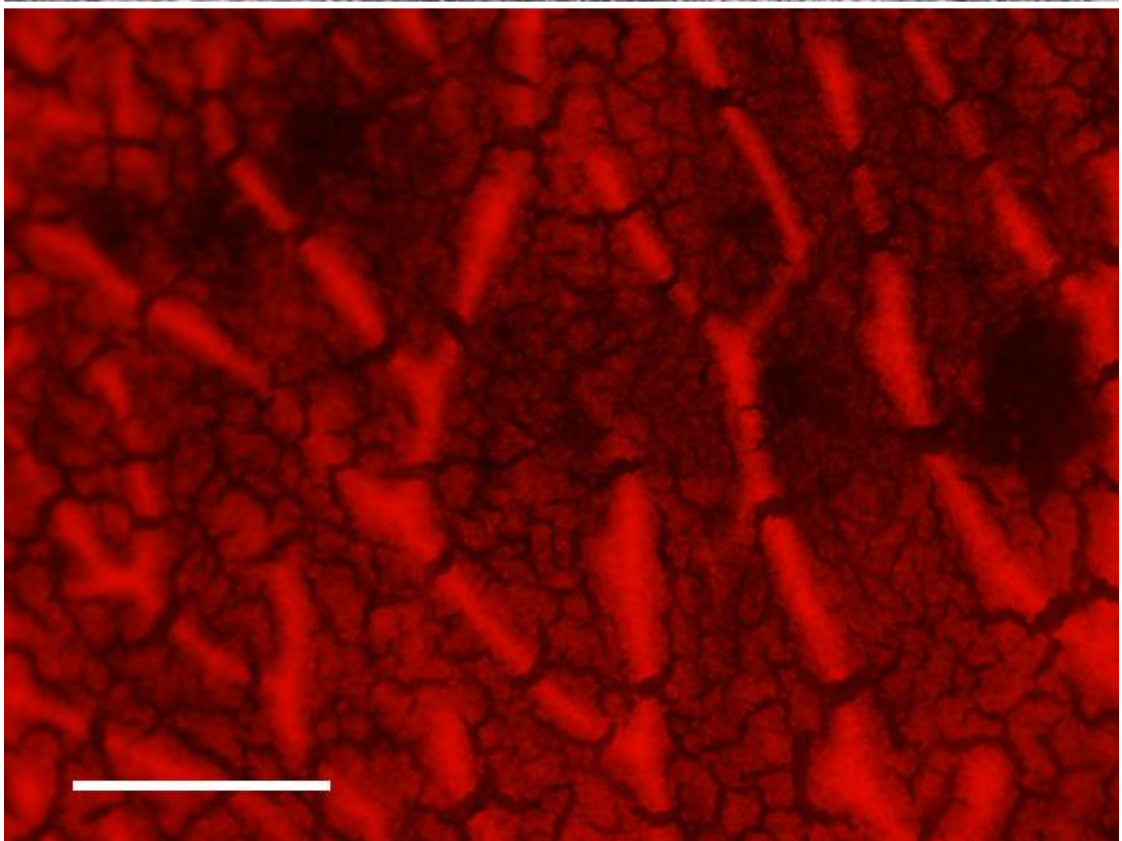


Figure 3.8 a) Bright field and b) fluorescence microscopy of the yeast cell layers produced on adhesive tape. Analysis showed that this method is susceptible to drying, compromising the use of such layers in bioimprint production. Scale bars represent 500 μm .

The method did not overcome the poor efficiency of cell deposition as large volumes were required. The method exacerbated the drying effect as the interaction between cells and the adhesive material was not significant to prevent aggregates being formed during the drying of the cell layer. Aggregates of cells may compromise the transfer of cells shape and size information from the cell layer to the bioimprints due to the ‘channelling’ effect linking cavities which may prevent binding in adjacent sites. This method was also discontinued as no advantage was observed in the formation of uniform cell layer on the substrates.

3.2.3. Cytospin centrifuge method

Though traditionally used in cell pathology, a Cytospin centrifuge was used to deposit fixed cells onto cationic polyelectrolyte-coated glass substrates.¹²⁻¹⁶ With this approach, instead of a monolayer of cells being deposited, a multilayer of cells was produced. Though regions of the cell deposit may have relatively different heights due to different numbers of stacked cells, if a sufficient number were in suspension, the whole area of the substrate would at least be covered to some extent. The application of centrifugal force on the cell suspension ensures that fewer cells are wasted. The densely packed cell multi-layer also protects the cells from being engulfed by the uncured resin when the imprinting takes place; each cell would be close enough to neighbours to prevent the resin penetrating the space in between them.

The fixed cells were immobilised to the substrate whilst PBS solution was removed. By varying the centrifuge speed and the duration, greater control of the amount of residual solution remained in the immobilised cell layer. The higher the centrifugal force used to deposit cells, the more stably the biofilm was immobilised to polyelectrolyte treated slides. This was a key caveat in the paradigm design of the cell layer as a more brittle, fragile layer was more likely to break and result in a poor print surface. At higher centrifugation speeds, the cell layer dried out faster so durations were reduced. Optimum conditions for deposition were found using the Cytospin centrifuge at 550 g for 2 minutes at a concentration of 20×10^6 cells ml⁻¹. The cell layer could be reproducibly produced and afforded a very dense and uniform layer over the whole substrate area. See Figure 3.9, below, for bright field microscopy of fixed Jurkat cells deposited via the cytocentrifugation to glass substrates functionalised with KOH and PDAC under optimal conditions.

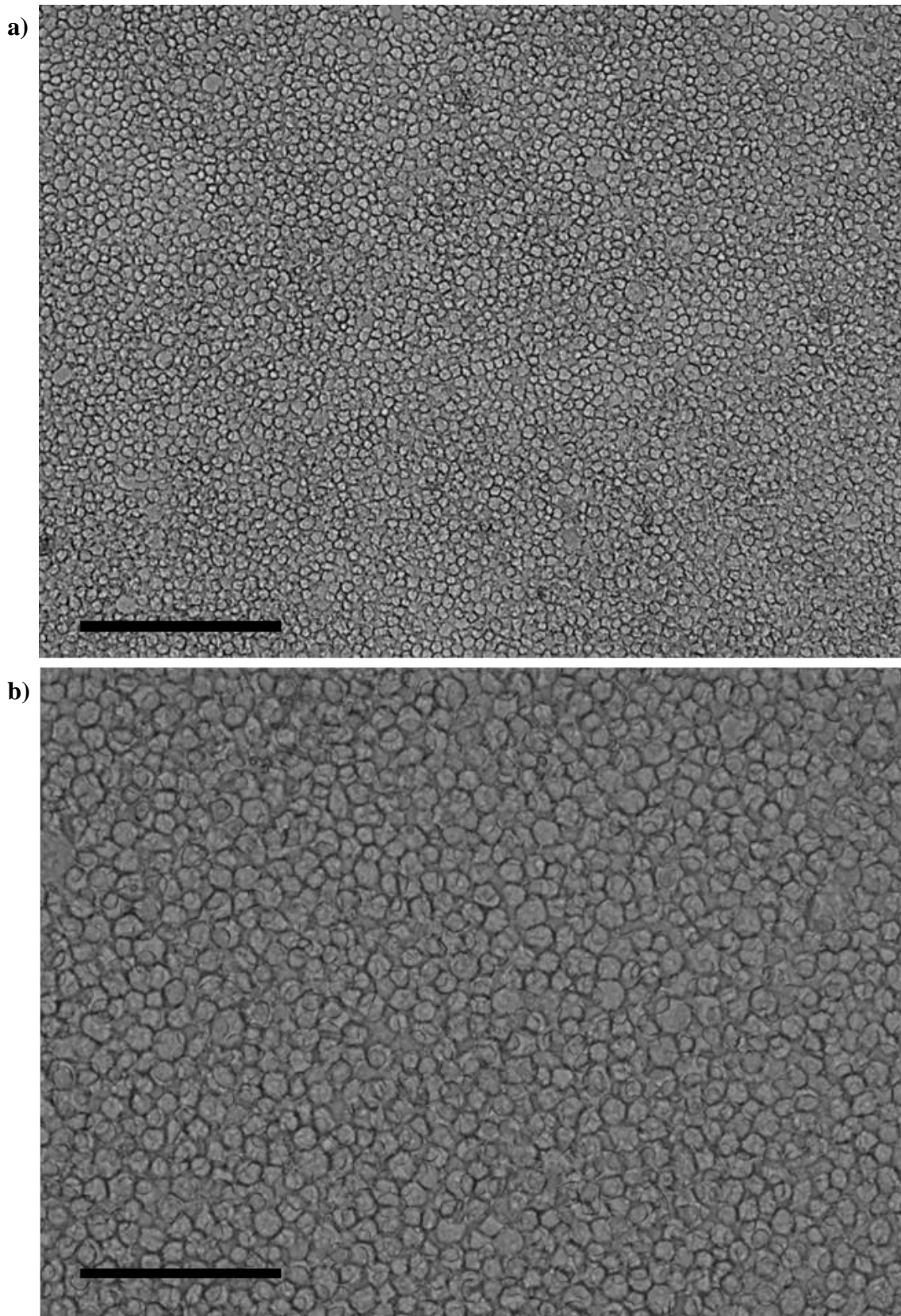


Figure 3.9 Fixed Jurkat cells immobilised to glass substrates pre-treated with 10% w/v KOH and 20% w/v PDAC after deposition of 1 ml of 20×10^6 cells ml^{-1} cytocentrifugation at 550 g for 2 minutes. Cell layers seen as bright field microscopy showing the densely packed lattice of cells immobilised to the surface. Scale bars represent a) 200 μm and b) 100 μm .

Cell layers produced using the Cytospin centrifuge showed optimal area density and excellent surface coverage with cells. Fewer of the cells from suspension were wasted as the applied centrifugal force directed their attachment to glass substrates. Ultimately, cell layers of 2 cm × 2 cm were prepared in an efficient and reproducible procedure.

3.2.4. Glucose protective coating spreading

Though the Cytospin provided a reliable and tuneable method to deposit template cells, the overall size of the cell patterned area is dictated by the device. The largest area that could be covered using the cyto-centrifugation method was 2 cm × 2 cm. Such cell layers would produce a bioimprint of a comparable size to those reported in literature (see Chapter 1), though is limited to this. In an attempt to produce an even smear of cells across a larger area an alternative method was developed.

Herein, cell suspensions were spread in a glucose solution over KOH and PDAC treated glass substrates.⁷ The water evaporates, however the glucose does not and settles to form a viscous layer beneath and in between cells deposited onto the substrate. The volume of glucose was calculated to account for voids between packed cells and fill the space up to a half of the cells height to ensure the cells were not entirely engulfed by glucose. To ensure an even coverage of cells, spreading of the cell suspension was trialled with a variety of tools including brushes and culturing equipment. However, it proved difficult to manually spread suspensions evenly.

To overcome this problem, an original tool was designed which consists of four glass strips joined at the ends to form a square (see section 2.2.2.3). One side of this square was offset by a height of 100 μm, arbitrarily designed due to the method of manufacture though deemed suitable as sufficient height for 5 – 7 layers of HL60 cells. The cell suspension was added to the tools interior and the tool moved along the glass substrate so that the side with the raised side was at the back. By moving the tool at a constant speed, an even film of cell suspension in glucose solution was made. Reproducing the glass tool with a larger perimeter, the method was easily scaled up; ultimately making a cell layer of 70 cm × 40 cm.

Unlike allowing cells to sediment from suspension, here the cell multilayers were allowed to dry out ensuring the cells remained in place on the substrate. Meniscus forces ensure the cells are close enough to the substrate for electrostatic interaction between cells and

polyelectrolyte coating on glass to bind them to the substrate.⁸ This ensures less cells are wasted which becomes more important when covering such a large surface area.

By using a glucose protective layer, the method removes the need to ascertain the water remaining in the deposited cell film. With previous methods trialled, this is difficult to judge by eye and drying was uneven across a large area. With a glucose protective layer preventing cells to aggregate, more control was gained of the proportion of cells exposed to the resin while preventing catastrophic rupture of the cell layer by finely adjusting the volume of glucose spread in cell suspensions. As the method required fine tuning of the volume of glucose used, exploratory studies were done using more readily available microparticle and yeast templates. The initial volume was calculated as the amount needed to fill the voids between randomly packed, spherical cells.

Visual and optical microscopy analysis of the deposited cell layer showed a uniform area across the substrate; see Figure 3.10 showing an example of a yeast bioimprint (dimensions 20 cm × 20 cm).

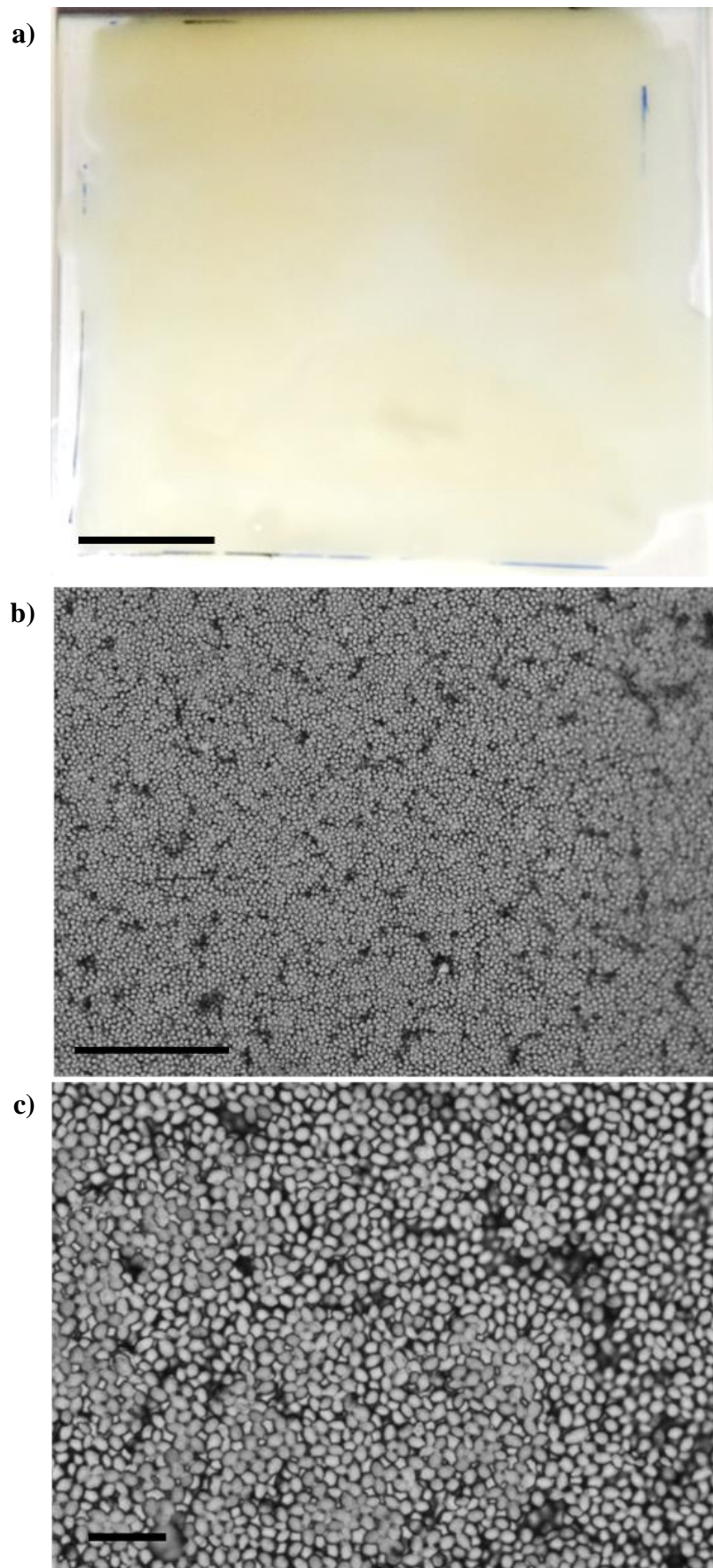


Figure 3.10 a) Fixed yeast cells spread from glucose suspensions after drying with the scale bar representing 5 cm and bright field microscopy of the substrate after the layer has been allowed to become fully dried scale bars represent b) 500 μm and c) 100 μm .

After troubleshooting and optimisation of glucose coating with yeast cells, bioimprints were made using fixed HL60 cells (Figure 3.11).

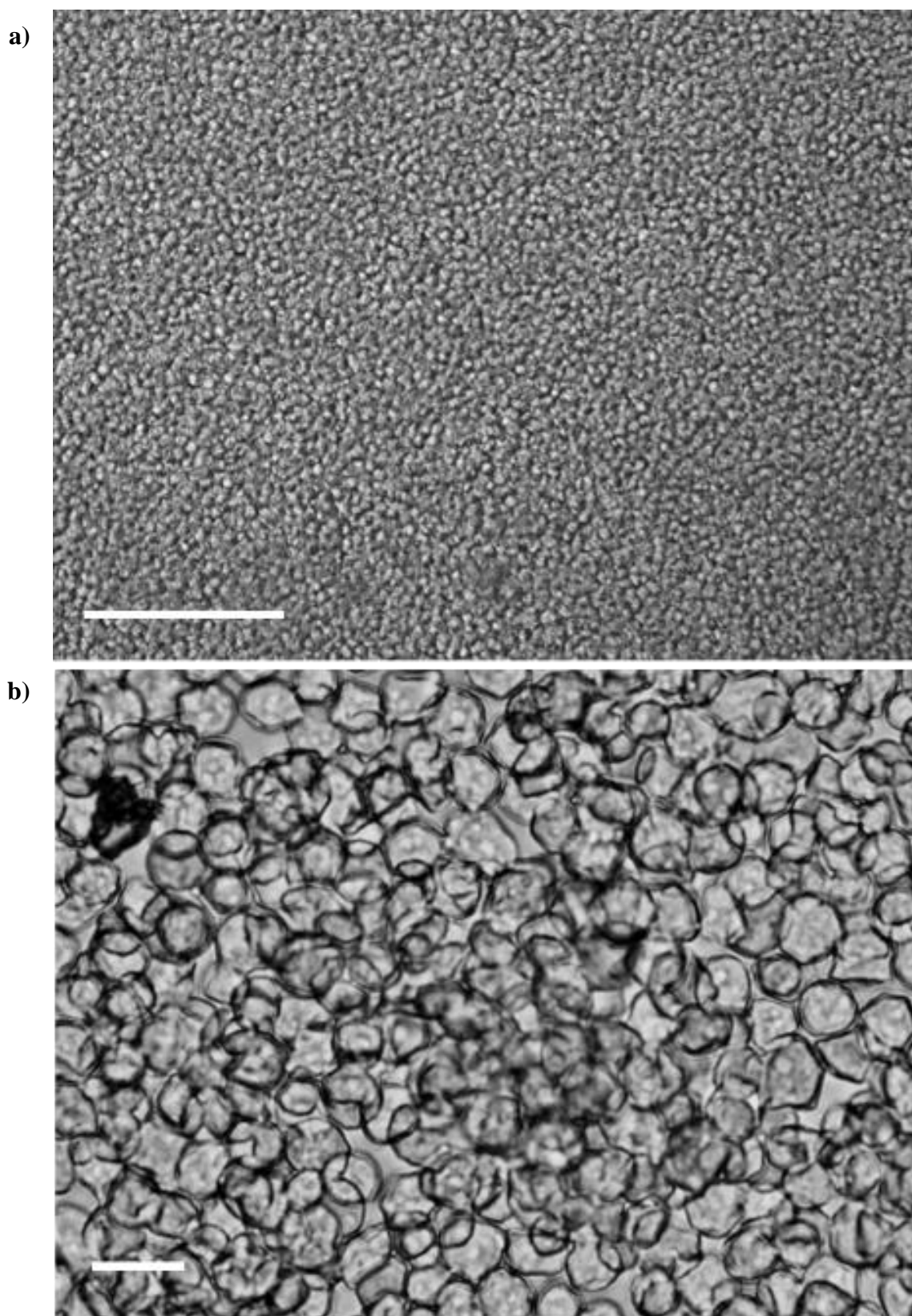


Figure 3.11 Bright field microscopy of HL60 cells spread from glucose suspensions and the layer has been allowed to become fully dried; scale bar represents a) 200 μm and b) 20 μm .

The method allowed a user defined area to be reliably covered with a relatively even layer of cell template material. Unlike the cell layers produced by cyto centrifugation, this method allowed cell deposition which can cover a significantly larger area. As the cell layer was fully dried, the residual volume of water left no longer determined the quality of the cell layer for bioimprinting purposes. Instead, minor adjustment of the volume of the glucose used allows control over the outcome between rupture of the cell layer and the template being entirely engulfed in the protective layer. The produced cell layers were exposed to curable resin to capture the cell size and shape information.

3.3. Bioimprint casting

Thus far, template cells have been chemically fixed and a variety of methods to spread an even layer of cells on functionalised glass substrates was trialled. Two of the methods were shown to be reliable and reproducible: being deposited by cyto centrifugation and by spreading from a glucose solution which sediments and provides protection against cell aggregates. The next step was to capture the topography of the cell layer in a polymer matrix in this instance, polydimethylsiloxane (PDMS) was used. The material is commercially available as a simple two-part kit which was easy to produce, relatively cheap, easy to handle and the ambient curing temperatures mean cell size and shape are unaffected by fluctuations in local temperature. PDMS is commonplace in a medical setting, used in numerous implants which corresponds to the intended use in a clinical myeloblast capture device.¹⁷⁻¹⁹

After being applied to the cell layer and allowed to cure at room temperature for 48 hours, the cured material is soft and elastic allowing easy separation from glass substrates. To add structural support to large bioimprints, a polyester sheet was incorporated in the PDMS during curing to act as a reinforcement; preventing tearing as PDMS was separated from glass substrates. Once separated, bioimprints were cleaned of debris by applying and removing adhesive tape (3M) and subsequently, sonication in ethanol.

3.3.1. Sedimentation imprints

Bioimprints were made by embossing yeast cell layers immobilised to functionalised glass substrates by sedimentation (Figure 3.5) captured into PDMS. The bioimprints were assessed by SEM (Figure 3.12).

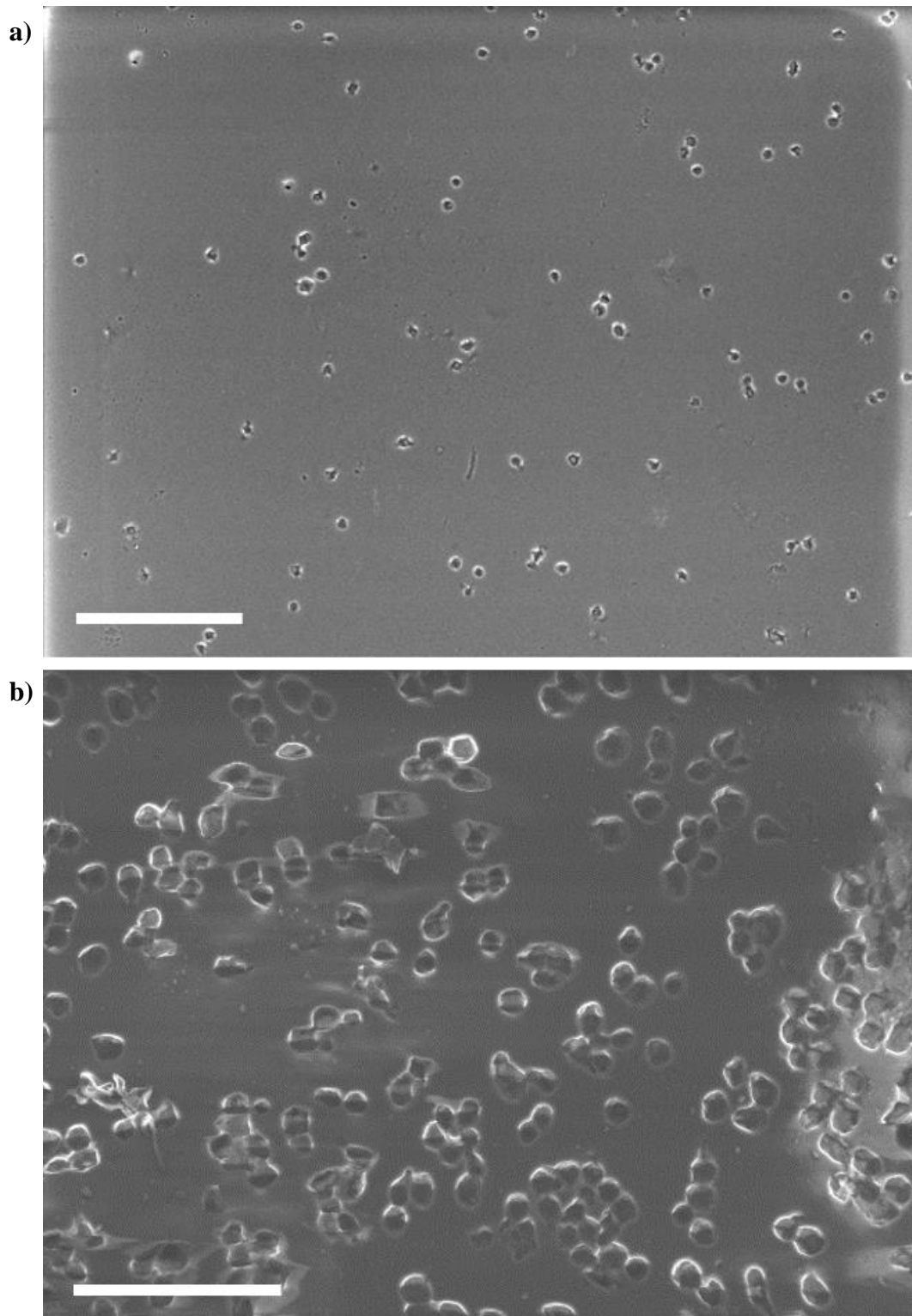


Figure 3.12 SEM of PDMS bioimprint made from sedimentation of yeast cells onto functionalised glass substrates. Scale bars represent a) 100 μm and b) 50 μm .

Analysis of the PDMS showed cavities have been introduced into the PDMS layer, representative of the shape and size of the yeast cell templates used. However, the substrates were not uniformly imprinted with the majority of areas remaining non-functionalized. The area density of the cavities achieved was poor, making the intended use of such type of bioimprints in a myeloblast capturing device highly inefficient. Producing cell layers from sedimentation of the template from suspension onto functionalised glass substrates offered no control over the volume of water left in the cell layer. When cells were allowed to over dry, aggregates of cells formed, disrupting the neighbouring areas. This effect can be seen in SEM analysis of PDMS bioimprints of such areas (Figure 3.13). Here, drying was not uniform across substrates so areas with too much and too little water were seen on the same cell layer.

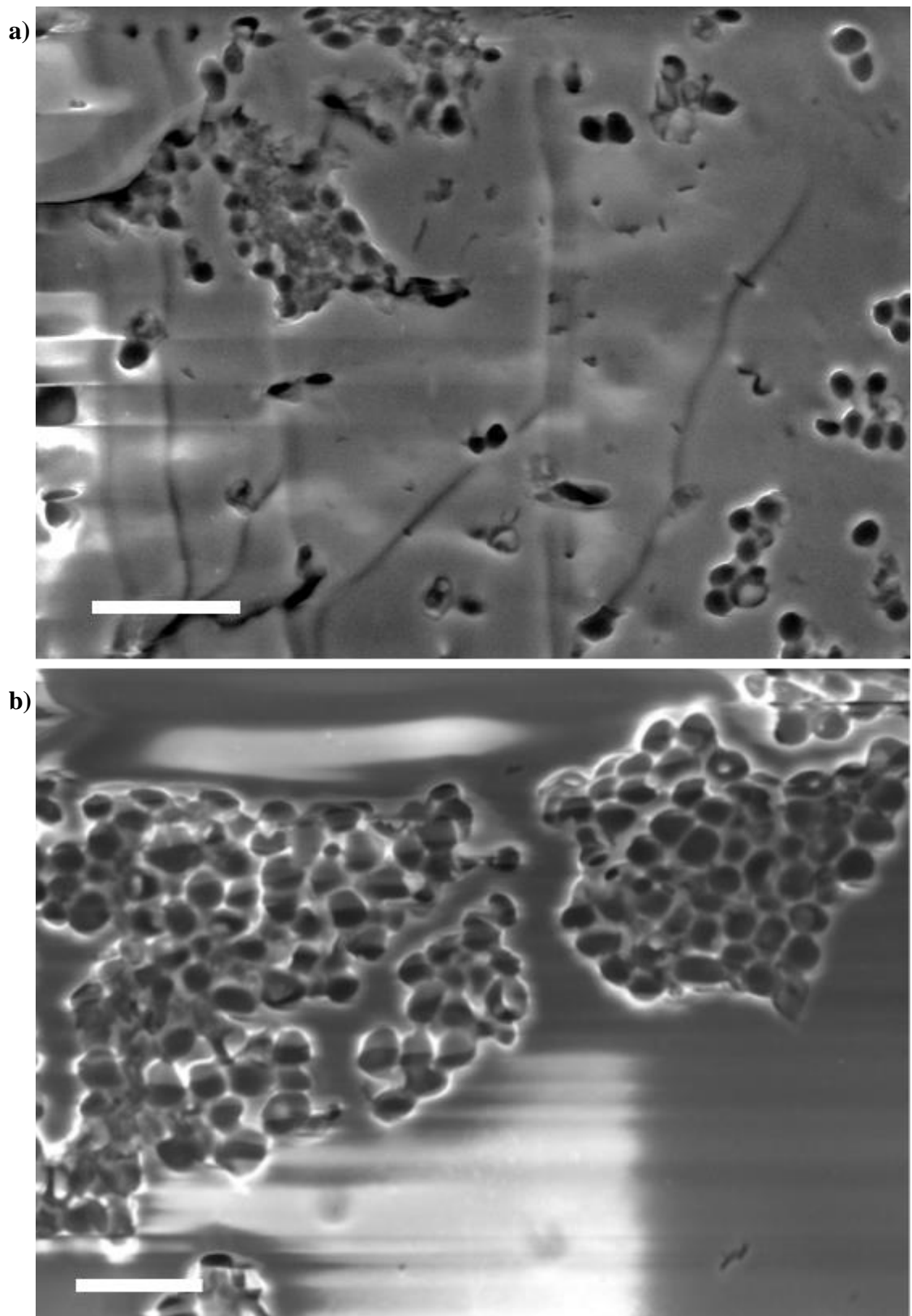


Figure 3.13 SEM analysis of PDMS bioimprints created from yeast templates that have been allowed to over dry forming aggregates. Scale bars represent a) 25 μm and b) 15 μm .

As shown previously (Figure 3.7), the method allowed no control over the water content in the cell layer. When cell concentration was increased in order to improve the surface density of the cell cavities produced, drying caused aggregation and cracking of the cell

layer at high cell concentration. Cell aggregates compromise the bioimprints as neighbouring cavities are linked preventing a cell to be retained to one or both sites. In forming the aggregate, cells have been disturbed from the surrounding area, leaving this area to be unimprinted.

3.3.2. Cytospin bioimprints

The following are images of bioimprints produced by curing PDMS over cell layers produced via a Cytospin centrifuge. Figure 3.14 shows a photograph of a Cytospin mediated bioimprints with dimensions of 2 cm × 2 cm.

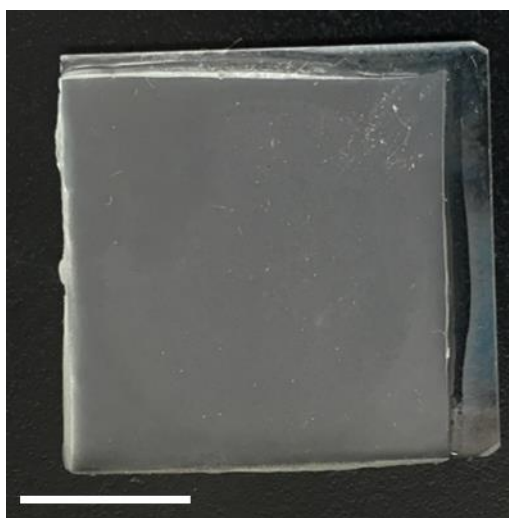


Figure 3.14 Photograph of bioimprints produced by exposing curing PDMS to a layer of fixed CA10 microparticles deposited on functionalised glass slides using Cytospin centrifuge. The cyto-funnel was cut to allow an area of 2 cm × 2 cm to be covered. Scale bars represent 1 cm.

By visual inspection, the bioimprinted substrate appears to be uniform across the entire surface area. CA10 bioimprints were analysed by SEM in order to assess the area density and quality of bioimprinted cavities present (see Figure 3.15).

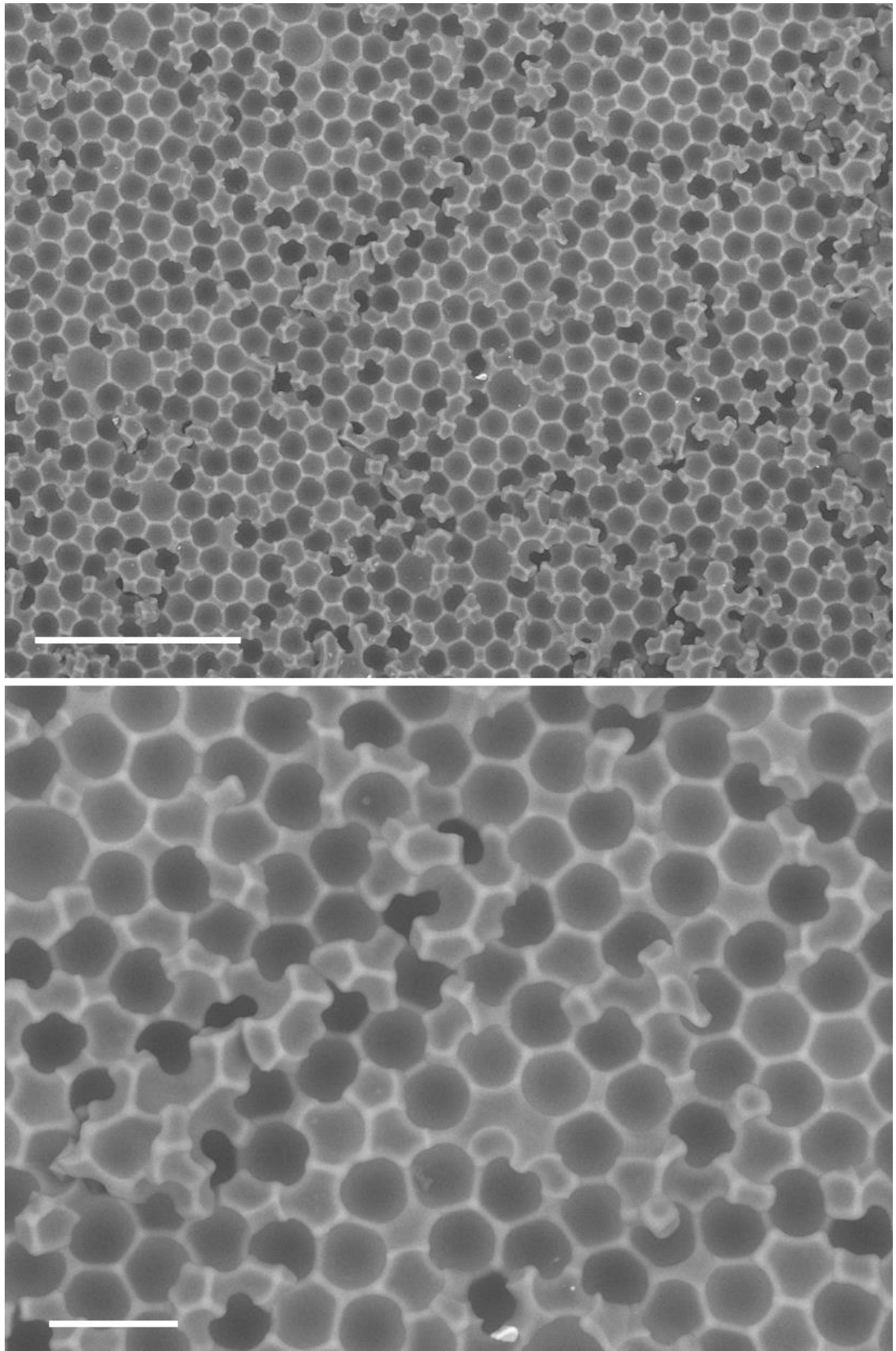


Figure 3.15 SEM of bioimprint produced by exposing curing PDMS to a layer of CA10 microparticles deposited on glass slides using the Cytospin centrifuge. Scale bars represent a) 100 μm and b) 25 μm .

Bioimprints of Jurkat cells were made via the Cytospin mediated deposition method (Figure 3.16).

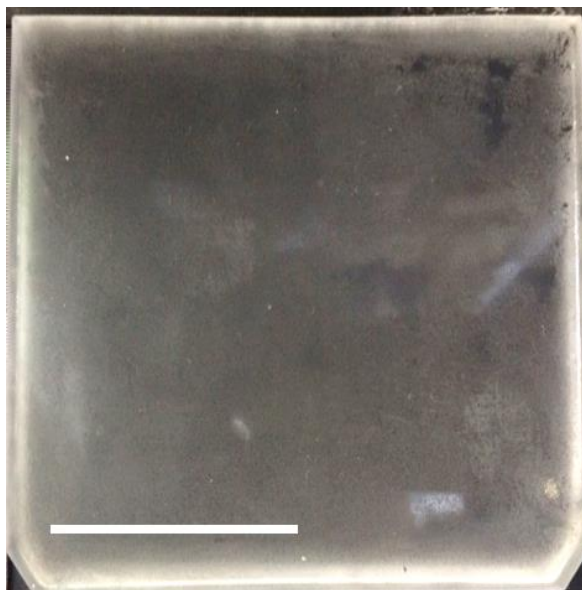


Figure 3.16 Photograph of bioimprints produced by exposing and curing the PDMS onto a layer of fixed Jurkat cells deposited on functionalised glass slides using the Cytospin centrifuge. The cytofunnel was cut to allow an area of 2 cm × 2 cm to be covered. Scale bar represents 1 cm.

Jurkat bioimprints produced into PDMS after exposure to cells deposited by the Cytospin centrifuge to functionalised substrates were analysed by bright field microscopy (shown in Figure 3.17). Visual inspection shows the layer to be evenly distributed across the entire bioimprint.

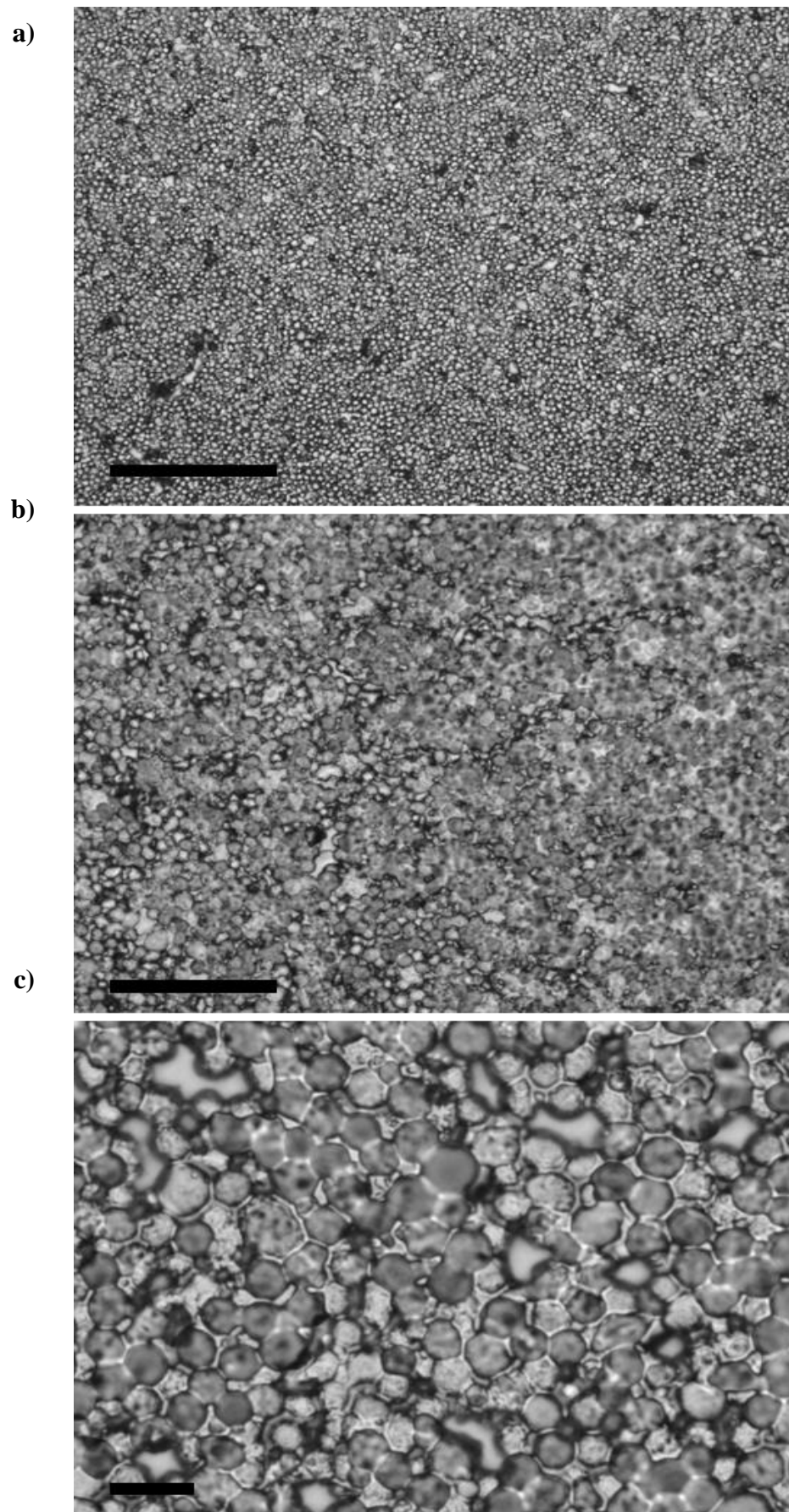


Figure 3.17 Bright field microscopy of a bioimprint produced by exposing and curing PDMS on to a layer of fixed Jurkat cells deposited on functionalised glass slides using the Cytospin centrifuge. Scale bars represent a) 200 μm , b) 100 μm and c) 50 μm .

As can be seen from the Figure 3.17, the cavities functionalised on to PDMS surface are representative of the images of immobilised cells (Figure 3.9). Even if the cells have been detached from the cell layer or engulfed by the polymer matrix, the multilayer coverage ensures that all areas of the bioimprints are patterned. Higher resolution analysis was carried out using scanning electron microscopy; see Figure 3.18 and Figure 3.19, below.

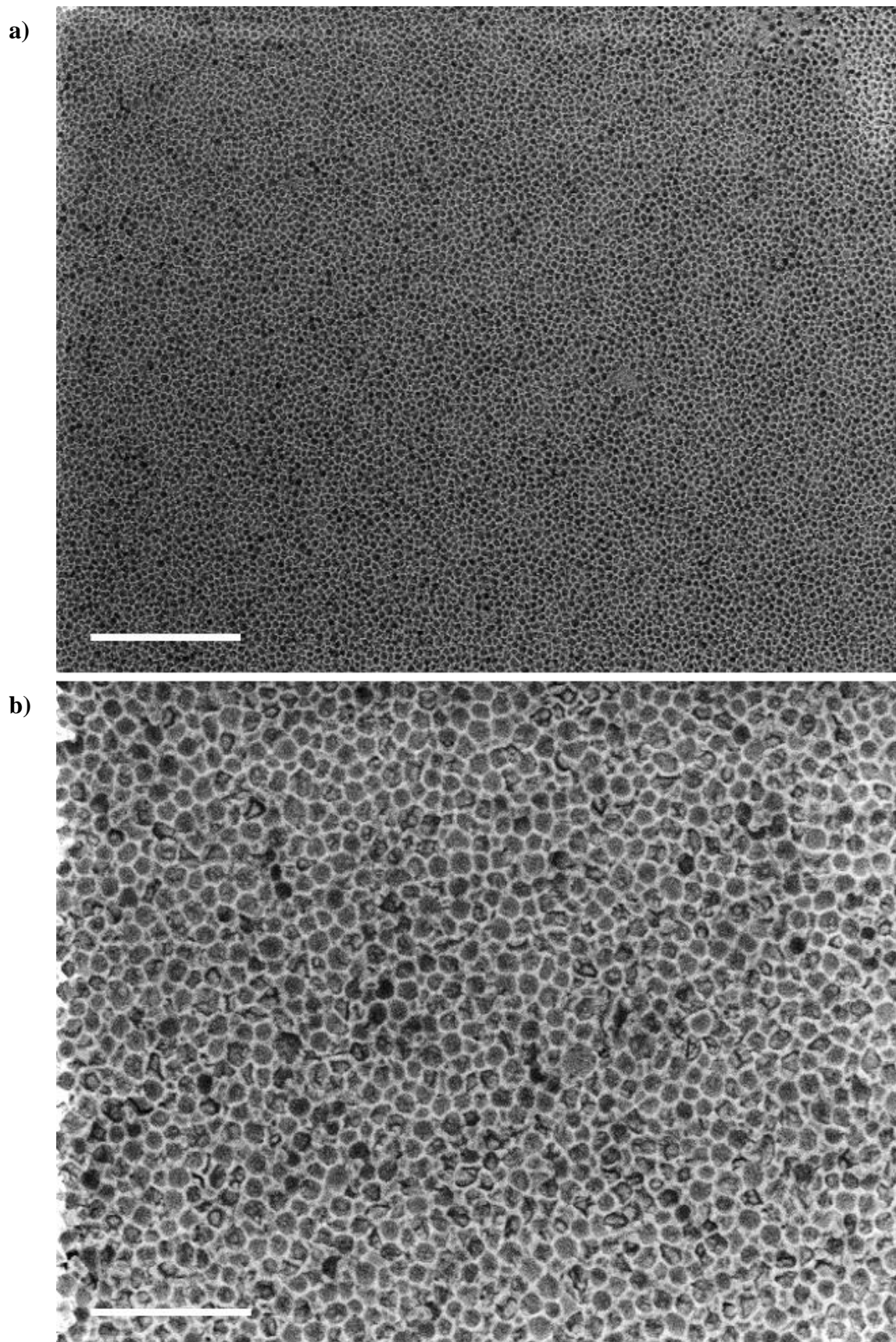
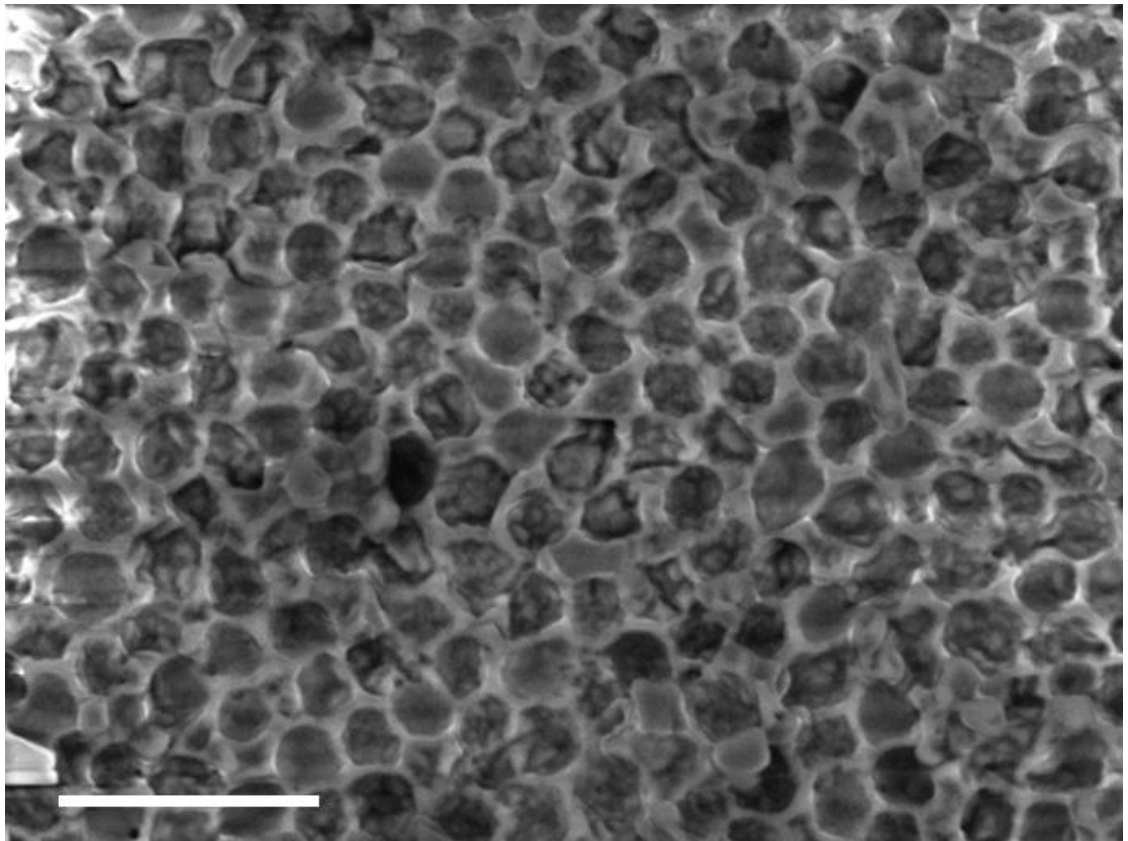


Figure 3.18 Scanning electron microscopy of PDMS bioimprints made using fixed Jurkat cells deposited by Cytospin centrifuge. Scale bars represent a) 250 μm and b) 100 μm , respectively.

a)



b)

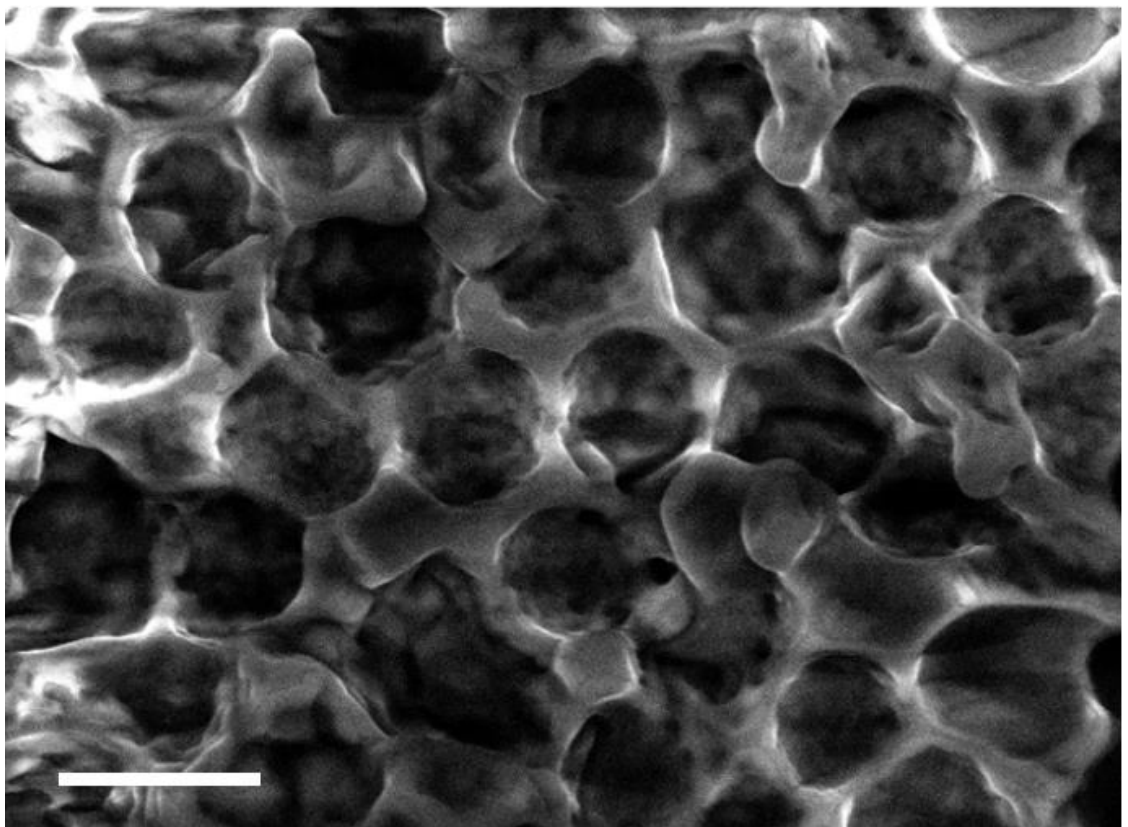


Figure 3.19 Scanning electron microscopy of PDMS bioimprints made using fixed Jurkat cells deposited by Cytospin centrifuge. Scale bars represent a) 50 μm and b) 15 μm , respectively.

Bioimprints fabricated by cyto-centrifugation showed great reproducibility, consistently affording densely packed cavities. Bioimprints were uniform over the full prints range and efficiently pack cell cavities into the surface.

3.3.3. Glucose imprints bioimprints

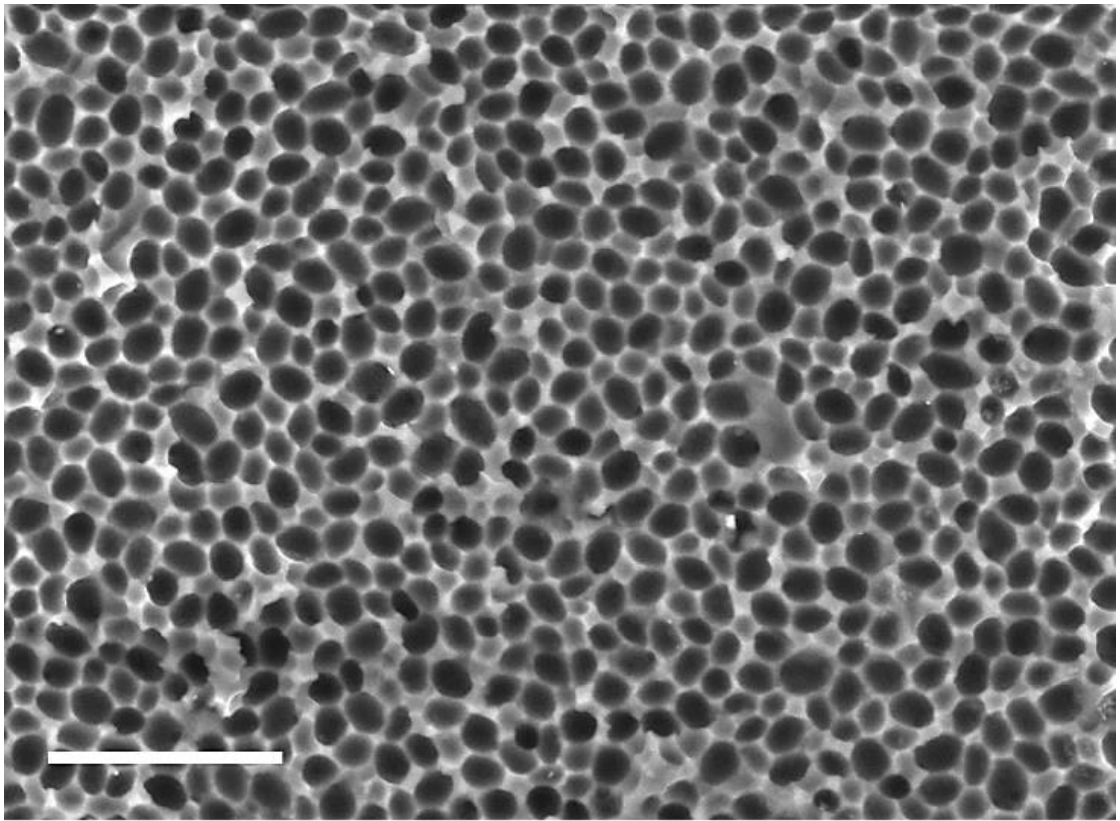
Identical analysis was made of the imprints into PDMS produced by spreading HL60 cells from glucose solutions. The advantage of such bioimprints was the user defined area covered unlike bioimprints produce via the Cytospin centrifuge which were limited to the device's capabilities. Such imprints were optimised with yeast and microparticles before progressing with the HL60 cell line. See Figure 3.20, below, showing the PDMS bioimprint made using a fixed yeast template, deposited from glucose solutions.



Figure 3.20 Bioimprint produced by exposing curable PDMS to a layer of fixed yeast cells deposited on functionalised glass slides from aqueous glucose solutions. The dimensions of the bioimprints are 2 cm × 2 cm. Scale bar represents 5 cm.

High resolution SEM analysis of bioimprints produced by spreading from aqueous glucose solutions; see below for bioimprints of fixed yeast a) and CA20 PMMA microspheres b).

a)



b)

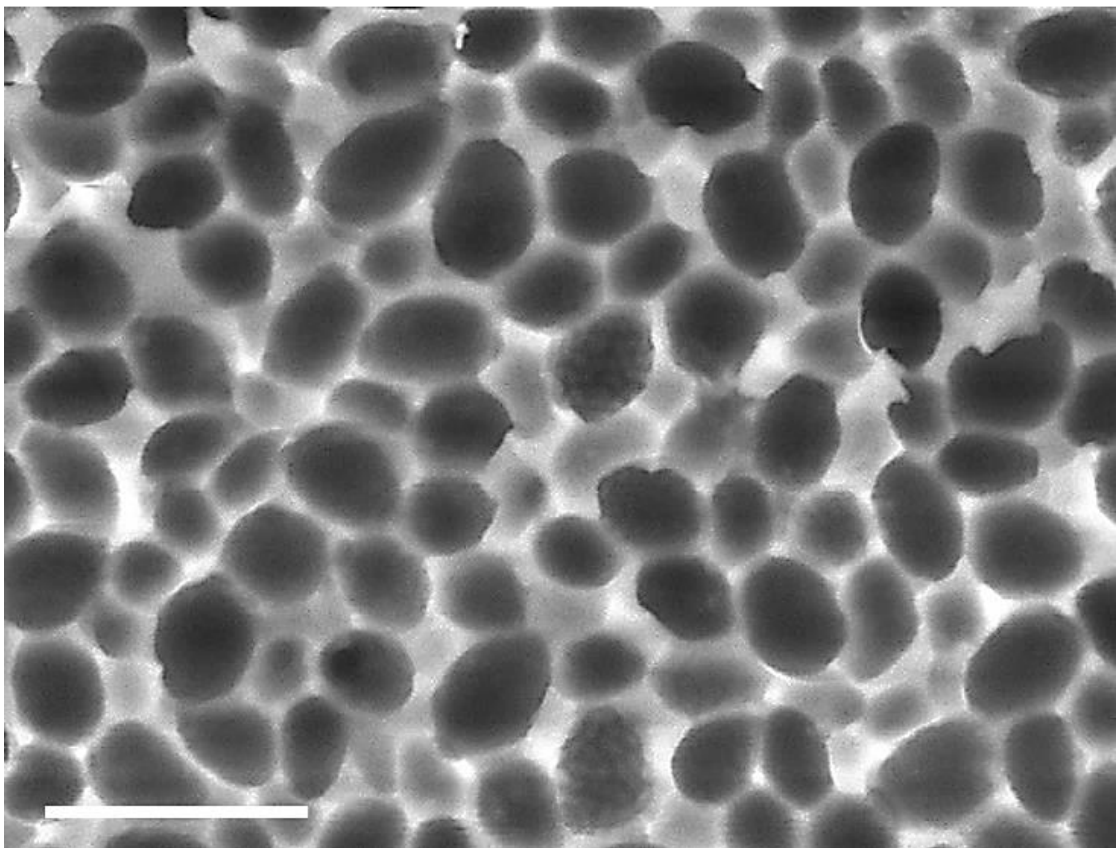
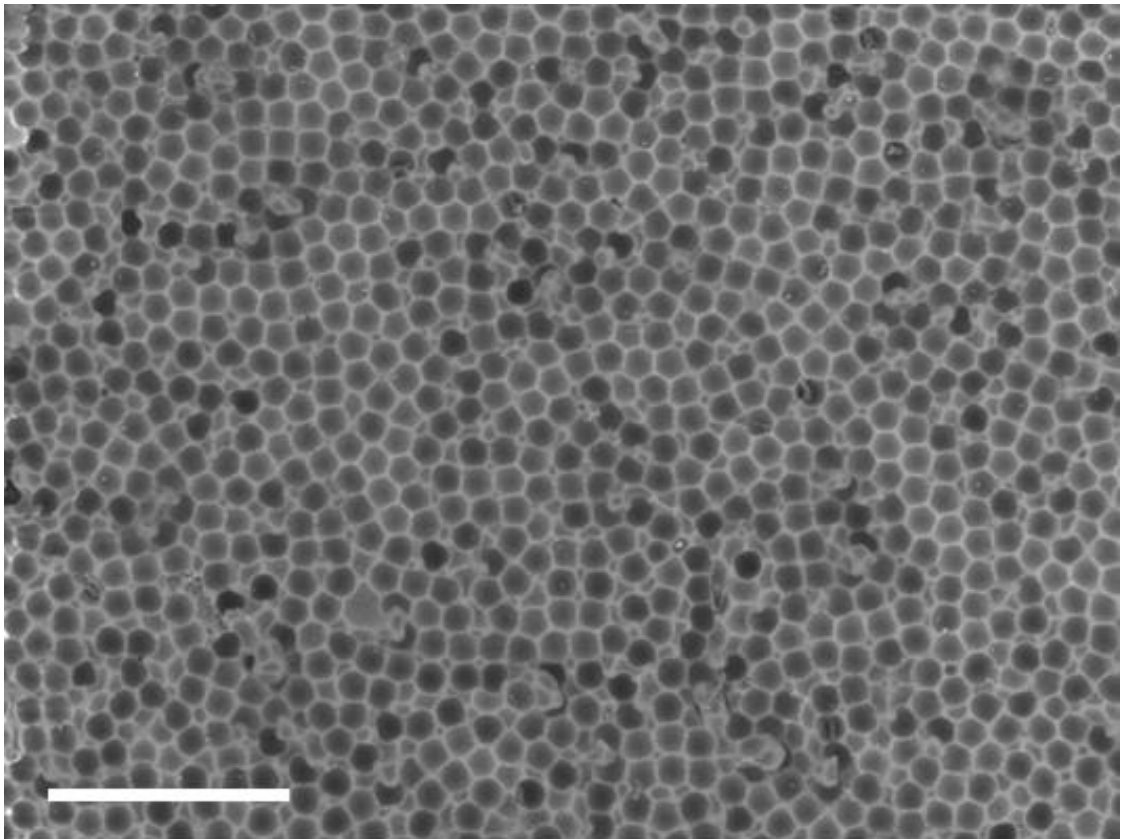


Figure 3.21 SEM of the bioimprint produced by exposing and curing PDMS to a layer of fixed yeast cells deposited on functionalised glass slides from glucose solutions. Scale bars represent a) 25 μm and b) 10 μm , respectively.

a)



b)

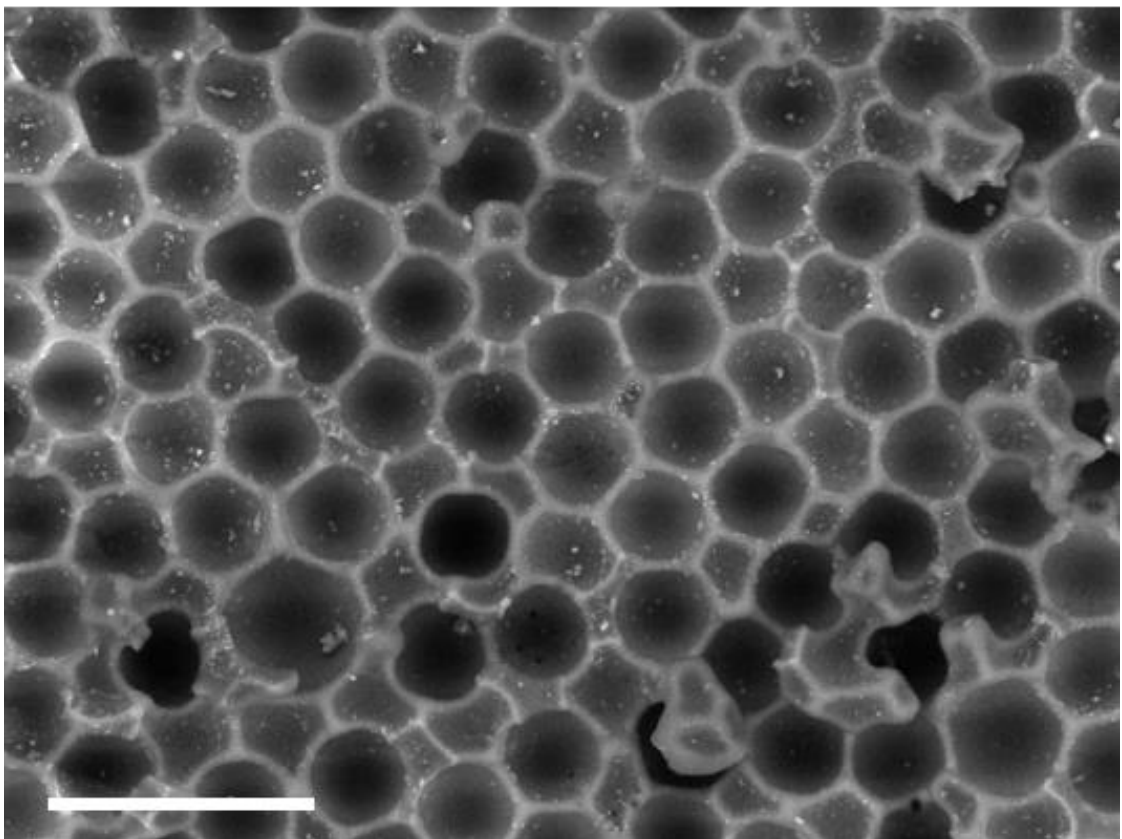


Figure 3.22 SEM of bioimprint produced by exposing curing PDMS to a layer of CA20 PMMA microparticles deposited on glass slides using the Cytospin centrifuge. Scale bars represent a) 100 μm and b) 50 μm , respectively.

Once proof of principle investigations where the volume of glucose was optimised, the methodology was used to produce HL60 bioimprints (Figure 3.23).

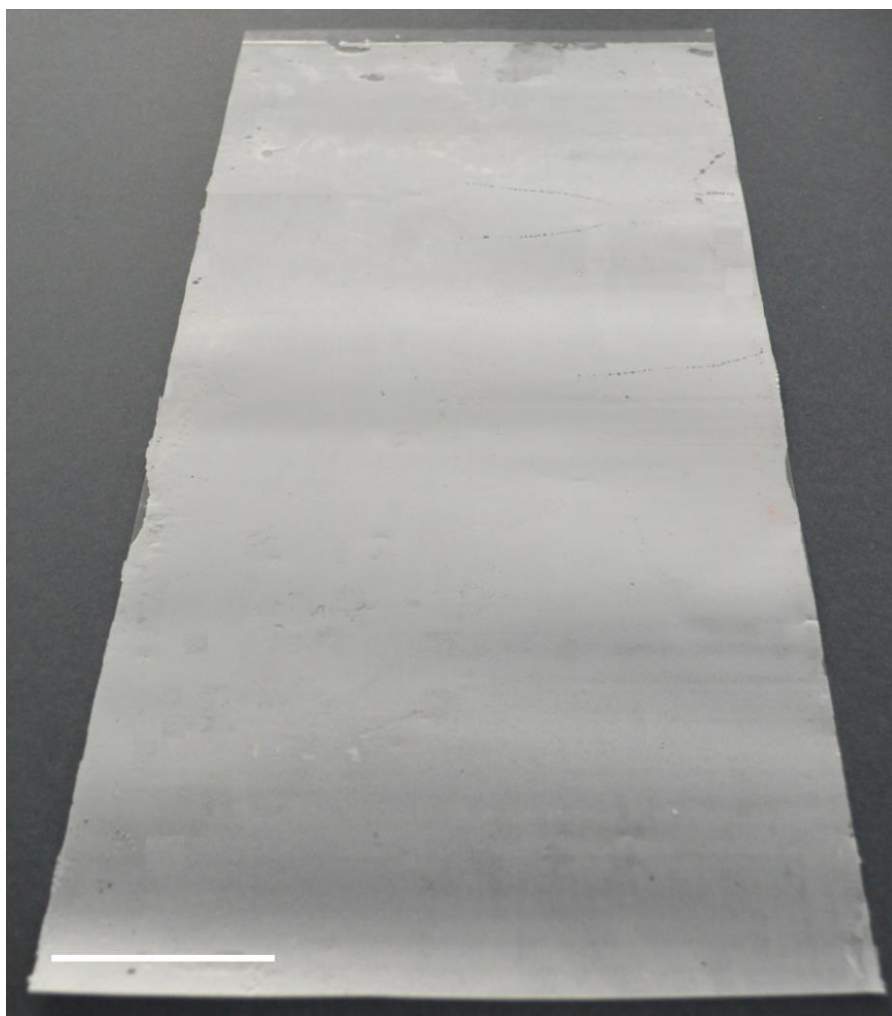


Figure 3.23 Photograph of bioimprints produced by exposing and curing PDMS to a layer of fixed HL60 cells deposited on functionalised glass slides from glucose solutions. The dimensions of the bioimprints are 70 cm × 40 cm. Scale bars represent 10 cm.

Visual inspection showed the imprint to have a good even coverage, unaffected by drying across the substrate. Further examination of the surfaces was carried out with bright field and scanning electron microscopy (Figure 3.24 to Figure 3.26). This showed that drying had not compromised the deposited cells which remained well spread over the substrate. The cell cavities were shown to not interlink as a result of overpenetration of over protection by water or the sedimented glucose. This allows the retention of cells to the cavities which show a size and shape representative of the template cell.

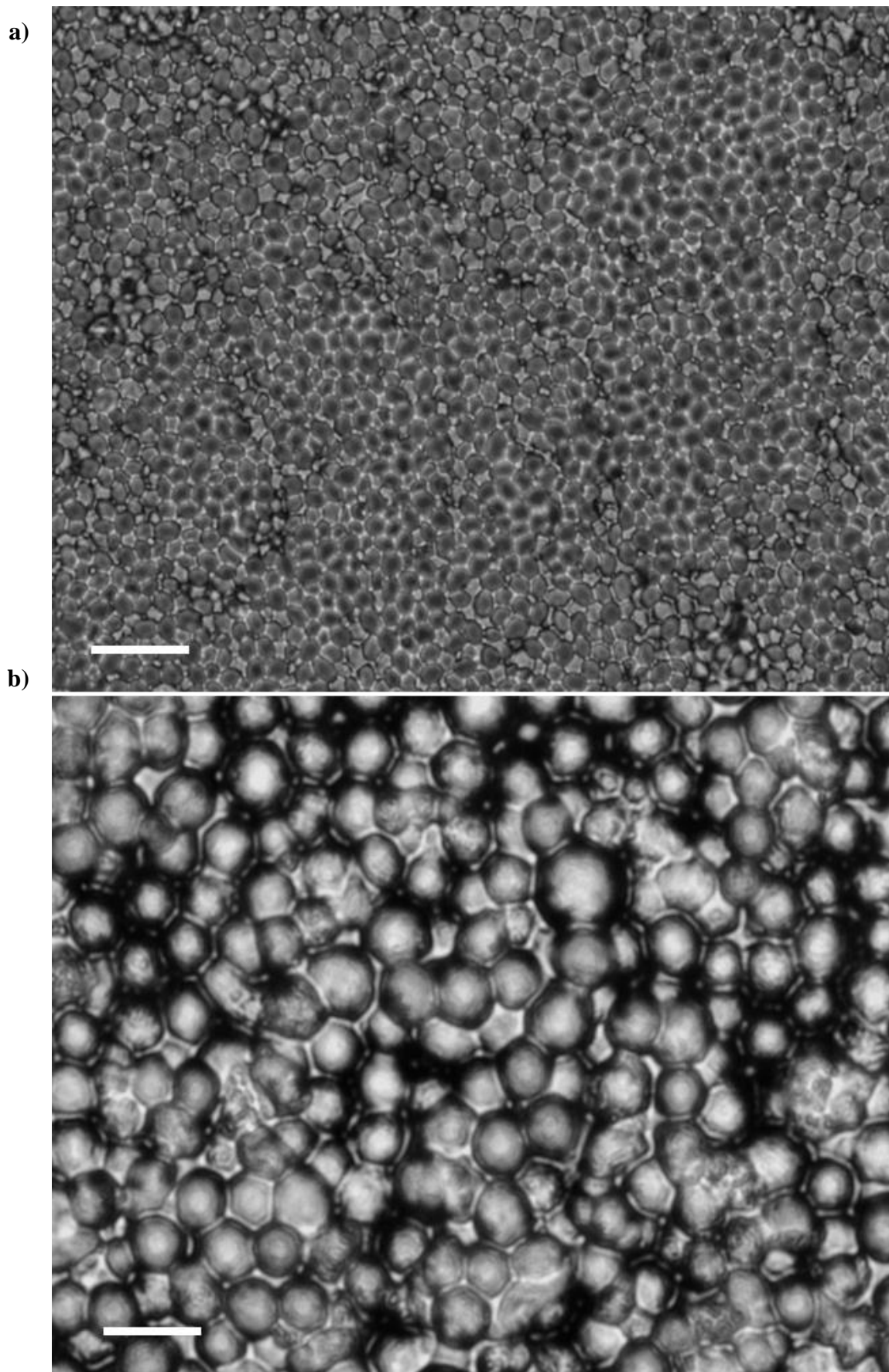


Figure 3.24 Bright field microscopy of various areas of the bioimprint produced by exposing curing PDMS to a layer of fixed HL60 cells deposited on functionalised glass slides from glucose solutions. Scale bars represent a) 100 μm and b) 20 μm , respectively.

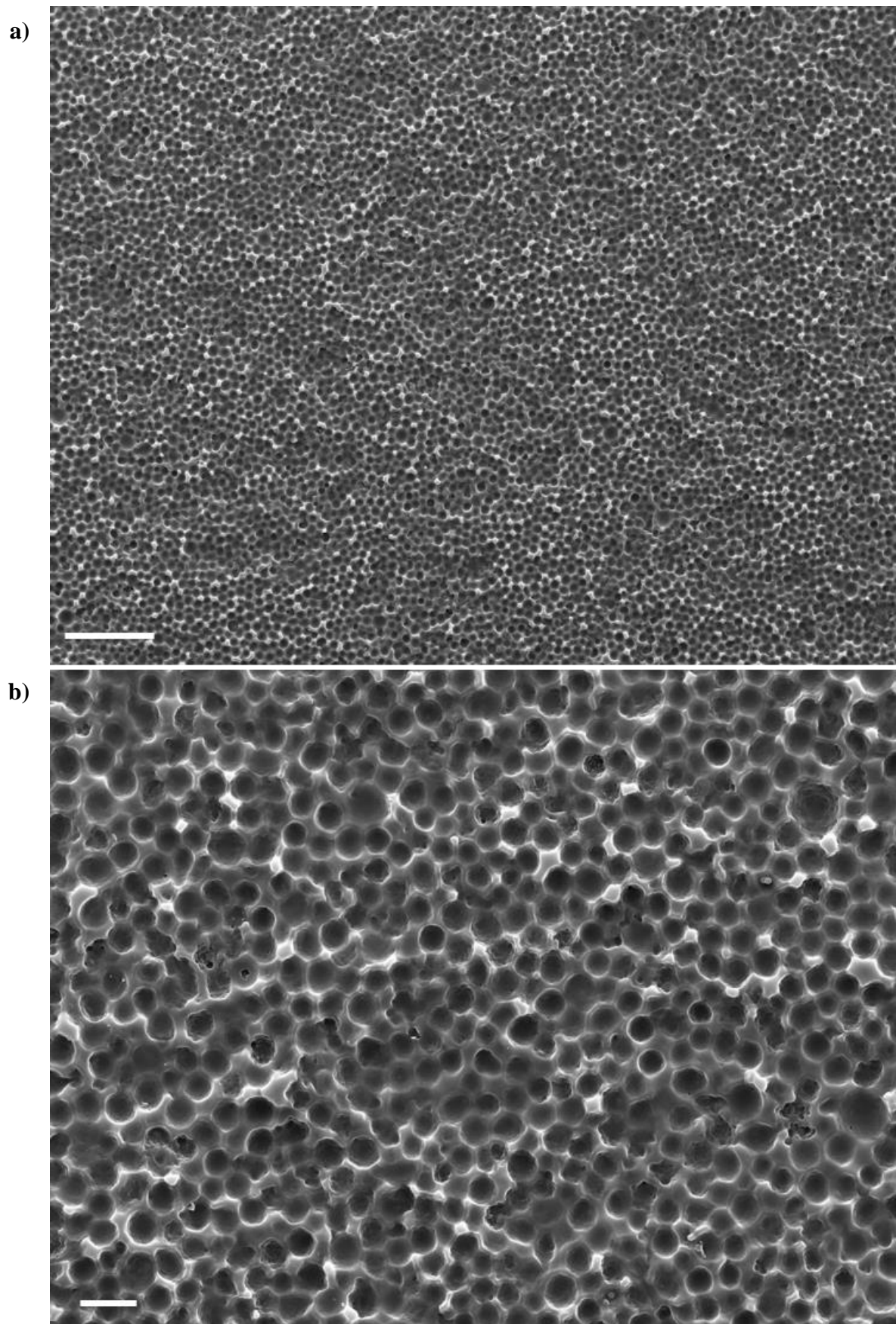
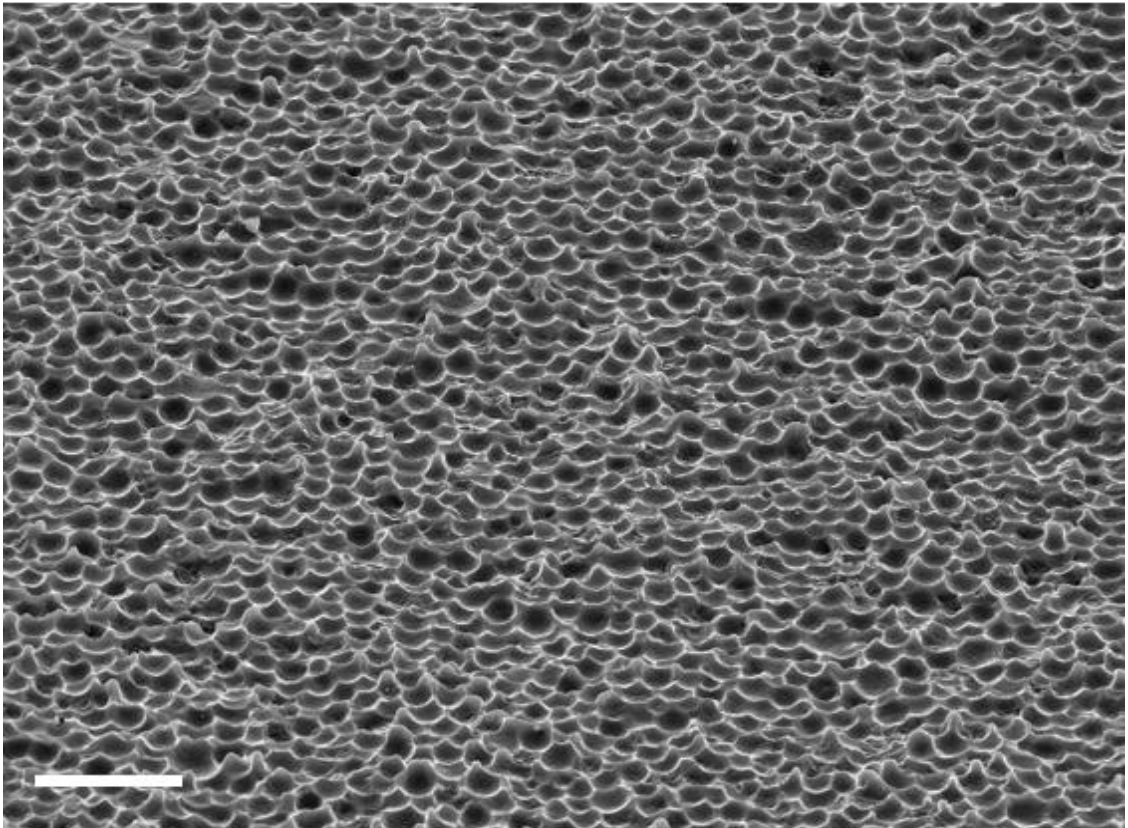


Figure 3.25 Scanning electron microscopy showing various areas of the bioimprint produced from curing PDMS in contact with HL60 layer deposited to glass substrates from glucose suspensions. Scale bars represent a) 100 μm and b) 50 μm , respectively.

a)



b)

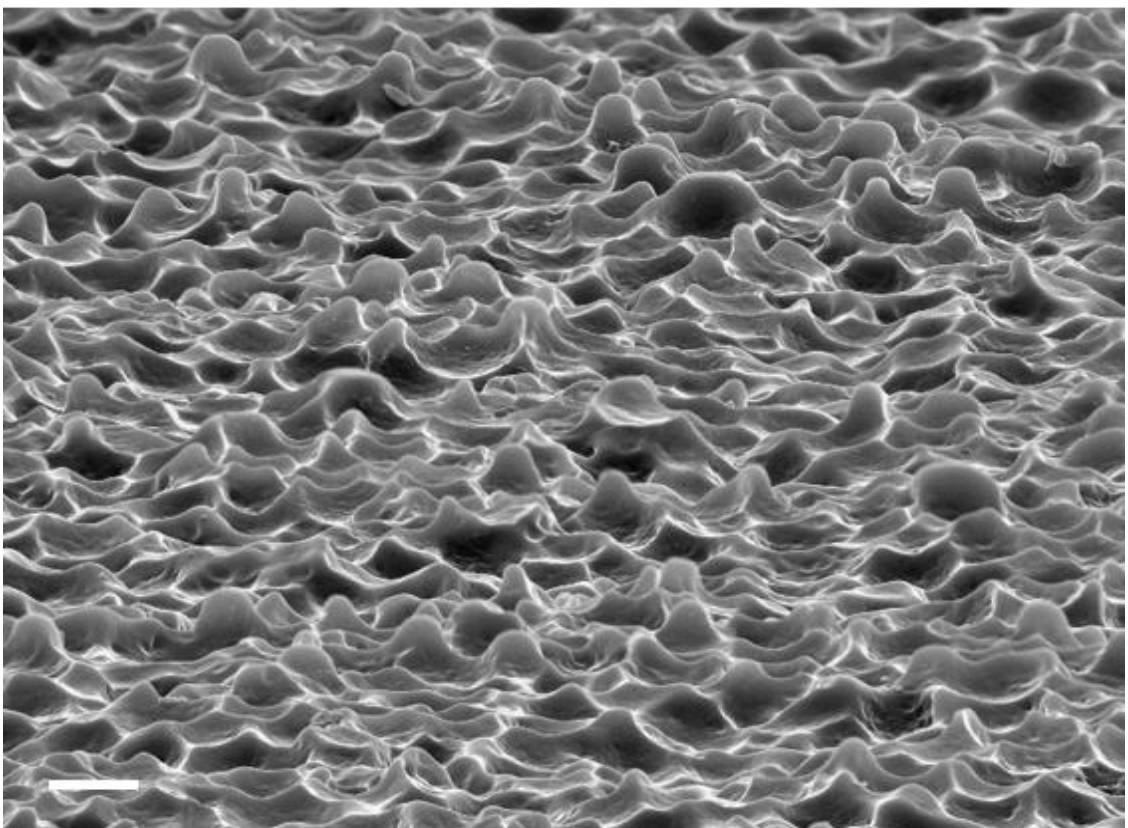


Figure 3.26 Scanning electron microscopy showing various areas of the bioimprint produced by curing PDMS in contact with HL60 layer deposited to glass substrates from glucose suspensions. Samples viewed from 70° offset. Scale bars represent a) 50 μm and b) 100 μm , respectively.

SEM images of the bioimprints surface show an ordered structure representative of the cells intended for capture. Cavities appear to be independent of neighbouring cavities which will allow for efficient capture when substrates are exposed to cell populations. In this instance, samples were tilted to provide a deeper perspective across the substrate. This analysis shows further information of the relative depth of each cavity indicative of what proportion of each cell embossed into the curing polymer material.

3.4. Positive imprints

Print positives of the PDMS bioimprints were made curing a further polymer resin on the bioimprint surface. The importance of positive imprints is twofold; firstly, in further analysis of the morphology of bioimprint cavities to assess the success of the imprint. Qualitative size, curvature and topological complexity examination of the negative imprint is difficult as features are obscured in the cavity. Secondly, in the same manner that the positive imprint is made from curing polymer on the bioimprint surface, multiple negative replica imprints can be made with another polymer resin by templating the positive imprint. This allows the positive imprint to be used to make numerous copies (negatives) for further experiments of retention of the cells used to make the first negative replica of the cell layer.

The combination of using hard and soft materials made the production of bioimprints and positive imprints easier as the surfaces could be released from each other easily. PDMS as a soft material was ideal to be separated from glass substrates and a hard-cured resin was best for the positive imprints.

The best results were found with an UV curable polyurethane (PU). The uncured material had a low viscosity so could be uniformly applied to the bioimprint, and air bubbles removed prior to UV irradiation. UV curing times had to be limited to <120 seconds using a 2 × 6 W lamp from 20 cm as if PU was overexposed, patches became difficult to separate from the bioimprint. This compromised the positive imprint being made and also the re-use of the bioimprint.

As with considering the negative bioimprints produced, the positive imprints will be considered separately for the Cytospin and glucose solution spread cells. Bright field microscopy was used to assess the packing of the cavities on the positive imprint though

further information was not available. The focus of analysis of positive imprints was by using SEM.

3.4.1. Cytospin-mediated positive imprints

A positive replica of the Jurkat cells bioimprints made into PDMS via the Cytospin centrifuge method were produced in NOA68. See Figure 3.27 for a photograph of the positive imprint created from bioimprints of a fixed Jurkat cell layer deposited by Cytospin centrifuge. Visual inspection shows the entire bioimprint to be imprinted in a uniform manner. Dimensions of the positive imprint are 2 cm \times 2 cm.

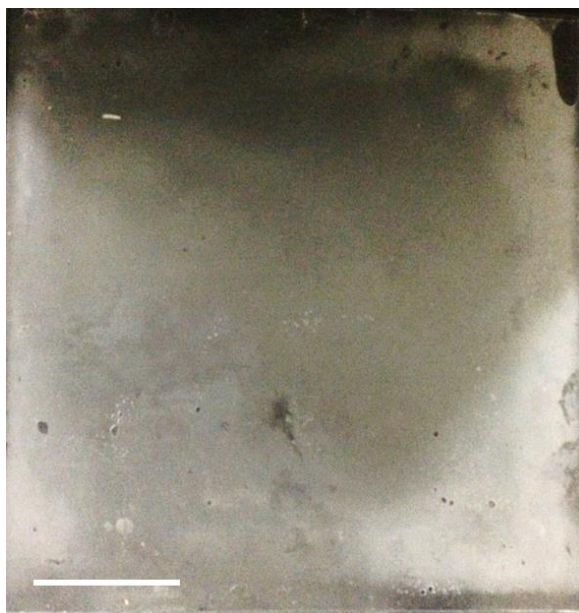


Figure 3.27 Photograph of a NOA68 positive imprint created from a bioimprint made via the Cytospin centrifuge. Scale bar represents 0.5 cm.

For the purpose of SEM imaging, approximately 100 nm of gold was evaporation coated onto the positive imprints to achieve higher resolution. This ensured, high-resolution analysis could be made without localised charging of the surface.

Figure 3.28 and Figure 3.29 show SEM images of the positive Jurkat imprints made from the Cytospin centrifuge mediated bioimprints.

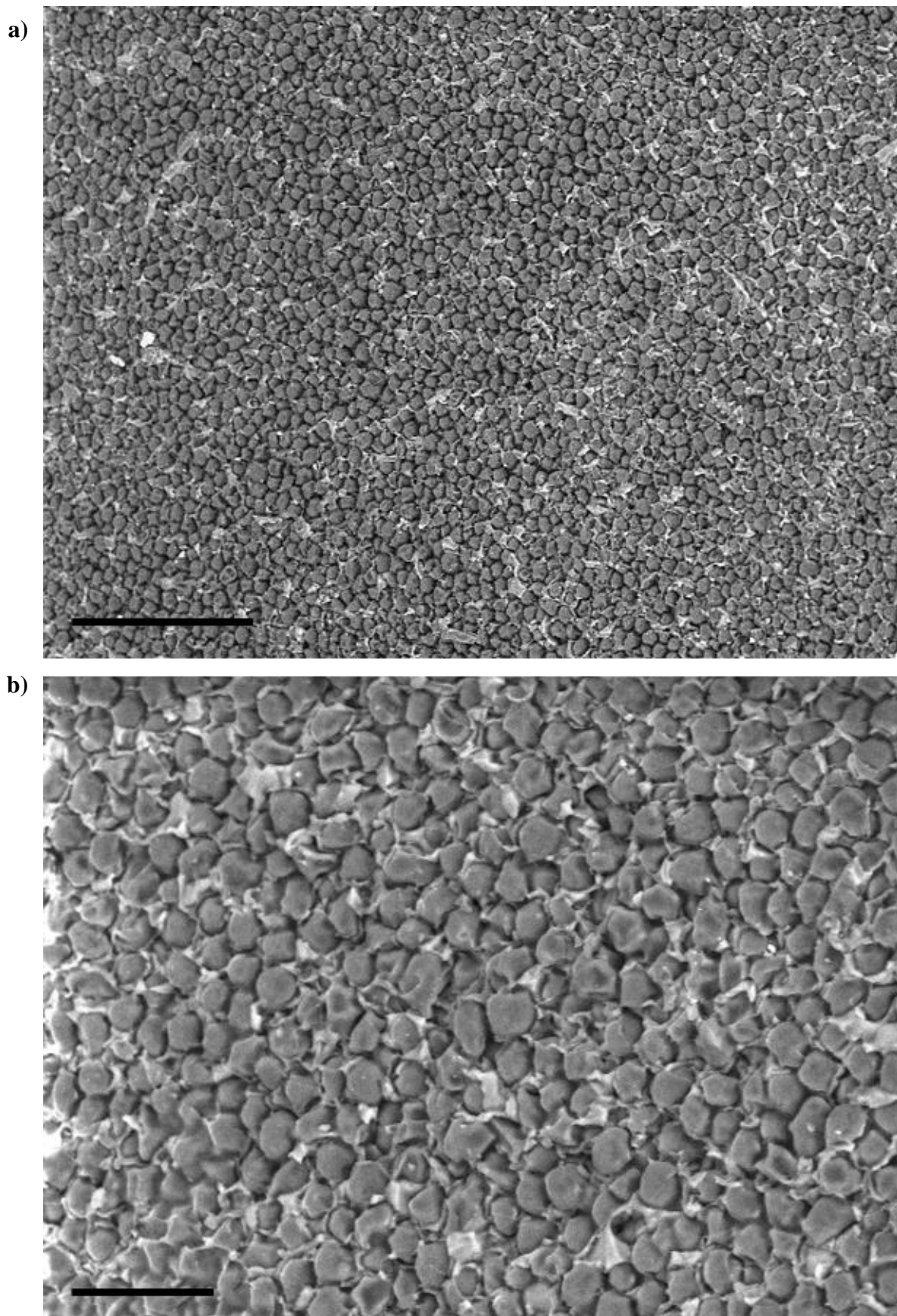
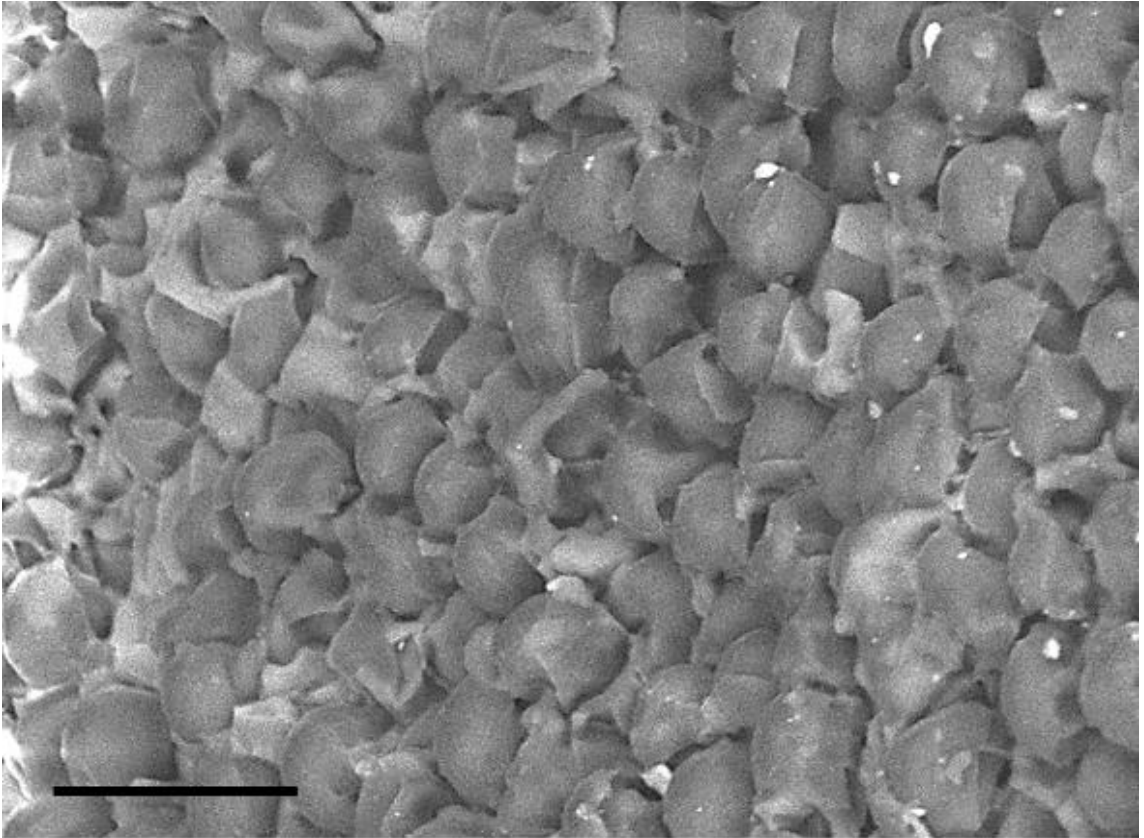


Figure 3.28 Scanning electron microscopy of PU positive imprints taken from Jurkat bioimprints made using Cytospin centrifuge induced cell deposition. Scale bars represent a) 150 μm and b) 50 μm .

a)



b)

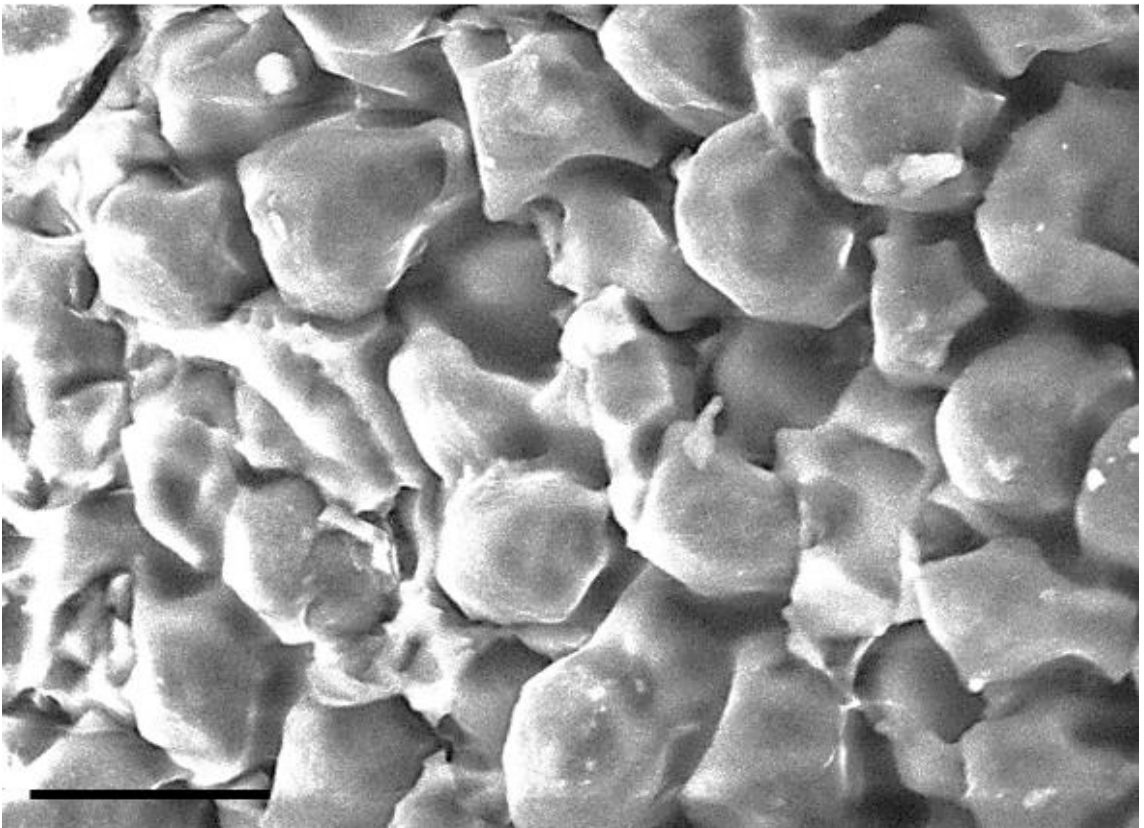


Figure 3.29 Scanning electron microscopy of PU positive imprints taken from Jurkat bioimprints made using Cytospin-induced cell deposition. Scale bars represent a) 25 μm and b) 15 μm .

The positive imprints show a good morphology, representative to that of the templated cell layer as seen in Figure 3.9. A dense layer of replica cells is observed with distinguishable features on separate cells. However, a tunnelling effect can be seen in which adjacent cells appear to be joined by a narrow seam of PU, indicative of over protection by residual water in the immobilised the Jurkat cell layers. This may potentially impact the retention of cells from suspension to bioimprints if cells cannot fit into the neighbouring cavities.

3.4.2. Glucose positive imprints

Positive imprints were also made of the cell layers created by spreading suspensions of fixed HL60 cells in aqueous glucose solutions. See a photograph of the positive imprint, with dimensions of 40 cm × 70 cm. By visual inspection, the imprint shows excellent uniformity over the large area covered shown in Figure 3.30.

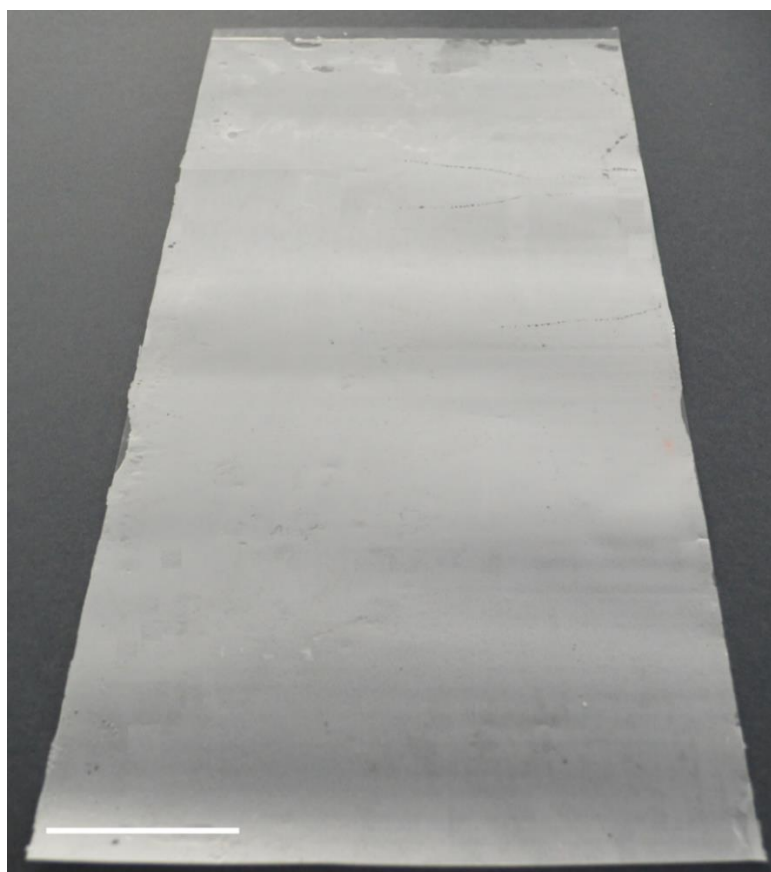
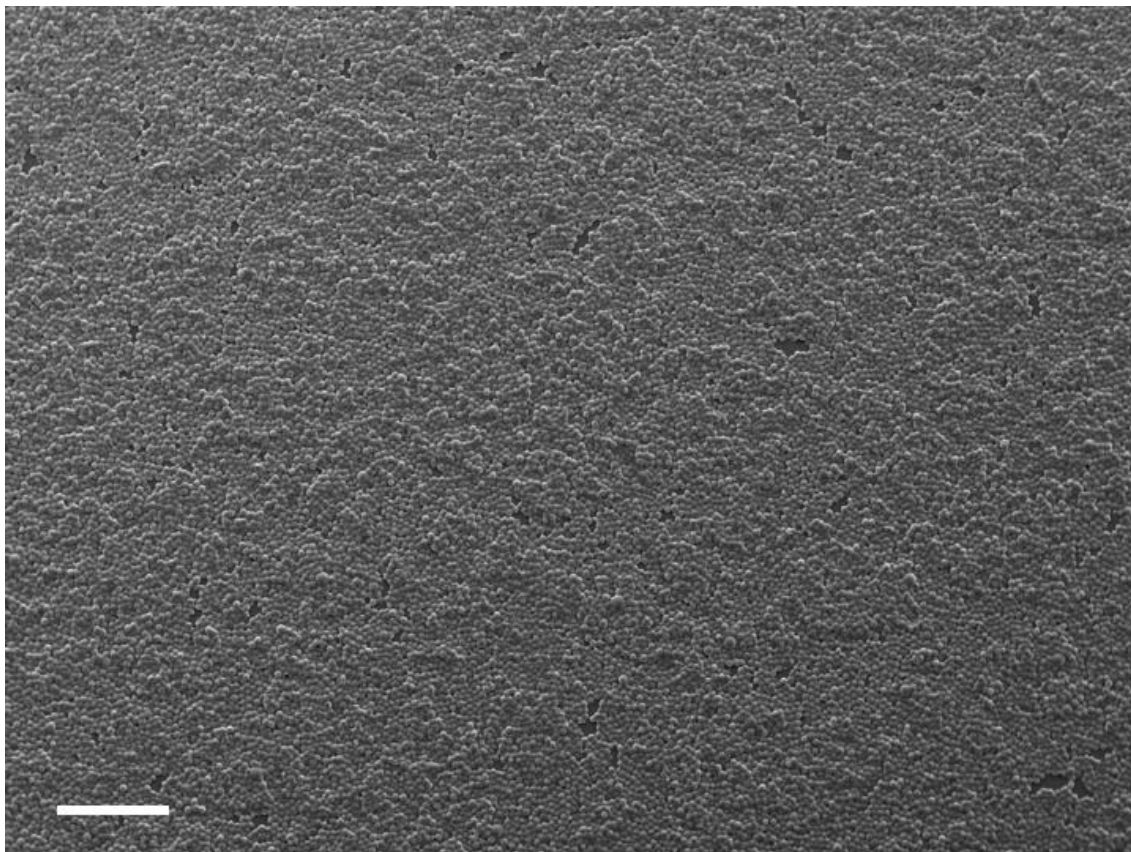


Figure 3.30 Photograph of the positive imprints created from bioimprints made from suspensions of fixed HL60 cells spread from aqueous glucose suspensions. Scale bar represents 5 cm.

SEM analysis was done of positive imprints created from bioimprints of HL60 cell layers produced by spreading HL60 suspensions in aqueous glucose solutions. Prior to the analysis, the samples of positive imprints had approximately 50 nm of gold deposited by evaporation. Analysis of various areas of positive imprints made via the cells in glucose solution method was carried using SEM (shown in Figure 3.31 and Figure 3.32).

a)



b)

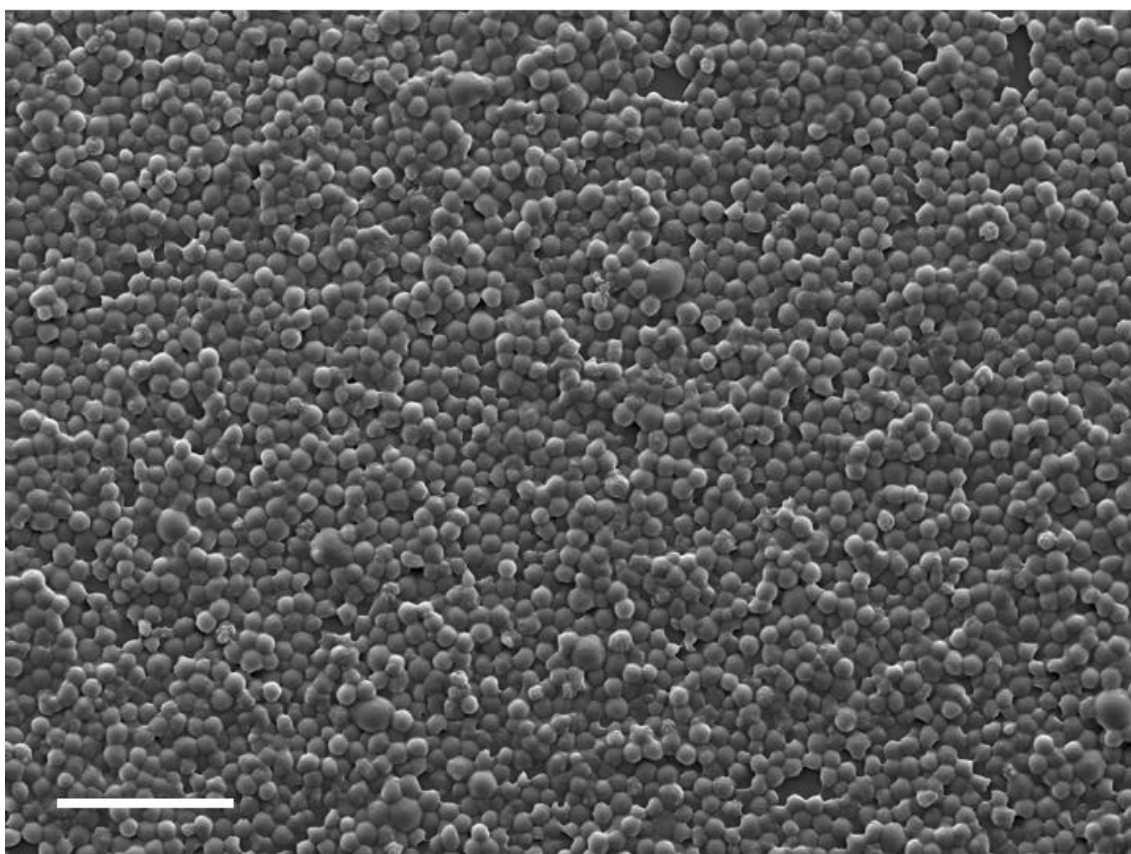


Figure 3.31 SEM examination of areas of the PU positive imprint taken from PDMS bioimprints of HL60 cells obtained from spreading HL60 cells in aqueous glucose solution on glass substrates. Scale bars represent a) 200 μm and b) 100 μm .

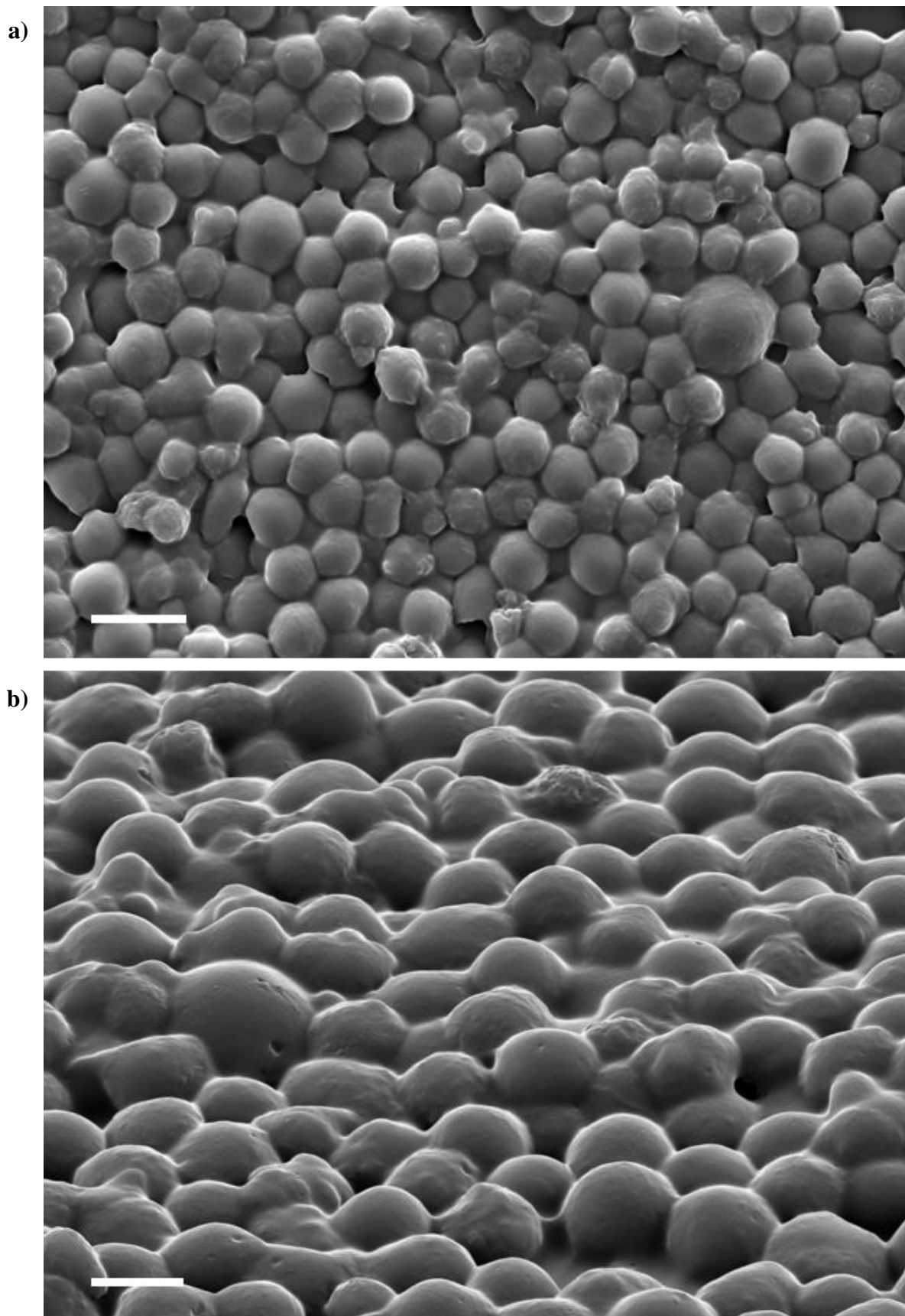


Figure 3.32 SEM images of areas of the PU positive imprint taken from PDMS bioimprints of HL60 cells suspensions in aqueous in glucose solutions spread on glass substrates. Scale bars represent a) 20 μm and b) 10 μm .

Images of the positive imprint show clearly defined cells surface morphology, representative of the size and shape of the HL60 template. In this instance, less of a channelling effect was observed meaning that the cavities in which a cell is adhered would have no competition with neighbouring sites. Extracellular features can be clearly seen on the cell surfaces indicating accurate copying of size and shape information on a low micron scale. Viewing positive imprints from an offset prospective allows a determination of the curvature of the imprinted cavities; qualitatively showing a rounded cell shape indicating template cells have not been deformed during bioimprint manufacture.

Bioimprints have been made and successfully replicated ready for cell retention testing. However, to be used as part of a cell capture device targeting AML myeloblasts the area needed is significantly larger. In doing, an augmentation step is required; roll-to-roll imprinting.

3.5. Imprint augmentation

Thus far, bioimprints have been produced showing similar dimensions to those reported in literature in the case of the Cytospin method (0.0004 m^2) and significantly larger for those spread from glucose solutions (0.28 m^2). However, in order to make the bioimprint relevant for a real-world, clinical application the total size of bioimprint needs to be increased further. Cytospin-mediated cell imprints are restrained by the size of the centrifuge setup and are already made to the maximum specification. Though the glucose spread solutions can be made to a user defined size, it is unfeasible to cover such a large area.

Roll-to-roll nanoimprint lithography (R2RNIL) was identified as a method of fabricating the nanometre to micron scale features of bioimprints onto substrates covering multiple square metres. In other commercial applications, the high throughput method is used for fabrication of nanoscale features, well below those needed in this project, with the ability to control imprint thickness by control of parameters such as roller pressure and speed.²⁰

In conjunction with the Joanneum Research Institute (Austria) positive bioimprints were mounted to the circumference of an imprinting drum. This cylinder is rolled in

conjunction with a film containing UV curable PU photoresist, with pressure maintain by a secondary cylinder. The process has a user defined speed, in this case at imprints were produced at 1, 2 and 3 m s⁻¹ with dimensions 0.4 m × 100 m.

The following sections will address the replication of prepared bioimprints beginning with Cytocentrifugation and followed by those made from spread glucose suspensions.

3.5.1. Cytospin augmentation

In order to fully cover imprinting drum, multiple imprints were made onto a PET foil substrate such that each was placed adjacent to the previous imprint. This created a patch work effect of 2 cm × 2 cm imprints across a total area of 15 cm × 5 cm. Though each imprint is separated by an unimprinted polymer the majority of the area would be comprised of bioimprinted cavities. This reduces the efficiency of an overall device as less of the substrate is patterned however, the flow device can be designed so that much of the unimprinted area is covered by channel walls to reduce inefficiency. See Figure 3.33, below, for a photograph of the patchwork of positive imprints made to cover a larger area which were then applied to the imprinting drum.



Figure 3.33 Photograph of a patchwork of multiple positive imprints made sequentially next to the previous one yielding a total imprinted area of 15 cm × 5 cm. Image taken after use in R2RNIL device; deterioration of metal coating is clearly visible. Scale bar represents 2 cm.

The patchwork of positive imprints was in turn applied to the circumference of the imprinting drum sequentially to cover an area of 30 cm × 10 cm. Positive imprints were evaporation coated with ~ 100 nm of nickel in order to prevent interaction between the positive and newly imprinted replica negative. The R2RNIL device was run at 1, 2 and 3 m s⁻¹ for a total distance of 100 m. Figure 3.34 shows images of replica Cytospin imprints augmented by R2RNIL.



Figure 3.34 Photograph of replica bioimprint embossed into UV curable PU photoresist R2RNIL from bioimprints made using Jurkat cells deposited by via the Cytospin centrifuge. Scale bar represents 6 cm.

As can be seen from Figure 3.34, R2RNIL was poor in copying the patchwork of Jurkat bioimprints with the replica imprints incompatible with the intended application. The method provides difficult control over the difference in thickness of each imprint resulting in a multilevel imprint. This proves problematic when the device is in action as first the metal coated layer is degraded over time followed by the positive imprint being removed. As the progress of the imprint continued, a greater proportion of the master positive imprint was worn off resulting in a poorer replica imprint. Damaged areas are recirculated on the master imprint and are seen periodically in the replica. Ultimately, the R2RNIL print was stopped as the master imprint had fully degraded. Early parts of the replica imprint were examined with bright field microscopy (shown in Figure 3.35).

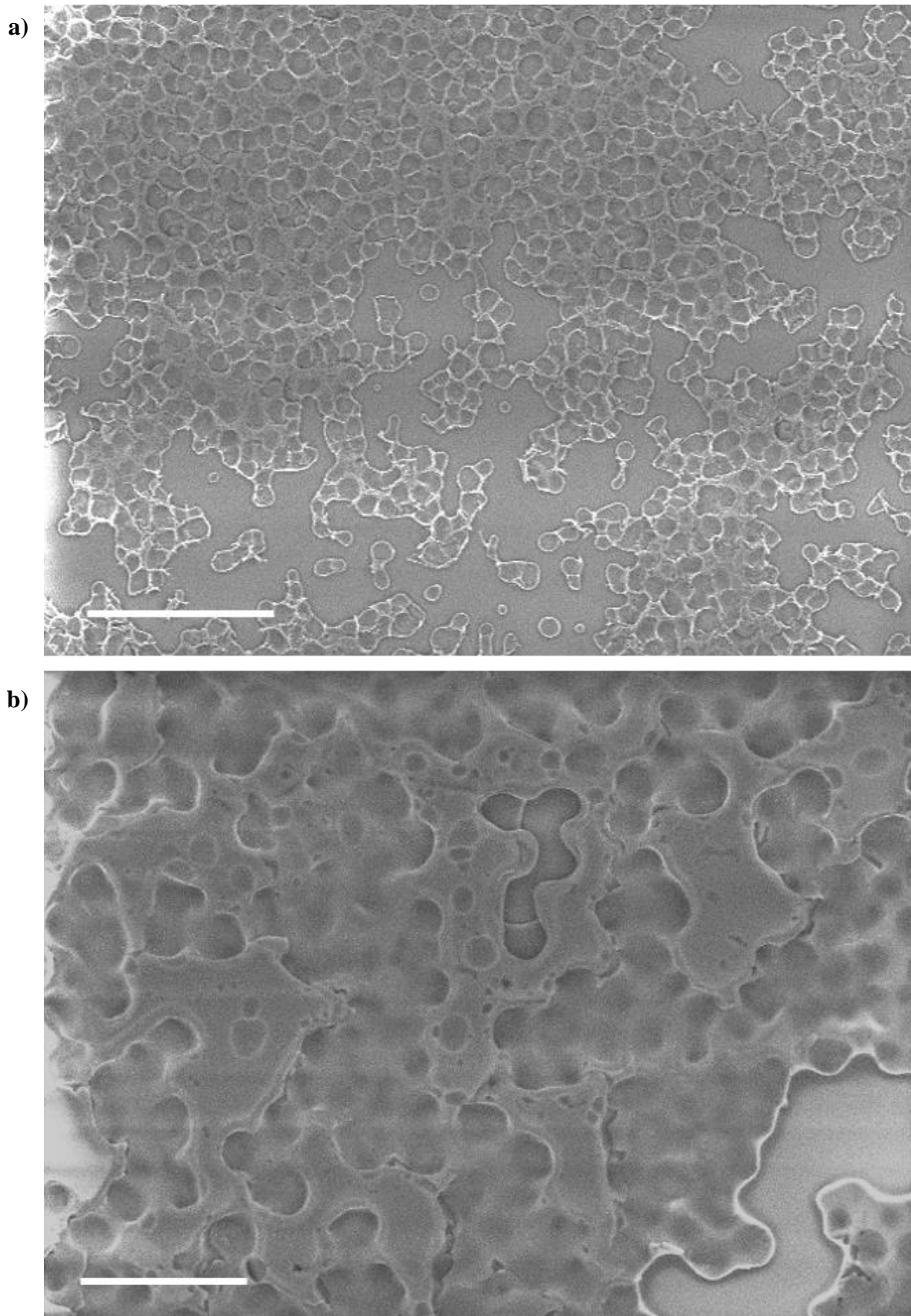
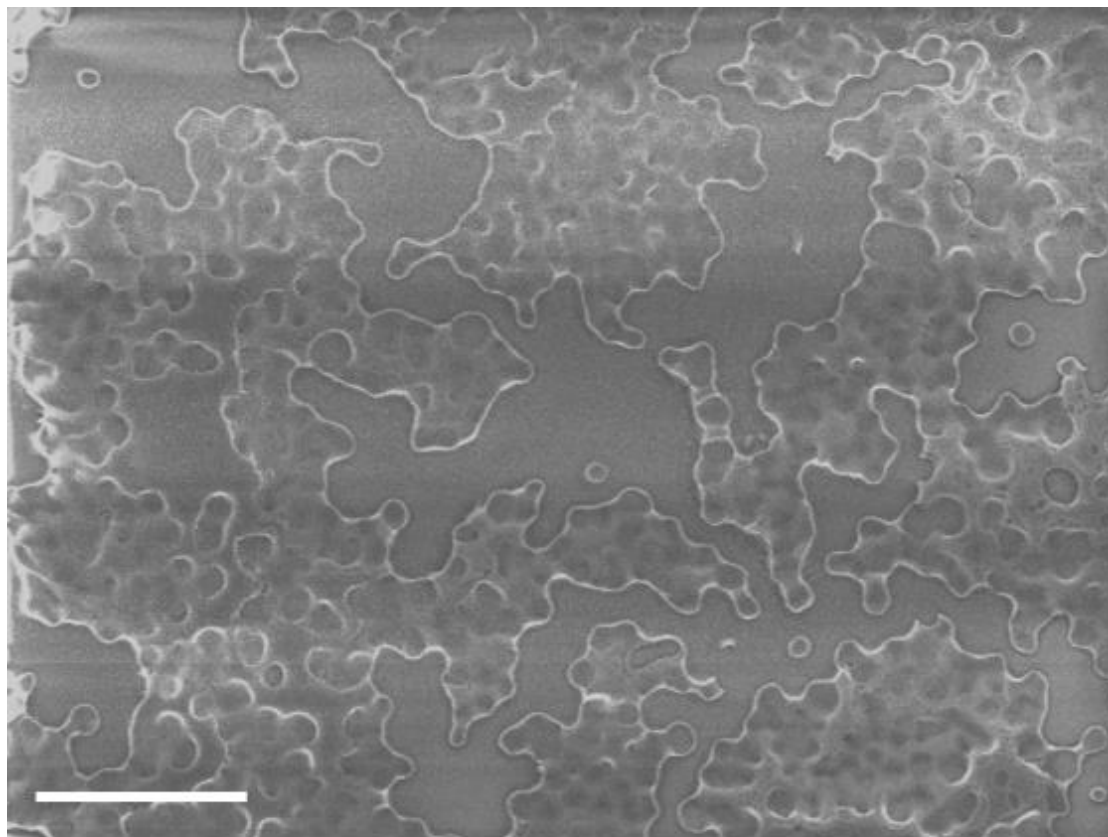


Figure 3.35 Bright field microscopy of early parts of the PU photoresist replica bioimprint. Scale bars represents a) 150 μm and b) 50 μm , respectively.

Latter sections of the imprints were either entirely non-imprinted or showed a very poor structure (see Figure 3.36). See below for bright field microscopy analysis of the replica imprint after catastrophic deterioration of the master positive imprint.

a)



b)

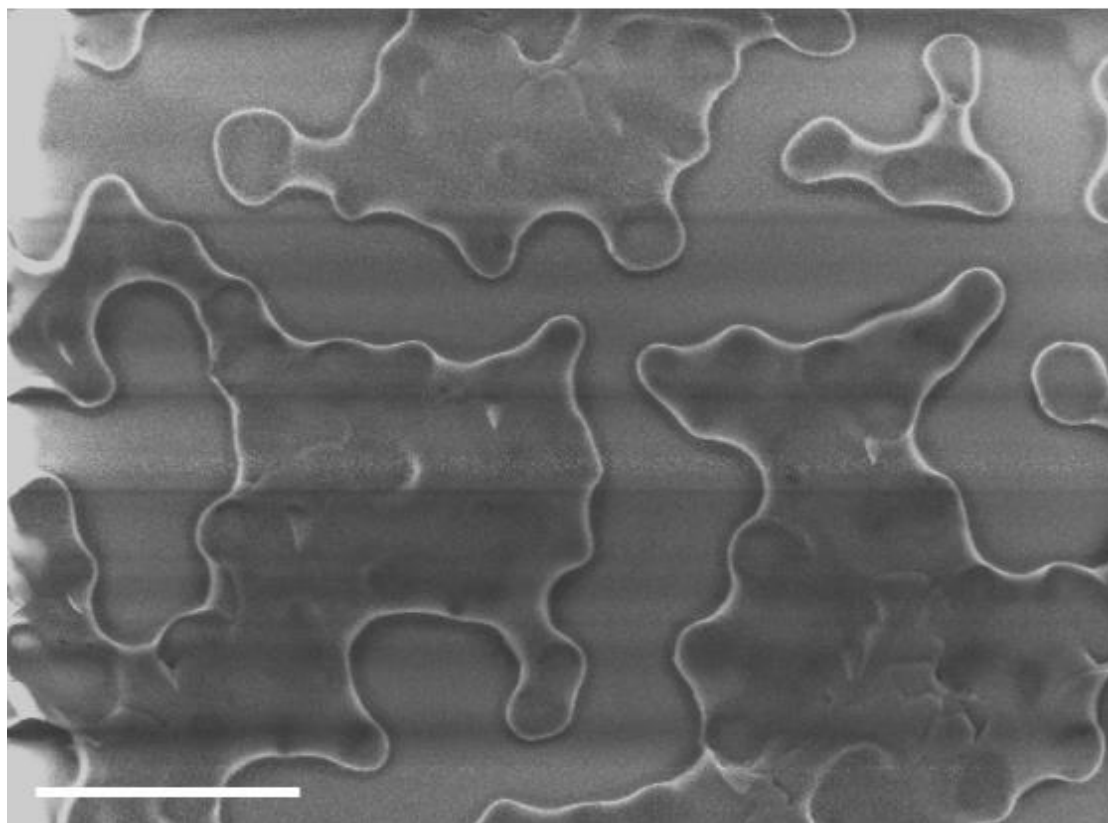


Figure 3.36 Bright field microscopy of early parts of the PU photoresist replica bioimprint. Scale bars represents a) 150 μm and b) 50 μm , respectively.

The un-imprinted polymer accumulation in the perimeter of each imprint forms a barrier preventing the thin film on the receiving PET foil to contact the bioimprint. This problem cannot be overcome by adding additional polymer to the imprinting drum as this is squeezed from the imprint by the pressure between the drums and contaminates the inner working parts of the device.

The replica imprint was of poor quality, entirely unrepresentative of that of the positive master imprint used to on the imprinting drum (see Figure 3.28 and Figure 3.29). Cell cavities can be seen in the PU; however the coverage is not uniform and vast areas of the replica are un-imprinted. In most areas, no size or shape information is discernible and no cavities were produced that the original cells can fit into. Though some areas of the imprint were better than others, a uniform surface imprint across the whole surface is needed.

Ultimately, bioimprints created using the Cytospin protocol are poorly replicated by R2RNIL and are incompatible with use in a myeloblast capture device. The largest size of the bioimprint is restrained to 2 cm × 2 cm, which in turn provided unable to be reliably copied by R2RNIL. All further work using cytocentrifugation to deposit template cell populations was discontinued.

3.5.2. Glucose protective layer

As mentioned previously, creating bioimprints from spreading fixed cells in glucose solutions does not suffer from the same experimental restraints. Instead, the imprints were made larger and larger from 10 cm × 10 cm and repeated to cover 40 cm × 70 cm which is able to fully cover the circumference of the imprinting cylinder. Therefore, the master positive imprint has one seam where the positive imprint is attached to the imprinting shim. Conversely, the Cytospin centrifuge mediated bioimprints contained a patchwork structure, with separate imprints of relatively different thickness. This uneven distribution made the nickel coating vulnerable to damage during processing which was not seen with glucose protective layer bioimprints. Figure 3.37 shows a photograph of the HL60 replica imprint after replication by R2RNIL.

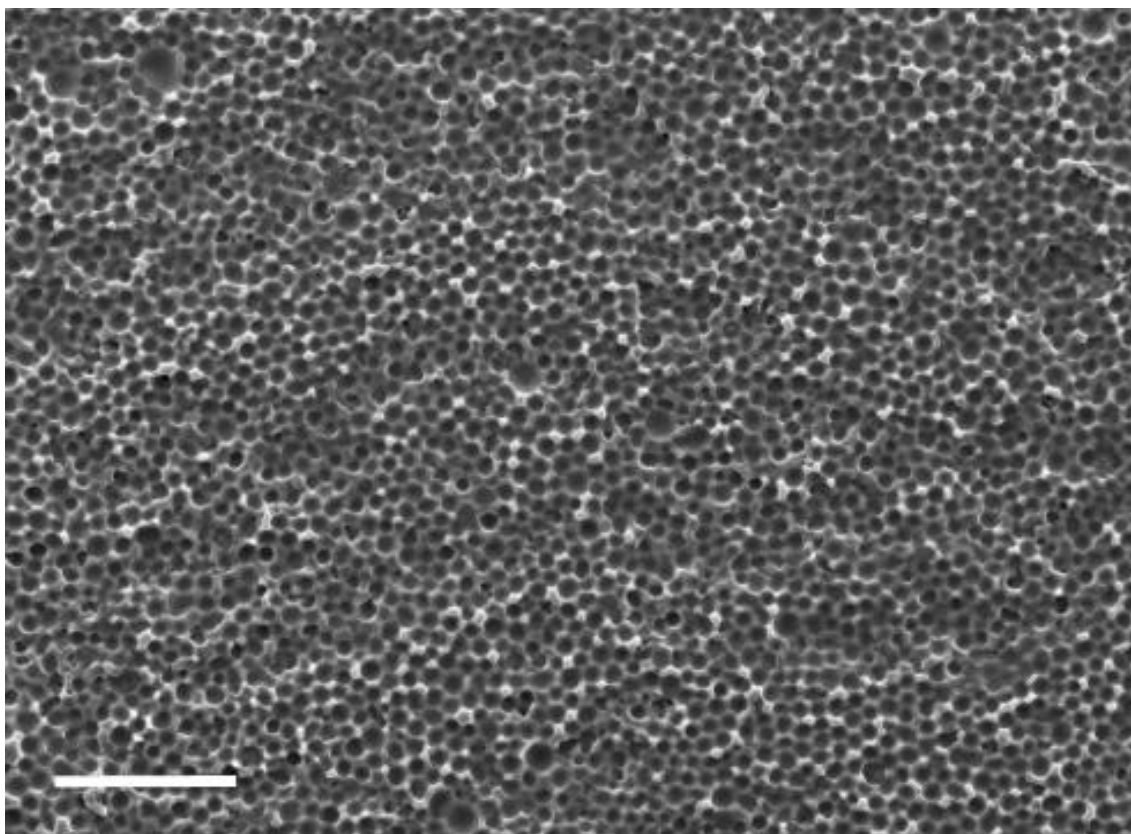


Figure 3.37 Photograph of the replica HL60 bioimprints augmented to cover $0.4 \text{ m} \times 100 \text{ m}$ by R2RNIL. Scale bar represents 20 cm.

Unlike the replica imprints from bioimprints produced via the Cytospin method, the glucose solution showed a uniform structure across the whole surface. A periodic fault can be seen to repeat every 70 cm though when used in a myeloblast capture device this area is negligible compared to the total area of bioimprint; also, significantly less than that seen with Cytospin-mediated imprints. Moreover, the fault can be incorporated into the design of the flow-through device so that cells are not eluted over this part. Variation between areas of the same imprint and subsequent imprints appears to be negligible.

No evidence of the positive master imprint degrading as the run continued was seen; the same master bioimprint could be reused and made replicas of $0.4 \text{ m} \times 100 \text{ m}$ using a run speed of 1, 2 and 3 m s^{-1} . The micrometre scale success of the bioimprint was confirmed by SEM analysis of various areas of the replica imprint (Figure 3.38 – Figure 3.39). Replica imprints were coated with $\sim 100 \text{ nm}$ of gold by evaporation coating prior to analysis.

a)



b)

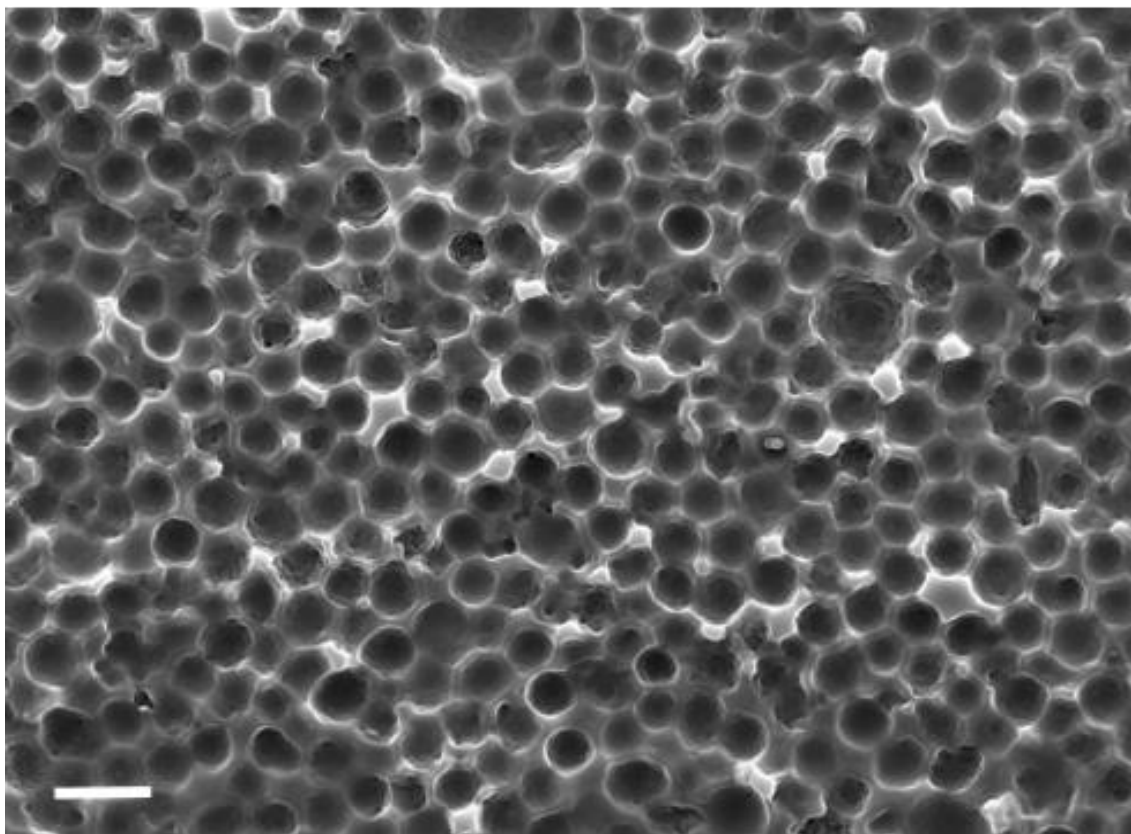


Figure 3.38 SEM images of the replica imprints of bioimprints created from HL60 cells spread in aqueous glucose solutions and replicated via R2RNIL. Scale bars represents a) 100 μm and b) 20 μm .

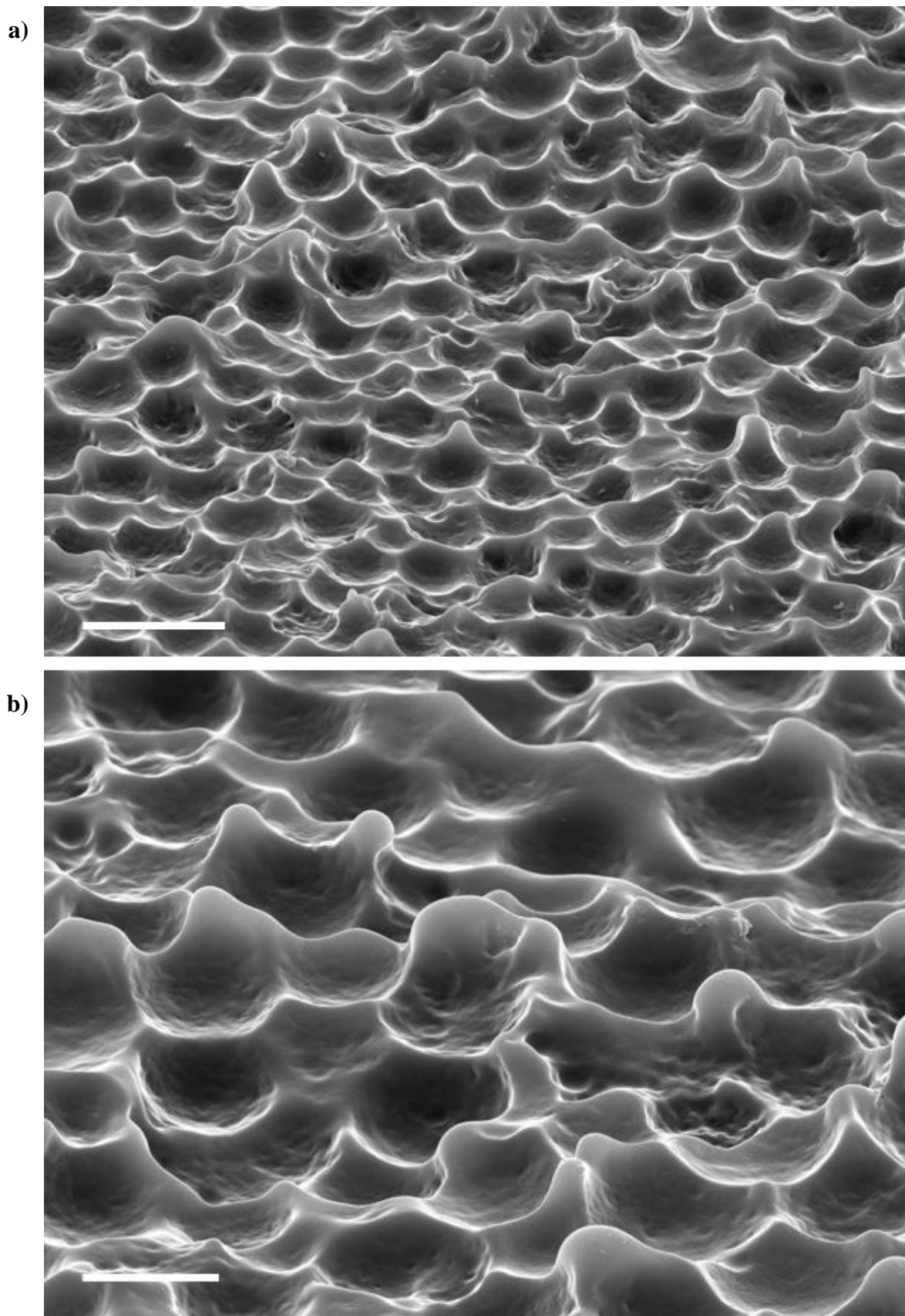


Figure 3.39 SEM images of the replica imprints of bioimprints created from HL60 cells spread in aqueous glucose solutions and replicated via R2RNIL. Scale bars represents a) 20 μm and b) 10 μm .

SEM analysis showed bioimprints to have excellent microstructure, uniform across the replica imprint and representative of the original bioimprints. Individual cavities are clearly seen with a size and shape representative of the template material and all stages of the imprinting process.

3.6. Conclusions

This chapter aimed to fabricate a bioimprinted replicas of blood cancer cells. Thus far, a more readily available immortalised cell line proxy and more readily available cell and particles templates of very similar size to myeloblast have been selected for the production of bioimprints.

To enable an accurate capture of cell shape and size information, unaffected by deformation from harsh cell handling or swelling as a result of osmotic pressure differences, the templated cells were chemically fixed. Numerous methods were trialled, aimed at preserving an accurate size and shape representation of live cells. All fixatives were assessed by flow cytometry to compare the size (by forward scatter) and surface complexity (by side scatter). Ultimately, glutaraldehyde was shown as the fixative of choice, least effecting the cells shape morphology as confirmed by flow cytometry and optical microscopy. By reducing the concentration of glutaraldehyde and using dropwise addition into a stirred solution, cell populations could be fixed with few aggregates formed.

Fixed cells and particles were deposited on activated glass substrates to produce a dense cell layer. It was important to consider an approach that could allow control over the proportion of the cell protruding from the cell layer. A protecting layer was designed in order to copy only a part of the cell surface, so that the resin matrix could engulf the cells which would form cavities that are inaccessible for cells to enter. Conversely, if too little of the cell was present, the cavities would have a poorer increase of the surface area coverage between the imprint and cells. Shielding in this instance was seen mostly from excess water in the immobilised cell layer; though added complexity arose if cell layers were allowed to over dry and the layer rupture and aggregate.

Various methods were trialled to reliably produce densely packed films of template material. Two methods in particular were successful; by Cytospin centrifuge and by spreading cells suspension in aqueous glucose solutions using a bespoke spreading tool.

The first offered the desired control as duration and spin speed could be optimised to yield an even cell layer with a predictable level of water. The latter relied on fine tuning of the glucose volume, acting as a viscous protection against film rupturing whilst not swamping cells. Both methods yielded excellent bioimprints cast into PDMS. The soft, elastic properties of PDMS proved convenient in bioimprint and positive imprint production as surfaces could be separated without damage.

Analysis of positive imprints created in PU photoresist showed a good structure; producing imitation cell layers. For the intended clinical use, the bioimprints total size needed to be augmented into a scale of hundreds of square metres. Roll-to-roll nanoimprint lithography was identified as a suitable method to upscale imprints, having been shown to be effective for features in the hundreds of nanometre scale. Bioimprints created using the Cytospin centrifuge were found to be incompatible with R2RNIL as their size was restrained to 2 cm × 2 cm, which could not effectively be applied to the imprinting drum. Bioimprints from the Cytospin method showed no scope in real world applications and efforts were discontinued.

Instead, imprints created from glucose solution spreading could be made larger so that a single bioimprint (40 cm × 70 cm) could be attached to the imprinting drum. The master positive in this case did not deteriorate and was reused to make three imprints of 0.4 m × 100 m. This total surface area coverage is vastly larger to any bioimprinting studied reported in literature which tend to be on a square millimetre scale. For use in a clinical AML cell capture device this area is sufficient to capture significant quantities of the large cell volumes anticipated. Replica imprints from this method showed an excellent packing of cells across the vast majority of the imprinted area. The imprints provide a good, efficient use of space; able to retain cells to cavities independent of each other.

As a reproducible procedure has been elucidated for the manufacture and the mass production of bioimprints of myeloblast layers. The next chapter will focus on quantitative analysis of the bioimprint topography and examine physical and chemical surface modifications in order to engineer a controllable attraction towards target cells.

3.7. References

- 1 O. Hayden and F. L. Dickert, *Adv. Mater.*, 2001, **13**, 1480–1483.
- 2 B. Alberts, A. Johnson, J. Lewis, M. Raff, K. Roberts and P. Walter, *Molecular Biology of The Cell*, Garland Science, New York, 6th ed., 2015, pp. 597–638).
- 3 M. Shehadul Islam, A. Aryasomayajula, P. Selvaganapathy, M. Shehadul Islam, A. Aryasomayajula and P. R. Selvaganapathy, *Micromachines*, 2017, **8**, 83.
- 4 J. S. Dickson, M. Koohmaraie and R. L. Hruska, *App and Env. Microbiol.*, 1989, **55**, 832-836.
- 5 O. V Bondar, D. V Saifullina, I. I. Shakhmaeva, I. I. Mavlyutova and T. I. Abdullin, *Acta Naturae*, 2012, **4**, 78–81.
- 6 Y. A. Ermakov and V. S. Sokolov, *Membr. Sci. Technol.*, 2003, **7**, 109–141.
- 7 Q. Liu, F. Lin and R. A. Hartwick, *J. Chromatograph. Sci.*, 1997, vol. 126-130.
- 8 V. N. Paunov, P. A. Kralchevsky, N. D. Denkov and K. Nagayama, *J. Colloid Interface Sci.*, 1993, **157**, 100–112.
- 9 H. Shinto, D. Komiyama and K. Higashitani, *Langmuir*, 2006, **5**, 2058-2064.
- 10 M. W. Wessendorf and T. C. Brelje, *Histochemistry*, 1992, **98**, 81–85.
- 11 C. Lefevre, H. Kang, R. Haugland, N. Malekzadeh, S. Arttamangkul and R. Haugland, *Bioconjugate Chem.*, 1996, **7**, 482-489.
- 12 B. Stokes, *Lab. Med.*, 2008, **35**, 434-437.
- 13 V. Schnadig, *Diagnostic Pathology of Infectious and Inflammatory Diseases*, Elsevier, Boston, 2010, ch.4, pp. 23–75.
- 14 M. Bibbo and D. C. Wilbur, *Comprehensive Cytopathology*, 3rd ed., Saunders/Elsevier, 2008, pp. 1120.
- 15 Z. Qing-fan, *J. Tongji Med. Univ.*, 1986, **6**, 256–261.
- 16 D. Hanson and M. Atlas, *Manual of Pediatr. Hematol. Oncol.*, 2016, 453–472.
- 17 L. Wolf, M. Lappé, R. Peterson and E. Ezrailson, *FASEB J.*, 1993, **7**, 1265–8.
- 18 T. Dang, M. Nikkhah, A. Memic and A. Khademhosseini, *Polymeric Biomaterials for Implantable Prostheses*, Elsevier, 2014, *Ch. 19*, pp. 309-331.
- 19 A. Subramaniam and S. Sethuraman, *Nat. Synth. Biomed. Polym.*, 2014, 301–308.
- 20 S. H. Ahn and L. J. Guo, *ACS Nano*, 2009, **3**, 2304–2310.

4. Bioimprint Characterisation and Modification

Thus far, methods have been elucidated and optimised to reliably produce bioimprints using various templates. This section aims to quantitatively characterise the topography and morphology of surface cavities by comparison with the template cell layers. Also described are the physical and chemical surface modifications performed on the bioimprints, aiming to improve cell retention onto imprints.

4.1. Bioimprint characterisation

4.1.1. Cavity diameter

Qualitative assessment of the success of bioimprints produced in Chapter 3 showed surfaces yielding a densely packed, honeycomb-like lattice of surface cavities, which are negative replicas of the cells on the surface of the original cell layer. High cavity surface density is required for the efficiency of the substrate when used as a cell-trapping device; however, the size and shape of the cavities are of particular significance. Here, the length mean diameter [1,0] of the bioimprint cavities was measured using high resolution SEM images of the Jurkat bioimprints and compared to the diameter of Jurkat cells. Measurements were made at the centre of the cell cavity horizontally, to negate any influence of the cells not being symmetrical. Figure 4.1 shows the analysis of SEM images of Jurkat cell bioimprints produced via the Cytospin-mediated method.

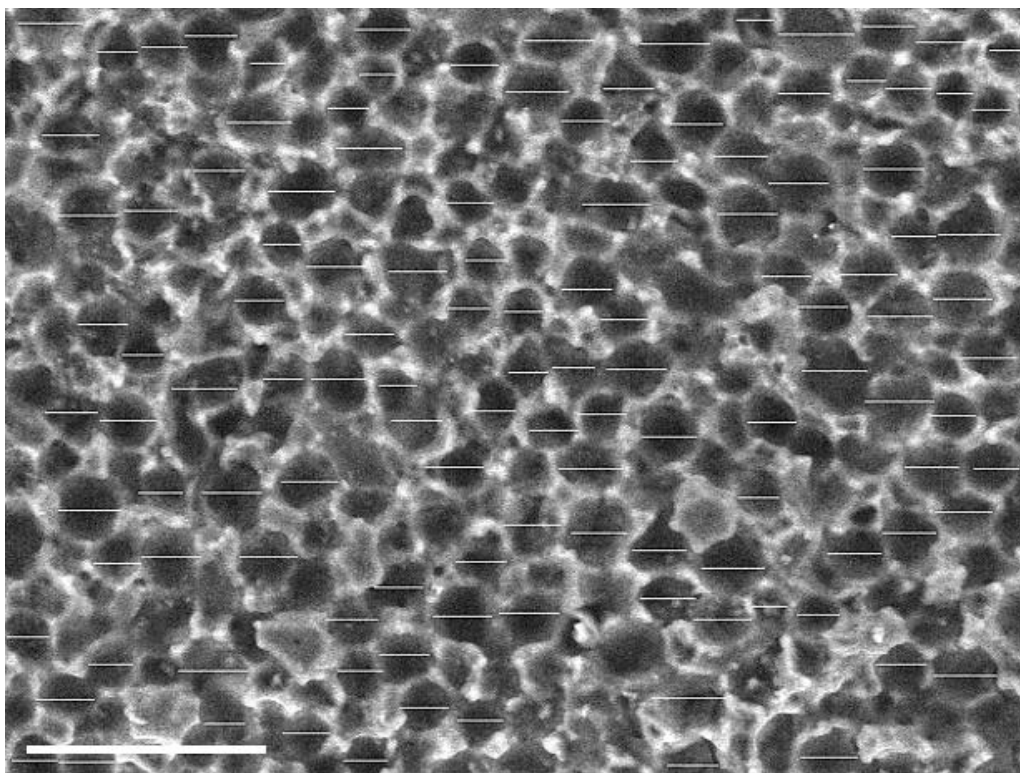


Figure 4.1 Scanning electron microscopy of PDMS bioimprint made using Jurkat cells deposited via the cytospin centrifuge. Measurements of the cavities size distribution used to calculate their length mean diameter are shown, represented by horizontal sections over the visible rim of the surface cavities. Scale bar represents 50 μm .

SEM images of the template cells could not be used for this purpose, as even after fixation, the vacuum required is likely to cause shrinking of the cells. The size distribution of fixed Jurkats was measured using bright field microscopy (see 2.2.2.5). The size distribution comparison of Jurkat cells and Jurkat bioimprint cavities can be seen in Table 4.1 and Figure 4.2.

Table 4.1 Tabulated comparison of the length mean diameter of fixed Jurkat cells and that of the bioimprinted cavities produced into PDMS via the Cytospin centrifuge mediated method. Number of cavities or cells assessed $n = >400$.

	Length mean diameter $d[1,0]$ (μm)			
	Minimum	Maximum	Mean	Standard Deviation (Mean)
Jurkat cells	7	20	12	2
Jurkat bioimprints	4	17	9	2

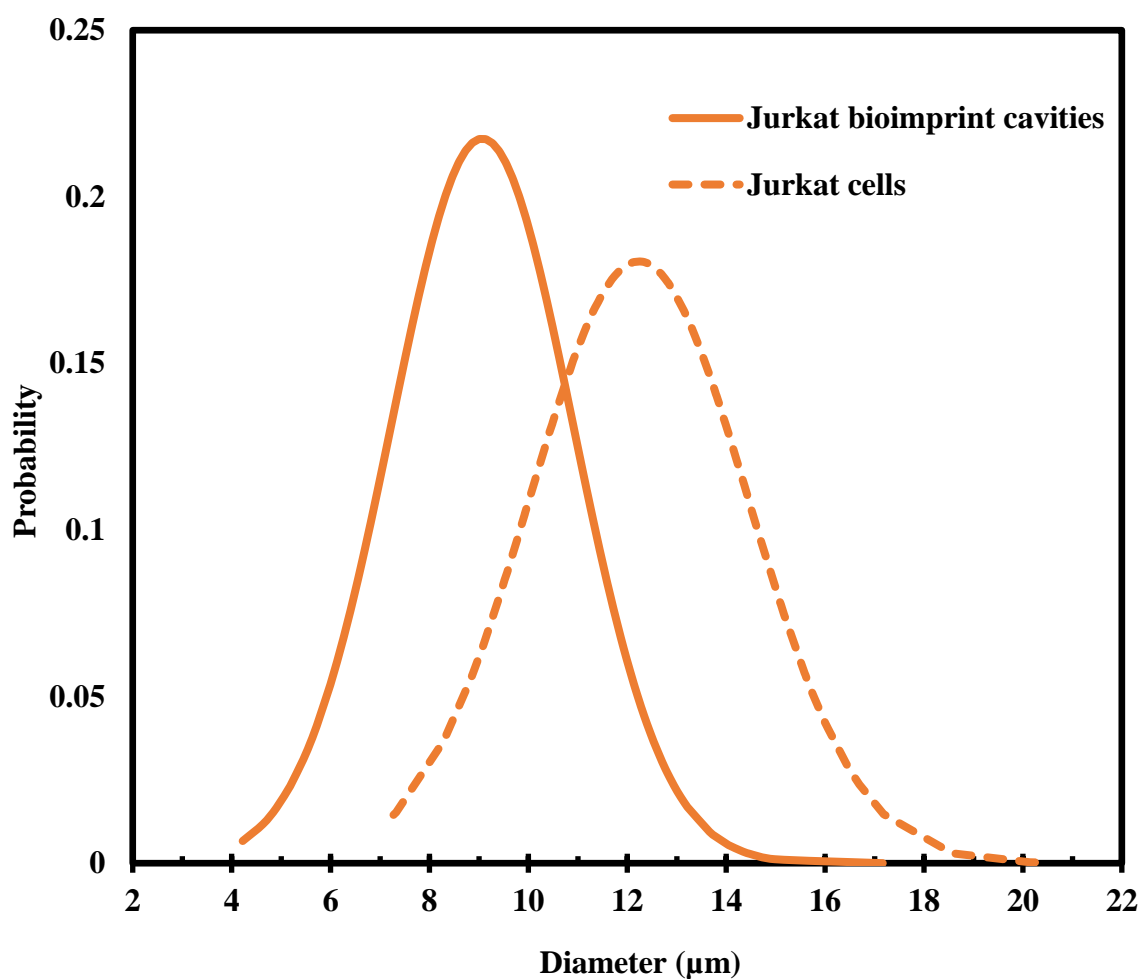


Figure 4.4.2 Overlaid side distributions comparison of the length mean diameter of fixed Jurkat cells and the same for the bioimprinted cavities produced into PDMS via depositing Jurkat cells using the cytospin centrifuge method.

The bioimprints produced by Jurkat cell layers depositing Jurkat cells with cytocentrifugation showed a smaller length mean diameter than the templated Jurkat cells. Here, less than half of the Jurkat cells are exposed to the curing PDMS as can be seen in Figure 4.3, below. The difference in size highlights an overprotection of the deposited

cells by residual water remaining in the multilayers. For the Cytospin method, this was difficult to control as if the cell layers were left to dry too long, meniscus forces caused aggregation and cell layers to be compromised (See Chapter 3).¹

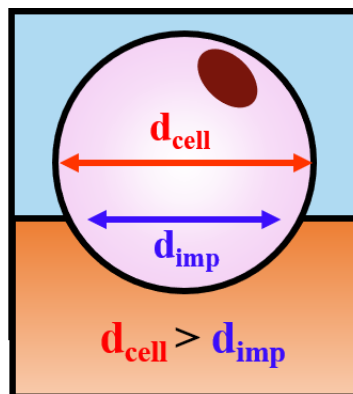


Figure 4.3 Schematic showing the difference between the imprint cavity rim diameter compared with the diameter of the imprinted cell.

This quantitative assessment can be compared with bioimprints produced using the glucose protective layer. Here, HL60 cells were preferred to Jurkats due to their closer likeness to AML myeloblast. Length mean diameter analysis of the bioimprints of HL60 cells made via the glucose protective layer method was also carried out to compare the size distributions of the cavities and the template HL60 cells; seen in Figure 4.4.

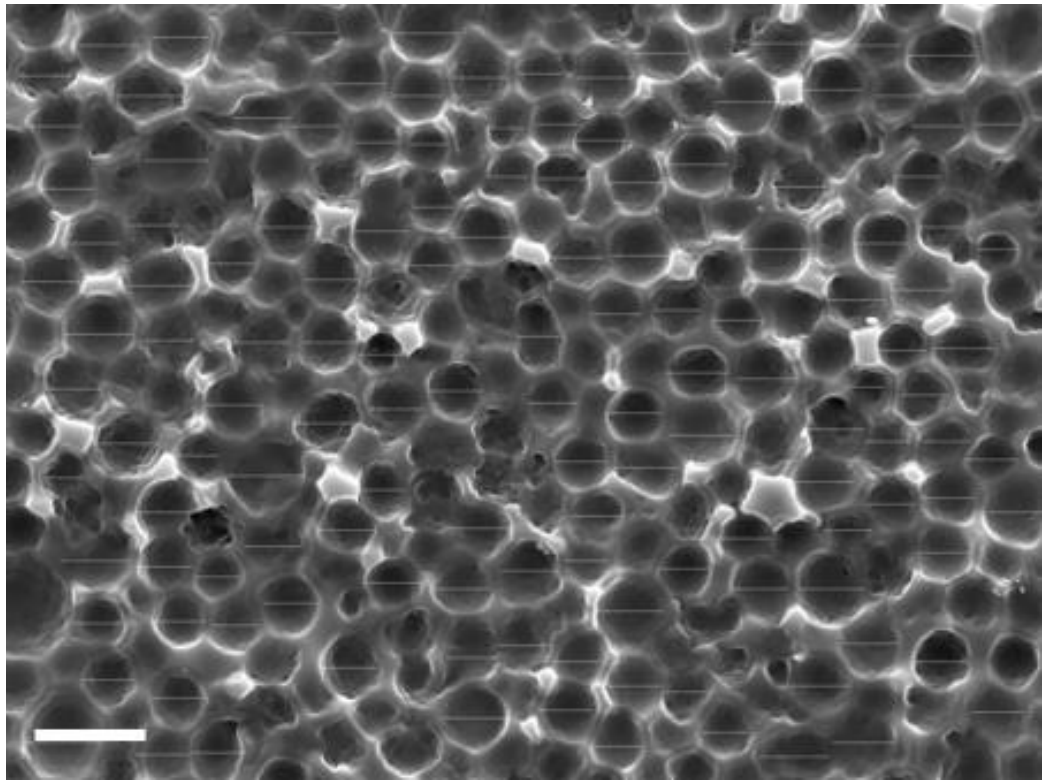


Figure 4.4 Scanning electron microscopy showing the horizontal measurements of cell diameter used to calculate the length mean diameter of HL60 bioimprint cavities, made via the spreading of the cells suspension in aqueous glucose solution to protect against drying. Scale bar represents 20 μm .

Tabulated and graphical plots of the length mean diameter [1,0] measurements of the HL60 cell imprints made by spreading template cells from aqueous glucose solutions can be seen in Table 4.2 and Figure 4.5, below.

Table 4.2 Tabulated comparison of the length mean diameter of fixed HL60 cells and the bioimprinted cavities in PDMS produced into via polyurethane the glucose protective layer method. Number of cavities or cells assessed $n = >400$.

	Length mean diameter (μm)			
	Minimum	Maximum	Mean	Standard Deviation (Mean)
HL60 cells	7	20	12	2
HL60 imprints	6	14	11	2

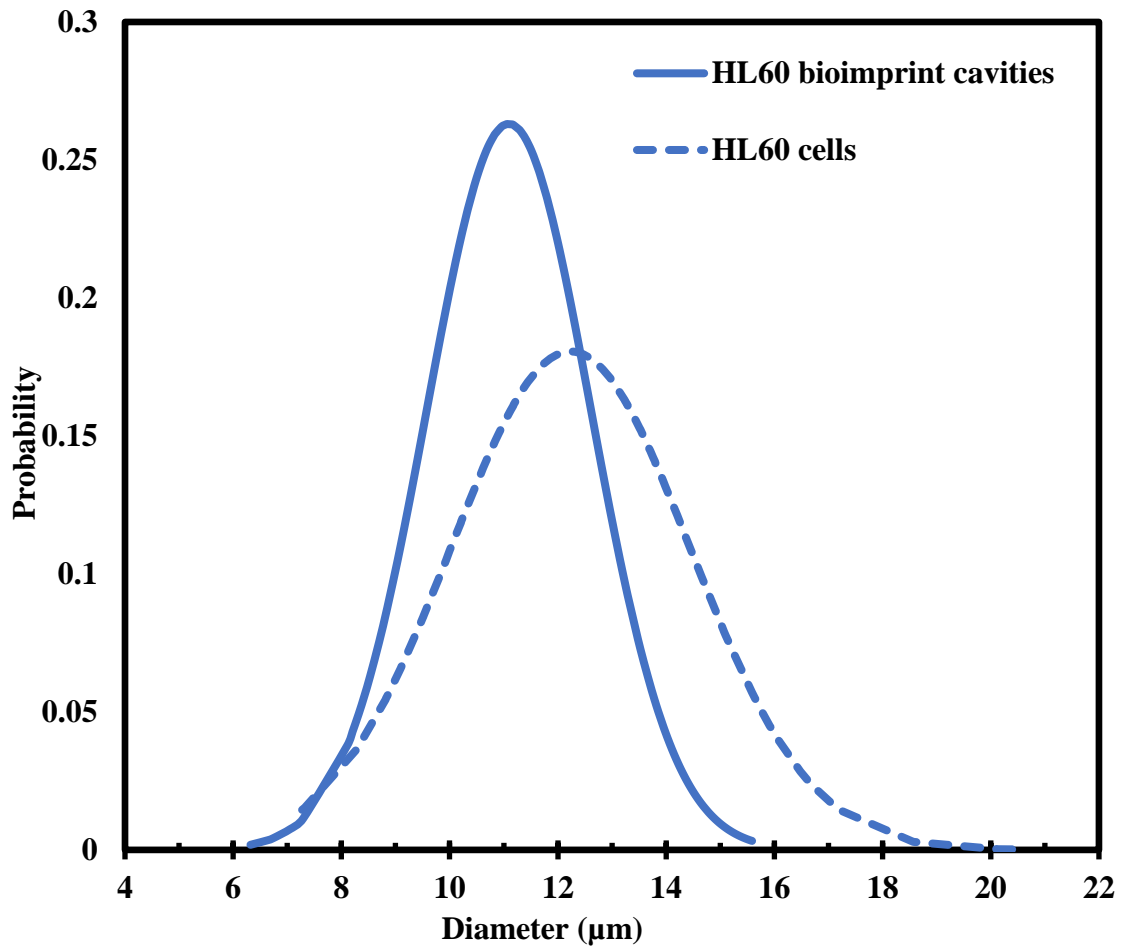


Figure 4.5 Overlaid side distribution comparison of the length mean diameter of fixed HL60 cells and the bioimprinted cavities produced into PDMS via depositing HL60 cells using the protective glucose method.

As with Cytospin mediated bioimprints, those produced by glucose show a smaller size distribution than the template cells (shown in Figure 4.3). In this instance, the overprotection has arisen from an excess of glucose in solution. Subsequent imprints tried to lower the volume of glucose in suspension though this resulted in areas of the cell multilayer drying and forming aggregates due to insufficient protection.

Comparison of the diameters of the bioimprint cavities and the cells can be made to calculate the proportion of the cell that is expressed in bioimprints. By dividing the length mean diameter of the bioimprint cavity by that of the template cell, the angle of the tangent made by the cell at the point of immersion (θ) can be found by the relationship in Eq.(4.1).

$$\frac{d_{[1,0]_{imprint}}}{d_{[1,0]_{cell}}} = \text{Sin}(\theta) \quad (4.1)$$

Where $\theta = 0$ gives the tangent when in contact with a planar substrate and $\theta = 90^\circ$ represents the tangent of a cell in a cavity with exactly half of the cell imprinted. Using this angle, it is possible to calculate the fraction of the cell surface (ϕ) that has been captured in imprints by Eq.(4.2).

$$\phi = \frac{(1-\cos(\theta))}{2} \quad (4.2)$$

How much of the template cell is captured into the curing polymer matrix (Figure 3.1) can be discussed in values of ϕ . If $\phi > 0.5$, more than half of the cell surface is imprinted and the resultant cavity is compromised by a rim preventing rebinding of cells (Figure 3.1c). Amplification of DLVO-style interactions is dependent on significant increase of the surface area contact between the cell and bioimprint.² Therefore, an ideal cavity would have as large a surface area contact possible, approaching $\phi = 0.5$ (Figure 3.1b). Comparisons of θ and ϕ were made of bioimprints made from the Cytospin mediated deposition (using Jurkat cells) and of spreading from aqueous glucose solution (using HL60 cells); see Table 4.3.

Table 4.3 The average diameters [1,0] of cell types compared to the average diameters d[1,0] of bioimprinted cavities made from depositing Jurkat cells via the Cytospin centrifuge and HL60 from aqueous glucose solutions. The immersion angle, θ , and the fraction of the cell imprinted, ϕ , for each case are shown.

	Jurkat	HL60
Imprint d[1,0] (μm)	9	11
Cell d[1,0] (μm)	12	12
Sin(θ)	0.8	0.9
(θ) (Degrees)	48.6	66.4
ϕ	0.2	0.3

Cellular imprints produced by both methodologies showed a close likeness to the template cells. In both cases the average diameter and distribution of cavities were smaller than the diameter of the cell or particle template used. The smaller average sizes are due to less than half of the cells surface being embossed into the curing polymer matrix. In the case of the glucose protective layers, the cell diameters matched more closely than their Cytospin centrifuge counterparts as $\phi_{\text{Glucose spreading}} > \phi_{\text{Cytospin mediated deposition}}$. The fractions

of the cell embossed are not in the range proposed in Chapter 3 of between one third and one half captured ($0.33 < \phi < 0.5$). However, the cavities show a significantly larger surface area contact when compared to a planar substrate. Particularly the bioimprint produced from aqueous glucose spreading of HL60 which shows a substantially larger proportion of the cell imprinted. Although the whole cell is not imprinted, the surface area offered by these bioimprints allows amplification of DLVO-style interactions (see Chapter 1). The difference in energy between a cell fitting closely in the cavity and a cell unable to receive full surface area contact with the bioimprint will be exploited for cell capture reliant on size and shape information. Moreover, the study shows that using a dense multilayer is an effective prevention for over exposing cells to the resin in the process of bioimprinting.

The effect of imprinting on the size distribution is confounded by the dividing nature of cell populations. Until fixation, cells are present at various stages of maturation resulting in a wide distribution and making comparison of cell and cavity size difficult. To examine this effect, bioimprints using monodisperse microparticles were also produced and analysed using the same methodology. Figure 4.6 shows measurements of bioimprint cavities produced with CA10 and CA15 monodisperse PMMA microspheres.

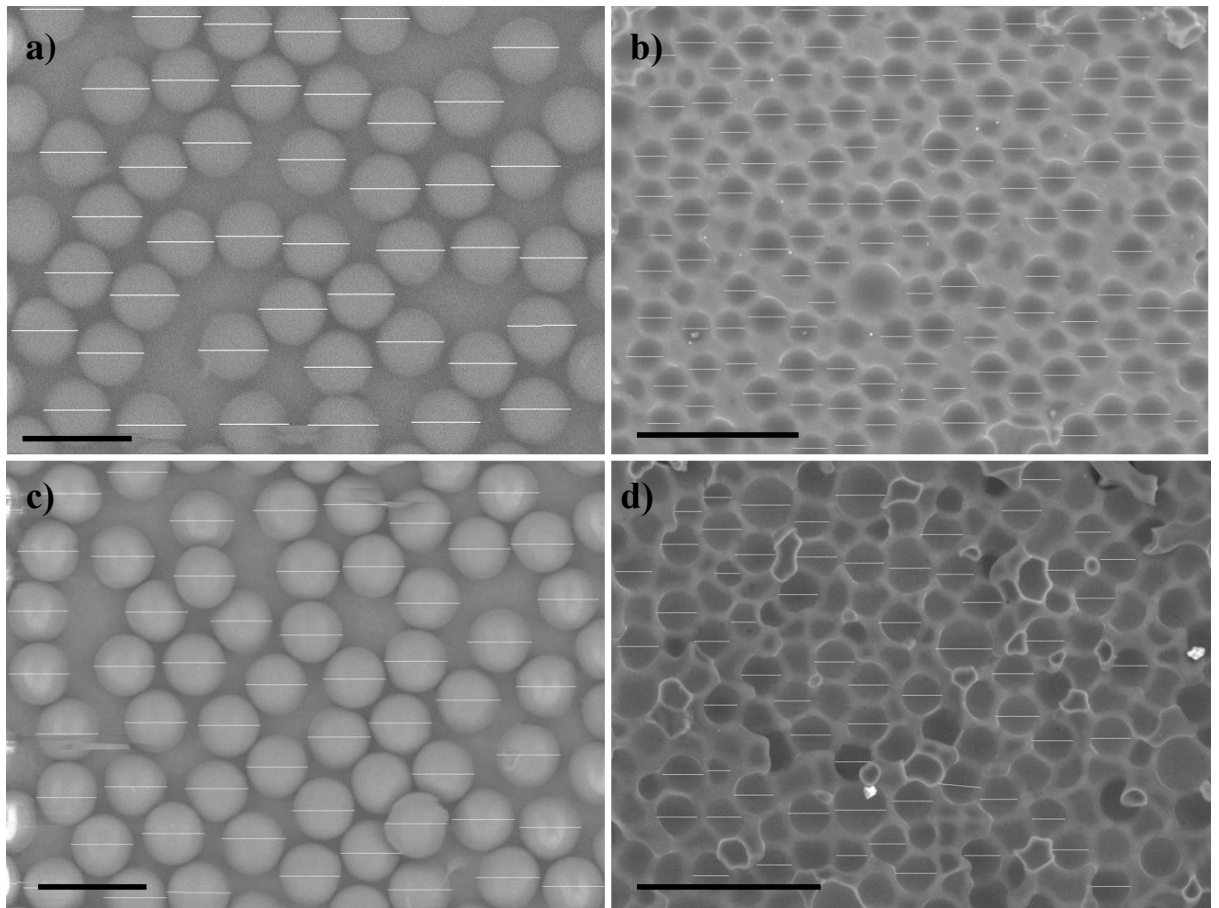


Figure 4.6 SEM images showing the length mean diameter measurements of CA10 a) particles (scale bar = 15 μm) and b) imprints (scale bar = 50 μm) and CA15 c) particles (scale bar = 25 μm) and d) imprints (scale bar = 50 μm).

Here, due to their non-biological nature, the length mean diameters are both measured using SEM images. This analysis results in a more precise comparison due to the SEM images superior higher resolution compared with optical microscopy. Comparison of the microparticles and resultant bioimprint cavities was made and can be seen in Table 4.4 and Figure 4.7, below.

Table 4.4 Tabulated comparison of the length mean diameter of monodisperse microparticles and the resultant bioimprinted cavities produced into polyurethane via the glucose protective layer method. . Number of cavities or cells assessed $n = >400$.

	Length mean diameter (μm)			
	Minimum	Maximum	Mean	Standard Deviation (Mean)
CA10 particles	8.7	10.3	9.6	0.2
CA10 imprints	6.8	9.6	8.0	0.7
CA15 particles	13.8	15.3	14.5	0.4
CA15 imprints	11.0	14.6	12.8	0.9

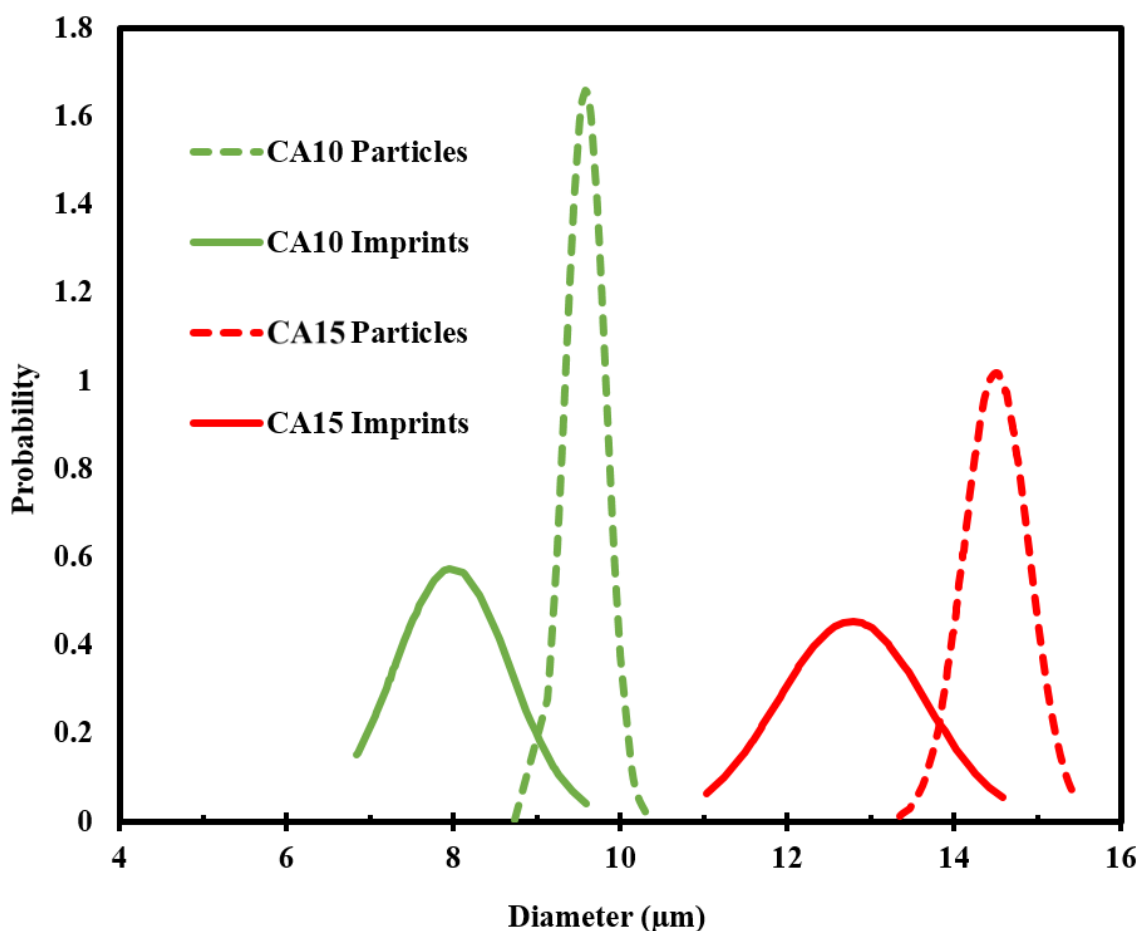


Figure 4.7 Overlaid size distributions from length mean diameter measurements of CA10 and CA15 particles and resultant bioimprint cavities.

This analysis shows that the particles have a very narrow distribution, which allows a better comparison with imprint cavities. As with cellular imprints produced using a glucose protective layer, the imprints mean diameter $d[1,0]$ shows a close likeness to the templated particles. Here, the wider distributions for the imprint cavities arises from the

different proportions of each particle exposed to the resin. Comparison of the θ and ϕ were also made for the particle imprints, both produced by spreading from glucose solutions (Table 4.5).

Table 4.5 Comparison of the average length mean diameters of CA10 and CA15 particles and the imprints made into PDMS from particle layers spread from aqueous glucose solutions. Also, the calculation of the angle of the tangent made from the particle in the cavity, θ , and the fraction of the cell surface captured into the polymer matrix, ϕ .

	CA10	CA15
Imprint d[1,0] (μm)	8	12.8
Cell d[1,0] (μm)	9.6	14.5
Sin(θ)	0.8	0.9
(θ) (Degrees)	56.4	62.0
ϕ	0.2	0.3

Both the CA10 and CA15 particle imprints yield a lower proportion of the cell surface captured in to the bioimprint. This highlights the importance in optimising the volumes of glucose used to spread cell and particle suspensions. However, in all cases an increased surface area is afforded by bioimprints when compared with a flat substrate, able to amplify favourable DLVO interactions to retain particles.

4.1.2. Nanoscale analysis

Qualitative SEM analysis showed both cell and particle bioimprints to have excellent microstructure, uniform across the replica imprint and representative of the original bioimprints. Further attempts to assess the depth and diameter of bioimprints were made. Cross sectioning of the bioimprint and analysing side-on was considered in order to examine cavity depth though this may potentially lead to inaccurate data as there is no control over what position of the cavity is examined. Surface profiling via dektak (DektakXT, Bruker) was trialled though the sensitivity of its probe was found to be insufficient to measure the low micron scale features of the bioimprint. Atomic force microscopy (AFM) (Dimension Edge, Bruker) in tapping mode provided a method to

semi- quantitatively assessment of the surface morphology of the master positive HL60 imprint and subsequent negative replica imprint and can be seen in Figure 4.8, below.

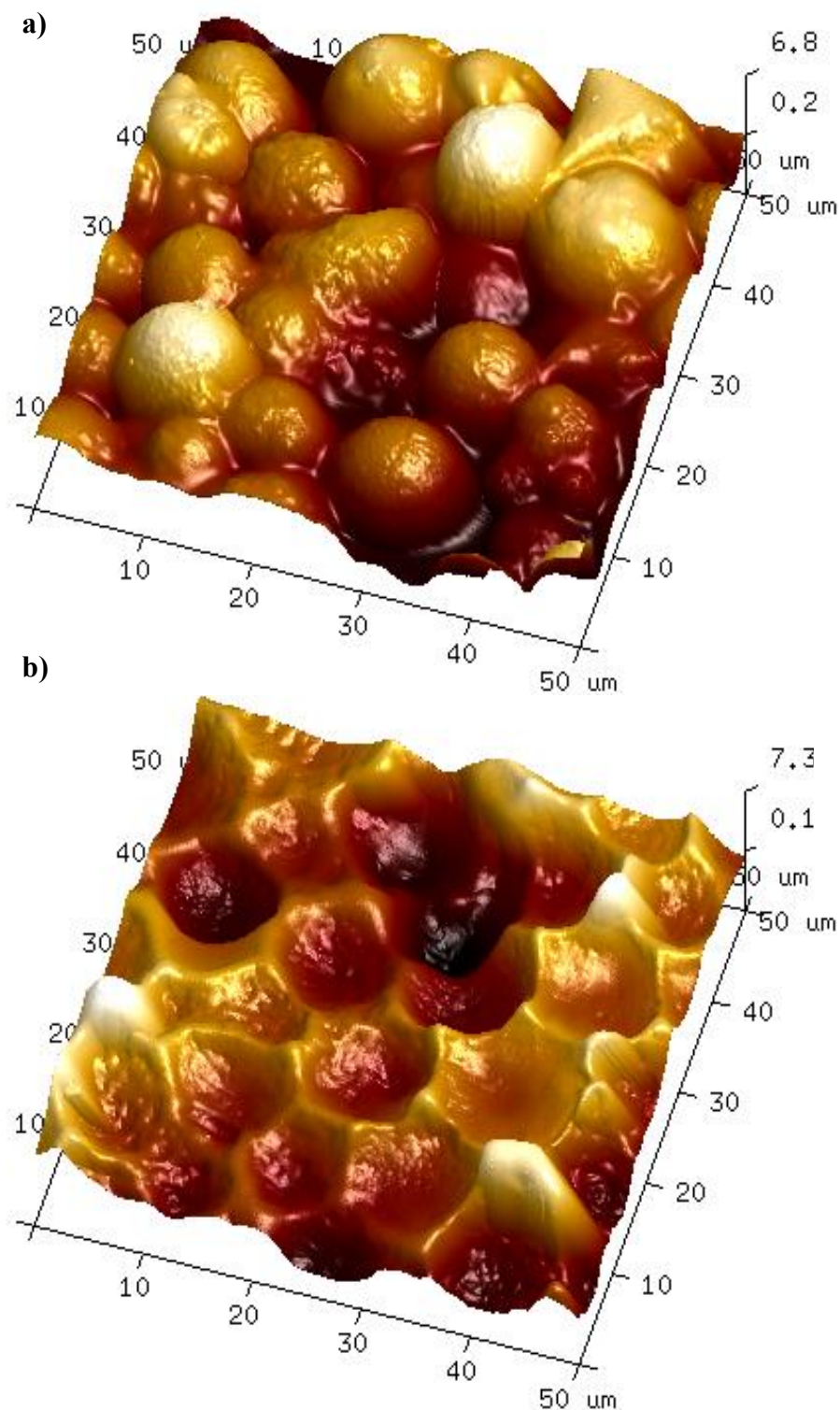


Figure 4.8 AFM analysis of HL60 a) positive master imprint used to create b) replica imprints in PU photoresist via R2RNIL augmentation. Images collected from a scan rate of 0.1 Hz using 1024 lines in 50 μm \times 50 μm scan range.

AFM was successfully used for high-resolution analysis of the bioimprint surfaces. Quantitatively, heights and diameters of the artificial cell and cavities are representative of the HL60 cell population. Images show that the PU photoresist is able to capture the overall cell size and shape on a sub-micron scale and also extracellular features on a significantly smaller length scale. Nanometre scale roughness can be seen on the positive imprint, in agreement of other publications studying cell signalling by studying extracellular features on cells. It was difficult to analyse even fixed cells to compare to via AFM due to deformation from the large forces exerted by the cantilever tip. Moreover, other studies cite bioimprinting as a possible route for nanometre scale analysis of the cell topology.^{3,4}

4.2. Surface modification

Thus far, bioimprints have been produced and shown to offer a significantly larger surface area contact with a cell than a planar substrate. However, the surface properties of the polymeric resin, like surface charge, was difficult to control as the composition of the commercially available UV-curable PU resins was not available from the manufacturer. In order to ensure that the surface charge of the imprint can be carefully controlled the bioimprint surfaces would need be chemically modified to promote weak electrostatic attraction towards cells from aqueous solutions to achieve spatial efficiency; particularly significant with very large cell volumes. The following section will examine methods to incur and control positive surface charge to bioimprints. Cells will be attracted to the modified surface of the bioimprint on account of their inherent negative surface charge which arises from dissociation of extracellular membrane proteins and carbohydrates.

Adding positive surface charge introduces attraction to cell populations which is amplified by the superior surface area coverage experienced by bioimprints. This effect is shown in the comparison of DLVO interactions between cells and bioimprints or flat substrates (see section 1.3). Here, interactions can be amplified over 2 - 3 orders of magnitude. Surface modifications protocols should be tuneable to yield control over the degree of positive charge administered to the substrate. The interaction should be sufficiently weak that cells are not retained indiscriminately to the rims of the cavities and unimprinted regions of the bioimprint. Polyelectrolytes with high isoelectric points were used to provide the cationic charge though methods to anchor the positive charge the surface were also trialled in this thesis.

4.2.1. Oxygen plasma & APTES

In this instance, surface modifications of imprints produced in PDMS were examined. PDMS is inherently hydrophobic due to an abundance of surface methyl groups which in aqueous media is problematic two-fold.⁵⁻⁷ Firstly, the cell suspension cannot fully wet the bioimprint, reducing the active surface area of imprint exposed to aspirate and allowing the entrapment of air in the bioimprint cavities. Secondly, the cured PDMS surface has a net negative charge surface charge is incurred; which will actively repel target cells. In this study the effect of oxygen plasma treatment of PDMS was examined; a procedure commonplace in the production and use of microfluidic chips to overcome

the inherent hydrophobic surface chemistry of PDMS which results in poor wetting and capillarity.^{6,8}

Exposure of the PDMS surface to high energy oxygen plasma causes substitution of surface methyl groups to silanol ($-\text{SiOH}$).^{5,6} These surface groups are able to dissociate in aqueous media, $-\text{SiOH} \rightarrow -\text{SiO}^- + \text{H}^+$, and electrostatically dock the cationic polyelectrolyte, anchoring the positive charges to the surface.^{5,8} Control can be achieved by varying the duration of the oxygen plasma treatment with excess polyelectrolyte washed away. Plasma treatment time is proportional to the number of silanol groups introduced to the surface which can be characterised by measurement of the contact angle made by water drops on non-imprinted PDMS substrates.^{5,8,9} Plasma functionalised substrates have a greater interaction with applied water molecules than native PDMS due to hydrogen bonding from silanol groups.^{5,8} Figure 4.9, shows the difference in chemical structure between native and oxygen plasma treated PDMS.

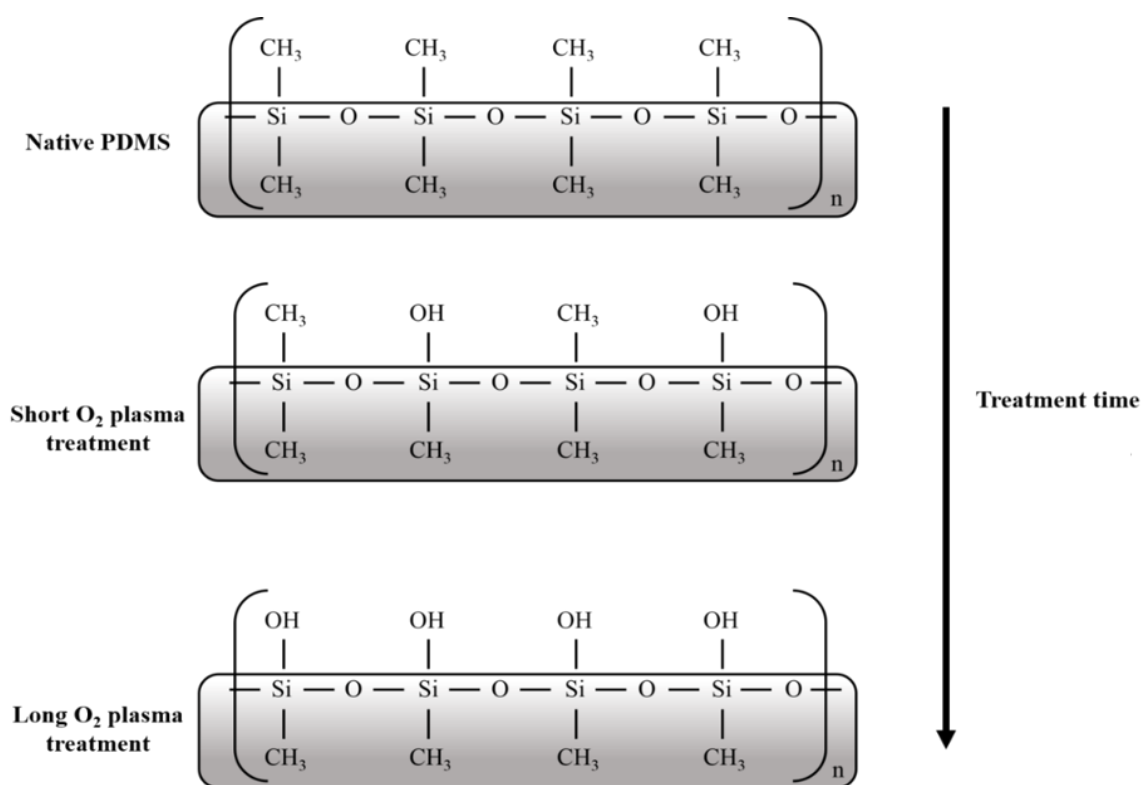


Figure 4.9 Schematic showing the changes in chemical structure of PDMS after exposure to oxygen plasma. Reproduced from information from reference Zhu *et al.*⁸

With polar surface groups, the interaction between the imprint and water drop is greater than methyl groups and thus, the water is better able to wet the surface.⁵ By measuring the contact angle of a sessile drop of water on the PDMS surface, a comparison of the degree of polar groups on the bioimprint surface could be made. Contact angle

measurements were made on unimprinted PDMS substrates to avoid pinning effects. Figure 4.10 shows the comparison of the hydrophobicity of Sylgard 184 PDMS before and after oxygen plasma treatment (147 Pa, 16 W) for 120 seconds.

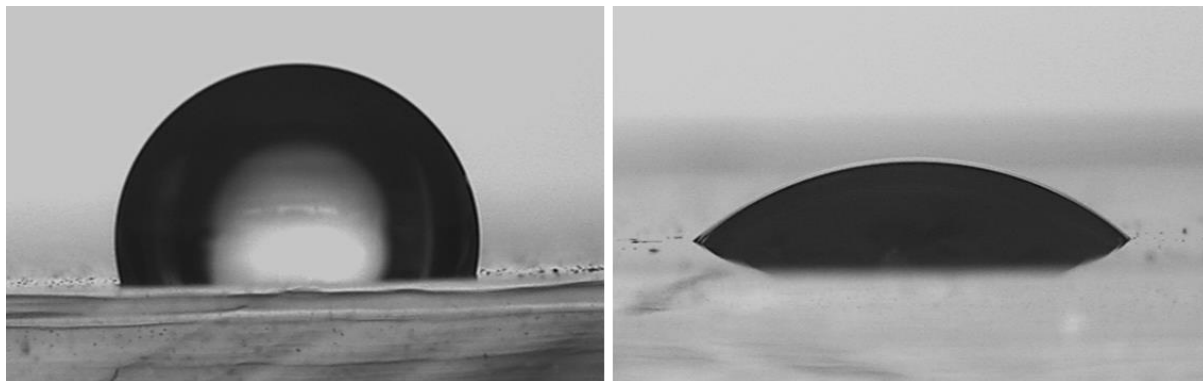


Figure 4.10 Difference in hydrophobicity between native and surface activated PDMS characterised by contact angle of sessile water drops (10 μ l) in air on a a) bare PDMS; contact angle $103 \pm 2^\circ$ and b) PDMS after treatment with oxygen plasma treatment (16 W, 147 Pa) for 120 seconds; contact angle $40 \pm 1^\circ$.

As can be seen, oxygen plasma treatment incurs hydrophilic nature. The contact angle decreases due to the increased interaction between the surface and water by hydrogen bonding. The interaction between surface and water competes with the hydrogen bonding between water molecules.

To incur a positive surface charge, the surface activated PDMS were immersed in an aqueous 20% (w/v) solution of (3-aminopropyl)trimethylsilane (APTES). The silanol groups on plasma activated PDMS can then be used to graft a cationic charge to the substrate by addition of APTES, shown in Figure 4.11.⁸ The extent of surface modification was controlled by adjustment of the oxygen plasma surface activation, monitored by contact angle measurements of sessile water drops. A more uniform surface modification is achieved by using APTES in excess and tuning the oxygen plasma treatment durations than the reciprocal situation.

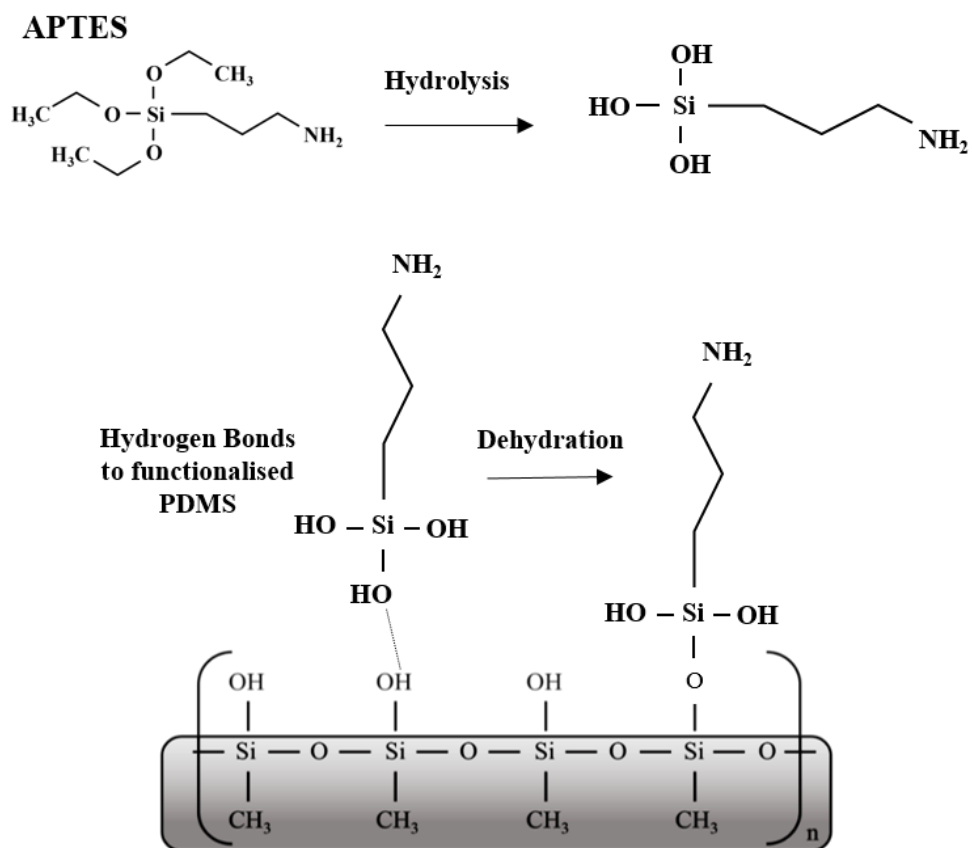


Figure 4.11 Schematic showing the anchoring of cationic charge to plasma activated PDMS by addition of APTES. Reproduced from information from Zhu *et al.*⁸

Binding of the 3-aminopropyl groups to the PDMS substrate is dictated by the number of polar silanol groups introduced. Longer treatment yields more polar groups which, in turn will bind lead to a larger positive surface charge from attachment of APTES. By using mild surface activation, a weak positive surface charge was made which can be amplified by the surface area contact. See Table 4.6 and Figure 4.12 for tabulated and graphical description of the effect on hydrophobicity of oxygen plasma treatment at 147 Pa, 16 W RF power as a function of treatment time.

Table 4.6 Tabulated data of the average sessile drop contact angle measurements of MilliQ water on PDMS as a function of treatment time in oxygen plasma (RF 16 W, pressure 147 Pa). Averages made from the contact angle on the left and right side (θ_L and θ_R) were taken over three separate drop repetitions.

Time in oxygen plasma (s)	Mean θ (degrees)	Standard deviation θ (degrees)
0	102	1
30	73	2
60	70	1
90	62	3
120	42	3
150	41	2
180	41	1

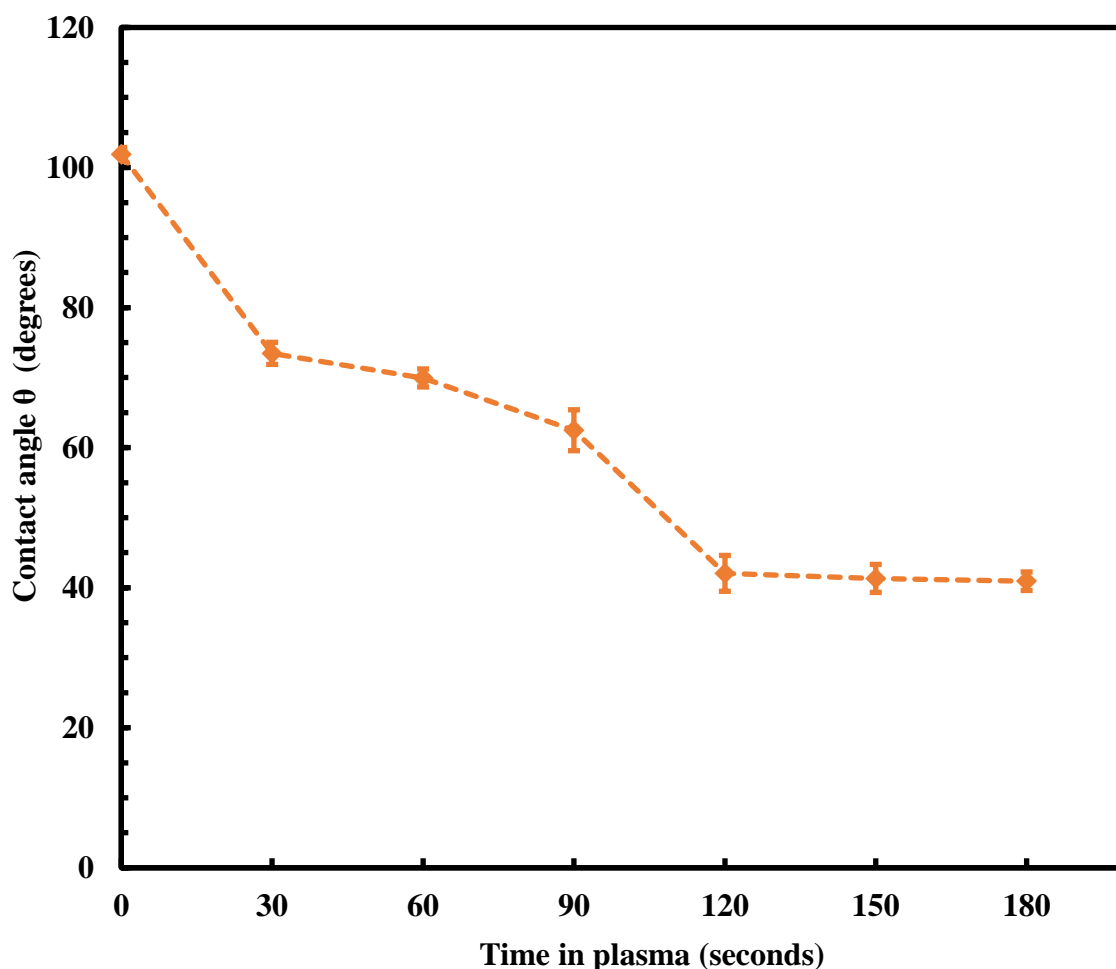


Figure 4.12 Average sessile drop contact angle measurements of MilliQ water on PDMS in air versus treatment time in oxygen plasma (RF 16 W, pressure 147 Pa). Averages were taken from the left and right contact angles of each drop (θ_L and θ_R) over three separate drop repetitions.

The examination showed the water contact angle to be inversely proportional to oxygen plasma treatment. Longer treatment times induced the substitution of more polar groups which are able to interact with water. After 120 seconds, the contact angle plateaus at $\approx 42^\circ$ as no further silanol groups are added to the PDMS surface. When longer durations are used, no further drop in the contact angle is observed.

Literature reports of damage to PDMS by over exposure to oxygen plasma with substrates becoming brittle.^{5,10} As short durations were trialled this was not observed to be an issue. This was confirmed as activated PDMS substrates showed no change in colour or surface alterations when analysed using high resolution SEM. In further studies, 120 seconds was the maximum treatment time for PDMS in oxygen plasma.

4.2.2. Hydrophobic recovery of PDMS

A complication was encountered with using PDMS bioimprints excited by oxygen plasma treatment due to its hydrophobic recovery.^{9,10} A possible explanation for this effect is that due to the low degree of crosslinking, the residual liquid silicone oil in the cured PDMS matrix was able to rearrange into the bulk of the material, lowering the entropy of the system.^{9,11} Hydrophobic recovery of PDMS substrates was monitored as a function of time after 120 seconds in oxygen plasma (16 W, 147 Pa). See Table 4.7 and Figure 4.13 which show the return of hydrophobic properties to PDMS substrates at 30 minute time intervals after oxygen plasma treatment.

Table 4.7 Tabulated data monitoring the contact angle of a sessile MilliQ water drop on an unimprinted PDMS substrate as a function of time after treatment in oxygen plasma (16 W, 147 Pa) for 120 seconds.

Time after treatment (minutes)	Mean θ (degrees)	Standard deviation θ (degrees)
0	42	2
30	44	2
60	46	2
90	51	2
120	55	1
150	63	4
180	77	1
210	85	1
240	95	1
270	98	1
300	98	1
330	102	1
360	103	1

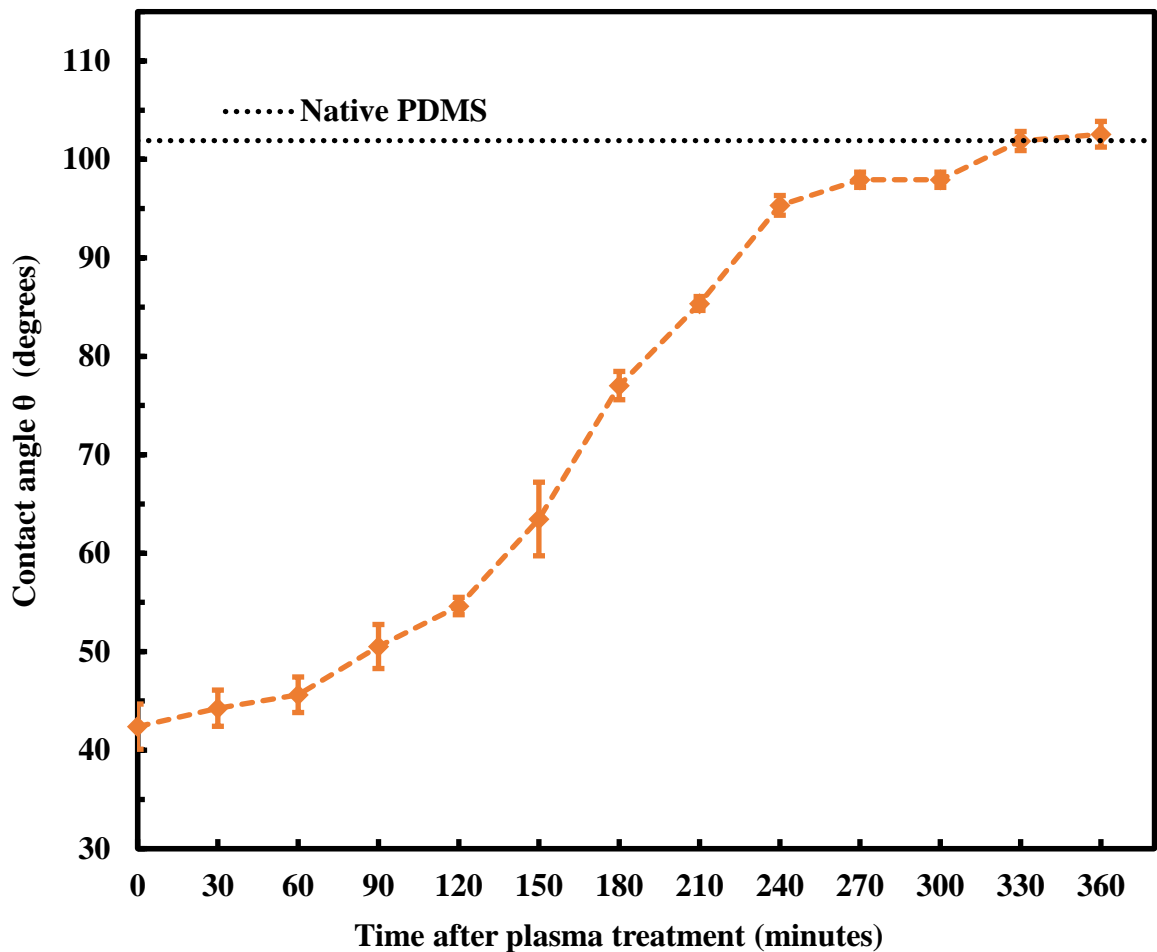


Figure 4.13 The hydrophobic recovery of PDMS characterised by measurement of the contact angle of a sessile water drop on PDMS substrates in air as a function of time after oxygen plasma treatment plasma (16 W, 147 Pa) for 120 seconds. Averages were taken from the left and right contact angles of each drop (θ_L and θ_R) over three separate drop repetitions.

Contact angle measurements show the hydrophobic recovery of the Sylgard 184 material to be proportional with time. After 360 minutes, all hydrophilicity introduced to the PDMS substrates is lost due to silanol group diffusion. As with native PDMS, the surface is comprised of predominantly methyl groups which have little interaction with water and inter-water hydrogen bonding is stronger than the interaction with the bioimprint.

4.2.3. Limitations of PDMS as a material for negative bioimprints

Poor wetting properties and rapid hydrophobic recovery of PDMS make it unsuitable for use in a clinical cell capture device. Regardless of the clinical setting used for bioimprints, all cell samples would be administered via aqueous media which requires very good

wetting of the bioimprint as an important criterion for the choice of bioimprint material. In particular, when incorporated into flow-through systems, large areas may be left unexposed to the cell suspension samples, lowering the surface area of the imprint in contact with the sample; and hence in turn reducing the efficiency of myeloblast capture device.

Ultimately, regardless of the oxygen plasma treatment, PDMS was completely incompatible with the intended real-world applications of bioimprints. Other additives to the PDMS mixture can also be used to incur hydrophilic properties at the formulation stage however this complicates the biocompatibility and use as a medical device. Moreover, though the elastic properties and softness of PDMS was advantageous when fabricating bioimprints via hard-soft combinations, PDMS would be difficult to incorporate on a large scale into a flow device. The elasticity is likely to cause deformation of channels and leakages by preventing a seal being formed when pressure is applied.

Further experiments assessed the suitability of PU as the bioimprinted surface. In this instance, carboxylic groups (-COOH) are substituted to the polymer surface which are able to immobilise the cationic polyelectrolyte in a similar fashion to the silanol groups on functionalised PDMS. The advantage of PU is that due to a higher degree of crosslinking, carboxylic groups are unable to revert back to the bulk of the material allowing an improved shelf-life as bioimprint compared with PDMS.^{5,12,13} The contact angle of a sessile water drop on unimprinted PU substrates was measured as a function of oxygen plasma treatment time; see Table 4.8 and Figure 4.14.

Table 4.8 Tabulated data of the average sessile drop contact angle measurements of MilliQ water on PU as a function of treatment time in oxygen plasma (RF 16 W, pressure 147 Pa). Averages made from θ_L and θ_R over three separate drop repetitions.

Time in oxygen plasma (s)	Mean θ (degrees)	Standard deviation θ (degrees)
0	96	3
20	78	2
40	70	5
60	56	2
80	48	1
100	40	4
120	40	2
150	37	2
180	40	1

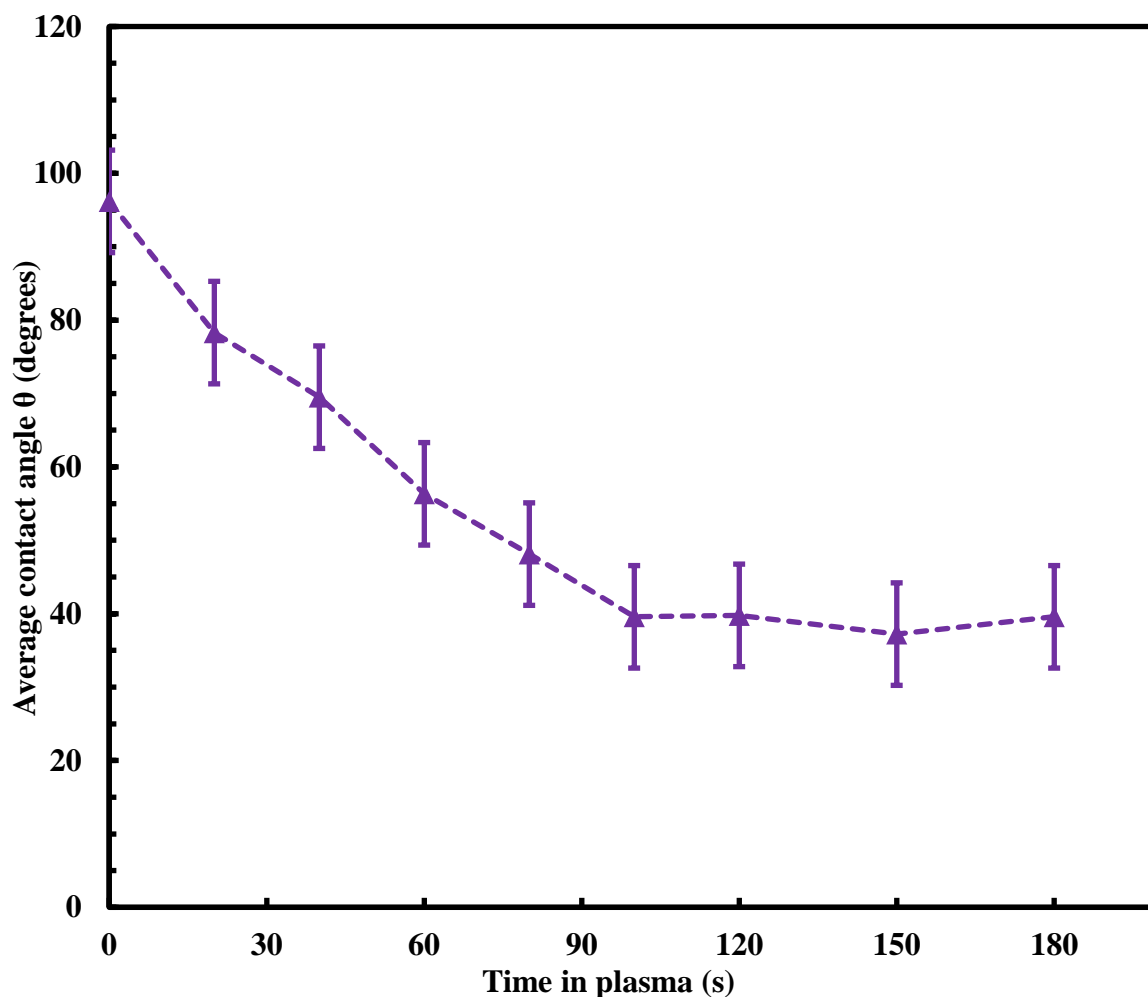


Figure 4.14 Average sessile drop contact angle measurements of MilliQ water on non-imprinted polyurethane in air versus treatment time in oxygen plasma (RF 16 W, pressure 147 Pa). Averages were taken from the left and right contact angles of each drop (θ_L and θ_R) over three separate drop repetitions.

As with PDMS, exposure to oxygen plasma makes the polyurethane substrates more hydrophilic. After oxygen plasma treatment, a positive surface charge can be administered by addition of a cationic polyelectrolyte in excess, with control achieved from the duration in oxygen plasma.

The disadvantage of this system is when grafting cationic polymers to the surface, the carboxylic-cationic polyelectrolyte interactions are relatively weak. This may compromise the bioimprints performance during use in a capture device; particularly as repeated perfusion may wash off the deposited polyelectrolyte material from the bioimprint surface. This is particularly problematic as free cationic polyelectrolytes are toxic to biological samples. Therefore, a stronger binding of the chosen polyelectrolyte was needed.

The following section describes the direct grafting of polyelectrolytes to substrates using trace amounts of the polymer matrix.

4.2.4. Matrix entanglement

When designing a method to produce a weakly positive surface charge on bioimprints, it was important to use a protocol that can be easily scaled up for use over bioimprint area of tens of square metres and can be directly implemented during the production stage of the imprint. As shown when producing bioimprints via the Cytospin method, all imprints were subject to the maximum parameters of the Cytospin device which was then difficult to augment. A preferred method will not rely on equipment with inherent limitations on working capabilities. Preliminary work has been trialled using the oxygen plasma device to functionalise PDMS which can also be used to introduce carboxylic groups on the PU surface. This first treatment is vital in order to retain the positive charge from cationic electrolytes. A similar alternative of UV ozone treatments are commercially available as part of a roller set up. However, to reduce costs and in an attempt to keep production of the device as simple as possible, this will also be avoided.

Instead, the positive charge was grafted directly to the substrate surface by evaporating cationic polyelectrolyte in conjunction with uncured PU photoresist. In this instance, ethanol was used as the solvent to spread a mixture of branched polyethyleneimine (bPEI) and PU resin. bPEI was ideal material for use in the study, providing the necessary cationic surface charge and also being approved for use in medical devices by the US

FDA and Medicines and Healthcare products Regulatory Agency (MHRA) of the UK.^{14,15} A layer of this in ethanol solution (<1% w/v) was applied to the surface of the bioimprint using a spreading tool like that used to spread cell suspensions. In this instance however, the sides of the tool were offset by 10 μm . The bPEI solutions were dried, and the PU cured by exposure to UV radiation. In this instance, the polyelectrolyte (bPEI) was encased in a network of covalently cross-linked PU polymer chains; yielding more attraction than the hydrogen bonding interactions from silanol or carboxylic groups, as the previously described methodologies can provide.¹⁶

The polyelectrolyte and PU polymer anchor were used in various proportions such that the combined additive was 1% (w/v) in ethanol as treatment. It was vital to use small concentration (1% w/v) so that after evaporation of the ethanol solvent the deposited film on the imprint did not compromise the bioimprint by filling or reducing the size of cavities. Films of this solution with a thickness $\sim 10 \mu\text{m}$, owing to the predetermined clearance of the spreading tool. As the polymer made up <1 % w/v, the expected bPEI/polymer coating of thickness less than 0.1 μm which is insignificant with target cells diameters in the range of 10 – 15 μm . SEM analysis of functionalised bioimprints showed no visible alteration of the imprint morphology by qualitative analysis. The method has the added advantage of being relatively simple to scale up to the tens of square metres required; possibly as a subsequent part of the R2RNIL.

4.3. Conclusions

This chapter focussed on the qualitative and quantitative characterisation of the bioimprints produced in Chapter 3. Comparison of the length mean diameter of the bioimprints to the template cell or particle size confirmed the cavities produced were representative of the template populations. The bioimprint cavity rim diameters did not match exactly that of the original cell. Cavities as less than half of the cell had been captured in the curing polymer matrix. Moreover, calculation of the fraction of the cell surface imprinted showed less than a third was imprinted. However, a significant increase of surface area of cell is seen when compared with planar substrates, allowing for amplification of DLVO type interactions between cells and bioimprints. By using surface profiling techniques, the nanometre scale resolution of extracellular features could be seen on positive and negative bioimprints. This agrees with publications citing bioimprinting a viable method of studying extracellular cell signalling.

Methods of chemically modifying the bioimprints surface to promote adhesion of target cells were examined. Firstly, oxygen plasma treatment was used to substitute methyl groups with polar silanol moieties on PDMS substrates. The effect was characterised by monitoring the contact angle of a sessile water drop on the PDMS surfaces. A positive charge could then be immobilised to the substrate by treatment with cationic polyelectrolytes, complementary to the negative charge exhibited by cells.

Due to the low degree of crosslinking present in PDMS, rearrangement of high energy groups to the material bulk caused a recovery in hydrophobic properties. The short shelf life made the use of PDMS incompatible for use in a real world setting due to the poor shelf life and storage conditions. A low viscosity, UV curable polyurethane was used as an alternative bioimprint matrix. When exposed to oxygen plasma in a similar fashion, the hydrophilic properties introduced did not decay due to a higher degree of crosslinking. However, in the interests of bioimprint longevity and safety, a method to provide stronger retention of added cationic polyelectrolytes was examined. Herein, thin films of polyelectrolyte were spread in conjunction with trace levels of uncured polymer matrix. The interaction was deemed superior, dependant on entanglement of the doping polyelectrolyte in a covalently grafted polymer matrix. bPEI was used as the polymer matrix in this instance, having the added advantage of better biocompatibility for use in medical devices. This surface coating and modification method was finally adopted for further experiments on myeloblast retention on bioimprints and their selectivity for myeloblasts compared with PBMCs, as described in the following chapters.

4.4. References

- 1 V. Paunov, P. Kralchevsky, N. Denkov and K. Nagayama, *J. Colloid Interface Sci.*, 1993, **157**, 100–112.
- 2 J. Borovička, S. D. Stoyanov and V. N. Paunov, *Phys. Rev. E - Stat. Nonlinear, Soft Matter Phys.*, 2015, **92**, 22–24.
- 3 A. L. Bole and P. Manesiotis, *Adv. Mater.*, 2016, 5349–5366.
- 4 F. Samsuri, M. M. Alkaisi, J. J. Evans, K. Chitcholtan and J. S. Mitchell, *Microelectron. Eng.*, 2011, **88**, 1871–1874.
- 5 M. J. Owen and P. J. Smith, *J. Adhes. Sci. Technol.*, 1994, **8**, 1063–1075.
- 6 S. H. Tan, N. T. Nguyen, Y. C. Chua and T. G. Kang, *Biomicrofluidics*, 2010, **4**, 1–8.
- 7 D. Munday, *Surfaces, Interfaces and Colloids — Principles and Applications*, ed. 2, D. Myers, Wiley-VCH, New York, 1999, vol. 51, pp. 20-60.
- 8 Z. Zhu, P. Chen, K. Liu and C. Escobedo, *Micromachines*, 2016, **7**, 1-14.
- 9 D. Bodas and C. Khan-Malek, *Sensors Actuators, B Chem.*, 2007, **123**, 368–373.
- 10 J. Bacharouche, H. Haidara, P. Kunemann, M. F. Vallat and V. Roucoules, *Sensors Actuators, A Phys.*, 2013, **197**, 25–29.
- 11 J. L. Fritz and M. J. Owen, *J. Adhes.*, 1995, **54**, 33–45.
- 12 A. Reghunadhan and S. Thomas, *Polyurethane Polym.*, 2017, 1–16.
- 13 M. A. Minnath and E. Purushothaman, *Polyurethane Polym.*, 2017, 17–44.
- 14 J. Wang, S.-S. Feng, S. Wang and Z. Chen, *Int. J. Pharm.*, 2010, **400**, 194–200.
- 15 M. Andersen, A. Lichawska, A. Arpanaei, S. Rask Jensen, H. Kaur, D. Oupicky, F. Besenbacher, P. Kingshott, J. Kjems and K. Howard, *Biomaterials*, 2010, **31**, 5671–5677.
- 16 J. U. Sommer, *Eur. Phys. J. B*, 1999, **10**, 537–542.

5. Cell retention on Bioimprints

Previous chapters have discussed the fundamentals of using bioimprints to retain specific blood cancer cells, the methods for the bioimprint fabrication and their functionalisation and characterisation. This next chapter will focus on the bioimprints' ability to capture the target cells from suspension and the role of the applied surface modifications from Chapter 4 on the cell retention.

5.1. PDMS bioimprints

Preliminary cell retention experiments were carried out prior to receiving the PU replica imprints produced by R2RNIL. These imprints were produced from a master imprint, replicated in-house by curing PDMS on a polyurethane master imprint.

5.1.1. Jurkat Bioimprint

Bioimprints made using Jurkat cells as templates, deposited from suspension by a Cytospin centrifuge, were used to produce a positive imprint into NO68 optical adhesive layer. In turn, this master positive was cast using PDMS to produce replica bioimprints; PDMS casting was repeated to yield numerous copies of the imprint surface. The master imprint was sputter coated with ~ 50 nm of gold to prevent a cross-reaction between curing PDMS and the NOA68. When positives were uncoated, PDMS crosslinking failed to fully cure at the contact with the NOA68 surface. Qualitative SEM comparison of the PDMS replicas via bright field and scanning electron microscopy showed no deterioration of the master imprint or the transfer of cell size and shape information. Using copies of the same bioimprint reduced variation in the imprinting process.

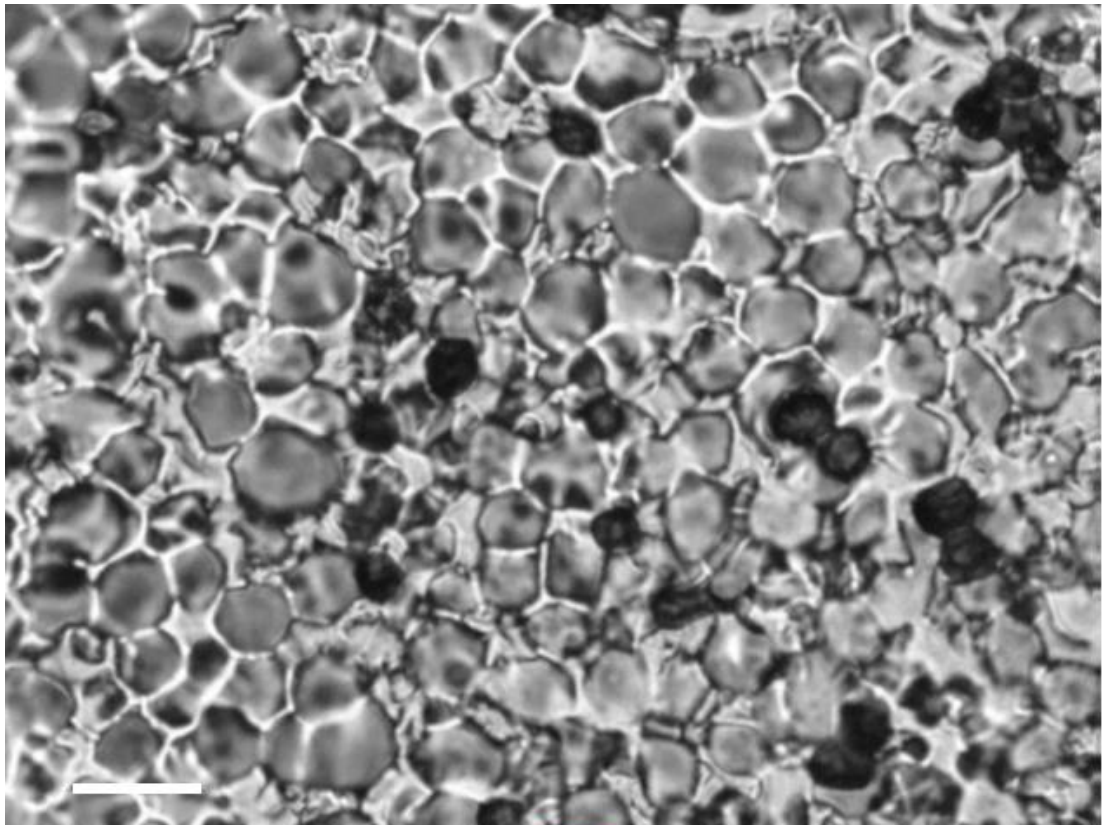
For these proof-of-principle studies, the bioimprint was not incorporated into a flow-through device. Instead, fluorescently tagged cell suspensions were deposited on the imprint surface and allowed to sediment for a fixed time (1 hour); prevented from drying by sealing with a coverslip. Excess cells, unbound to the imprint were washed away by

immersion in water, the coverslip was replaced and the cells enumerated via fluorescence microscopy.

5.1.2. Jurkat Cells

The retention of fixed Jurkat cells to bioimprints made using a Jurkat cell temple was examined. Initially, cells were stained with trypan blue, traditionally used in viability assays to detect dead cells, and then counted manually using bright field microscopy of various sites of the imprint.^{1,2} Subsequently, Jurkats were fluorescently tagged with lissamine-rhodamine for automated counting in ImageJ.^{3,4} Figure 5.1 shows sites on a Jurkat cell bioimprint after incubation with fixed Jurkat cells at a concentration of 40×10^6 cell ml⁻¹; a) Bright field microscopy with Trypan Blue providing contrast for viewing cells and b) fluorescence microscopy of the PDMS bioimprint at the same site with cells highlighted in red.^{5,6} The latter was used in conjunction with ImageJ software for automated counting of 20 areas of the bioimprint.^{3,4} The process involved using the watershed feature in order to differentiate multiple cells from aggregates (see 2.2.4.2).

a)



b)

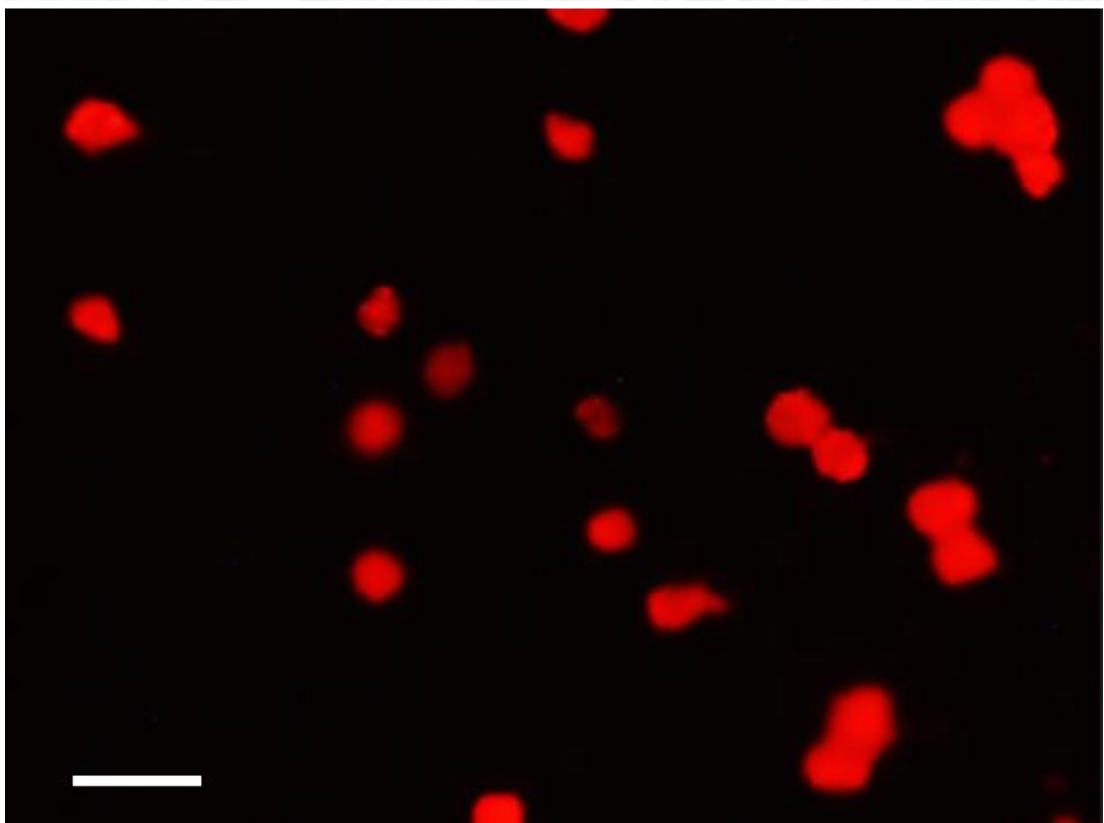


Figure 5.1 PDMS Jurkat bioimprint after exposure to cell suspension of for 1 hour. a) Bright field microscopy of the bioimprint and the associated Jurkat cells seen as dark circles due to Trypan Blue staining and b) fluorescence microscopy using a FITC of the same site on the bioimprint. Once can see the collocation of the cells on the imprint and the fluorescence microscopy image. Scale bars represent 20 μm respectively.

5.1.3. Jurkat cells retention onto PDMS imprints

Further assessment of the Jurkat cells retention on bioimprints was carried out using SEM to produce high resolution images. After analysis via bright field and fluorescence microscopy, coverslips on the bioimprint surface were removed and the substrates allowed to dry. Figure 5.2 below for SEM images of fixed Jurkat cells adhered on to bioimprints produced into PDMS from Jurkat templates.

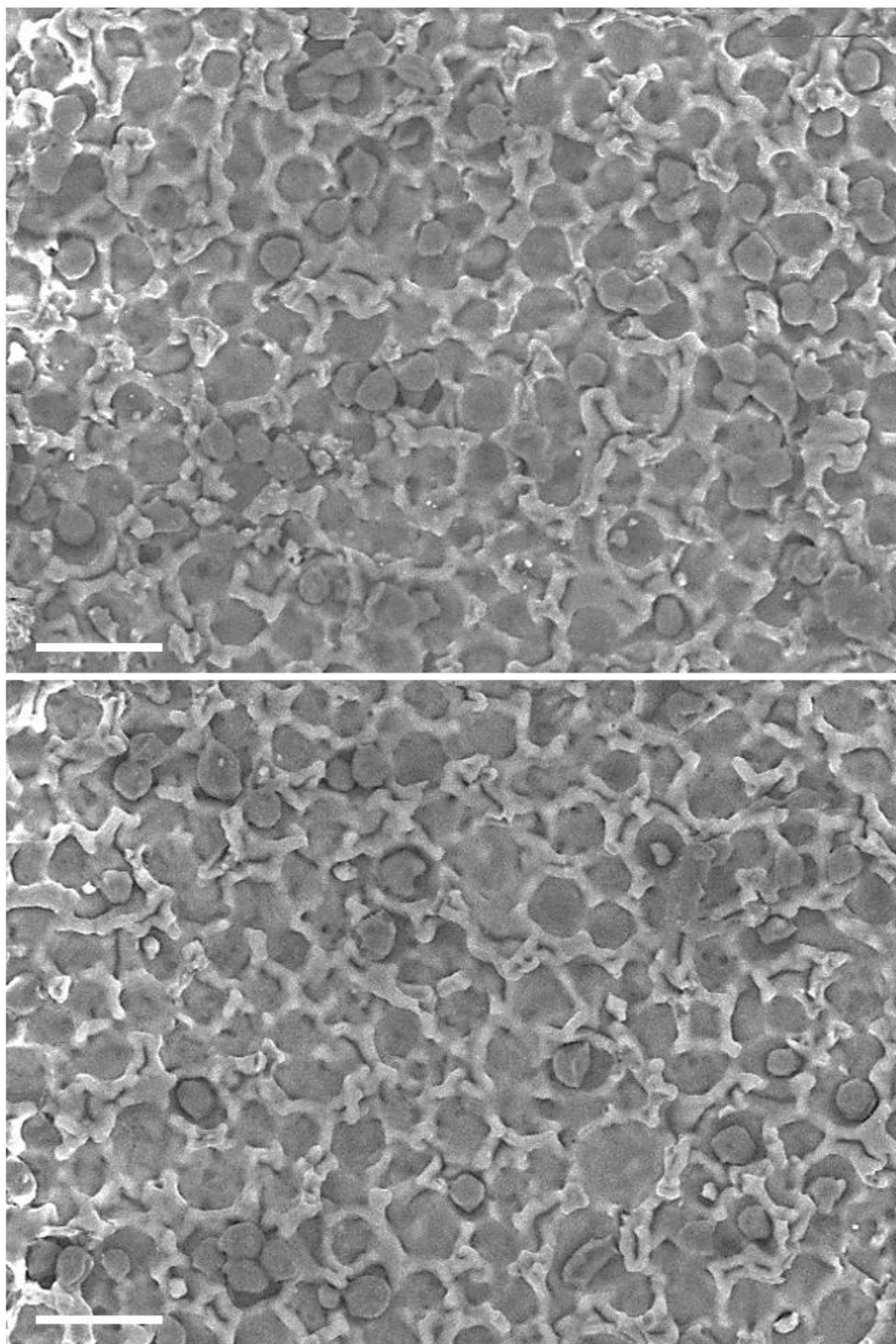


Figure 5.2 SEM images of Jurkat bioimprints after exposure to a suspension of 50×10^6 Jurkat cells ml^{-1} for one hour and unbound cells removed by immersion in MilliQ water. One can clearly identify the Jurkat cells slotted into the imprint cavities. Please note that the drying has caused cells to shrink. Scale bars represent 25 μm .

The SEM images in Figure 5.2 show the Jurkat cells are retained in bioimprint cavities. However, though the high-resolution images give a better indication of the cells location on the bioimprint, this could be as a result of the drying process. Meniscus forces may result in cells moving to the lowest nearby position on the bioimprint rather than being viewed where they were deposited.⁷ Though not already achieved, further confirmation could be found by AFM analysis of the bioimprint after seeding with cells under an aqueous phase.⁸⁻¹⁰

The retention of fixed Jurkat cells onto PDMS Jurkat bioimprints was studied as a function of incubated cell suspension concentration. For proof of principle experiments, Jurkat suspensions ranging from $1 - 100 \times 10^6$ Jurkats ml^{-1} were used. This range is far in excess of the real-world application; at AML diagnosis 20% of the white count constitutes myeloblasts suggesting a target range of $\sim 0.8 - 2 \times 10^6$ blasts ml^{-1} .¹¹⁻¹³ Figure 5.3 shows microscopic analysis of PDMS Jurkat bioimprints after exposure to a suspension of $40 \times 10^6 \text{ ml}^{-1}$ Jurkat cells. After incubation, unbound cells were washed away from the bioimprint by immersion in MilliQ water. Cells were automatically counted using fluorescence microscopy at various sites on the bioimprint ($n = 20$)(see 2.2.4.3.). The number of cells were calculated per metre squared, termed the area density, as a function of the incubated Jurkat cell concentration (Table 5.1 and Figure 5.4).

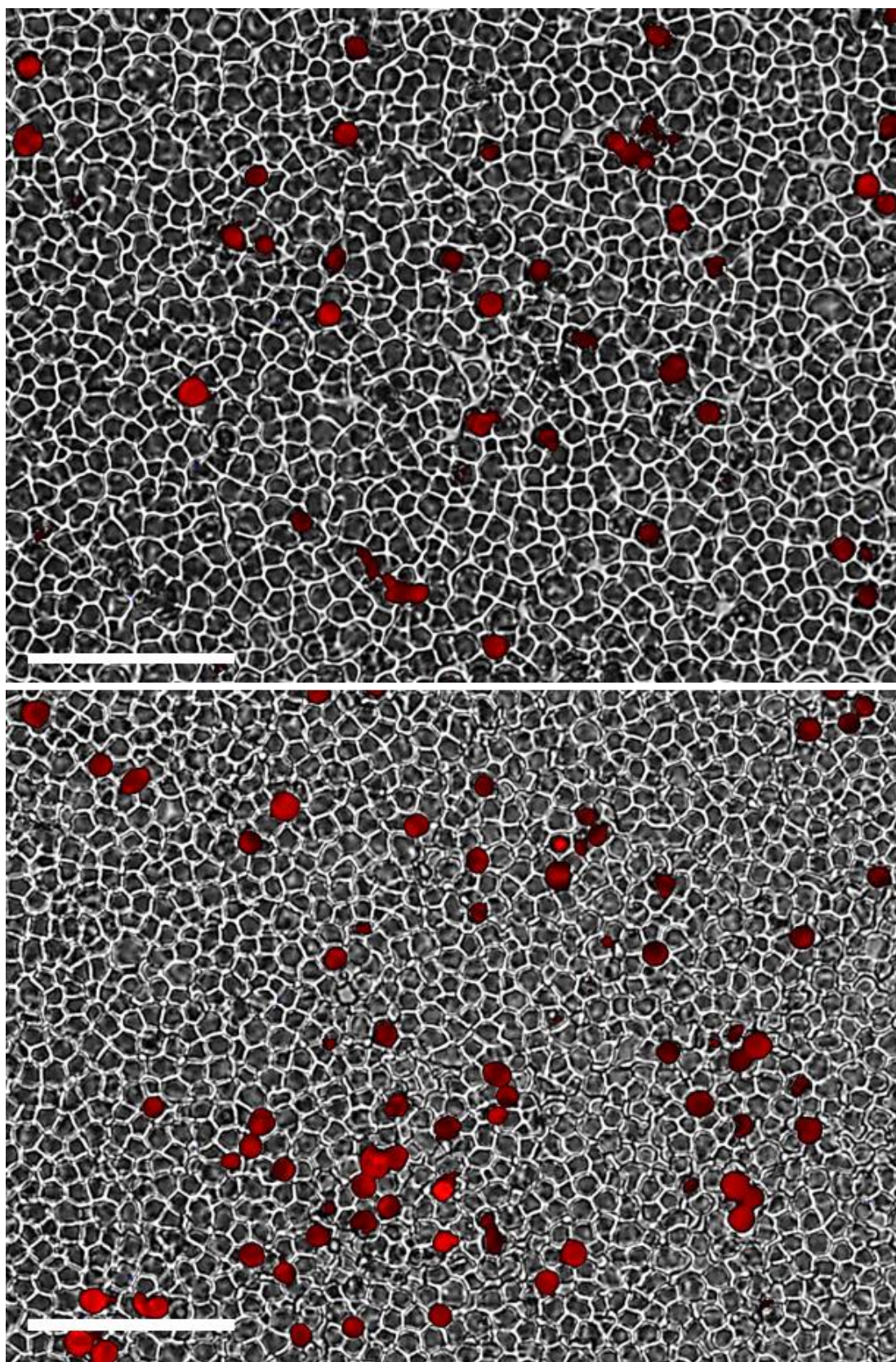


Figure 5.3 Fluorescence microscopy images showing Jurkat cells tagged with lissamine-rhodamine overlaid with bright field images of the PU bioimprint whilst. Suspension of $40 \times 10^6 \text{ ml}^{-1}$ Jurkat cells were incubated under static conditions for 1 hour and unbound suspension removed by perfusion of MilliQ water at 100 ml h^{-1} . Scale bars represent $100 \mu\text{m}$.

Table 5.1 Average values of the percentage of cavities filled and retained cells per unit area for Jurkat cells on native PDMS bioimprints made from Jurkat cell templates. Each value comprises of 10 fields of view.

Seeded [Jurkat] ($\times 10^6$ cells ml^{-1})	Cell area density ($\times 10^9$ cells m^{-2})	Standard deviation area density ($\times 10^9$ cells m^{-2})
10	0.12	0.03
20	0.15	0.05
30	0.25	0.07
40	0.48	0.08
50	0.5	0.2
60	0.7	0.3
70	1.3	0.3
80	1.4	0.2
100	1.4	0.2

Retention was measured as the percentage of cavities retained and as an area density of cells on the bioimprint. The former may be subjective as the user defines what appears to be an imprint cavity using bright field microscopy, which does not indicate the height of the rims around them. Cell area density was calculated as the number of cells per square metre. This comparison relies on the areas being uniform which was confirmed across areas of the bioimprint surface with no loss of quality seen in subsequent replications. Hereafter, the percentage of bioimprint cavities filled was discontinued as the process could not be automated causing analysis to be time consuming whilst not providing additional information compared with cell area density.

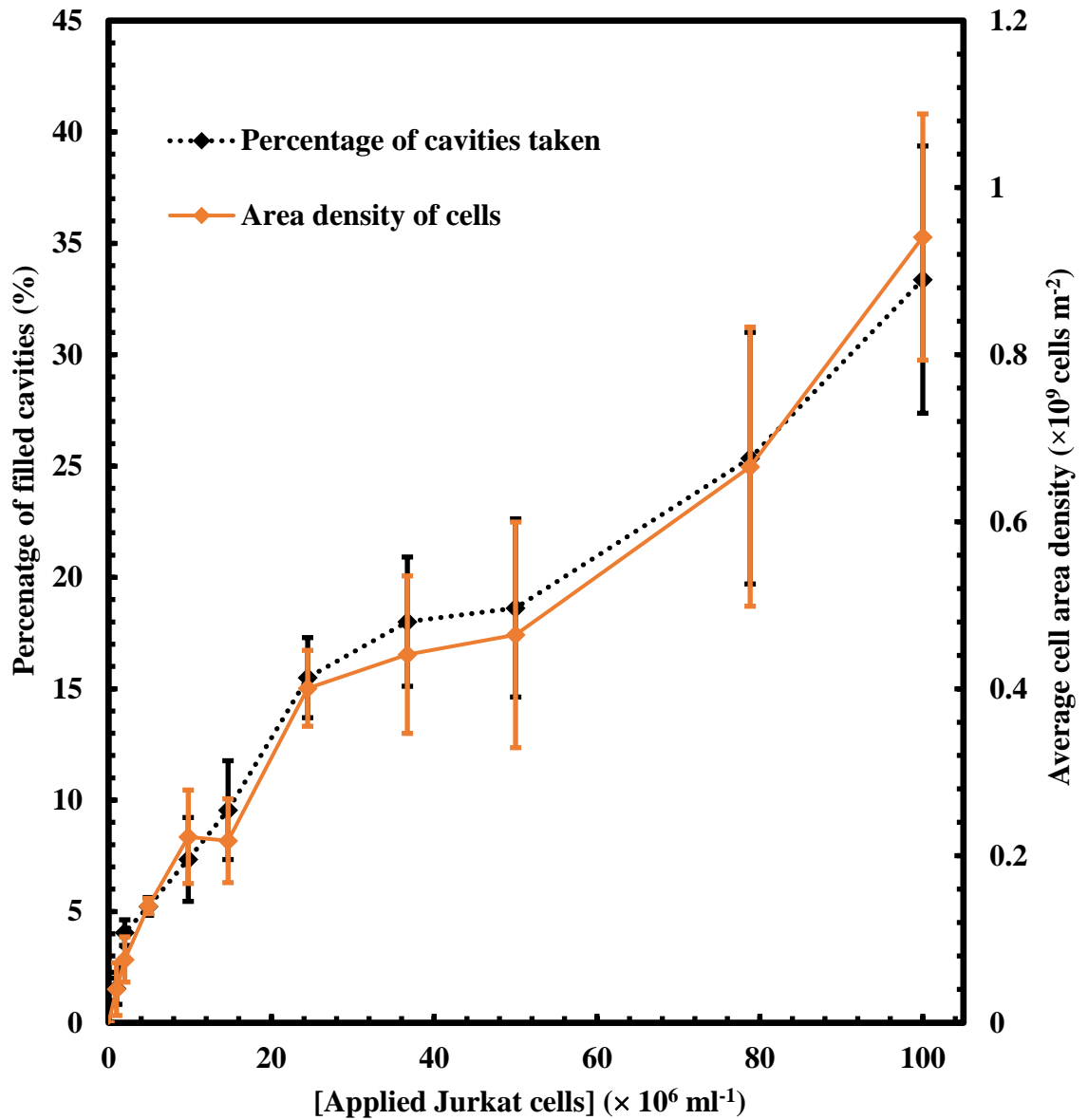


Figure 5.4 Retention of fixed Jurkat cells to PDMS Jurkat bioimprints as a function of the incubated cell suspension concentration. Cell retention was measured as the percentage of cavities filled (*left axis*) and cell area density (*right axis*).

The results show an affinity between the bioimprint and cell suspension of the same cell line as the template used to make the bioimprint. Analysis of the bioimprint showed that Jurkats adhered to the bioimprint, localised to the bioimprinted cavities; no cells were observed in the un-imprinted areas surrounding the bioimprint. Moreover, by overlaying fluorescence and bright field microscopy, it appears that cells are held in the imprinted cavities rather than indiscriminately on the surface. This shows the capture is a result of the complementary size and shape relationship provided by the bioimprint. As expected, by increasing the number of cells added to the imprint surface, more cells are retained. However, despite a greater concentration of cells retaining to the surface with greater cell

concentrations, overall, retention was poor. Even at the higher concentrations, exceeding those seen in the AML patients at diagnosis, the majority of the bioimprint surface remained free of cells; the highest concentration examined was a factor of 10 higher than that of the upper boundary expected at the total healthy white-count.^{12,14} This makes real-world application of this type of bioimprint problematic due to efficiency.

To further understand this behaviour, the number of cells per unit area were calculated and rationalised. See Table 5.2 for the calculation of cells per unit area of the bioimprint in the case of 50 μl of 100×10^6 Jurkat cells ml^{-1} suspension. The length mean diameter of the Jurkat cells was measured as 12 μm , corresponding to an area of $4.5 \times 10^{-10} \text{m}^2$. Therefore, the area of the whole cell population used (5×10^6 Jurkats) is calculated as $2.3 \times 10^{-3} \text{m}^2$, which considering Jurkats as spherical particles with no interactions have a packing efficiency of 0.68 (for body centred cubic lattice). By dividing the area of packed cells by the total imprinted area, it is possible to estimate approximately 9 layers of cells could potentially come over the bioimprint.

Table 5.2 Calculation of the area taken by the maximum Jurkat cell population compared with the area of the bioimprint used.

Jurkat cells		Bioimprint area	
r (μm)	12	l (cm)	2
r (m)	1.2×10^{-5}	l (m)	0.02
Cell area (m^2)	4.5×10^{-10}	Area (m^2)	4.0×10^{-4}
Total number of cells	5.0×10^6		
Area of all cells (m^2)	2.3×10^{-3}		
Area considering packing (m^2)	3.3×10^{-3}		

Layers of cells on the bioimprint = Total area of all cells / bioimprint area

$$= \frac{2.3 \times 10^{-3}}{2.7 \times 10^{-4}} \approx 9 \text{ cell layers}$$

This figure should be treated only as a rough estimate as the deposition area is not strictly controlled and excess cell suspension may be displaced by adding the coverslip to the surface. However, as the value is far in excess of the available bioimprint area it indicates cells numbers used are far in excess of that needed to completely cover the bioimprint. Increasing the number of cells deposited on the bioimprint will not increase the number of cells that come into contact with the bioimprint. As the retention rate remains poor

after exposure to an overpopulation of cells, this highlights a poor interaction between bioimprints and target cells. The inherent hydrophobic nature of PDMS prevents cell suspensions fully wetting the bioimprint and incurs no attraction to target cells.¹⁵

5.2. Flow cell experiments

Thus far, bioimprints have been produced and replicated. Initial experiments were trialled using in-house replicas of bioimprints made into PDMS, though the material has proved incompatible and the experimental procedure offers little control over parameters that may influence performance. In this section, bioimprints were incorporated into a microfluidic flow cell to provide more a reproducible and representative assessment of the bioimprints ability to retain cells from suspension.

Using channels of the same dimensions, each bioimprint is subjected to a liquid flow of comparable and controllable hydrodynamics. Suspensions of a controllable volume can contact a pre-defined area of the bioimprint. For this, channels (area of 5 cm × 0.5 cm by 100 μm deep) were imprinted into curing PDMS substrates (area of 7.5 cm × 2.5 cm by 0.5 cm deep). The PDMS bioimprint was positioned between the PDMS substrate and a microscope slide. In order to seal the chip, the PDMS and glass slide were treated in oxygen plasma (16 W, 147 Pa) for 180 seconds. The channel was protected from hydrophilising during oxygen plasma treatment. In this setting, the hydrophobic nature of PDMS is an advantage this will minimise the number of cells adhering to the channel walls. Figure 5.5 shows a photograph of the microfluidic chip produced to improve accuracy of cell retention experiments.

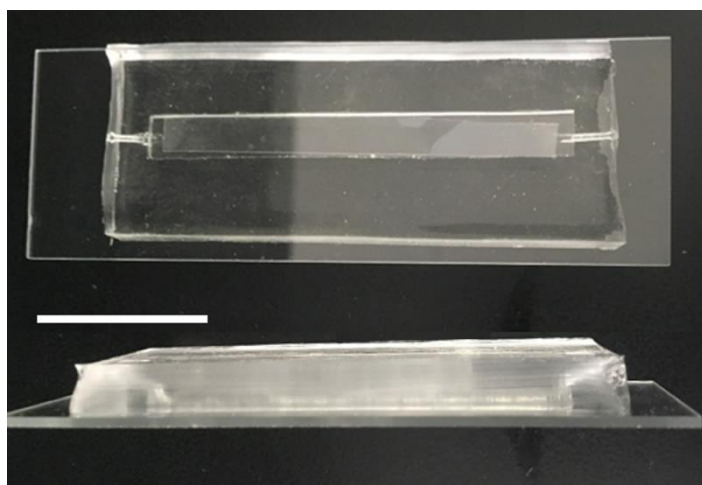


Figure 5.5 Images of the bespoke PDMS microfluidic flow chip used to examine the retention of cells to bioimprints with channel dimensions of $5\text{ cm} \times 0.5 \times 0.01\text{ cm}$ viewed a) Top down and b) side-on. Scale bar represents 2 cm.

Retention of fixed myeloblast cells to bioimprints was measured under static conditions using the microfluidic chip. The cell suspension was applied to the imprint, allowed to sediment for a fixed time (1 hour) and the unbound cells washed away using MilliQ water at a user defined and reproducible flow rate (100 ml h^{-1}). This was calibrated using the minimum flow rate in order to remove cells from an un-treated and non-imprinted PU substrate. The chip was kept sealed for the microscopic analysis to prevent evaporation of the remaining solution on the bioimprint. This method avoids introducing an artefact to retention by aberration from meniscus forces whilst drying, previously highlighted as an issue for analysis. Though analysis continued to be done via inspection of the bioimprint another advantage of this method is the scope for analysing the effluent cell suspension.

5.2.1. Substrate

Replicas of bioimprints produced by spreading HL60 cells in glucose solutions, copied by R2RNIL, were incorporated into microfluidic cells. Replica imprints comprised of a $\sim 10\text{ }\mu\text{m}$ layer of PU on a polyethylene terephthalate (PET) layer. The harder nature of the PU allows a good seal in the microfluidic chip when pressure is applied; likely to be advantageous when the total area is scaled up. The retention of HL60 cells was measured to untreated PU HL60 replica imprints; Figure 5.6 and Figure 5.7 show fluorescence microscopy images of retained HL60 cells on HL60 bioimprints, examined within the microfluidic flow cell.

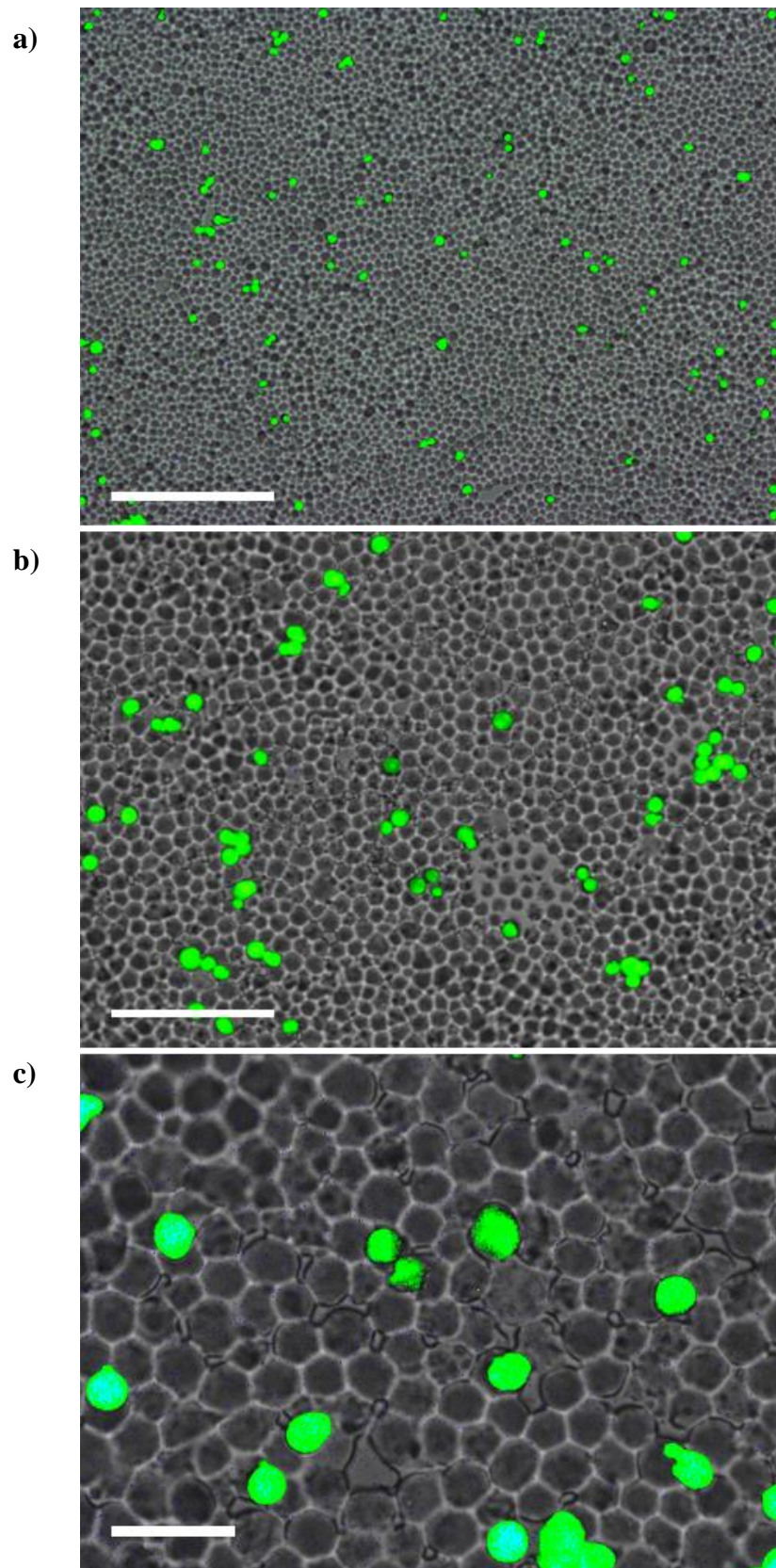


Figure 5.6 Fluorescence microscopy showing HL60 cells tagged with carboxyfluorescein overlaid with bright field images of the PU bioimprint whilst incorporated into a microfluidic chip. Suspension of $10 \times 10^6 \text{ ml}^{-1}$ incubated under static conditions for 1 hour and unbound suspension removed by perfusion of MilliQ water at 100 ml h^{-1} . Scale bars represent a) $200 \mu\text{m}$, b) $100 \mu\text{m}$ and c) $20 \mu\text{m}$ respectively.

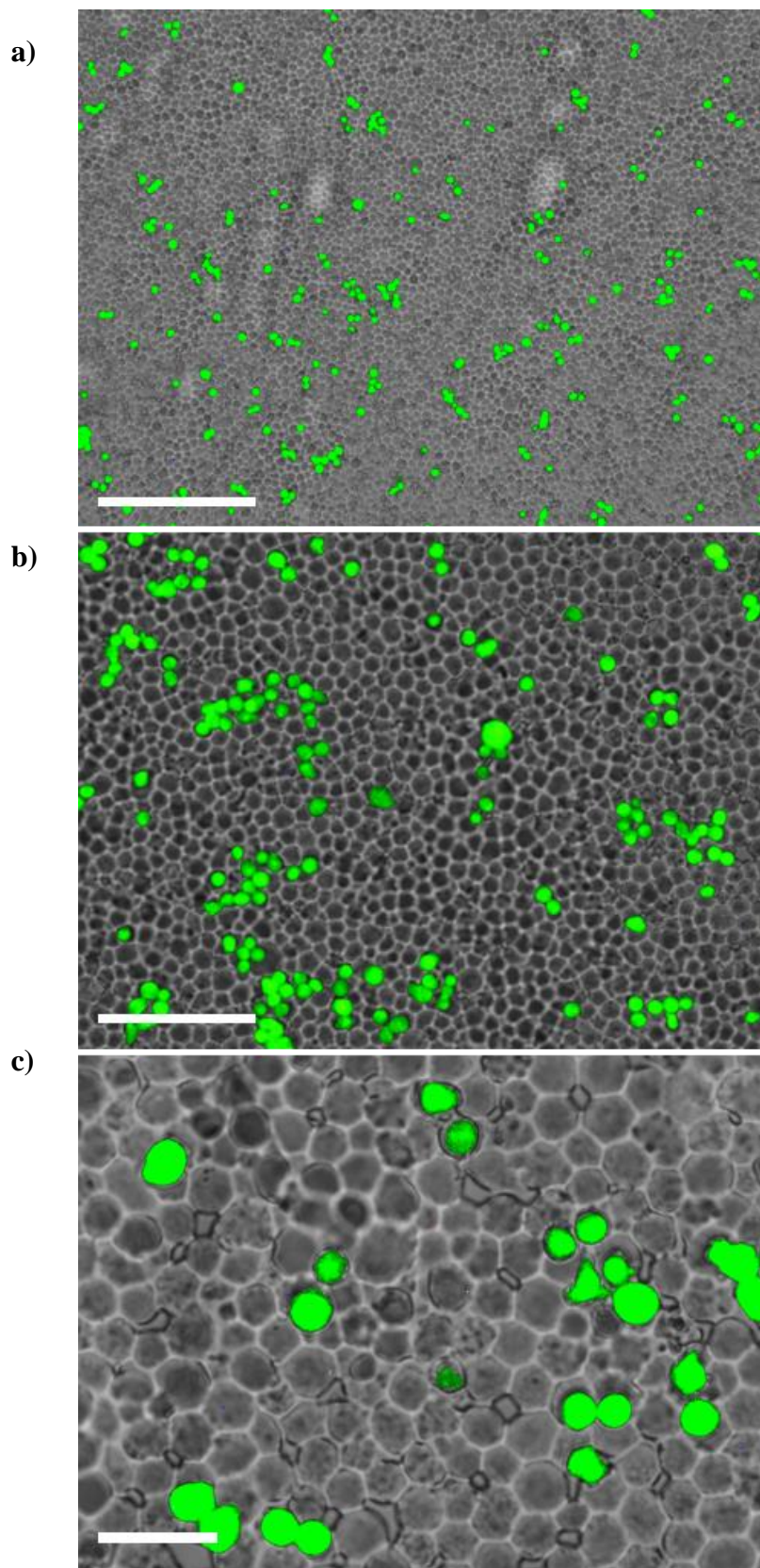


Figure 5.7 Fluorescence microscopy showing HL60 cells tagged with carboxyfluorescein overlaid with bright field images of the PU bioimprint whilst incorporated into a microfluidic chip. Suspension of $30 \times 10^6 \text{ ml}^{-1}$ incubated under static conditions for 1 hour and unbound suspension removed by perfusion of MilliQ water at 100 ml h^{-1} . Scale bars represent a) $200 \mu\text{m}$, b) $100 \mu\text{m}$ and c) $20 \mu\text{m}$ respectively.

Results show that as the concentration of the seeded cell suspension was increased, more cells were retained to the bioimprint. Table 5.3 and Figure 5.8 present the results of the analysis of the retained cells per metre on the bioimprint as a function of the seeded cell suspension concentration. Figure 5.8 compares the retention data of bioimprints in static conditions under benchtop conditions and whilst incorporated into a microfluidic chip. The former involved removing unbound cells from the bioimprint by washing manually and offers little control over the resultant hydrodynamic forces on the bioimprint surface.

Table 5.3 Tabulated data for the retention of fixed HL60 cells to HL60 PU imprints produced from bioimprints using a glucose protective layer and replicated by R2RNIL as a function of the applied cell suspension concentration. Cell area density is the average of 20 sites on the bioimprint with the standard deviation also calculated.

[HL60] ($\times 10^6$ cells ml ⁻¹)	Cell area density ($\times 10^9$ cells m ⁻²)	Standard deviation area density ($\times 10^9$ cells m ⁻²)
2.5	0.04	0.02
5	0.09	0.04
7.5	0.16	0.03
10	0.20	0.07
20	0.35	0.07
30	0.7	0.2
50	1.3	0.2

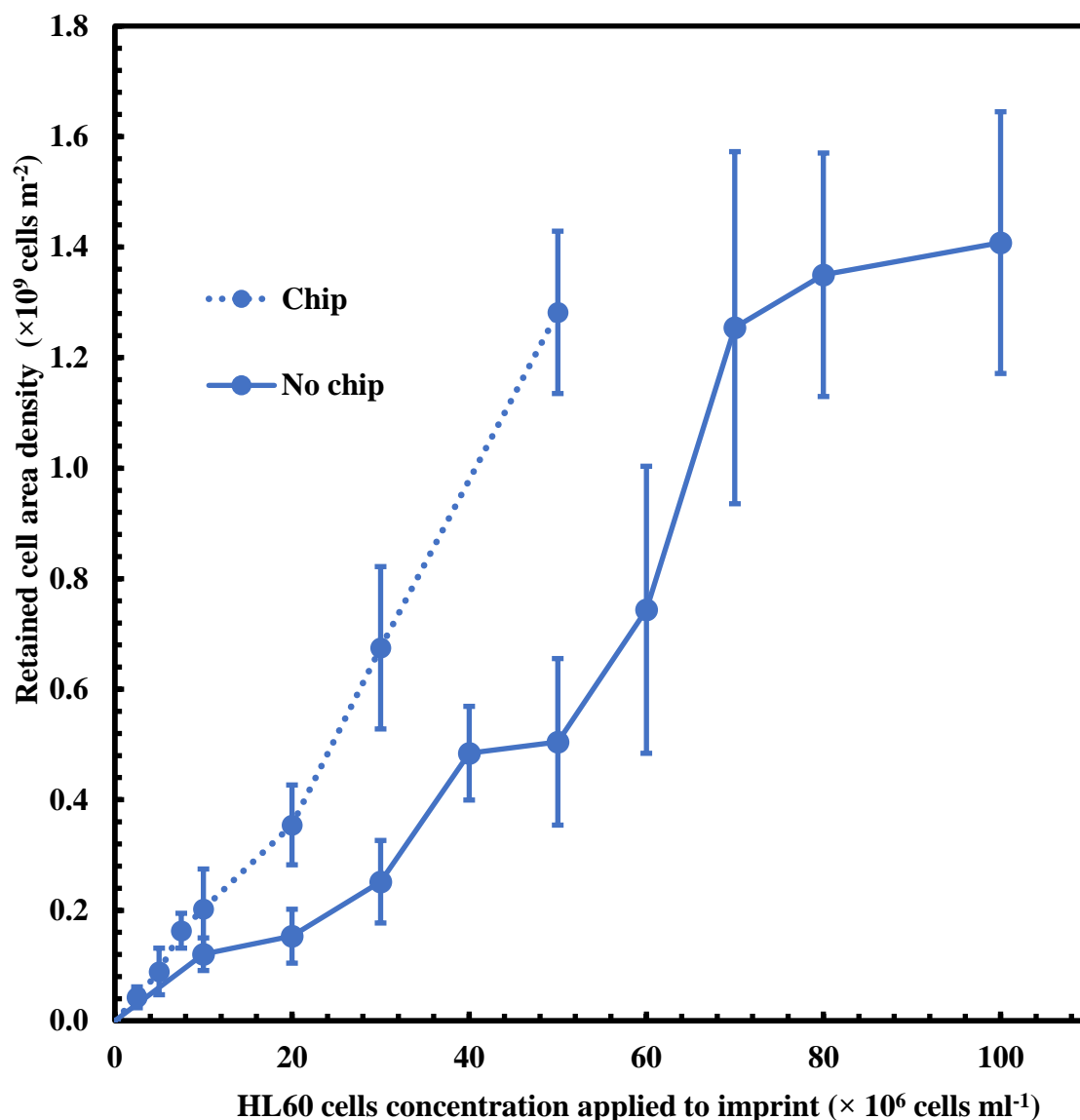


Figure 5.8 Retention of fixed HL60 cells to HL60 imprints versus the applied cell suspension concentration on to native PU bioimprints. The uptake was measured in static conditions after incorporation into a bespoke microfluidic device.

Both chip and no chip show the retention to bioimprints was proportional to the concentration of cells applied to the imprinted surface (Figure 5.8). Retention whilst incorporated into a microfluidic chip shows greater uptake, which can be attributed to the lack of meniscus forces but can also be attributed to the greater levels of cell excess in the smaller area. Calculations of the area taken by the cell population for the case of 50×10^6 HL60 ml⁻¹ can be seen in Table 5.4, below.

Table 5.4 Tabulated parameters of the area of HL60 cells, the area of the bioimprint as part of the microfluidic flow cell and the number of layers of HL60 cells expected to form from 200 μl of a 50×10^6 HL60 cells ml^{-1} .

HL60 cells		Bioimprint area	
r (μm)	13	w (cm)	4
r (m)	1.3×10^{-3}	w (m)	0.04
Cell area (m^2)	5.3×10^{-10}	l (cm)	0.5
Total number of cells	1.0×10^6	l (m)	0.005
Area of all cells (m^2)	5.3×10^{-3}	Area (m^2)	2.0×10^{-4}
Area considering packing	7.8×10^{-3}		

Layers of HL60 on the bioimprint = Total area of all cells / bioimprint area

$$= \frac{7.8 \times 10^{-3}}{2.0 \times 10^{-4}} = \sim 32$$

As with Jurkat bioimprints, cells were used in excess on the bioimprint surface; the majority of cells will not come into contact with the bioimprint. Increasing the suspension concentration is unlikely to cause more cells to be retained. However, as is clear from microscopic analysis of the imprints after unbound cells have been washed away (Figure 5.6 and Figure 5.7), much of the bioimprint area was left unused. When incorporated into a myeloblast capture vehicle, such imprints with poor retention would lead to an inefficient device. To improve the cell capture, the bioimprint surface is treated to yield a weak positive charge.

5.2.2. Retention of cells from single cell suspension

Retention of fixed HL60 cells was measured as a function of the incubated suspension concentration per bioimprints treated with various ratios of PU:bPEI. Solutions of 0.1%, 0.25%, 0.5%, 0.75% and 0.9% bPEI, made up to 1% (w/v) with uncured PU in ethanol were used to treat the PU bioimprints. Once functionalised and the deposited PU layer was UV cured, the substrates were incorporated into the flow-through device (Figure 5.5) and the same procedure as used with un-treated bioimprints. Fixed HL60 cells were

stained with lipid conjugated carboxyfluorescein in order to be automatically counted. Table 5.5 and Figure 5.9 present the tabulated and graphical data of fixed HL60 cells retention to functionalised bioimprints as a function of the seeded cell suspension concentration.

Table 5.5 Area cell density of retained HL60 cells to HL60 imprints as a function of seeded cell suspension concentrations repeated for various treatment parameters of PU bioimprints. Cell area density is the average of 20 sites on the bioimprint with the standard deviation also calculated.

[bPEI] (wt. %)		Retained cells per area ($\times 10^9$ cells m^{-2})						
		Incubated [HL60] $\times 10^6$ cells ml^{-1}						
		2.5	5	7.5	10	20	30	50
0.9	Mean	0.5	1.4	2.1	3.2	3.3	3.5	3.4
	SD	0.1	0.3	0.3	0.3	0.3	0.3	0.3
0.75	Mean	0.31	0.8	1.6	2.5	3.2	3.4	3.5
	SD	0.06	0.1	0.2	0.3	0.3	0.3	0.2
0.5	Mean	0.19	0.5	1.2	1.8	3	3.5	3.4
	SD	0.06	0.1	0.3	0.4	0.5	0.5	0.5
0.25	Mean	0.15	0.21	0.4	0.7	1.9	3	3.4
	SD	0.06	0.06	0.1	0.3	0.2	0.2	0.2
0.1	Mean	0.06	0.16	0.25	0.3	0.7	1.2	1.8
	SD	0.03	0.03	0.08	0.1	0.1	0.2	0.2
0	Mean	0.04	0.09	0.16	0.2	0.35	0.7	1.3
	SD	0.02	0.04	0.03	0.07	0.07	0.2	0.2

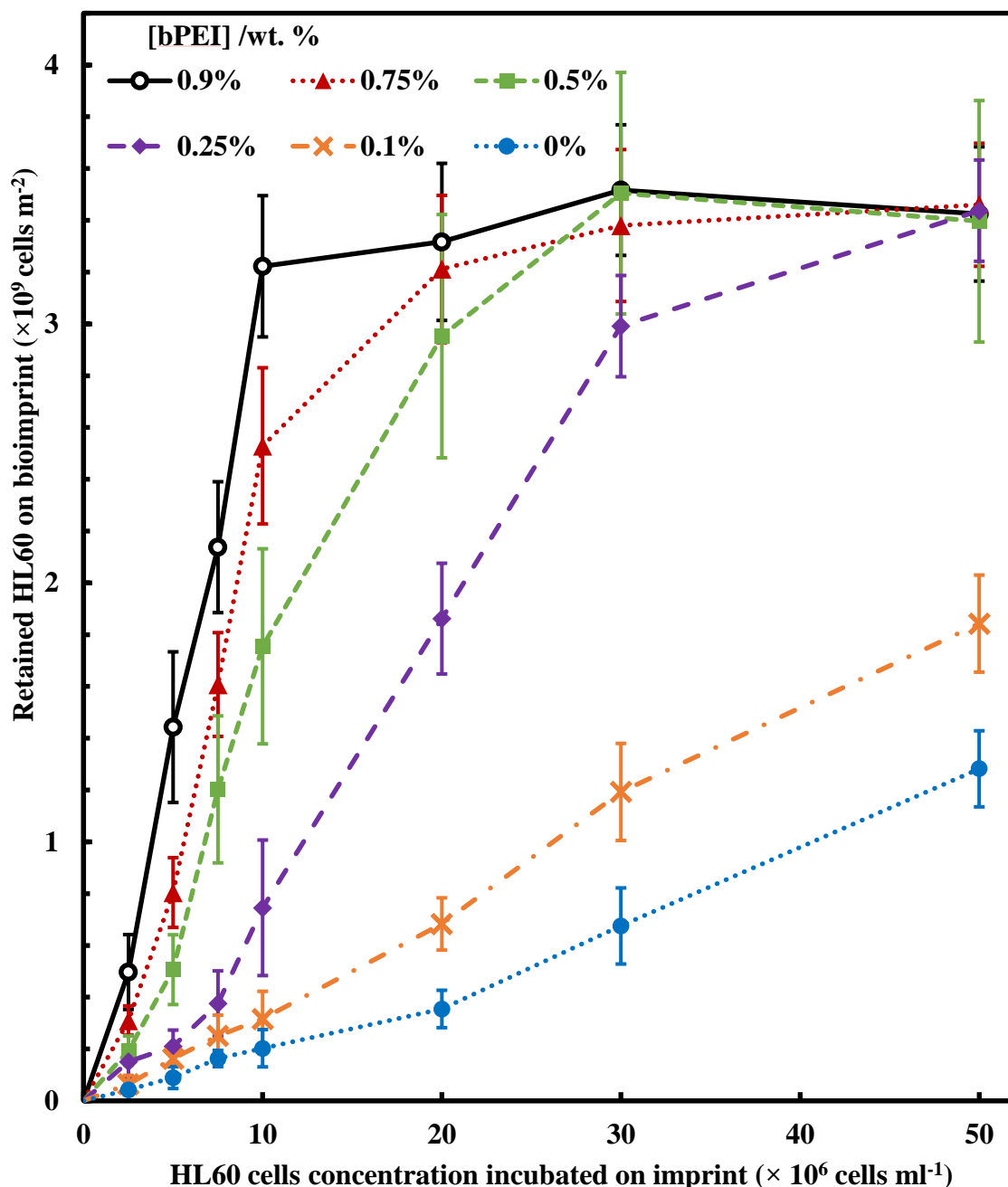


Figure 5.9 Area cell density of retained HL60 cells to HL60 imprints as a function of seeded cell suspension concentrations repeated for various treatment parameters of PU bioimprints using bPEI and PU mixtures. Unbound cells were removed by perfusion of 100 ml h^{-1} of MilliQ water.

Results show that more rigorous surface modifications procedures lead to an improved capture of HL60 cells to the bioimprints. More cells are retained to the bioimprint for bioimprints treated with a higher proportion of bPEI due to increased immobilised grafted cationic charge, grafted to the surface by residual volumes of PU. Apart from native PU and imprints treated with 0.1% (w/v) bPEI, the effect appears to plateau at $3.4 \times 10^9 \text{ cells ml}^{-1}$; despite the excess of target cells optical microscopy analysis of the

imprints showed that some fraction of the areas are not fully occupied. This may be due to the uniformity of the bPEI:PU functionalisation though the method was similar to that used to spread cells evenly. Instead, the problem is more likely the interaction is insufficient however, by increasing the bPEI proportions further would reduce the volume of PU holding the charge on the surface. If the PU were also increased, this may compromise the size and shape of the bioimprinted cavities which in turn would reduce the capacity for shape and size recognition.

However, the aim was to produce a weak attraction between bioimprint surface and the target cells in order to prevent indiscriminate adhering of cells to all areas of the surface. For more adequate assessment of the surface treatment parameters the bioimprints ability to discriminate against a target cell type from binary mixtures will be assessed in the Chapter 6. If the bioimprint is more selective, poor retention may be overcome by recirculating cell suspensions to achieve a maximum capture.

5.2.3. HL60 retention to particle imprints

The effect of the cell shape was examined by assessing the retention of HL60 cells to bioimprints produced from microparticles of a comparable size. Due to their relatively smooth spherical surface of the particle little asperity is observed in particle imprint cavities as seen with cell imprints. All interactions dependent on the extracellular features are not seen with microparticle bioimprints and retention is dependent only on size matching between the cells and the particle imprint cavities. CA15 particles were used as they are representative of cell size.¹⁶ The sizes were comparable; length mean diameter of HL60 cells was $13 \pm 2 \mu\text{m}$ and the length mean diameter of the microparticle imprint cavities was $14.5 \pm 0.4 \mu\text{m}$. The retention of HL60 cells was measured on CA15 negative bioimprints produced in PU by R2RNIL. The assessment was carried out over a range of bPEI and PU concentrations with a total additive concentration of 1 wt. % (Table 5.6 and Figure 5.10).

Table 5.6 Area cell density of retained HL60 cells to CA15 particle imprints as a function of seeded cell suspension concentrations repeated for various treatment parameters of PU bioimprints. Cell area density is the average of 20 sites on the bioimprint with the standard deviation also calculated.

[bPEI] (wt. %)		Retained cells per area ($\times 10^6$ cells m^{-2})						
		Incubated HL60 cell concentration $\times 10^6$ cells ml^{-1}						
		2.5	5	7.5	10	20	30	50
0.9	Mean	5	13	26	54	140	188	257
	SD	4	4	11	20	13	44	47
0.75	Mean	5	14	20	41	104	174	203
	SD	1	4	8	10	42	35	34
0.5	Mean	3	10	16	47	82	145	179
	SD	2	7	10	17	29	40	64
0.25	Mean	4	10	11	25	67	110	141
	SD	3	3	4	9	24	31	52
0.1	Mean	4	7	12	23	57	91	136
	SD	4	5	5	9	15	19	55
0	Mean	3	4	8	12	37	68	108
	SD	3	3	5	5	14	27	33

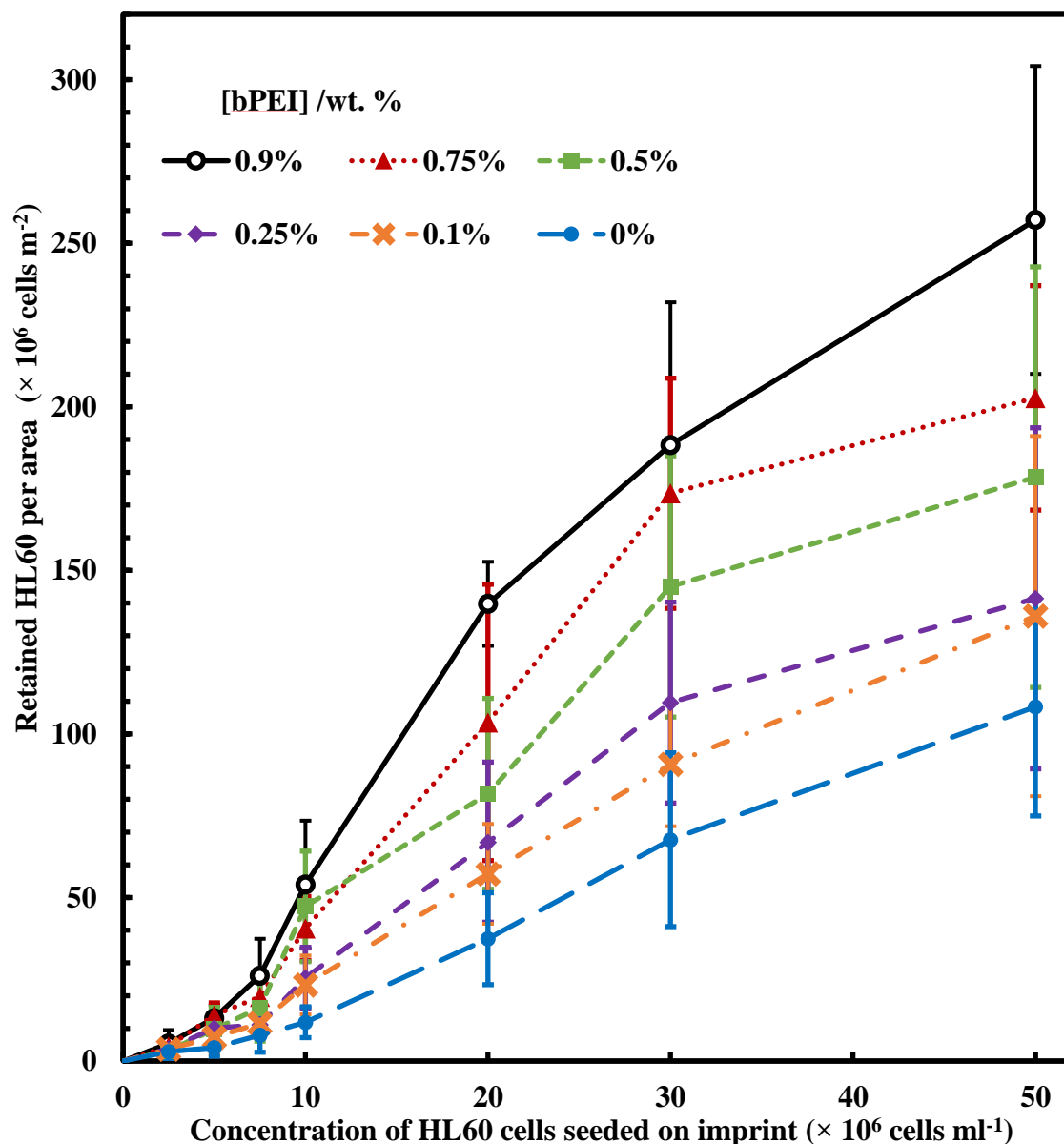


Figure 5.10 Area cell density of retained HL60 cells to PU CA15 imprints as a function of seeded cell suspension concentrations repeated for various surface modification parameters of PU bioimprints using bPEI and PU mixtures. Unbound cells were removed by perfusion of 100 ml h^{-1} of MilliQ water.

As with HL60 retention to cell formed bioimprints, the retention increased as a function the incubated suspension concentration. In this case the overall retention was around a factor of 10 lower. As the sizes were similar, the poor retention could be attributed to mismatched radii of curvatures and the lack of extracellular roughness in the cavities, observed in Chapter 4. Recognition of extracellular features mean great specificity in the intended clinical setting; particularly as extracellular features are specific to cell types. This effect will be further assessed in chapter 6 with mixtures of cell types.

5.3. Conclusions

This chapter aimed to assess the bioimprints ability to retained cells of the templated cell line to the substrate.

Initially, fixed Jurkat cell suspensions were seeded on Jurkat bioimprints made of native PDMS. The overall capture of cells by the surface was poor with large areas showing no bound cells. The retention of HL60 cells was measured to native PU bioimprints in static conditions. Though the bioimprints were produced via different methods and from different template cells, the myeloblast cell retention showed a similar trend. Data showed regions of both bioimprint types being largely devoid of cells.

To gain control of the conditions in which the retention was assessed, bioimprints were incorporated into a flow-through type of cell. Each device offered the same dimensions and when coupled with a user defined flow rate, hydrodynamics and flow present in the incubation and washing steps could be controlled. Bioimprints were analysed with the device intact to negate the impact of drying and meniscus forces on cell adsorption.

The retention of HL60 cells to native imprints whilst incorporated into a microfluidic flow chamber yielded more reproducible results. This plot showed a higher percentage retention though a large proportion of the imprint area did not contained immobilised cells. Greater attraction between the bioimprint and cells were sought, so a method to chemically modify the surface to introduce a weak attraction towards target cells was examined. The retention of single cell suspensions was examined as a function of the cell suspension concentration was repeated for bioimprints functionalised with a range of polyelectrolyte treatments. With a higher proportion of polyelectrolyte grafted to the bioimprint surface, the retention of HL60 cells improved. This is due to an electrostatic attraction being introduced by immobilising a positive surface charge from cationic polyelectrolyte with a high isoelectric point. Cell retention plateaued at high concentrations of the incubated cell suspension.

The importance of cell membrane topography on cell retention was examined by assessing retention of cell populations to imprints created from monodisperse microparticles with a comparable cell radius to HL60. As with cell imprints, retention increased as a function of the incubated suspension concentration though showed a significantly lower retention. This highlights the importance of the nanoscale membrane

feature are important in shape recognition and not captured in spherical microparticle imprints.

All cell suspensions used for retention experiments were fixed in order to preserve the size and shape information and avoid interference from damage during the experimental procedure. However, for the intended use in a myeloblast capture device, where all cells will be live, the effect of fixation will need to be addressed. In this instance cell retention is likely to be improved as cells can deform to achieve a flush fit with cell cavities.

5.4. References

- 1 W. Strober, *Curr. Protoc. Immunol.*, 1997, **111**, 1-3.
- 2 S. Atلمان, L. Randers and G. Rao, *Biotechnol. Prog.*, 1993, **9**, 671–674.
- 3 J. Lozano-Gerona and Á.-L. García-Otín, *Anal. Biochem.*, 2018, **543**, 30–32.
- 4 D. Cadena-Herrera, J. E. Esparza-De Lara, N. D. Ramírez-Ibañez, C. A. López-Morales, N. O. Pérez, L. F. Flores-Ortiz and E. Medina-Rivero, *Biotechnol. Reports*, 2015, **7**, 9–16.
- 5 C. Lefevre, H. C. Kang, R. P. Haugland, N. Malekzadeh, S. Arttamangkul and R. P. Haugland, *Bioconjug. Chem.*, 1996, **7**, 482–489.
- 6 M. W. Wessendorf and T. C. Brelje, *Histochemistry*, 1992, **98**, 81–85.
- 7 V. N. Paunov, P. A. Kralchevsky, N. D. Denkov and K. Nagayama, *J. Colloid Interface Sci.*, 1993, **157**, 100–112.
- 8 D. J. Müller and Y. F. Dufrêne, *Trends Cell Biol.*, 2011, **21**, 461–469.
- 9 P. Zachee, J. Snauwaert, P. Vandenberghe, L. Hellemans and M. Boogaerts, *Br. J. Haematol.*, 1996, **95**, 472–481.
- 10 S. Kasas, V. Gotzos and M. R. Celio, *Biophys. J.*, 1993, **64**, 539–544.
- 11 Cancer Research UK, <https://www.cancerresearchuk.org/health-professional/cancer-statistics/statistics-by-cancer-type/leukaemia-aml>, Accessed December 2017.
- 12 D. Harmening, *Clinical & fundamentals of Hemostasis*, F. A. Davies Company, Philadelphia, 1997.
- 13 G. J. Schuurhuis, M. Heuser, S. Freeman, M.-C. Béné, F. Buccisano, J. Cloos, D. Grimwade, T. Haferlach, R. K. Hills, C. S. Hourigan, J. L. Jorgensen, W. Kern, F. Lacombe, L. Maurillo, C. Preudhomme, B. A. van der Reijden, C. Thiede, A. Venditti, P. Vyas, B. L. Wood, R. B. Walter, K. Döhner, G. J. Roboz and G. J. Ossenkoppele, *Blood*, 2018, **131**, 1275–1291.
- 14 S. Oberoi, T. Lehrnbecher, B. Phillips, J. Hitzler, M. C. Ethier, J. Beyene and L. Sung, *Leuk. Res.*, 2014, **38**, 460–468.
- 15 S. H. Tan, N. T. Nguyen, Y. C. Chua and T. G. Kang, *Biomicrofluidics*, 2010, **4**, 1–8.
- 16 W. Ladines-Castro, G. Barragán-Ibañez, M. A. Luna-Pérez, A. Santoyo-Sánchez, J. Collazo-Jaloma, E. Mendoza-García and C. O. Ramos-Peñafiel, *Rev. Médica del Hosp. Gen. México*, 2016, **79**, 107–113.

6. Bioimprint Selectivity

In Chapter 5, the retention of single cell suspensions was examined. Though target cells remain adsorbed to the bioimprint, no consideration has been paid to the preference to target cells from competitive cell mixtures, mimicking patient blood aspirate. The following section will assess how selective bioimprints are toward the template cell type from cell mixtures. In order to mimic the conditions of the intended myeloblast capture device, HL60 cells will be targeted as a cancerous proxy with competition provided by a control population of healthy peripheral blood mononuclear cells (PBMCs).

6.1. Cell populations

The preference of the bioimprint to one cell type on account of the cell size and shape differs with the rest of the cells in the complex mixture. Therefore, it is important to define the morphologies of both populations. As the study has used a myeloblast proxy, it is important to confirm the size and shape difference of HL60 and healthy blood cells. In this case, peripheral blood mononuclear cells (PBMCs) were harvested from whole blood samples to act as a control. An ideal device would not interact with PBMCs, allowing them to elute from the device, only the capturing the myeloblast substitute HL60. The length mean diameter of both cell types was measured using high resolution bright field microscopy images of cells. See Table 6.1 and Figure 6.1 for the size distributions of HL60 and PBMCs; both compared to the bioimprint cavities created using HL60 cells as templates. The normal distribution of the length mean diameters was calculated in conjunction with the mean and standard deviation of the measurements.

Table 6.1 The minimum, maximum, average and standard deviations of length mean diameter $d[1,0]$ of fixed HL60 cells, PBMCs and the bioimprint cavities created using HL60 cells.

	Minimum (μm)	Maximum (μm)	$d[1,0]$ (μm)	SD (μm)
HL60 bioimprints	6	14	11	2
HL60 cells	7	18	13	2
PMBC cells	5	14	9	2

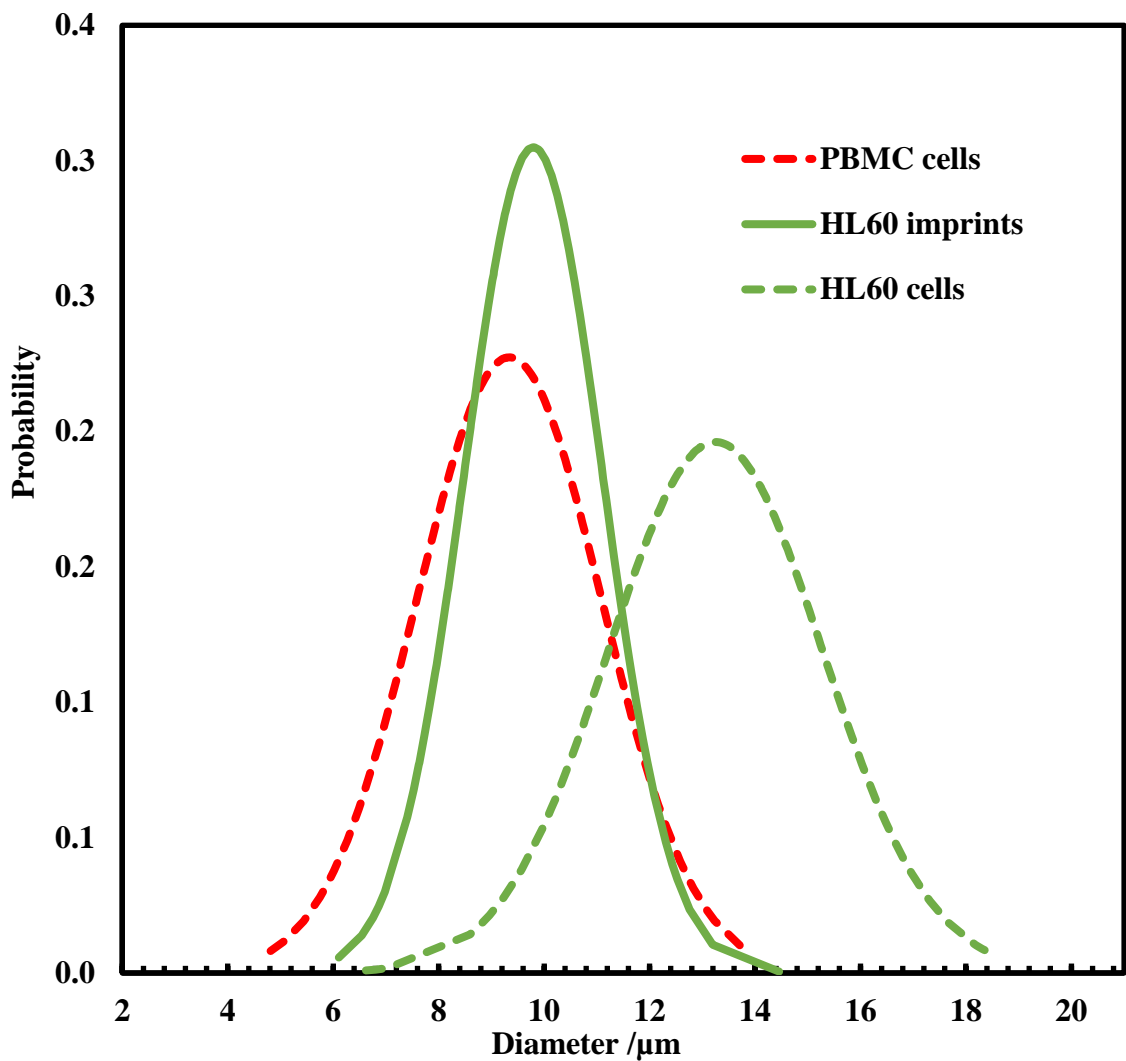


Figure 6.1 Overlaid size distributions calculated by length mean diameter measurements of fixed PBMC and HL60 with the size of bioimprinted bioimprint cavities produced from HL60 cells via the glucose protective layer method.

HL60 cells, the cancerous surrogate, show a larger average cell diameter to the ‘healthy control’ PBMC control. Bioimprinted cavities created using a HL60 template have a smaller diameter than the cells as less than half of the cell is exposed to the curing polymer matrix as discussed in Chapter 2. Note, that the diameter of the HL60 imprints matches the rim of the imprint rather than its radius of curvature. Therefore, though the size of the bioimprint cavities is closer to the size of the healthy control cell population, due to a difference in the radii of curvature the surface area will not be significantly increased as in the case of the correctly matched cell.

The bioimprint will aim to target this size difference by allowing cells of the correct match to fit flush into the cavities. When the cell mixture of HL60 and PBMC cells gets in contact with the imprint, both types of cells are electrostatically attracted to the surface

of the cationically functionalised imprint.¹ However, the HL60 cells attraction to the surface is stronger as their contact area with the imprint surface is much larger than this of the PBMCs, as it matches the surface of the hole much closer. When the flow-through device is flushed, the loosely bound PBMC cells are detached easier from the imprint as they make merely a point contact with the interface, while HL60 fit closely and remain in the bioimprint cavities. The substantially larger contact area of the matching myeloblast cells with the imprint amplifies the otherwise weak electrostatic interaction and provides a differentiation in their retention in comparison with the PBMCs.

It is also important to consider the morphology of the target, myeloblast cells which have irregular shapes and variation in cell membrane expression. As seen in Chapter 5, the nanometre scale surface roughness also directs retention. Therefore, the size and cell membrane complexity of HL60s and PBMCs was compared via forward and side scatter assessment using flow cytometry (Figure 6.2).

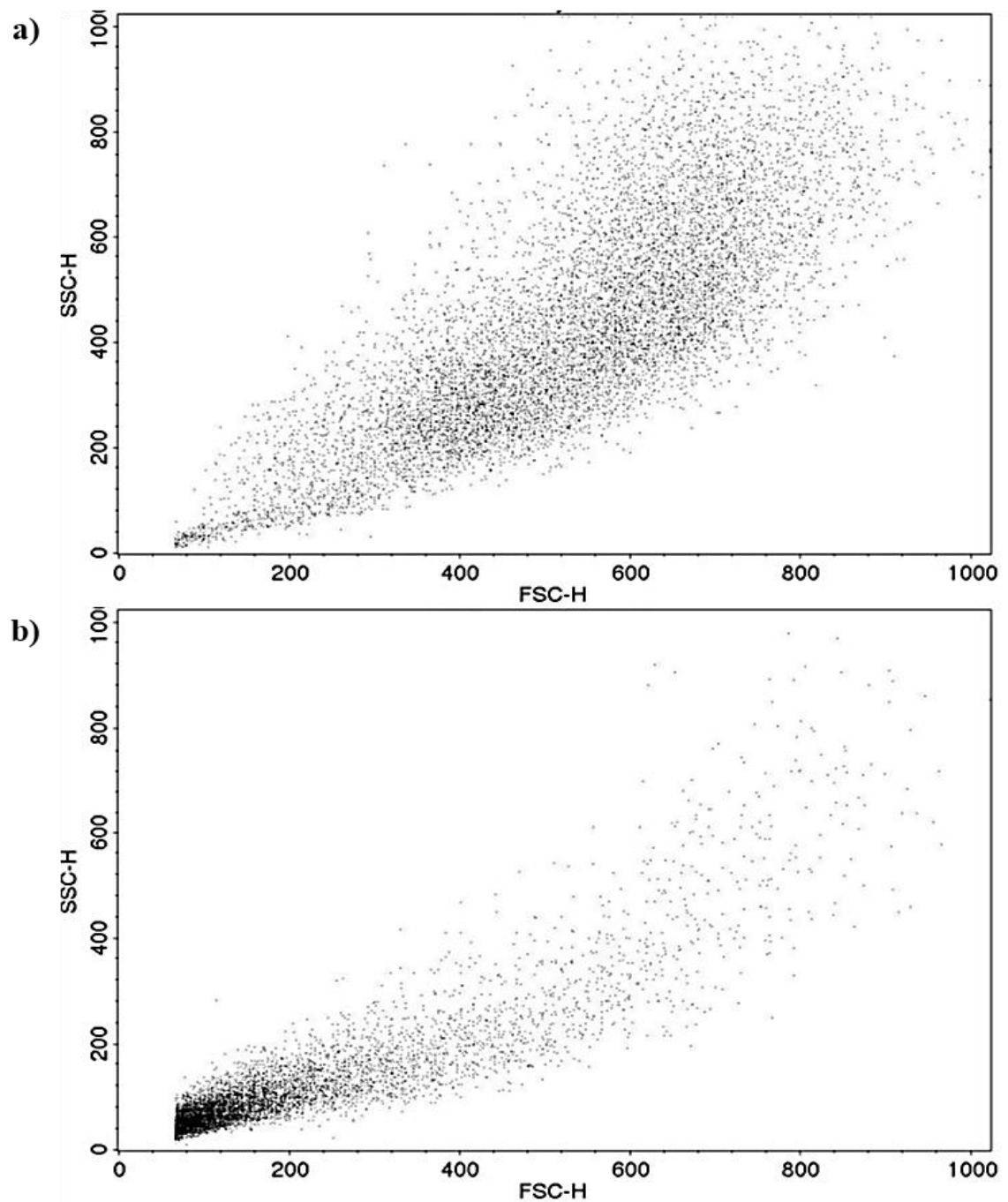


Figure 6.2 Flow cytometry analysis showing forward scatter (size size) versus side scatter (cellular granularity) for fixed a) HL60 and b) PBMCs.

The forward and size scatter show the HL60 cells to have both a larger and more granular structure when compared to PBMCs. The heterogeneity in size of HL60 cells corresponds to the poor grouping shown by forward scatter. This may be due to HL60 cells being fixed with cells at various stages of proliferation, however, circulating myeloblasts circulate in a range of stages of differentiation making this representative of the real-world application. Comparatively, PBMCs are significantly smaller with a distinctive size grouping characteristic of cells differentiating fully in the bone marrow before circulating

in the blood. HL60 show poor grouping with regards to membrane complexity indicating variation in the cellular features expressed in cells, as expected from myeloblasts. In both cases 100,000 cells were analysed in order to yield a sufficient representative sample.

Flow cytometry analysis confirms the size and shape difference between the cancerous proxy and healthy control that can be exploited with bioimprinting.

6.2. Cell staining

For myeloblast-PBMCs cell mixtures, which mimics the blood of an AML patient, a method was needed to identify and enumerate both cell types on the bioimprint surface. Other studies (reviewed in Chapter 1) have coupled imprinted substrates with a detection entity based on differences in, for example, heat transfer or mass variation distinguishing between retained cell types.²⁻⁸ In this instance, cell populations were separately tagged with fluorescence moieties and analysed via fluorescence microscopy using a combination of filter setups to differentiate cell emission. The tag was required to remain localised to one cell type, not stain the entire cell population indiscriminately. It was important to ensure dye combinations did not leach or affect each other, introducing unwanted artefacts into the results. Dye pairings were selected so that excitation and emission spectra did not significantly overlap; which may cause an emission from one cell type to excite a neighbouring cell, thus giving a false positive. Another requirement was the tag should remain localised to one cell type, not stain the entire cell population indiscriminately.

Using fluorophores covalently bonded to antibodies is commonplace in literature and provide a specific stain which do not transfer between cell populations. However, antibodies are expensive and inaccessible in large quantities needed; though the greatest disadvantage for bioimprinting applications was deemed changing the cell surface membrane shape. As shown in Chapter 5 and in other studies, nanometre scale alterations of the cell shape can influence the uptake of cell types.⁹⁻¹²

A CFSE proliferation kit was trialled to stain the cell population prior to fixing; advantageous as subsequent passages remain tagged. Though an excess of the fluorescent tag was used, a poor fluorescence stain is achieved, only visible on the edges of the cell when multiple focal depths are viewed. This makes distinguishing between different cell types difficult and unsuitable for use to identify cells as poorly tagged cells may not be

counted. Other problems with photobleaching and leaching to all cells were seen using stilbene 420.

Ultimately, the best results were seen with systems comprised of a fluorescent moiety attached to a lipid chain. Such dyes were retained in target due to the lipophilic nature of the cell with partition into the aqueous suspension highly disfavoured.^{13,14} Here, the size of the lipid chains is insignificant compared to the size of the cell and nanoscale topography. Lipid conjugated lissamine rhodamine and lipid-carboxyfluorescein were used to tag extracted PBMCs and HL60 cells respectively.^{13,14} Rhodamine moieties were viewed with TRITC filters, seen as red, and carboxyfluorescein, FITC; seen as green. See Figure 6.3 showing cells separately stained with lipid-lissamine rhodamine and lipid-carboxyfluorescein. Exposure times were calibrated by assessment of equal mixtures of stained and unstained cells. This ensure that the cells inherent auto-fluorescence was not observed.

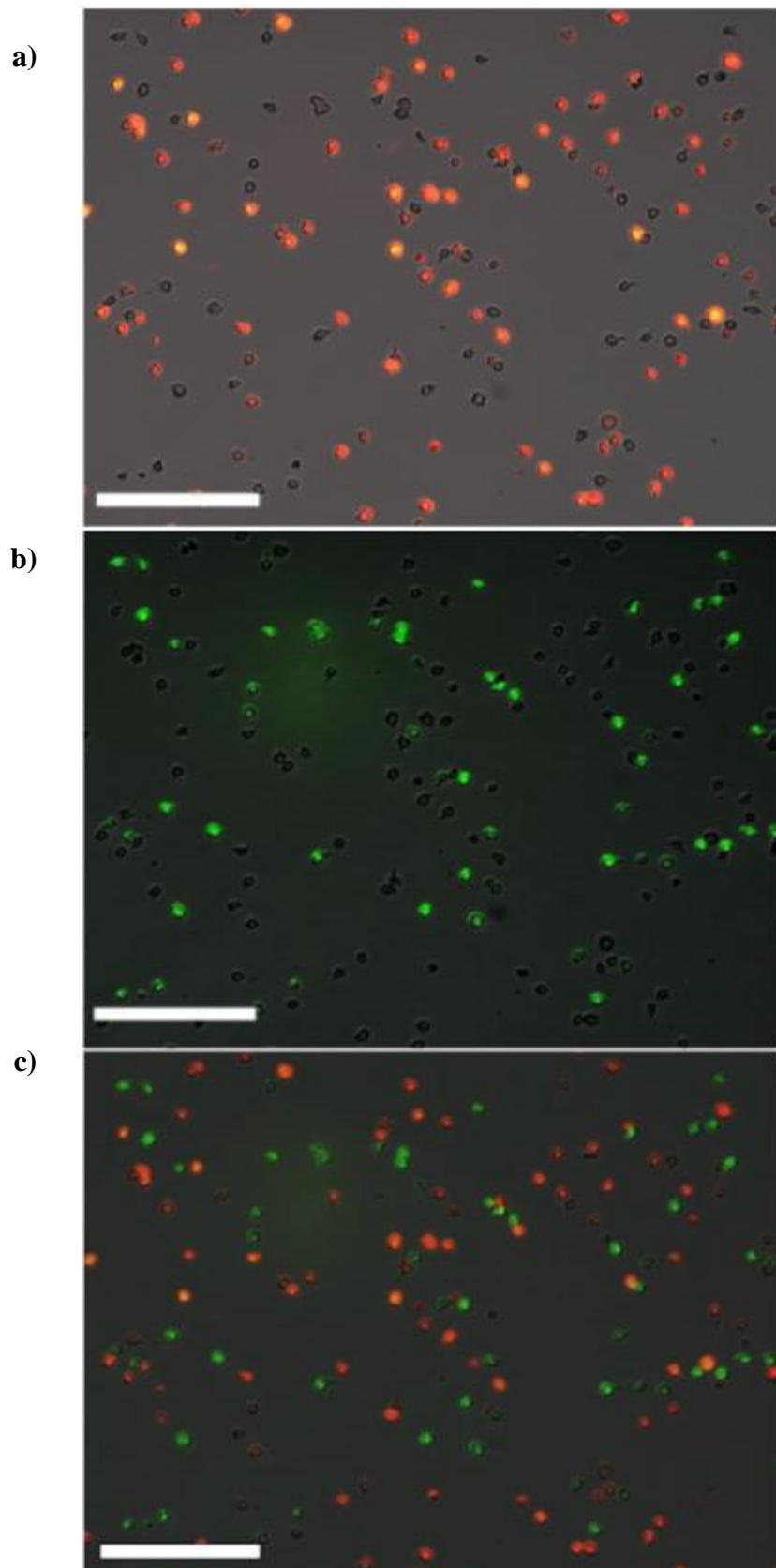


Figure 6.3 Mixed suspension of lissamine rhodamine and carboxy fluorescein labelled cells viewed using a) TRITC filter set; cells appear green b) FITC filter set; cells appear red and c) overlaid TRITC and FITC filter sets showing all cells are labelled and can be identified. Scale bars represent 100 μm .

Although not soluble in aqueous media, it was expected that dyes may transfer if cell suspensions were pelleted together by centrifugation. This effect was tested and no measurable transfer was observed. Results showed good distinction between the two cell types with cells not being identified in both filter sets.

6.3. Examination of the bioimprint selectivity towards myeloblasts

The retention of HL60 and PBMCs in mixed solutions was measured on PU bioimprints of HL60 cell layers. Each measurement was made under static seeding conditions whilst incorporated into a flow-through device (see Chapter 5). Bioimprints were functionalised with bPEI, grafted onto the bioimprint by matrix entanglement (see Chapter 4). The total cell concentration of the suspensions was kept to 20×10^6 cells ml^{-1} at a range of proportions of HL60 to PBMCs; 10%:90% 25%:75%, 50%:50% and 75%:25%. This cell concentration was shown to yield the maximum retention of cells in single cell suspensions (see Chapter 5). In this setting, it was possible to examine if the competitive interaction of the healthy control prevented plateau.

Cell populations were analysed under bright-field, FITC and TRITC emission filters to show that cell populations were not appearing in both channels. Here, HL60 were seen using TRITC (green), PBMC cells FITC (red) and the bioimprint imaged in bright field. Analysis was carried out at 20 sites across each bioimprint. Figure 6.4 shows the overlaid fluorescence and bright field microscopy images of various sites of the bioimprint after seeding with equal numbers of HL60 and PBMC cells from a suspension with a total concentration of 20×10^6 cells ml^{-1} for 1 hour.

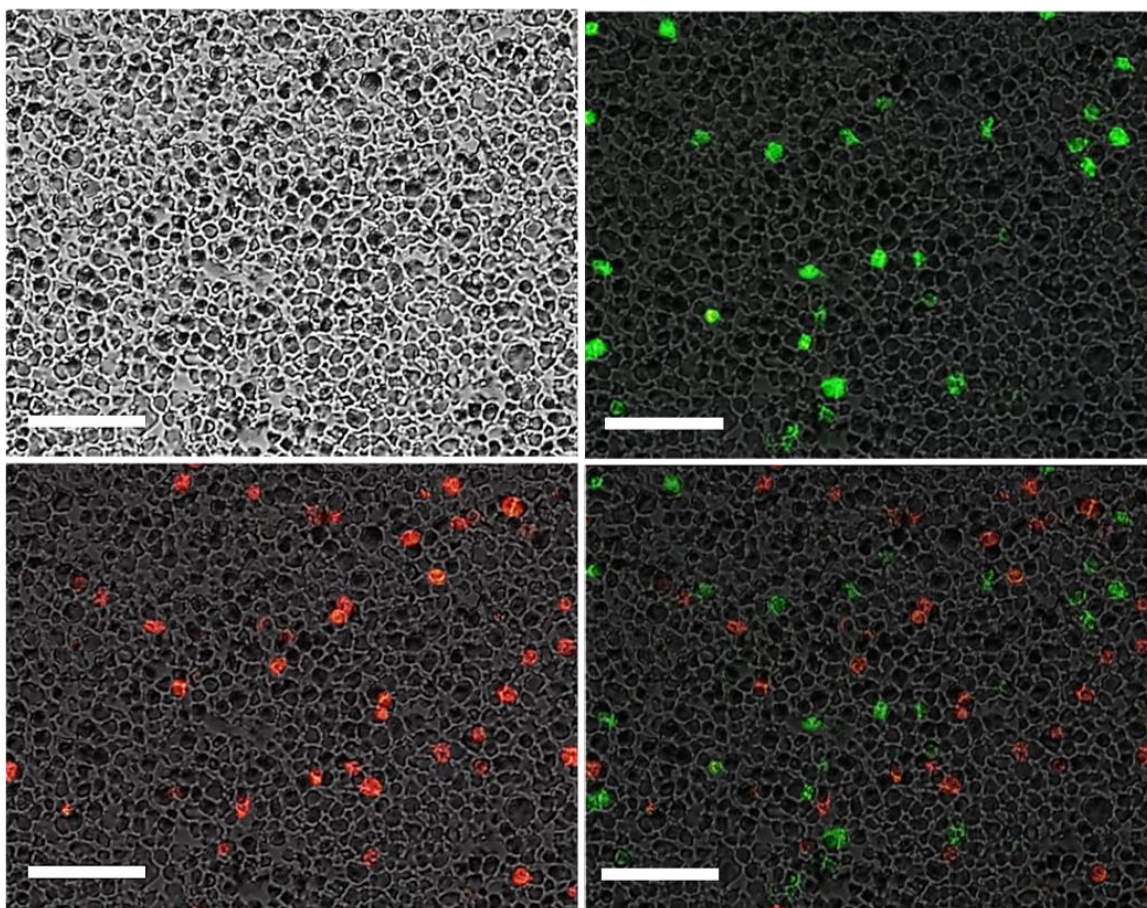


Figure 6.4 Fluorescence and bright field microscopy of HL60 bioimprints after exposure to equal ratios of HL60 and PBMCs from a suspension with total cell concentration of 5×10^6 cells ml^{-1} for 1 hour. Bioimprints were functionalised with 0.1% (w/v) bPEI and 0.9% (w/v) PU. Selectivity towards HL60 cells was measured under static conditions whilst incorporated into a flow-through cell. PBMCs are shown in red and HL60 in green. Scale bars represent 100 μm .

Selectivity experiments were carried out on bioimprints functionalised with 0.1%, 0.5% and 0.9% (w/v) bPEI, each solution containing uncured PU to make the additive concentration 1% (w/v) overall in ethanol, a layer of which was deposited, dried and UV-cured on the imprint (see Chapter 4). Each imprint treatment was examined at the four ratios of HL60 to PBMCs cell concentrations. Overlaid images showing fluorescence microscopy via TRITC and FITC filters showing PBMCs (red), HL60 (green) and the bright field image of the bioimprint for the case of 0.5% (w/v) bPEI and 0.5% (w/v) PU are seen in Figure 6.5 and Figure 6.6 after being exposed to a) 10% HL60, b) 25% HL60, c) 50% HL60 and d) 75% HL60 .

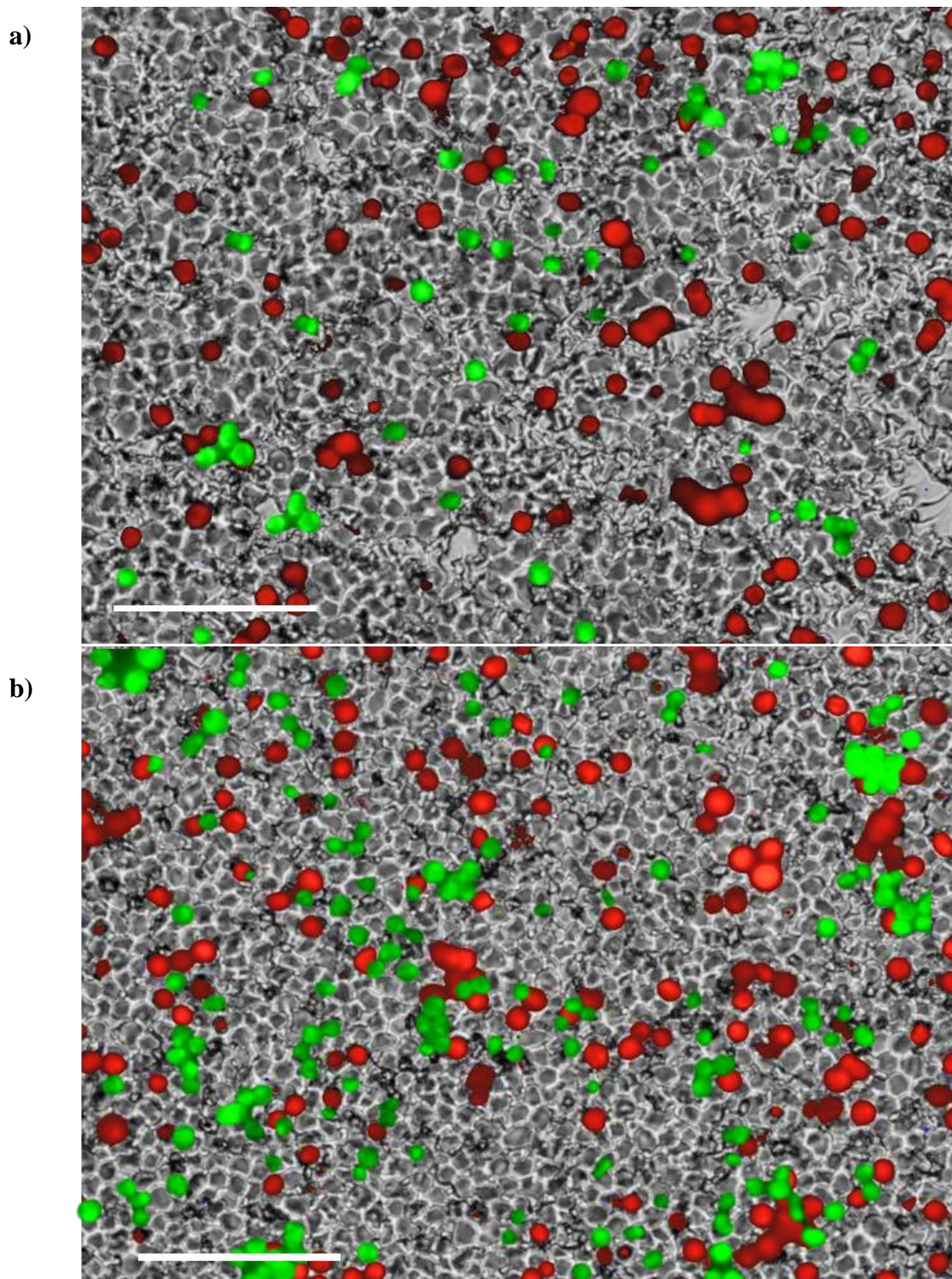


Figure 6.5 Overlaid fluorescence and bright field microscopy of HL60 bioimprints after exposure to a) 10% and b) 25% HL60 with PBMCs from a mixed suspension with total concentration of 20×10^6 cells ml^{-1} for 1 hour. Bioimprints were functionalised with 0.5% (w/v) bPEI and 0.5% (w/v) PU deposited as a thin layer in ethanol. Selectivity was measured under static conditions whilst incorporated into a flow-through cell. PBMCs are shown in red and HL60 in green. Scale bars represent 100 μm .

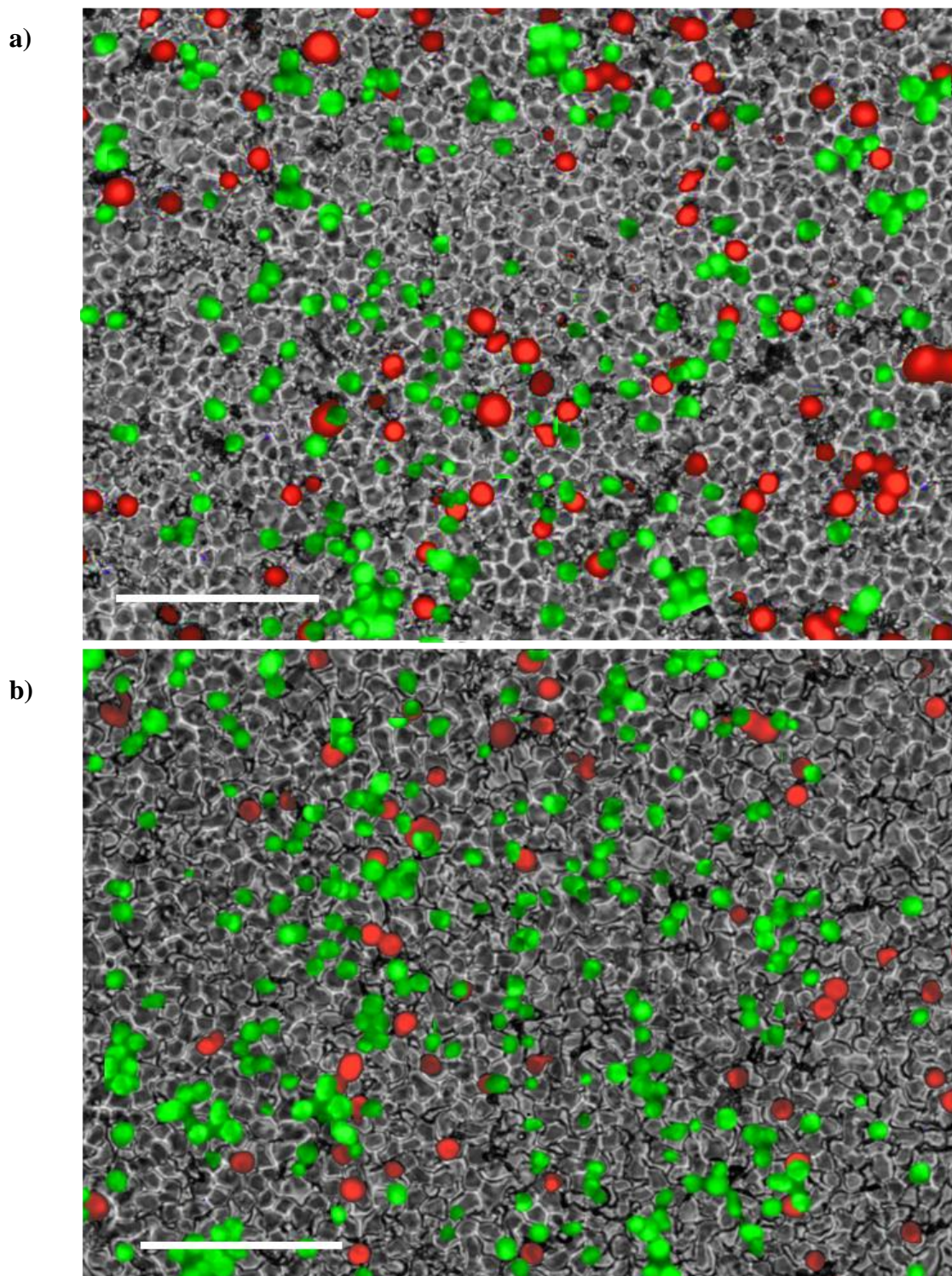


Figure 6.6 Overlaid fluorescence and bright field microscopy of HL60 bioimprints after exposure to a) 50% and b) 75% HL60 with PBMCs from a mixed cell suspension with total concentration of 20×10^6 cells ml^{-1} for 1 hour. Bioimprints functionalised with 0.5% (w/v) bPEI and 0.5% (w/v) PU. Selectivity was measured under static conditions whilst incorporated into a flow-through cell. PBMCs are shown in red and HL60 in green. Scale bars represent 100 μm .

The selectivity study examines four proportions of cell types. Here, the surface modification parameters with bPEI were also examined in order to optimise the uptake of HL60 whilst maintaining a preference in retention compared with PBMCs. In each instance, the cell suspension was applied to the bioimprints whilst incorporated into the flow device (see section 5.2), allowed to sediment for 1 hour and the unbound material washed away by perfusion of 10 ml of water at a rate of 100 ml h⁻¹. Fluorescence microscopy was used to acquire images at 20 sites on the bioimprint using TRITC and FITC filter sets. Each cell type was numerated in ImageJ and the average numbers of each cell type calculated. Table 6.2 and Figure 6.7 show the cell types retained to bioimprints.

Table 6.2 The area density of retention of HL60 and PBMC cells from binary suspensions of 20×10^6 cells ml⁻¹ incubated various proportions of cell types and repeated for a range of surface modifications of bPEI and PU. Retention was measured in static conditions on PU HL60 bioimprints incorporated into PDMS microfluidic chip. Unbound cells were removed by perfusion of water (10 ml) at 100 ml h⁻¹.

		Proportion of HL60 in the incubated solution							
		10% HL60		25% HL60		50% HL60		75% HL60	
[PEI] (wt.%)	Cells retained to imprint / $\times 10^6$ cells m ⁻²								
	PBMC	HL60	PBMC	HL60	PBMC	HL60	PBMC	HL60	
0.9	156	33	73	74	55	322	27	370	Mean
	26	7	46	18	20	56	11	38	SD
0.75	165	32	96	94	54	298	27	327	Mean
	44	10	31	49	18	36	12	38	SD
0.5	168	26	133	134	64	258	30	279	Mean
	41	10	43	36	15	66	10	75	SD
0.25	160	24	148	137	74	240	27	280	Mean
	29	10	40	23	26	24	13	25	SD

The number of each cell type retained to the bioimprint as a function of the proportion seeded in suspension is shown in Figure 6.7. This was repeated for bioimprints treated with 0.25%, 0.5%, 0.75% and 0.9% bPEI, grafted to the bioimprint by matrix entanglement in PU.

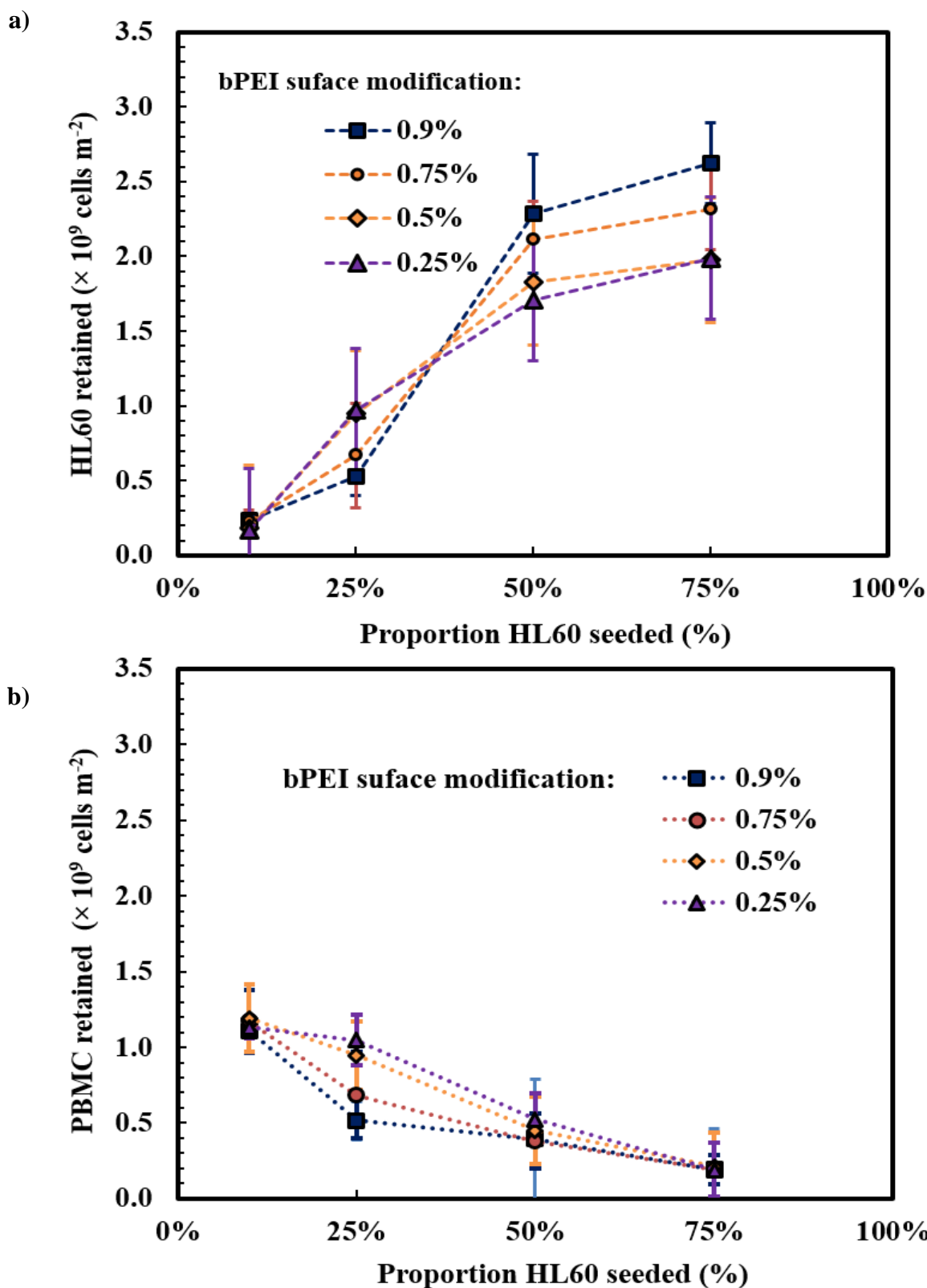


Figure 6.7 Retention of fixed a) HL60 and b) PBMC cells from mixed cell suspensions versus the proportion of HL60 in the seeded suspension of overall concentration of 20×10^6 cells ml^{-1} . Cell retention was measured in static conditions on PU HL60 bioimprints incorporated into PDMS microfluidic chip. Unbound cells were removed by perfusion of water (10 ml) at 100 ml h^{-1} .

When exposed to binary mixtures, the bioimprints show a preference to the target cell type. Results show that as the proportion of the target HL60 cells increases, more HL60s are retained on the bioimprint. In each case the ratio of HL60s retained to the bioimprint is larger than the proportions in the seeded solutions, showing the preference of HL60 over PBMCs.

The range of proportions of each cell type were designed to represent those expected in AML patient aspirate. At diagnosis, 20% of the mononuclear cells found in a blood sample are blasts.¹⁵ This translates to around $0.8 - 2.2 \times 10^9$ blasts per litre of blood, which with between 4.5 – 5.5 L of blood per person gives a total of $\sim 3.6 - 12.1 \times 10^9$ blasts in a patients' system.^{15,16,25} In the system representing diagnosis (25% HL60:75% PBMCs), between $0.5 - 1 \times 10^9$ HL60 cells were retained to the bioimprint. Therefore, around 10 – 20 m² of the bioimprint is needed to fully accommodate the myeloblast population from a patient in the diagnosis stage which is well within the range that can be practically produced by R2RNIL. In doing, further attention needs to be paid to arranging bioimprints into a flow system able to expose this area to patient aspirate. If successful, this would allow patients to undergo therapy to reduce blast numbers whilst in remission to prevent relapse and prolong disease free survival. Such treatment would be significantly less invasive and dangerous than traditional consolidation therapies allowing more frequent use, even for high risk patients.

Alternatively, the cell populations can be recirculated over the bioimprint to reduce the need for large areas of imprint. The greater affinity of the bioimprint towards the target cell enriches the proportion of the control cell type in the effluent media. If this is reapplied to the imprint, preferential capture of the HL60s allows a further depletion of the mixture from the myeloblasts. By sequential capture phases, the cancerous material could potentially be reduced below the minimal residual disease concentration whilst retaining the healthy white blood cells which can be returned to the patient to recover their immune system.

Though recirculation reduces the practical capacity of a bioimprint device, using a bioimprint of sufficiently large surface area can result in removal of HL60 cells from the applied sample. By constructing a bioimprint based device with a sufficiently channel long path length a complete depletion of the blood from the cancerous cells can potentially be achieved. This channel path length is dependent on the percentage of selectivity achieved towards the target cell type as an ideal system, 100% selective towards HL60s, all PBMCs would remain unbound reducing the wasted area. Moreover,

to ensure the quantities of the enriched healthy cell population are useable, a higher selectivity toward to malignant cells is preferred.

The retention of HL60 out of mixtures with PBMCs is of the same magnitude as from single cell suspensions indicating little competition for cavities between the two cell types (see Chapter 5). However, in the interest of spatial efficiency of the device, further examination of surface modification parameters should be done to improve the poor uptake of cells as from Figure 6.7. By analysis of the retention data as a function of the concentration of bPEI added to the bioimprint it is possible to better understand the effect of surface modification on selectivity. Figure 6.8 shows the effect of surface modifications with bPEI on the bioimprints selectivity towards HL60 cells from the cell mixtures.

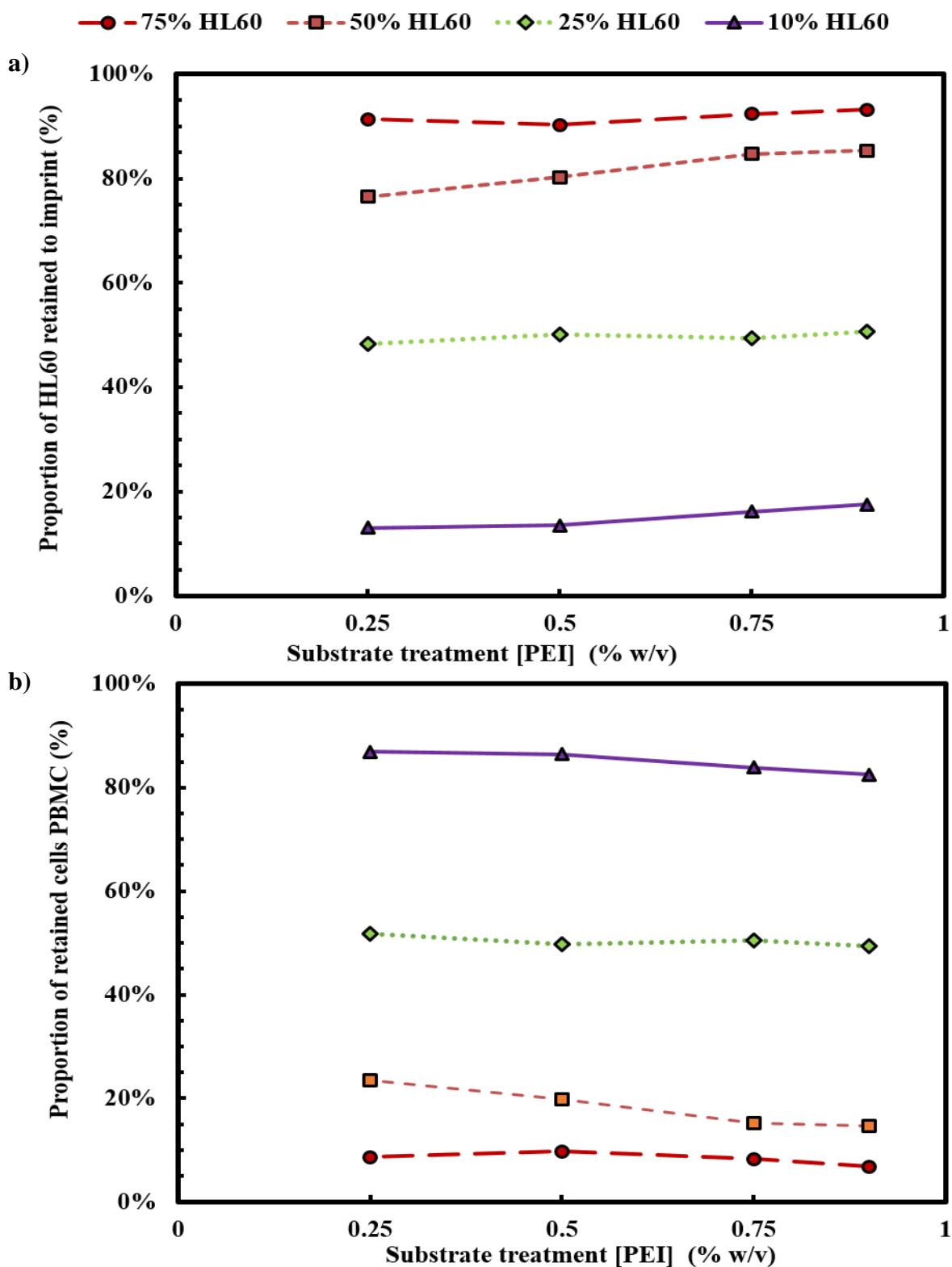


Figure 6.8 The proportion of a) HL60 and b) PBMC cells retained to the bioimprint versus the concentration of cationic polyelectrolyte bPEI used to functionalise the bioimprint surface. Selectivity measured as retention from binary cell mixtures of concentration kept constant at 20×10^6 cells ml^{-1} . Retention tested under static condition whilst incorporated in to PDMS microfluidic cell.

Results show the surface modification to be independent of the selectivity of the device. Though the number of cells retained to the bioimprint increases proportional to the bPEI treatment concentration, the percentage of HL60 cells remains relatively constant for treatment parameters. This effect was observed across all compositions of the binary cell mixture. The results show that the surface treatment protocols trialled did not offer good control over the selectivity of the bioimprint. This may be due to the treatment being carried out in a range that affects selectivity or the flow rate of flushing is not suitable for the attraction between the cells and the bioimprint surface. For instance, the bPEI is probably too far in excess of the effective range. In this case, excess polyelectrolyte could be washed away from the bioimprint prior to cell adhesion.

In future work, a lower bPEI concentration can be trialled, despite the poorer association between cells and the bioimprint. In such a system, recirculation of samples across the surface or using a larger surface area may offer provide adequate cell depletion. The following section will analyse if the selectivity of bioimprints is dependent on the path length of bioimprint used.

6.3.1. Channel path length comparison

The bioimprint selectivity towards HL60 cells was measured on bioimprints of varying length with a constant cell concentration mimicking the case of cell suspensions being recirculated over the bioimprint. The number of cells used was calculated as that required to cover the fully cover the entire area of the smallest chip length, 2 cm. As when with the effect of surface modification, three ratios of HL60 and PBMCs were trialled (Table 6.3 and Table 6.4, and graphically in Figure 6.9).

Table 6.3 Retention of HL60 cells to a polyurethane, HL60 cell bioimprint functionalised by grafting of 0.5% bPEI with 0.5% PU. Binary mixtures of fluorescently tagged HL60 and PBMCs were incubated at three discreet ratios with a constant cell concentration of 5×10^5 cells ml⁻¹. Retention of HL60 was examined under static conditions whilst incorporated into microfluidic flow cells as a function of the bioimprint path length.

Column length (cm)	Proportion of HL60 incubated (%)					
	25		50		75	
	HL60 retained ($\times 10^9$ cells m ⁻²)					
	Mean	SD	Mean	SD	Mean	SD
2	0.4	0.2	0.7	0.2	0.9	0.3
4	0.31	0.05	0.6	0.2	0.8	0.3
8	0.4	0.2	0.6	0.3	0.7	0.3

Table 6.4 Retention of PBMC cells to a polyurethane, HL60 cell bioimprint functionalised by grafting of 0.5% bPEI with 0.5% PU. Binary mixtures of fluorescently tagged HL60 and PBMCs were incubated at three discreet ratios with a constant cell concentration of 5×10^5 cells ml⁻¹. Retention examined under static conditions whilst incorporated into microfluidic flow cells as a function of the bioimprint path length.

Column length (cm)	Proportion of HL60 incubated (%)					
	25		50		75	
	PBMC retained ($\times 10^9$ cells m ⁻²)					
	Mean	SD	Mean	SD	Mean	SD
2	0.7	0.2	0.4	0.1	0.25	0.09
4	0.5	0.2	0.3	0.2	0.14	0.09
8	0.5	0.2	0.3	0.3	0.13	0.05

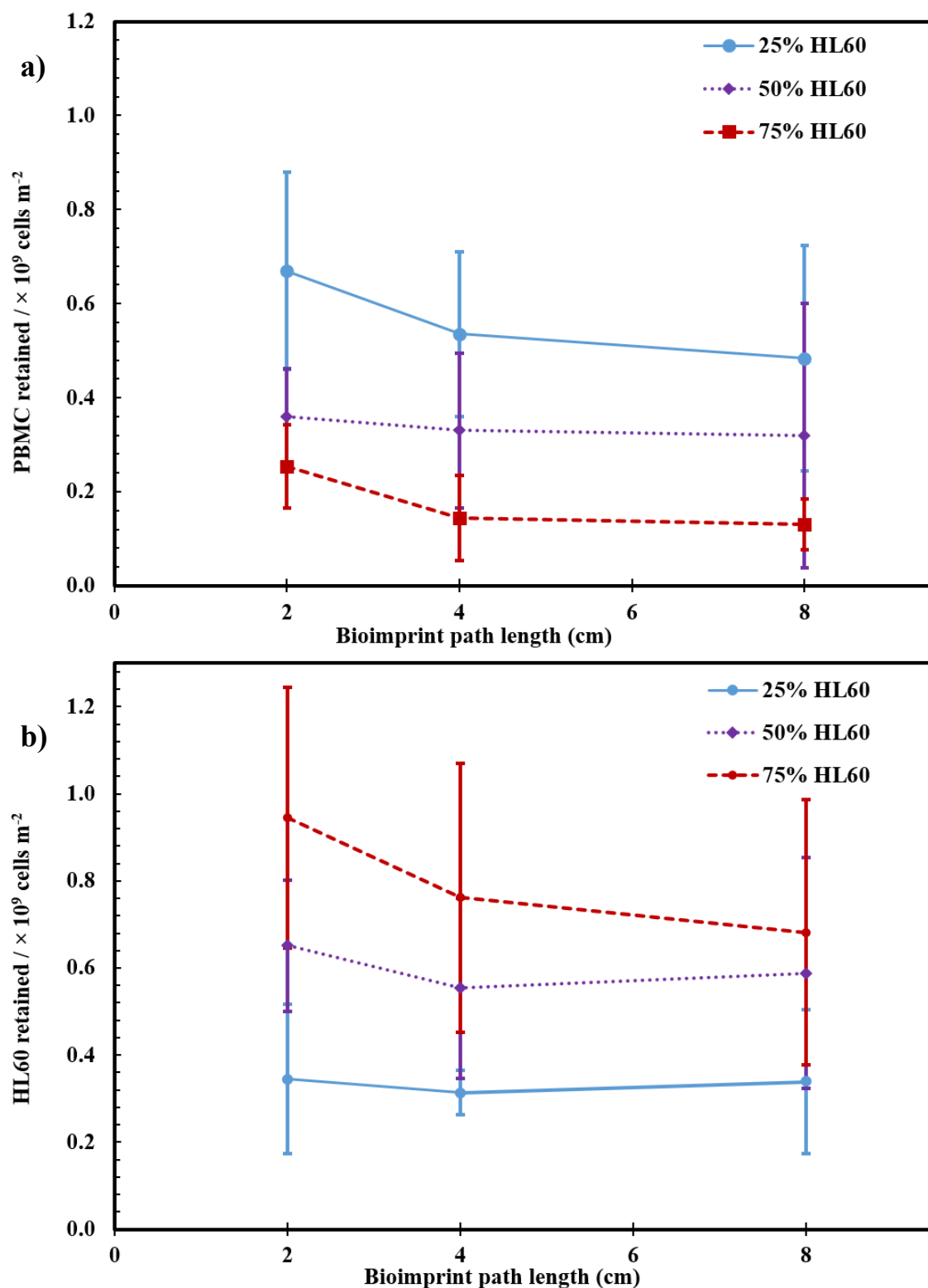


Figure 6.9 Area density of retention of a) PMBC and b) HL60 cells to a polyurethane from binary mixtures versus the path length of the polyurethane, HL60 cell bioimprint functionalised by grafting of 0.5% bPEI with 0.5% PU. Binary mixtures of fluorescently tagged HL60 and PBMCs were incubated at three discrete ratios with a constant number of 5×10^5 cells. Retention examined under static conditions whilst incorporated into the flow-through type of cell.

The selectivity towards HL60 cells can also be shown as the proportion of each cell type observed on imprints see Table 6.5 and Figure 6.10, below.

Table 6.5 Proportion of HL60 and PBMC retained to polyurethane, HL60 cell bioimprint functionalised by grafting of 0.5% bPEI with 0.5% PU as a function of the bioimprint path length. HL60 and PBMCs were incubated at three discreet ratios with a constant cell concentration of 5×10^5 cells ml⁻¹. Retention was examined under static conditions whilst incorporated into flow-through cell.

		Proportion of HL60 incubated (%)					
		25		50		75	
Column length (cm)	Cell type retained						
	PBMC	HL60	PBMC	HL60	PBMC	HL60	
2	66%	34%	33%	67%	21%	79%	
4	63%	37%	38%	62%	16%	84%	
8	59%	41%	36%	64%	16%	84%	

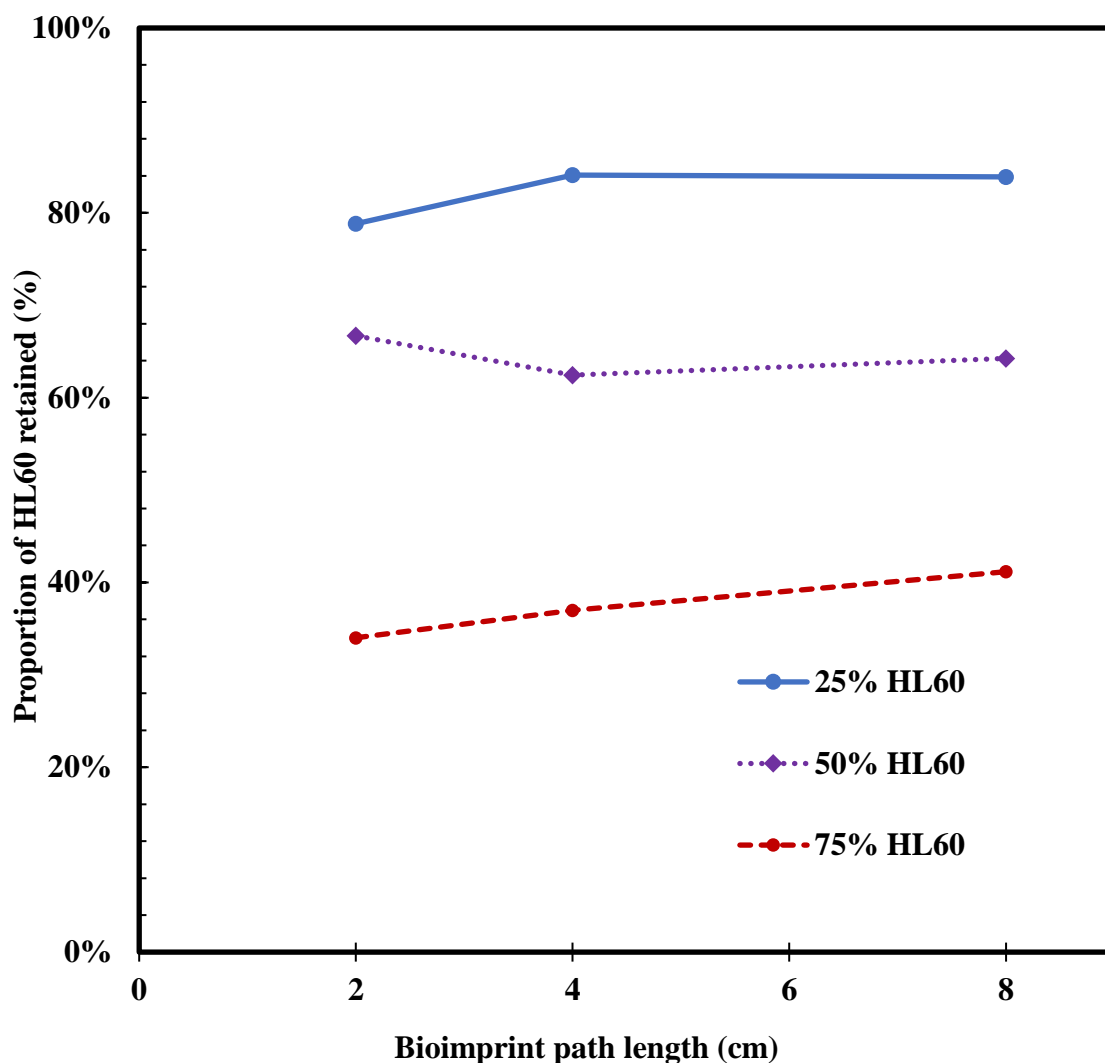


Figure 6.10 Selectivity of bioimprints towards HL60 from mixtures with PBMCs as a function of the bioimprint path length. Suspensions of a constant 5×10^5 cells ml^{-1} were incubated on polyurethane, HL60 cell bioimprints functionalised by grafting of 0.5% bPEI with 0.5% PU. Retention examined under static conditions whilst incorporated into a flow-through type of cell.

This analysis confirms the surface modification examined do not affect the selectivity, despite the change of cell concentration.

6.4. Conclusions

This chapter aimed to examine the ability of bioimprints to recognise template myeloblast cells from complex, mixed populations. Here the proof-of-principle is carried out using a myeloblast surrogate, HL60, in competition with control of healthy peripheral blood cells.

The preference towards the target cell type was examined from such cell mixtures, by seeding them on the imprint surface under static conditions whilst incorporated into a microfluidic flow cell (see Chapter 5). The composition of the binary cell suspension used model ratios of cancerous to healthy cells expected from patient's aspirate. A trade-off was expected between the volume of cells retained and the selectivity of the device. This balance dictates in what capacity the bioimprinted myeloblast capture device can be used; diagnostic or direct therapy. In a diagnostic setting, selectivity towards the myeloblasts remains paramount. Here the device can be used to capture myeloblasts from patient aspirate during the minimal residual disease phase who, by definition, have too few cells to be statistically relevant by morphological analysis. Detection at an early stage of relapse is highly favourable for a positive prognosis. An improved therapeutic classification of FAB or WHO AML subtypes can also be found. The selectivity achieved by bioimprints treated with polymer grafted bPEI was not sufficient for use in a diagnostic device.

Though the target cell type were retained to imprint, so too are a number of the healthy control. If bioimprints were used in this setting the number of healthy cells from patient aspirate would also be retained in high quantities. However, classical morphological analysis may be carried out on an enriched population on the bioimprint in an attempt to lower the detection limits and identify relapse of acute myeloid leukaemia (AML). Such a device would allow very small cell populations to be isolated and identified from large volumes of tissue.

Alternatively, if the focus of the device were in direct treatment, cell retention on large scale would be key. Such a device would need a sufficient throughput to make a significant difference in the 10^{10} – 10^{11} cells present in an AML patient. Use in therapy to directly remove myeloblasts from patient aspirate may be possible as the large quantities expected in AML aspirate will be available for capture, allowing healthy tissue to be reinfused to the patient. Collateral capture of healthy tissue is undesirable though if a preference towards malignant cells is observed, fewer myeloblasts remain in the patient's system.

By recirculation of the patient aspirate the myeloblast target can be depleted fully as each successive pass yields an increased purification of healthy cells. These can be reinfused in a patient in order to restore the immune system and negate problems of graft versus host disease seen in allogeneic transplantation. It is possible to design such a therapy may be used as an alternative to leukapheresis which to date does not clinically relate to improved remission or survival. Herein, the bioimprint offers the advantage of reintroducing healthy white cells to help maintain sufferers prior to or during chemotherapy.

An examination of the bioimprint path length confirmed the surface modification parameters trialled were insufficient to affect the selectivity achieved. However, the number of cells retained to the bioimprint remained relatively constant in cases where the incubated suspension concentrations were lower. The examination also confirmed that if a sufficient area of bioimprint was used, target cells could potentially be completely depleted from the sample allowing healthy white blood cells to be reinfused.

6.5. References

- 1 A. Bole and P. Manesiotis, *Adv. Mater.*, 2016, 5349–5366.
- 2 K. Eersels, B. Van Grinsven, A. Ethirajan, S. Timmermans, K. L. Jiménez Monroy, J. F. J. Bogie, S. Punniyakoti, T. Vandenryt, J. J. A. Hendriks, T. J. Cleij, M. J. A. P. Daemen, V. Somers, W. De Ceuninck and P. Wagner, *ACS Appl. Mater. Interfaces*, 2013, **5**, 7258–7267.
- 3 A. Ahmed, J. V. Rushworth, N. A. Hirst and P. A. Millner, *Clin. Microbiol. Rev.*, 2014, **27**, 631–646.
- 4 T. Cohen, J. Starosvetsky, U. Cheruti and R. Armon, *Int. J. Mol. Sci.*, 2010, **11**, 1236–1252.
- 5 O. Hayden, K. J. Mann, S. Krassnig and F. L. Dickert, *Angew. Chemie - Int. Ed.*, 2006, **45**, 2626–2629.
- 6 M. Jenik, A. Seifner, P. Lieberzeit and F. L. Dickert, *Anal. Bioanal. Chem.*, 2009, **394**, 523–528.
- 7 P. Qi, Y. Wan and D. Zhang, *Biosens. Bioelectron.*, 2013, **39**, 282–288.
- 8 J. J. Muys, M. M. Alkaisi and J. J. Evans, *J. Biomed. Nanotechnol.*, 2006, **2**, 11–15.
- 9 J. J. Muys, M. M. Alkaisi, D. O. S. Melville, J. Nagase, P. Sykes, G. M. Parguez and J. J. Evans, *J. Nanobiotechnology*, 2006, **4**, 1-10.
- 10 F. Samsuri, M. M. Alkaisi, J. J. Evans, K. Chitcholtan and J. S. Mitchell, *Microelectron. Eng.*, 2011, **88**, 1871–1874.
- 11 F. Samsuri, J. S. Mitchell, M. M. Alkaisi and J. J. Evans, *AIP Conf. Proc.*, 2009, **1151**, 71–74.
- 12 X. Zhou, J. Shi, F. Zhang, J. Hu, X. Li, L. Wang, X. Ma and Y. Chen, *Lab Chip*, 2010, **10**, 1182–1188.
- 13 H. Goodall and M. H. Johnson, *Nature*, 1982, **295**, 524–526.
- 14 M. W. Wessendorf and T. C. Brelje, *Histochemistry*, 1992, **98**, 81–85.
- 15 D. Harmening, *Clinical & fundamentals of Hemostasis*, F. A. Davies Company, Philadelphia, 1997.
- 16 H. Döhner, E. H. E. Estey, S. Amadori, F. R. F. R. Appelbaum, T. Büchner, A. K. a. K. Burnett, H. Dombret, P. Fenaux, D. Grimwade, R. a. R. A. Larson, F. Lo-Coco, T. Naoe, D. Niederwieser, G. J. Ossenkoppele, M. A. Sanz, J. Sierra, M. S. Tallman, B. Löwenberg, C. D. Bloomfield and Others, *Blood*, 2010, **115**, 453–474.
- 17 G. Ossenkoppele and B. Lowenberg, *Blood*, 2015, **125**, 767–774.
- 18 J. Saultz and R. Garzon, *J. Clin. Med.*, 2016, **5**, 33.

- 19 S. Oberoi, T. Lehrnbecher, B. Phillips, J. Hitzler, M. C. Ethier, J. Beyene and L. Sung, *Leuk. Res.*, 2014, **38**, 460–468.
- 20 I. Berber, I. Kuku, M. A. Erkurt, E. Kaya, H. Gozukara Bag, I. Nizam, M. Koroglu, M. Ozgul and S. Bazna, *Transfus. Apher. Sci.*, 2015, **53**, 185–190.
- 21 M. Schulz, G. Bug, H. Bialleck, H. Serve, E. Seifried and H. Bönig, *Vox Sang.*, 2013, **105**, 47–53.
- 22 E. Paietta, *Blood*, 2018, **131**, 1265–1266.
- 23 G. J. Schuurhuis, M. Heuser, S. Freeman, M.-C. Béné, F. Buccisano, J. Cloos, D. Grimwade, T. Haferlach, R. K. Hills, C. S. Hourigan, J. L. Jorgensen, W. Kern, F. Lacombe, L. Maurillo, C. Preudhomme, B. A. van der Reijden, C. Thiede, A. Venditti, P. Vyas, B. L. Wood, R. B. Walter, K. Döhner, G. J. Roboz and G. J. Ossenkoppele, *Blood*, 2018, **131**, blood-2017-09-801498.
- 24 C. U. Michael J. Burke, Linda Burns, Michael A. Linden, Bruce Lindgren, Michael R. Verneris, Daniel Weisdorf, *Am. J. Hematol.*, 2014, **88**, 826–827.
- 25 E. H. Estey and H. Dohner, *Lancet*, 2006, **368**, 1894–18907.

7. Summary of Conclusions and Future Work

7.1. Conclusions

This thesis has focussed on acute myeloid leukaemia; a heterogeneous condition characterised by a fast onset of symptoms, resulting in death within months of diagnosis. Despite advances in the knowledge of the condition and aetiology, prognosis and outcome remain very poor. Treatment relies on chemotherapy and bone marrow transplant which are unsuitable for a large proportion of patients due to iatrogenic damage. Moreover, treatment related mortality remains a concern in the majority of patients who present at adverse age and condition. AML therapy is maligned by the inability to specially target neoplastic tissue. This study aimed to develop bioimprinting technologies to produce a vehicle for myeloblast depletion dependent only on their size and shape differences when compared with healthy white blood cells. To date, no publications detail the imprinting of leukaemia cells or use bioimprinting in this field.

7.1.1. Bioimprint production

In order to produce accurate imprints of biological material, cells were chemically fixated to prevent membrane deformation and damage during handling. Glutaraldehyde was identified as a suitable fixative, shown to preserve the morphological information of the templated cell. The next stage of the project aimed to elucidate a method to reliably immobilise the templated cells to form layers on solid support which could then be cast into a curing polymer resin. Densely packed cell layers were sought to provide spatial efficiency of the ultimate myeloblast capture device. A key design caveat was to protect a part of the cell surface in the templated layer which dictates the proportion of each cell that is exposed for capture by the imprinting resin. A balance was achieved between over protection from water, yielding shallow cavities and complete drying compromising the cell layer due to cracking and cell aggregation.

Two of the methods trialled proved successful in reliably immobilising cell templates; by using Cytocentrifugation and by spreading in conjunction with aqueous glucose solutions.

The latter involved fully drying the cell layer which was prevented from cracking by fine adjustment of the glucose concentration. Fabrication of bioimprints produced by this methodology were of an area 2 - 3 orders of magnitude larger than currently reported in the literature for various cell templates. Bioimprints were cast into PDMS, ideal in this application due to the ambient curing conditions minimised the damage on the biological template and the soft, elastic nature of the curable silicone allowed cell substrates to be replicated without compromising the bioimprint structure.

Replication was achieved by in-house plate-to-plate style imprinting; the positive imprint made by applying a UV curable photoresist enabling fabrication of a copy of the original negative by subsequent application of PDMS or PU resin. Industrial roll-to-roll nanoimprint lithography was used to upscale the imprinted area by two orders of magnitude. The master imprint was not damaged as a result of the imprinting process and can be readily used to further reproduce bioimprints at a user defined length. This augmentation was poor from bioimprints created by deposition of template cells by cyto centrifugation making the method incompatible with producing a myeloblast capture device. As such, spreading cells using the cyto centrifuge was discontinued.

7.1.2. Bioimprint characterisation and modification

Quantitative analysis of the diameters of the myeloblast bioimprint cavities showed a close likeness between cell templates, bioimprints and replica imprints. This analysis was confirmed by assessing bioimprints produced from a population of monodisperse particles. Here, the effect of the proportions of the cell exposed to the curing polymer could be seen from the wide distribution of cavity diameters achieved. Surface profiling of PDMS and PU substrates was able to detect nanoscale features on the bioimprints, representative of extracellular features.

The project then aimed to create a methodology to introduce an attraction towards target cells by chemical modification of the bioimprint surface. The protocols trialled attempted to immobilise cationic polyelectrolytes to provide favourable increased electrostatic interactions. By fine control of this attraction, the selectivity of the bioimprints could be achieved through amplification of classical DLVO-style forces towards cells fitting into cavities. Initially this was achieved via oxygen plasma treatment of PDMS substrates to produce negative surface groups to anchor cationic polyelectrolytes. However, due to a

low degree of crosslinking, hydrophobic recovery was observed in PDMS substrates making it incompatible for use in a myeloblast capture device.

In the interest of device storage and longevity, an alternative surface modification procedure was examined involving the entrapment of polyelectrolytes by grafting in a matrix from trace amounts of the polymer material. Here, care was taken to ensure the polymer material was not added in sufficient amount to compromise the cavity shape which constitutes the *raison d'être* of bioimprint selectivity. Polyelectrolyte branched PEI was trialled in this study which offered the dual advantage of being soluble in polar solvents and being non-toxic and thus, ratified for use in medical devices. Analysis of the modified bioimprints confirmed the materials applied to the surface showed no significant adulteration of the structure.

7.1.3. Retention of single cells to bioimprints

The ability of bioimprints to immobilise cells from suspension was examined. Here, a methodology was developed that involved incorporation of bioimprints into a bespoke flow cell in order to remove artefacts in data collection. This enabled the control of the hydrodynamic environment and prevented evaporation of the cell suspension seeded on the bioimprint surface; both of which could impact results. Cells were identified on the bioimprint localised to the bioimprint cavities, not indiscriminately on the surface. A protocol for automatic enumeration reliant on fluorescence microscopy analysis of the bioimprint was developed.

The surface of the bioimprint cavity on cell retention was examined as function of the incubated cell suspension concentration. When investigating surface charge, the area density of retention was shown to be proportional to both the cell and polyelectrolyte concentration and achieved a plateau at high concentration. Surface topography was investigated by assessing the retention of cells to an imprint produced from particles of a comparable size though with relatively little asperity. The uptake of cells to particle imprints was a factor of ten lower than to cellular imprints indicating the importance of the cell curvature and cell membrane features on retention.

7.1.4. Selectivity from binary mixtures

The preference of the bioimprint towards the target cell type was measured from competitive mixtures. In this instance, the cancerous target cells were mixed with healthy peripheral blood cells to mimic the situation of myeloblasts in leukaemia patient aspirate. Cell types were fluorescently tagged for identification and numeration. Dye combinations were chosen so cross-talk and leaching did not cause cells to appear in both fluorescence channels.

Selectivity of the bioimprints was examined by seeding binary cell suspensions of HL60 cells, representing the myeloblasts, and healthy PBMCs. Various proportions of each cell type, in suspensions of fixed concentration, were examined to mimic samples from AML sufferers in the early stages of the condition through to the situation where significantly more cancerous cells than healthy from pre-enrichment of populations. In all scenarios, the proportion of cancerous cells retained to the bioimprint was higher than in suspension added, showing some degree of selectivity for the target cell population. Comparison of surface charge showed the selectivity to be independent of the surface modifications trialled. Further surface activations should be trialled to improve discrimination of the cancerous cell type.

The result was promising as a proof of principle for a myeloblast capture device. Any preference can be exploited by subsequent reapplication of the effluent media to fresh bioimprints. As bioimprints deplete the blood cancer cells preferentially, after sufficient 'washings', they will be completely removed from the mixed cell sample. The effluent material becomes enriched with a population of healthy peripheral blood which could potentially be reinfused to the patient in a similar procedure as leukapheresis. Here, the clinical significance of returning healthy cells to patients may be examined.

In terms of a flow-through device, if the pathlength of the bioimprint is sufficiently long, all myeloblasts can be totally excluded due to the preferred affinity to bioimprints. This was mimicked in small scale conditions by varying the length of the flow cell used to examine retention with constant cell volume. The preference towards a cell type was unaffected by the increased surface area however, the numbers of cells retained to the imprints also remained relatively unchanged despite the difference in the incubated cell population. This also indicates that additional surface modification parameters should be trialled to improve selectivity at fixed flow rate.

7.2. Future work

7.2.1. Optimise surface modification

As discussed previously, the surface modification parameters trialled were unable to improve the affinity of the bioimprint towards the target cell type. By using lower concentration of cationic polyelectrolyte, the reliance on the amplification of electrostatic forces by superior surface area contact may become evident. Alternatively, other materials may provide a better selectivity towards myeloblasts, thus reducing the amount of collateral capture of healthy tissue. An alternative route of improving selectivity is to functionalise the bioimprints with myeloblast-specific antibodies, for instance CD33.

7.2.2. Examination of effluent

The selectivity in this study concerned only the cells adsorbed to the bioimprint. It is possible to also assess the effluent media in order to quantify the enrichment of healthy cells and characterise the depletion of cancerous cells. Flow cytometry assessment of suspensions before and after eluting can indicate the populations being targeted by the bioimprint. As discussed previously, the cancerous cell type can potentially be totally removed from samples using a sufficiently long path-length of the bioimprint. This length can be characterised by changing the number of cells added to the imprint and monitoring the collected media for complete depletion.

7.2.3. Unfixed cells

For this proof of principle study, cell retention has only been examined using chemically fixed cells. Crosslinking of the surface proteins gives fixed cells structural rigidity and resistance to deformation. As part of a clinical procedure, aspirate will be comprised entirely of unfixed cells. The effect of cell deformation with should be investigated by exposing bioimprints to single and multi-cell suspensions of unfixed cells.

7.2.4. Flow conditions

For practical real world use, the cell retention and preference to target cell should be examined under flow conditions. This may involve a sequential pattern of start/stop periods to allow the cell populations to sediment on the bioimprint. This flow can also be used to detach unbound cells from the bioimprint. It is also important to consider the design of the flow system which are available in various conformations: serpentine or parallel channels.